GERAGHTY, LEX RODGER

GEOCHEMICAL CHARACTERISTICS AND RARE EARTH ELEMENT TRENDS OF THE UPPER ZONE IN THE WESTERN BUSHVELD COMPLEX

MSc **UP** **1994**

Geochemical characteristics and rare earth element trends of the Upper Zone in the western Bushveld Complex.

by
Lex Rodger Geraghty

Submitted in partial fulfillment of requirements
for the degree of
MASTER OF SCIENCE
in the Faculty of Science
University of Pretoria
Pretoria

April 1994

ABSTRACT

The geochemical trends of the Bierkraal 1 drill core are investigated to document the behaviour of various elements. Special emphasis is placed on the rare earth elements during the final stages of crystallization of the Upper Zone in the western Bushveld. The geochemical characteristics of the western Bushveld Upper Zone are also briefly compared to the Upper Zone of the eastern Bushveld as exposed in the Roossenekal district.

The rock types intersected by the Bierkraal 1 borehole consist largely of gabbro, magnetite gabbro, lesser magnetite and anorthosite layers. Plagioclase comprises 50 to 70 volume percent of most samples investigated. Up to 87 volume percent plagioclase is found in anorthosite while magnetitite layers consist of up to 97 volume percent oxide. Unlike the eastern Bushveld, olivine occurs throughout the Bierkraal 1 borehole and, is generally limited to the range of 15 to 30 volume percent. Pyroxene is generally well below 10 volume percent with hornblende becoming a major constituent only in the upper part of the borehole.

Apatite, which generally occurs in the percent range, is the mineral with the highest concentration of rare earth elements in the Upper Zone. The accessory minerals are K-feldspar, quartz and zircon are limited to the uppermost parts of the sequence, while biotite occurs throughout.

Closely spaced samples indicate that the overall trend in the Bierkraal 1 borehole can be subdivided into 4 cycles. The 4 cycles are identified by means of apatite and olivine composition, whole rock and trace element contents. The individual cycles undergo normal fractionation.

The modelling of overall Rb enrichment suggests a trapped liquid content of 15 to 37 percent. Modelling each cycle individually, shows that the cycles undergo crystallization in an open system with residual liquid escaping and, probably mixing with overlying fluid.

Four cycles, corresponding to the whole rock geochemistry, are evident in the whole rock and apatite rare earth element content. The rare earth element trends are shown to be largely dominated by modal proportions of apatite and plagioclase and, to a lesser extent, by normal fractionation. Alteration and metamorphism are shown to have little effect on the rare earth element patterns.

Apatite samples are light rare earth enriched, at approximately 1000 times chondrite. The light rare earth element enrichment is typical of late stage differentiation, while certain light rare earth element ratios imply contamination of the mafic magma by Transvaal sediments.

A specific melt type, from which the Upper Zone crystallized, is not clearly indicated by the whole rock rare earth element patterns. The replenishment by a less fractionated magma and the resulting mixing, rather than the introduction of new magma, are thought to be responsible for cyclic trends. It is not clear whether these mixing events are due to, 1) pulses of the same, but less

fractionated magma, 2) convectional overturning resulting from the disintegration of a stagnant layer, or 3) whether prestratification of the magma in the magma chamber existed.

Rare earth element distribution coefficients (calculated by the ratio of rare earth element content of apatite to rare earth element content of host matrix) indicates that the apatite in magnetite and apatite rich zones crystallized under conditions nearer to equilibrium than apatite in any other rock units. This lends credence to the theory that an immiscible Fe-P_2O_5 rich melt forms during the crystallization of the Upper Zone.

Various interwoven geochemical twin trends following in stratigraphic sequence, are identified in some cycles and are found to be similar in geochemical behaviour. These trends are associated with normal fractionation processes. The presence of interwoven twin trends are tentatively ascribed to crystallization being alternatively dominated by adjacent convection cells within the magma.

SAMEVATTING

Monsters van die Bierkraal 1 boorgat is ondersoek met die doel om die geochemiese eienskappe van 'n verskeidenheid elemente, veral die seldsame aardelemente, tydens die finale kristallisasie van die Bosone in die westelike Bosveld Kompleks te beskryf. Chemiese resultate van die westelike Bosveld Kompleks is ook met resultate afkomstig van die Roossenekal distrik vergelyk.

Die Bierkraal 1 boorgat bestaan hoofsaaklik uit gabbro, magnetiet gabbro met ondergeskikte anortosiet en magnetiet lae. Die gesteentes bevat meestal tussen 50 en 70 volume persent plagioklaas, maar anortosiet lae bevat tot 87 volume persent plagioklaas. Magnetiet lae daarenteen, bevat tot 97 volume persent oksiedes. Olivien kom deurgaans in die gesteentes voor en beslaan ongeveer 15 to 30 volume persent van die gesteentes. Gesteentes bevat hoogstens 10 persent pirokseen, en horingblende is slegs 'n hoof bestandeel in die boonste dele van die boorgat.

Apatiet, wat oor die algemeen beperk is tot die persentasie interval, is die belangrikste seldsame aardelement ryke mineraal in die Bosone. Bykomstige minerale is biotiet, met voorkomste van K-feldspaat, kwarts en zirkoon, wat beperk is tot die boonste dele van die opeenvolging.

Resultate van naby gespasieerde monsterneming dui aan dat die algehele geochemiese patroon in die Bierkraal 1 boorgat in vier eenhede onderverdeel kan word. Die vier siklusse kan deur middel van 1) apatiet en olivien samestelling en 2) heel gesteente en spoor element analise geëien word. Die individuele siklusse ondergaan normale fraktionering.

Modellering van die algehele Rb verryking toon dat 15 tot 37 persent van die magma as vasgevangde vloeistof kristalliseer. Daarenteen toon die modellering van die individuele siklusse dat residuele vloeistof ook ontsnap en waarskynlik met oorligende magma meng.

Die vier siklusse, soos teenwoordig in die heelgesteente geochemie, is ook teenwoordig in die heelgesteente en apatiet seldsame aardelementpatrone. Seldsame aard element patrone is grootliks deur modale apatiet en plagioklaas beheer, en tot 'n mindere mate deur normale fraksionering. Metamorfose het geen effek op die seldsame aardelementpatrone nie.

Relatief tot kondrietwaardes, is apatiet tot 1000 keer verryk, veral in die ligte seldsame aardelemente. Alhoewel hierdie tipe verryking tipies is van laat differensiate, toon sekere ligte seldsame aardelementverhoudings dat die magma deur Transvaal sedimente gekontamineer is.

Die spesifieke magma waaruit die Bosone gekristalliseer is kan nie deur middel van seldsame aardelementpatrone geëien word nie. Die byvoeging van 'n minder gefraksioneerde magma en die gevolglike magma vermenging, eeder as 'n nuwe

magma, is beskou as die oorsaak van ritmiese siklusse. Of vermenging die gevolg was van 1) pulse vars magma 2) konveksiestroom omkering of 3) die disintegrering van gestagneerde lae, is nie duidelik nie.

Distribusie koeffisiente is bepaal deur die verhouding van seldsame aardelemente in apatiet tot die in die gasheer heelgesteentes. Hierdie koeffisiente dui aan dat die apatiet wat in die magnetiet-apatietryke sones voorkom onder omstandighede gekristalliseer is, wat die naaste aan ekwilibriumtoestande kom, as in enige ander eenheid. Hierdie feit ondersteun die teorie dat 'n ontmengbare Fe-P_2O_5 smeltsel gevorm is tydens die kristallisasie van die Bosone.

Verskeie vervlegte tweeling-geochemiese tendense wat in stratigrafiese volgorde volg, is in sommige siklusse geidentifiseer en toon dieselfde patroon. Alhoewel hierdie tendense verband hou met normale fraksionering, is die vervlegte tweeling-aard van die tendense toegeskryf aan kristallisering wat alternatiewelik deur aangrensende konveksieselle, in die magma, gedomineer is.

CONTENTS

LIST OF ILLUSTRATIONS

LIST OF TABLES

1 INTRODUCTION

Numerous rare earth and trace element investigations of layered igneous complexes such as the Kiglapait (Morse, 1981; Morse and Nolan, 1985), Skaergaard (Haskin and Haskin, 1968; Paster et al., 1974) and Stillwater (Lambert and Simmons, 1987) exist in the literature. These kinds of investigations are, by and large, aimed at a broad overview of geochemical trends rather than studying detailed variations. From detailed trace element investigations of the Upper Zone of the Bushveld Cawthorn and MacCarthy (1985) conclude that the Upper Zone crystallized from one batch of magma. This is supported by Kruger et al., (1987) who argue on the basis of the Rb/Sr isotopes that the Upper Zone is homogeneous, while Merkle and Von Gruenewaldt (1986) document distinct cycles.

The study of the Upper Zone of the Bushveld Complex provides an ideal opportunity to document geochemical trends and to reconstruct processes during final crystallization of a large layered complex. The aim of the present investigation is to document and interpret the detailed geochemical trends of the rare earth elements during the crystallization of the Upper Zone of the Bushveld.

Three stratigraphic boreholes drilled by the Geological Survey of South Africa on the farm Bierkraal 120 JQ (Fig. 1), referred to as Bk-1, Bk-2 and Bk-3 allowed detailed sampling of the Upper Zone of the western Bushveld. Chemical and modal analyses were done on samples collected by Merkle and Von Gruenewaldt (1986) for their investigation of borehole Bk-1 and on samples from the eastern Bushveld collected by Von Gruenewaldt (1971) for his PhD dissertation.

For the purpose of simplifying the text, several words and geological concepts are abbreviated. Rare earth element is abbreviated as REE, while prefixes such as L, M and H refer to light (La to Nd), medium (Sm to Ho) and heavy (Er to Lu) REEs respectively. Other abbreviations are:

meq	-	milli-mole-Equivalent (charge)
Bk-1	-	Bierkraal 1 borehole
Bk-2	-	Bierkraal 2 borehole
Bk-3	-	Bierkraal 3 borehole
A	-	Apatite as prefix see chapter 7.4
O	-	Olivine as prefix see chapter 7.4
MgN	-	Magnesium number (MgO/MgO + FeO)
Eua	-	Europium anomaly
Kd	-	Distribution coefficient
lld	-	Lower limit of detection
v %	-	Volume percent
( )	-	Refers to relevant sample number. In the case of Bk-1 this refers to the collar depth, eg. (1320) = 1320 m depth.
T	-	Total (used as a prefix to REEs)

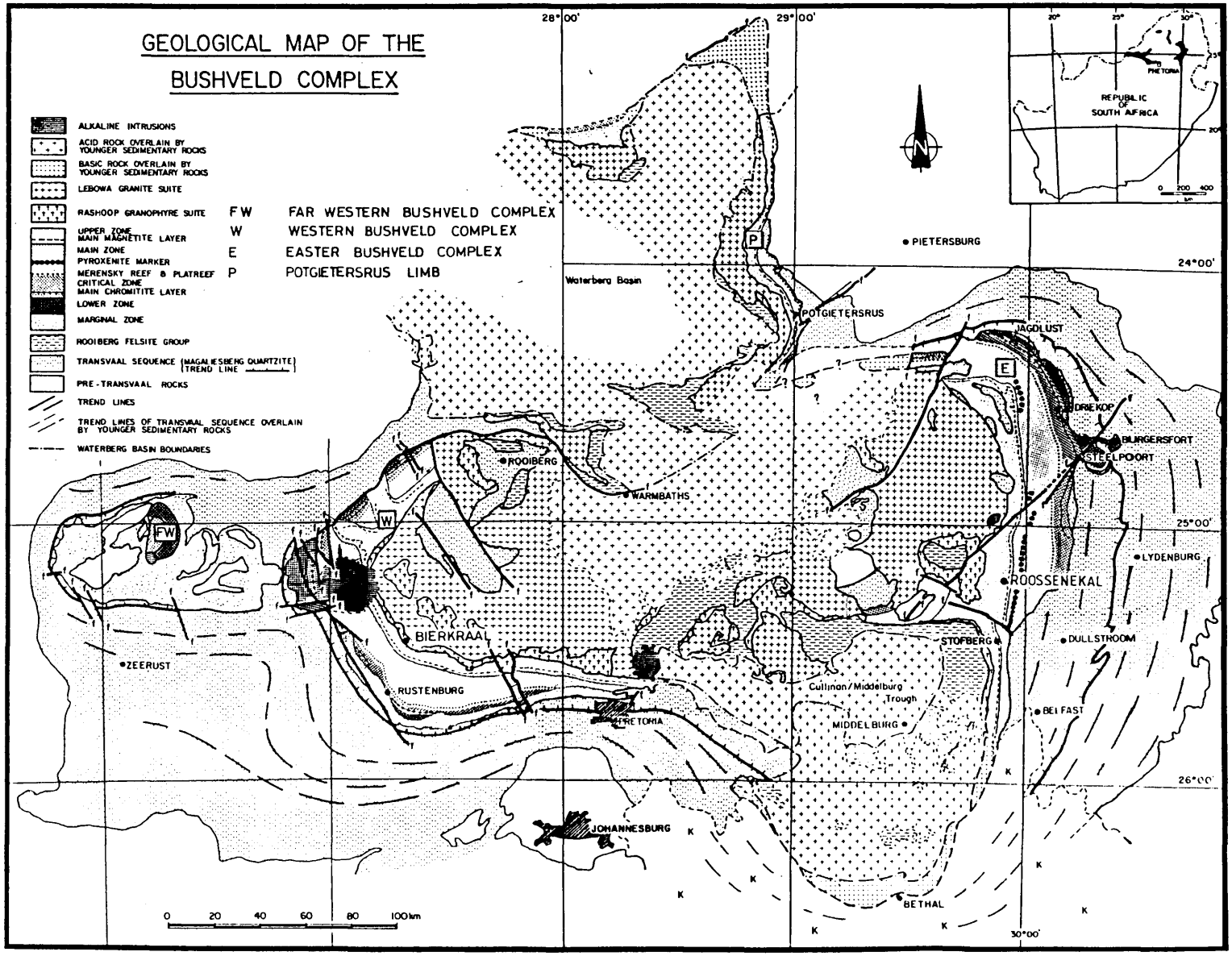

Figure 1: The relative positions of the Bierkraal and Roossenekal sites are plotted on this locatity map of South Africa. The various lobes or compartments of the Bushveld Igneous Complex are also shown.

All other abbreviations in use are strictly according to scientific notation as defined by the Commission on Symbols, Terminology and Units, International Union of Pure and Applied Chemistry, (IUPAC). REE concentration patterns are normalized to the chondrite values reported by Evensen et al. (1978), (Appendix 4), unless otherwise specified.

Where limitations prevented the accurate detection of certain of the REEs, such as Lu, values were estimated by linear interpolation of the chondrite normalized patterns. This technique is employed throughout this text to calculate TREE, LREE, MREE, HREE and REE ratios etc.

The Eu anomaly (Eua) is defined throughout as the analyzed Eu value divided by the value calculated by interpolating the chondrite normalized lines from Sm to Gd.

1.1 Sample Selection

Of the collection of samples taken from the Bk-1 borehole and used by Merkle and Von Gruenewaldt (1986), thirty four samples were selected for mineral separation. These samples are spaced at a maximum of 50 m apart in the sequence, except for the lower 200 m. The Y content of the lower 200 m is low which suggests a relatively low REE content. A further six whole rock samples were selected from the lower 200 m, but no mineral separation was attempted with these six samples. In order to compare the western Bushveld with the eastern Bushveld, twenty two samples were selected from a previous study conducted by Von Gruenewaldt (1971) in the Roossenekal area and kindly made available by him (Appendix 10). The Roossenekal samples are not spaced equally across the stratigraphic interval but, are representative of all the sub-zones of the Upper Zone as defined by Von Gruenewaldt (1971).

All XRF data used in this investigation is that of Merkle and Von Gruenewaldt (1986) and is used here in conjunction with the REE data to interpret the observed geochemical trends. The XRF data of the Bk-1 borehole consists of 139 whole rock major and trace element analyses, and 217 analyses of trace elements alone.

2 SAMPLE PREPARATION

2.1 Mineral Separation

The mineral separation was executed as illustrated in Figure 2 and includes sieving, magnetic separation and density techniques. These techniques are discussed in detail by Hutchison (1974). The product of each step is checked by binocular microscope and, where necessary, hand picking was employed for final cleaning of the concentrates.

The separation procedure was greatly complicated by the abundance of magnetite and ilmenite, as well as ilmenite and magnetite inclusions in the silicates, specifically clinopyroxene. Due to the high magnetic susceptibility and relatively high density of magnetite and ilmenite, neither magnetic nor density separations are very effective when applied to these samples. While the individual silicate phases could not be isolated, apatite, feldspar and zircon were readily concentrated. Apatite often contains biotite inclusions (Von Gruenewaldt, 1971; see also chapter 5.4) and is partially lost during magnetic separation. The separation of pyroxene and biotite was abandoned due to ineffective concentration.

2.2 Rare Earth Element Analysis

The analytical procedure for the REE applied in this study is similar to that used by Robinson et al. (1986). The samples were decomposed, the REEs concentrated by a cation exchange procedure, and finally adsorbed on cation exchange loaded paper prior to analysis by XRF spectrometry. The cation exchange column and decomposition procedures were modified to facilitate a less complex and time consuming process. Analytical grade reagent and de-ionised water was used throughout the procedure.

2.2.1 Dissolution Procedure

Major elements, and in particular silicon, were not determined and an open vessel, low temperature hydrofluoric-perchloric acid dissolution technique was employed. Sodium peroxide fusion techniques were applied where required (Appendix 1).

2.2.2 Cation Exchange Procedure

The purpose of the cation exchange procedure is to concentrate the REEs and to remove any elements that might interfered spectrographically during XRF analysis. For this purpose 10 g (dry) Bio-Rad AG50W-X8, 200 - 400 mesh polystyrene resin was used. The final sample preparation for XRF analysis was to absorb the REE concentrate onto cation exchange paper. See Appendix 2 for a complete description of the method.

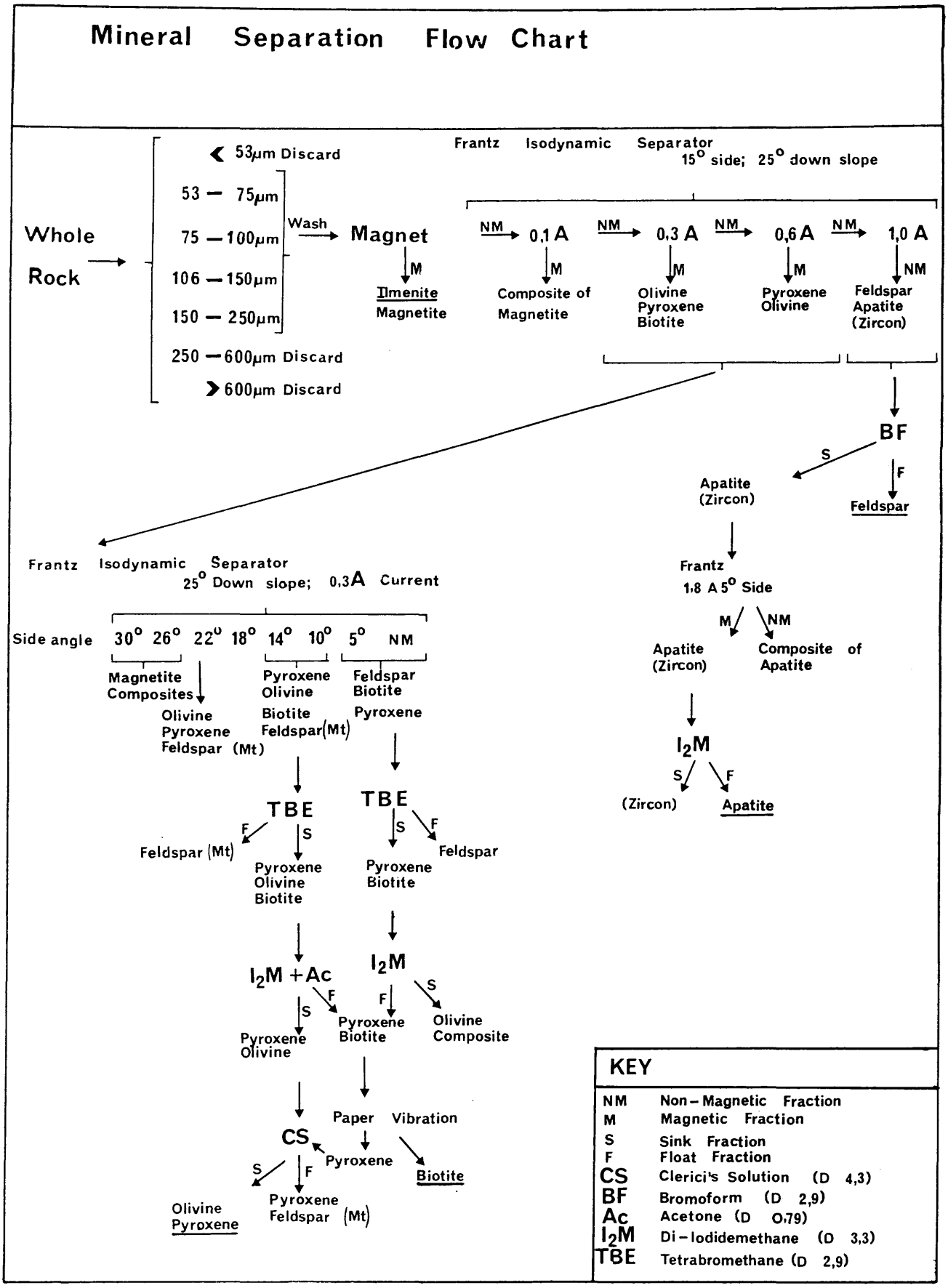

Figure 2: Mineral separation flow chart. The underlined minerals refer to the dominant mineral phase separated. Note that pyroxene cannot be concentrated effectively. Biotite can be concentrated but, the procedure is extemely time consuming.

2.2.3 Discussion

The hydrofluoric-perchloric acid dissolution procedure was used for the magnetite gabbro, feldspar, biotite, pyroxene and apatite samples, but fusion was necessary for some of the gabbro samples containing zircon. For the dissolution of the apatite samples, hydrofluoric acid was not required and was omitted from the procedure.

The major problem during dissolution was a precipitate which forms during the treatment of samples containing a high concentrate of both phosphorous and titanium. A sodium peroxide fusion was effective for decomposing the precipitate but, the precipitation often re-occurs when the sinter was combined with the original sample solution. When this occurred, these samples were discarded as a major percentage of the REEs can be lost due to co-precipitation (Reeves and Brooks, 1978).

The column cation exchange procedure consists of adsorbing the sample on to the column using a 200 ml 0,1 M HCl solution. Selective leaching was achieved with 130 ml 0,1 M HCl 90 % acetone and 220 ml 2 M HNO_3 solutions. The final extraction of the REEs from the column was achieved by leaching with a 300 ml 5 M HCl solution (see Appendix 2A and Fig. 3).

The column cation exchange procedure effectively concentrates the REEs in all the samples. Due to the high proportion of aluminium in the feldspar and gabbro samples, the aluminium could not be completely separated from the REEs using this method. The final 20 ml aliquot of the 220 ml nitric acid eluent was monitored in the case of the whole rock samples by AA spectroscopy, which indicated a maximum absolute aluminium content of 250 milli mole equivalent charge (meq). Such low values would neither overload the cation exchange loaded filter paper (Appendix 2), nor would the absorption of the REEs be affected. The same order of magnitude aluminium levels could be expected for the feldspar samples but this was not the case. Extensive overloading of the cation exchange loaded paper occurred (Fig. 3).

Six random feldspar samples were selected and their final 300 ml aliquots containing the REEs were analyzed for aluminium by Atomic Absorption Spectrometry (AAS). Five samples contained between 50-100 ppm aluminium (in total 1700-3300 milli-mole equivalent charge), while the sixth contained an exceptional 175 ppm (in total 5800 milli-mole equivalent charge) aluminium. The latter exception could possibly have been due to an operator error in confusing the nitric and hydrochloric acid concentrate reagents during eluting (see Strelow, 1960).

A synthetic feldspar solution was prepared to determine the reason for the large aluminium content in the final aliquot, and the elution of aluminium was monitored by AAS (Fig. 3). This figure shows that large quantities of aluminium was included in the final aliquot as a direct result of the column conditions.

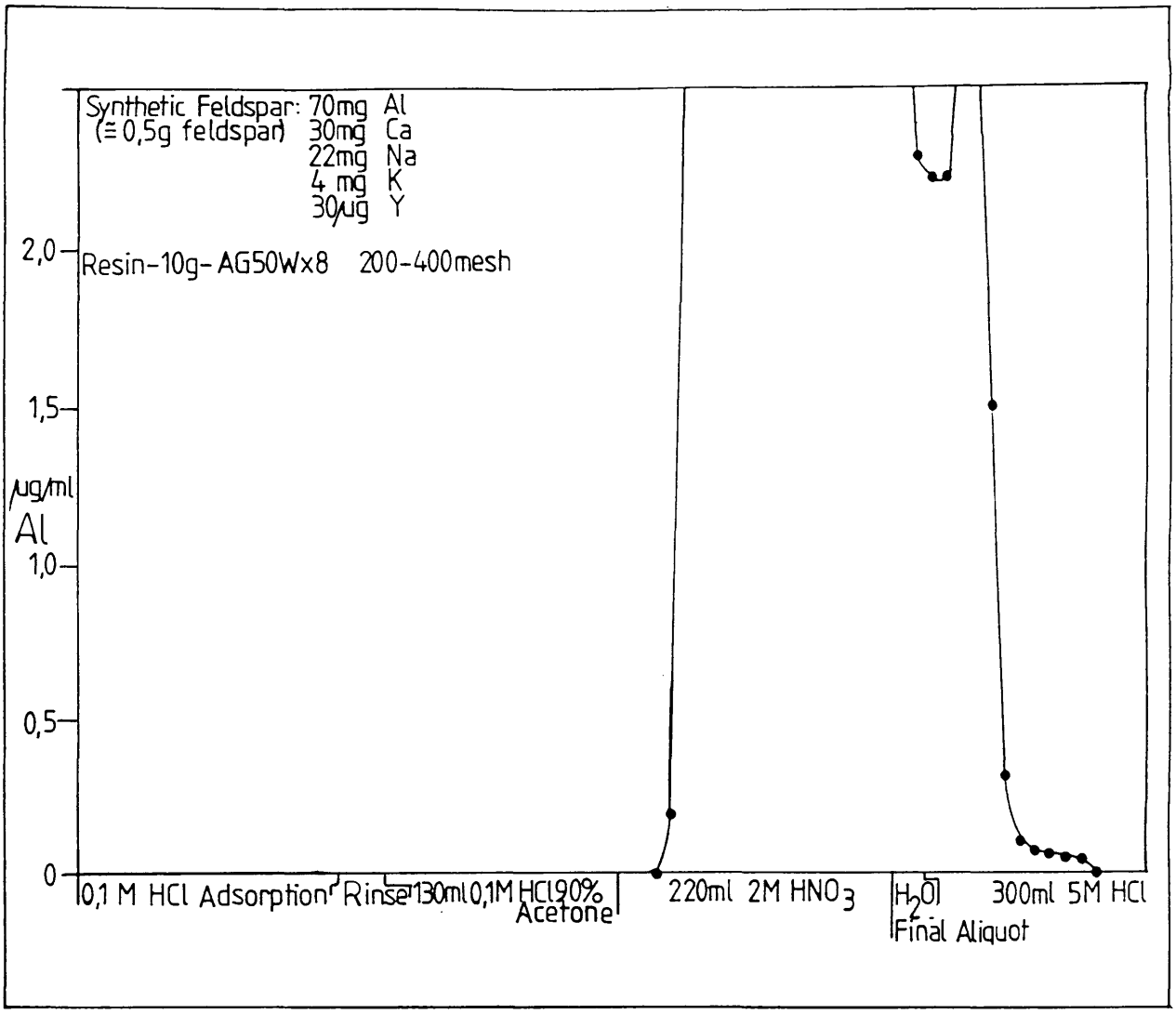

Figure 3: Elution curve of aluminium. This figure illustrates the concentration and leaching of aluminium from the cation exchange column. The final aliquot is absorbed onto the cation loaded filter paper. The excessive aluminium can exceed the capacity of the cation loaded filter paper and lead to the partial loss of the REEs when feldspar samples are prepared.

The cation exchange column procedure used in this investigation is considered insufficiently effective in the separation of the aluminium from the REEs for the feldspar samples. The procedure is satisfactory for the whole rock samples. This can be explained by the shift of the aluminium elution peak, or increased tailing with increasing deviation from equilibrium conditions (Strelow, 1973). This implies that the aluminium can be separated from the REEs by increasing the column size, or by developing a different elution procedure which will leach the aluminium more readily from the column.

2.2.4 Alternative Column Procedures

The absorption of the sample on the column in an oxalic-hydrochloric acid solution will allow a large proportion of aluminium to be leached as an anionic species (Strelow, et al., 1969; Strelow and Van der Walt, 1984). The REEs will form lower charged cation complexes in this medium and can be partially leached (Strelow pers. commun.; see also Cantrell and Bryne, 1987). Alternatively an anion exchange column using the same eluent will absorb the aluminium (Strelow et al., 1969), allowing the REEs to be leached. The REEs can then be separated from the other major cations by standard cation exchange procedure. The difficulty with this approach is that the REEs precipitates in an excess oxalic acid medium (Schoeller and Powell, 1985) and such an approach will have to be further investigated before such a technique can be recommended.

Alternatively, the REEs can be precipitated by an excess of oxalic acid prior to absorption on to the column, the precipitate filtered off and ignited to obtain the oxides (Schoeller and Powell, 1985). The oxides can then be re-dissolved in hydrochloric acid and absorbed on to a smaller cation exchange column, which will separate the REEs from the co-precipitates such as calcium and thorium. Other co-precipitants that can be considered for precipitation procedures are: aluminium hydroxide, calcium fluoride and lanthanum 8-hydroxyquinoline (Reeves and Brooks, 1978). This approach can greatly simplify the column procedure but the manipulation of a precipitate is not practical and is avoided.

2.2.5 Complications of the Cation Exchange Procedure

An excess of aluminium will not necessarily prevent the absorption of the REEs into the paper since the REEs affinity for the strongly acidic type resin of the paper in 0,1 M HCl is far greater than that of aluminium (Strelow, 1960). The REEs will replace the aluminium on the resin of the paper during lengthy absorption periods. To encourage this replacement, a 3 day absorption period was used while preparing the plagioclase samples. Using an AAS, the Y content of synthetic feldspar solution was determined after this absorption period. Traces of Y were still present in solution, which indicates that the REE replacement of the aluminium was not complete.

Additional difficulties occurred during the procedure used in this study when samples rich in zirconium and hafnium were re-dissolved after drying on the water bath. The zirconium and hafnium did not readily re-dissolve in hydrochloric acid during this step and hydrofluoric acid digestion was necessary to re-dissolve these elements. Since zirconium and hafnium were not to be determined, this difficulty could have been averted by absorbing such samples onto the column as a tartaric-nitric acid solution (Strelow and Van der Walt, 1982), thus allowing the zirconium and hafnium to be partially leach during the absorption step.

Effective concentration of the REEs, using an ion exchange column, can only be achieved by considering each type of sample independently through examination of its composition and relative concentrations of its constituent elements. This does not only apply to the dissolution technique, but also to the column procedure.

2.2.6 X-Ray Fluorescence Spectroscopy (XRF)

Extensive effort and time was spent in investigating a thin film XRF analysis technique for the determination of REEs (Appendix 3). It was found to be a feasible technique, but the time required to calibrate the XRF was too prohibitive for the purposes of this study. The samples were finally analyzed by inductively coupled plasma-atomic emmission spectroscopy (ICP-AES).

2.3 Inductively Coupled Plasma-atomic Emmision Spectroscopy, (ICP-AES)

The instrumentation for the analysis of the samples was the ICP-AES housed at the University of Stellenbosch and the instrument procedure was the same as that used routinely in that laboratory (Cornell et al., 1988). The samples were leached from the Whatman SA-2 resin loaded paper and prepared as a 5 ml, 4 M HCl solution.

2.3.1 Leaching

Several semi-quantative experiments were run to determine the most efficient method of sample extraction from the Whatman SA-2 paper. These experiments consist of soaking the paper disc in 10 ml 4 M HCl solution and decanting the acid at 10 minute, 30 minute and 4 hour intervals. The results of the tests for various REEs are illustrated in Figure 4. Based on these results, the paper samples were soaked for 1 hour in 10 ml 4 M HCl and the acid decanted. The discs were then soaked in 10 ml 4 M HCl for 30 minutes and the acid decanted. The 30 minute soaking procedure was repeated three times and all aliquots combined.

The paper samples partially decomposed during the leaching process and the solution was filtered before bringing it to dryness over a hot plate. The samples were then dissolved in 5 ml 4 M HCl and filtered once more before ICP-AES analysis.

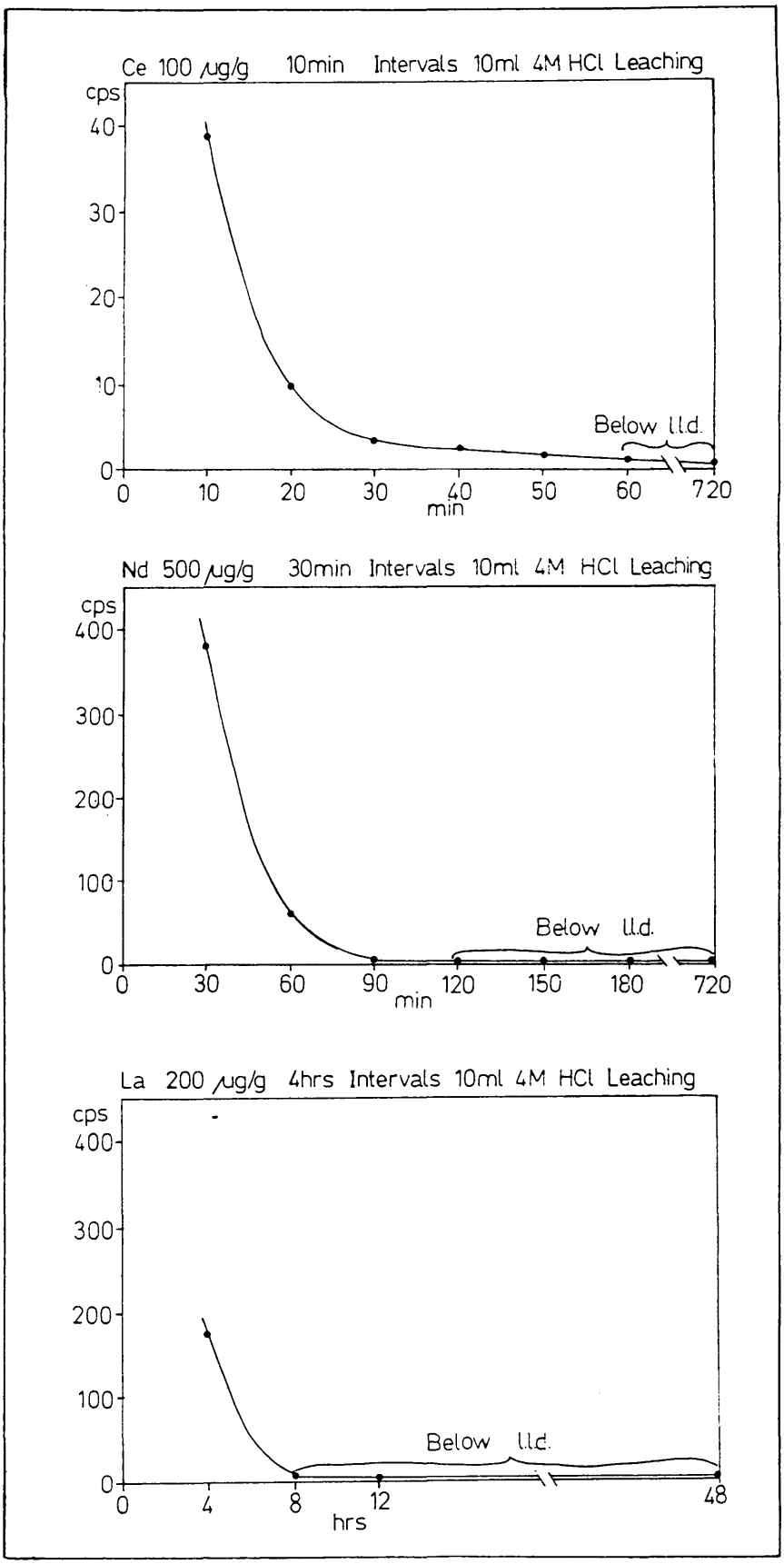

Figure 4: Leaching of the Whatman SA-2 paper in preparation for ICP-AES analysis. The plots illustrate the concentration of Ce, Nd and La in the leached solution (expressed in counts per second by ICP-AES analysis) as a function of time.

2.3.2 ICP-AES Analysis

Samples were analyzed by using a Philips inductively coupled plasma source with an RSV optical spectrometer which had been modified to count sixteen channels simultaneously. Groups of three samples and standards were aspirated with multi-element drift correction references and a spectrometric blank before and after each group. Standards are prepared from dried spectropure oxides.

Each element was corrected for peak and blank drift. Interference corrections were made for inter-analyte line overlaps and for Ca, Fe and Th. Batch blanks were monitored, but found to be below lower limits of detection.

2.4 Accuracy

The accuracy of the ICP-AES technique, was tested by analyzing two geological reference materials: NIM L, a zircon containing granite and Sy 3, a syenite. The standards were included in the first batch of samples prepared (Appendix 11).

Compared to the accepted values for NIM L and Sy 3 (Jackson and Strelow, 1975), (Abbey, 1983) the results obtained in this investigation are slightly depressed. The major element matrix of the geo-standards differ greatly from the apatite samples. Several apatite samples which were analyzed by neutron activation analysis (Von Gruenewaldt, unpublished data) are included as an appropriate accuracy check in the investigation (Table 1). The REE concentrations obtained by these two methods compare very well and are largely within the expected statistical standard deviation (approximately 10 percent). Two Nd values as determined by the ICP-AES seem high but are just within the 3σ range assuming a standard deviation of 10 percent for the neutron activation analysis. The ICP-AES Gd values are also consistently higher than indicated by the neutron activation analysis. This systematic error seems to be related to the relatively high lower limit of detection of the neutron activation analysis technique for Gd.

The results of the geo-standards are lower than the accepted values but have trends that are parallel (Fig. 5, Appendix 11). The concentrations found in the two geo-standards are systematically lower which exclude the possibility that a REE rich mineral (such as zircon) was incompletely dissolved. The presence of such an undissolved or partially dissolved mineral will, because of its preferential incorporation of specific REEs, alter the REE pattern of the standards and therefore result in a non-parallel deviation.

The apatite ICP results on the other hand are within the 2σ statistical error range of the neutron activation analysis. The depressed values obtained for the geo-standards cannot be ascribed to the incorrect calibration of the ICP-AES technique, but is rather a function of major element matrix compositional contrasts. Since the apatite and the geo-standards differ significantly in composition it follows that the samples behave differently during the absorption of the sample solutions on to the cation exchange paper and the cation exchange column. Strelow (pers. commun.) points out that cation columns respond under equilibrium conditions only if 10 percent or less of its carrying capacity is used. This level is exceeded in the

Table 1:
Comparison of Rare Earth Analisies of apatite by neutron activation analysis (NAA) and induced coulped plasma (ICP)

Analysis	NAA	ICP	NAA	ICP	NAA	ICP	NAA	ICP	NAA	ICP
Sample Number	G208/eb4d		G253/eb7d		G271/eb11d		G257/eb9d		G264/G264	
La	1008	904	653	569	252	269	209	186	318	289
Ce	1780	1597	1048	936	502	516	295	379	595	531
Pr	N.D.	248	N.D.	144	N.D.	91	N.D.	71	N.D.	88
Nd	1040	1016	360	589	284	417	340	344	380	386
Pm	--	--	--	--	--	--	--	--	--	--
Sm	225	187	93	110	95	83	86	72	77	74
Eu	19	16	23	20	18	21	22	26	22	16
Gd	<50	178	<50	108	<50	83	<50	74	<50	75
Tb	26	N.D.	21	N.D.	18	N.D.	14	N.D.	13	N.D.
Dy	179	157	110	94	44	67	121	60	64	64
Ho	N.D.	29	N.D.	17	N.D.	12	N.D.	11	N.D.	12
Er	N.D.	74	N.D.	46	N.D.	30	N.D.	27	N.D.	30
Tm	N.D.	N.D.	N.D.	N.D.	N.D.	N.D.	N.D.	N.D.	N.D.	N.D.
Yb	43	39	27	27	13	16	16	16	12	16
Lu	4.9	N.D.	2.1	N.D.	3.7	N.D.	2.1	N.D.	1.0	N.D.

All values given in ppm
N.D. Not determined

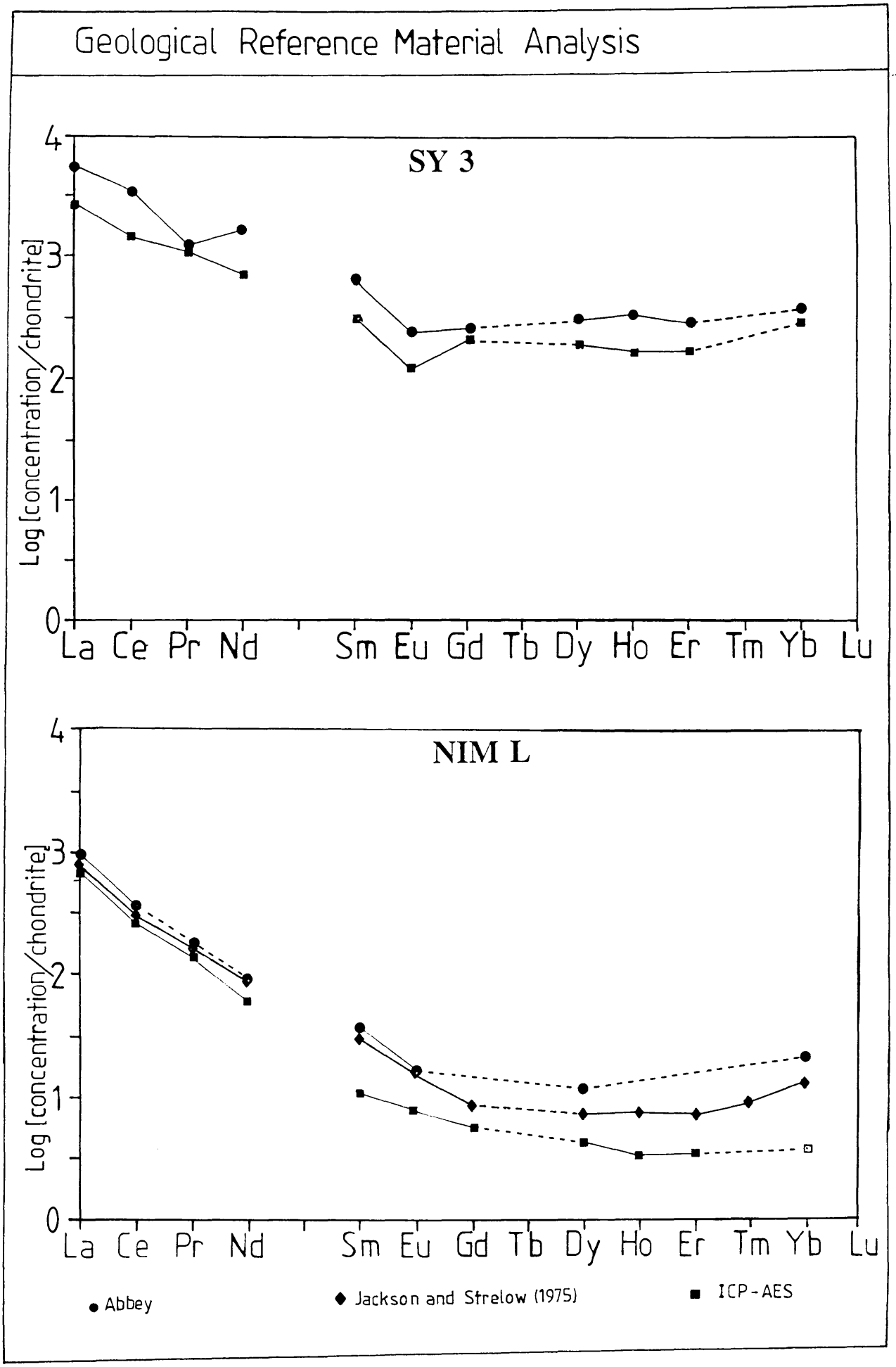

Figure 5: Analytical results of geological reference materials. Note that the analyzed ICP-AES values are depressed but parallel to the accepted values.

very first absorption step of the whole rock REE analysis and can possibly contribute to the partial loss of the REEs. This possibility is investigated while setting up the column procedure. A partial loss can be below the detection limit of the AAS technique which is applied to check the elution procedure of the columns.

A further difficulty of the geo-standards is that they are exceptionally difficult to redissolve after the REE concentrate is dried (Appendix 1). This can be ascribed to the presence of copious zircon (especially NIM L) and aluminium (especially Sy 3) which oxidizes during the complete evaporation step. This results in the formation of insoluble oxides and the co-precipitation and incorporation of some of the REEs. This co-precipitation then leads to the partial loss of the REEs and causes the depressed values.

It is concluded that the results of apatite REE analysis are fully quantitative while the whole rock samples can be seen as semi-quantitative. A complete list of the results is reproduced in Appendix 4.

3 PETROGRAPHY

3.1 Comparison of the Eastern and Western Bushveld Complex

3.1.1 The Eastern Bushveld

The excellent exposure of the Upper Zone in the eastern Bushveld permits the thorough description and investigation of the rock units. Molyneux (1970) and Von Gruenewaldt (1971; 1973) subdivide the eastern Bushveld Upper Zone into four subzones (Fig 6), whilst SACS (1980) subsequently only recognizes three subdivisions of the Upper Zone in the eastern Bushveld (Fig. 6).

The base of subzone A of the Upper Zone is defined where cumulus magnetite first appears in the sequence, usually in an anorthosite. Subzone A consists typically of magnetite gabbro with lesser olivine gabbro, mottled anorthosite and lower magnetitite layers 1 to 3. Some of the mottled anorthosite layers contain disseminated sulphides.

The Main Magnetite Layer is taken as the base of subzone B. Subzone B consists mainly of magnetite gabbros with a thin layer of feldspathic pyroxenite, mottled anorthosite and magnetitite layers 1 to 7.

Subzone C consists of olivine gabbro alternating with magnetite gabbro, anorthosite and troctolite. Magnetitite layers 8 to 14 occur in this subzone.

Subzone D is characterized by an abundance of olivine and apatite bearing cumulates as well as magnetite gabbro and anorthositic diorite. Diorite is limited to the uppermost part of the subzone D. Magnetitite layer 21 is typically, well developed in the eastern Bushveld. This layer and the nature of other magnetitite layers is discussed in detail by Molyneux (1970) and Von Gruenewaldt (1971).

3.1.2 Western Bushveld

The outcrop of the Upper Zone of the western Bushveld is generally poor and three deep stratigraphic boreholes have therefore been drilled in the Bierkraal area by the Geological Survey of South Africa. They are referred to as the Bk-1, Bk-2 and Bk-3 boreholes. The extent to which these boreholes are representative of the Upper Zone in this area is unclear due to the lack of marker horizons and difficulties in the correlation with the eastern Bushveld. The Bk-2 borehole seems to penetrate the pyroxenite marker (Fig. 7) (Walraven and Wolmarans, 1979).

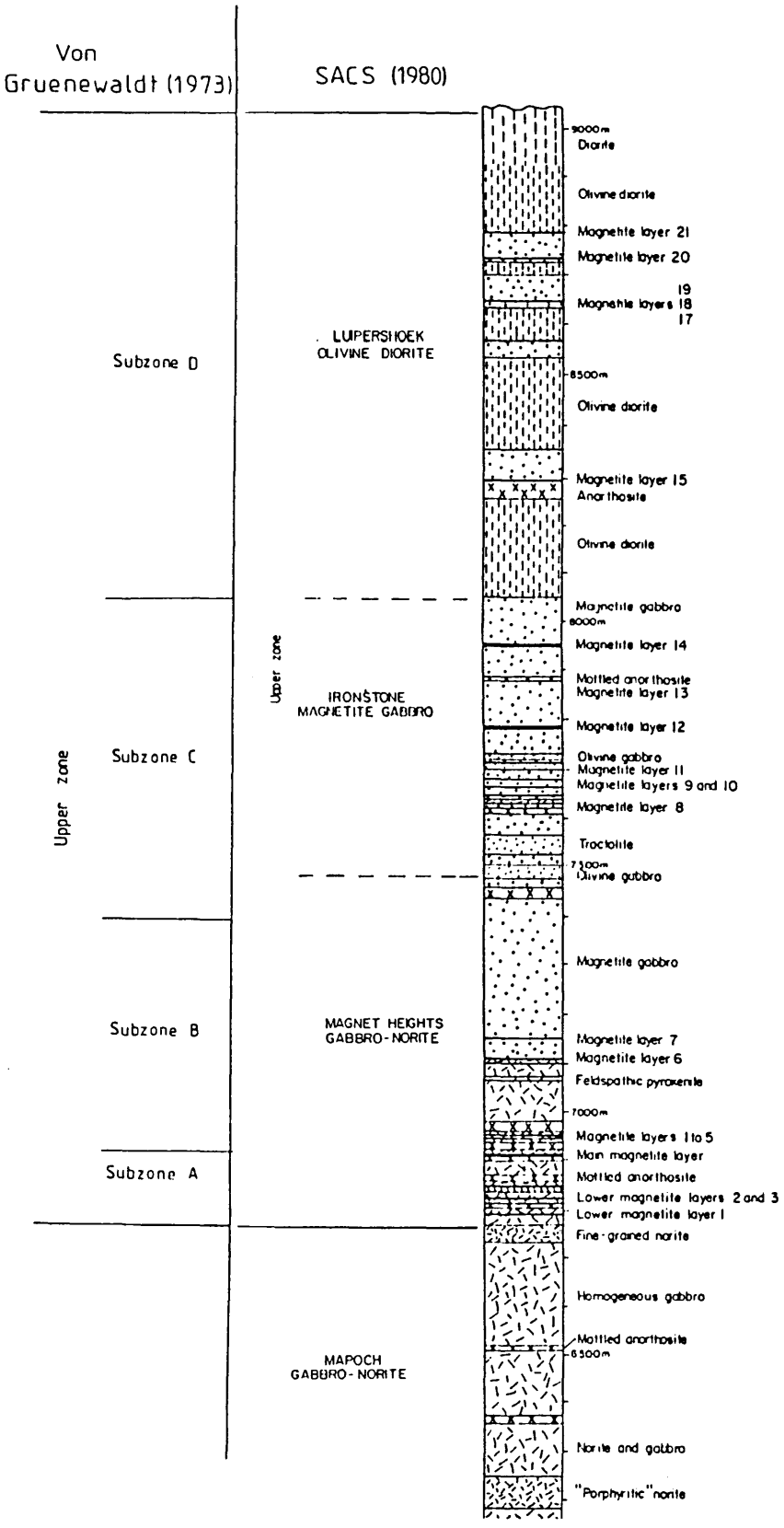

Figure 6: Stratigraphic comparison of the subzones as defined by Von Gruenewaldt (1970, 1971) and by SACS (1980).

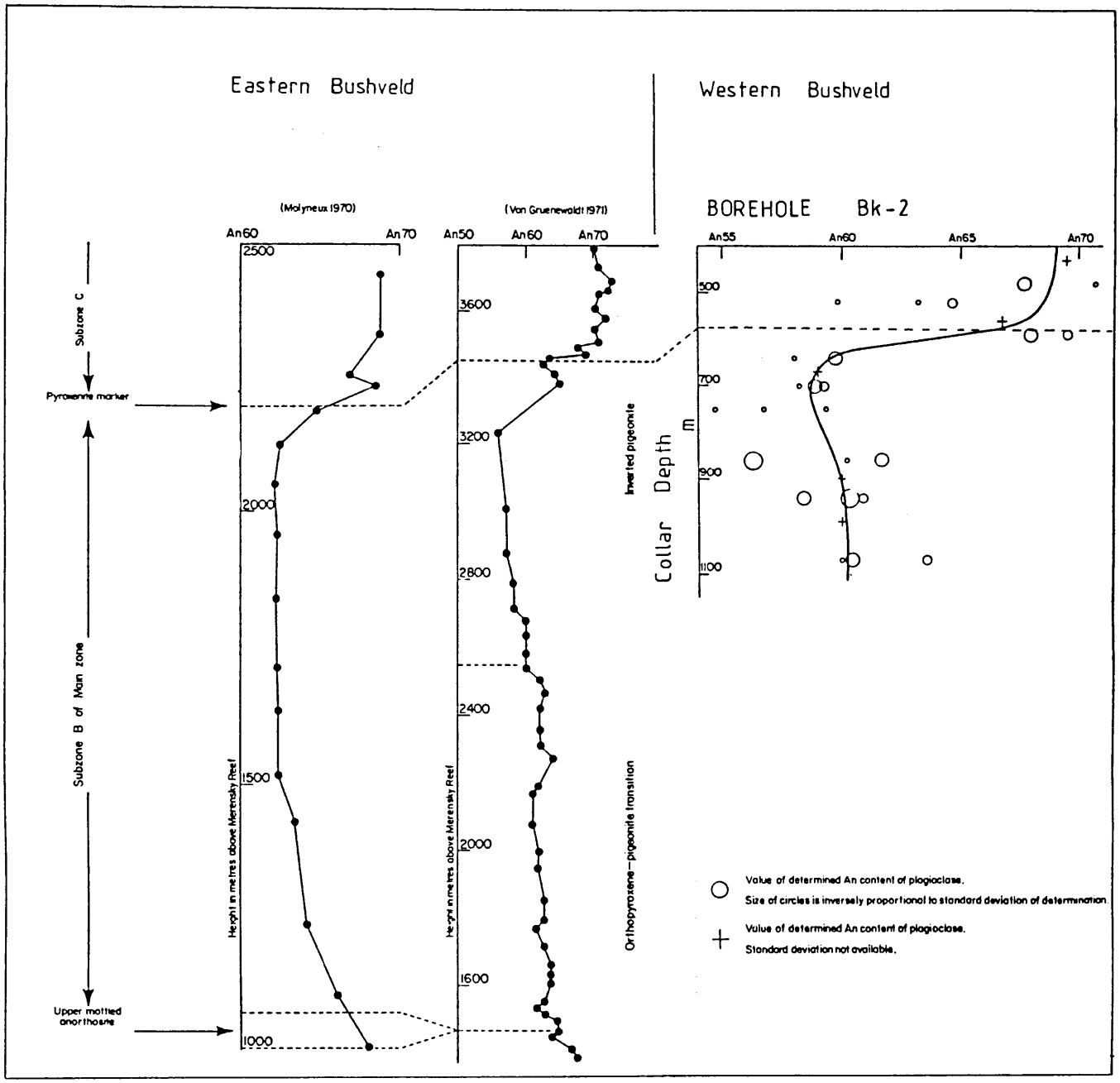

Figure 7: Stratigraphic comparison of the variation in plagioclase composition. The change in plagioclase composition in Bk-2 of the western Bushveld is compared to similar variations across the pyroxenite marker in the eastern Bushveld. The figure is adapted from Walraven and Wolmarans (1979).

The present investigation of the Upper Zone is confined to the uppermost 1200 m intersected by borehole Bk-1. The stratigraphic succession consists mainly of olivine gabbro and lesser magnetite gabbro, while a ferrodiorite tops the column (Fig. 8). A major magnetitite layer at a collar depth of 1 450 m is associated with prominent anorthosite layers on either side of the magnetite. Below this, two more prominent layers are present, both are associated with magnetite gabbro and anorthosite (Fig. 8). A further 12 minor magnetitite layers, usually associated with magnetite gabbro or anorthosite, occur in the sequence.

3.1.3 Comparison of Eastern and Western Bushveld Upper Zone

The sequence of lithologies in the Upper Zone in the eastern and the western Bushveld is similar though, the correlation of individual layers is not possible. Olivine is present throughout the stratigraphy of borehole Bk-1 (Merkle and Von Gruenewaldt, 1986). The well developed magnetitite layer found at collar depth +- 1 471 m to 1 494 m in borehole Bk-1 is, on grounds of apatite and titanomagnetite content, correlated with magnetitite layer 21 of the eastern Bushveld by Reynolds (1985). The magnetitite layer 21 in the eastern Bushveld is approximately 500 m below the roof contact (Von Gruenewaldt, 1971). Assuming that the magnetitite layer 21 is at the same relative stratigraphic height in both lobes of the Bushveld complex, it implies that the Upper Zone in the western Bushveld is at least twice as thick as in the eastern Bushveld.

Walraven and Wolmarans (1979) document a sharp increase in An content of plagioclase within gabbronorites of the Main Zone at a depth of 600 m in the Bk-2 borehole. This inflection is correlated with a similar change in plagioclase composition found across the pyroxenite marker in the eastern Bushveld (Fig. 7).

4. MODAL COMPOSITIONS AND CIPW NORMS

Borehole Bk-1 intersects a thick sequence of relatively monotonous olivine-magnetite gabbro. Borehole logs show that the sequence is interlayered with comparatively thin layers of magnetitite, anorthosite and overlain by olivine diorite at the top of the Upper Zone. The purpose of modal analysis is to determine whether mineralogical trends exist in the sequence. Modal analyses are needed to calculate certain distribution coefficients and to determine theoretical trends of element compatibility.

Modal proportions of the 45 samples chosen for whole rock REE analysis, were determined by using a Swift Automatic Point Counter with a fixed grid in the microscope ocular (Fig. 8). A minimum of 1 900 points were counted per thin section using transmitted light to distinguish the silicates, apatite and ore. Ore minerals were distinguised by using oil immersion reflected light microscopy. Four thousand points were counted on each section. The results given in terms of magnetite, ilmenite and sulphide are plotted in Fig. 8. Where magnetite-ilmentite intergrowths proved too fine for point counting, a visual estimate of proportions was applied to the point counting. The trace minerals such as K-feldspar, zircon and quartz were not counted.

Whole rock analyses from Merkle and Von Gruenewaldt (1986) were used to calculate CIPW norms. Samples containing more than approximately 30 % FeO are nepheline normative. To enable comparison with modal trends, nepheline is recalculated to albite regardless of SiO_2 deficiency and the norm normalized to one hundred percent. The modal and normative trends (Fig. 8) are broadly similar (Fig. 9) although, the normative and modal concentrations of individual minerals do not compare well (Fig. 10A to 10G).

The poor correlation of CIPW norms and modal analyses seems to be related to the limitations of CIPW norms. CIPW calculations work with end-member compositions such as albite, anorthite and hypersthene etc.. Discrepancies related to such end-member compositions arose in the proportions of magnetite and ilmenite. The natural magnetite contains fine exsolutions of ulvospinel while the CIPW norm only calculates pure magnetite and ilmenite and this leads to a gross over calculation of ilmenite.

Less significant discrepancies arise due to textural features. Magnetite-ilmenite exsolutions in clinopyroxene are taken as part of the modal pyroxene. The CIPW norm does not make provision for hornblende and its presence leads to several norm calculations having anomalously high clinopyroxene values when compared to modal proportions (Fig. 10F).

4.1 Plagioclase

Plagioclase is by far the most important component of the gabbroic rocks in borehole Bk-1 and generally varies from 50 to 70 v %. A maximum of 87 v % plagioclase is found in anorthosite (1 508.6) while less than 3 percent total silicates (1 466.6) is found in a typical magnetitite layer.

BIERKRAAL 1

Modal Analysis (V %)

C I P W Norm

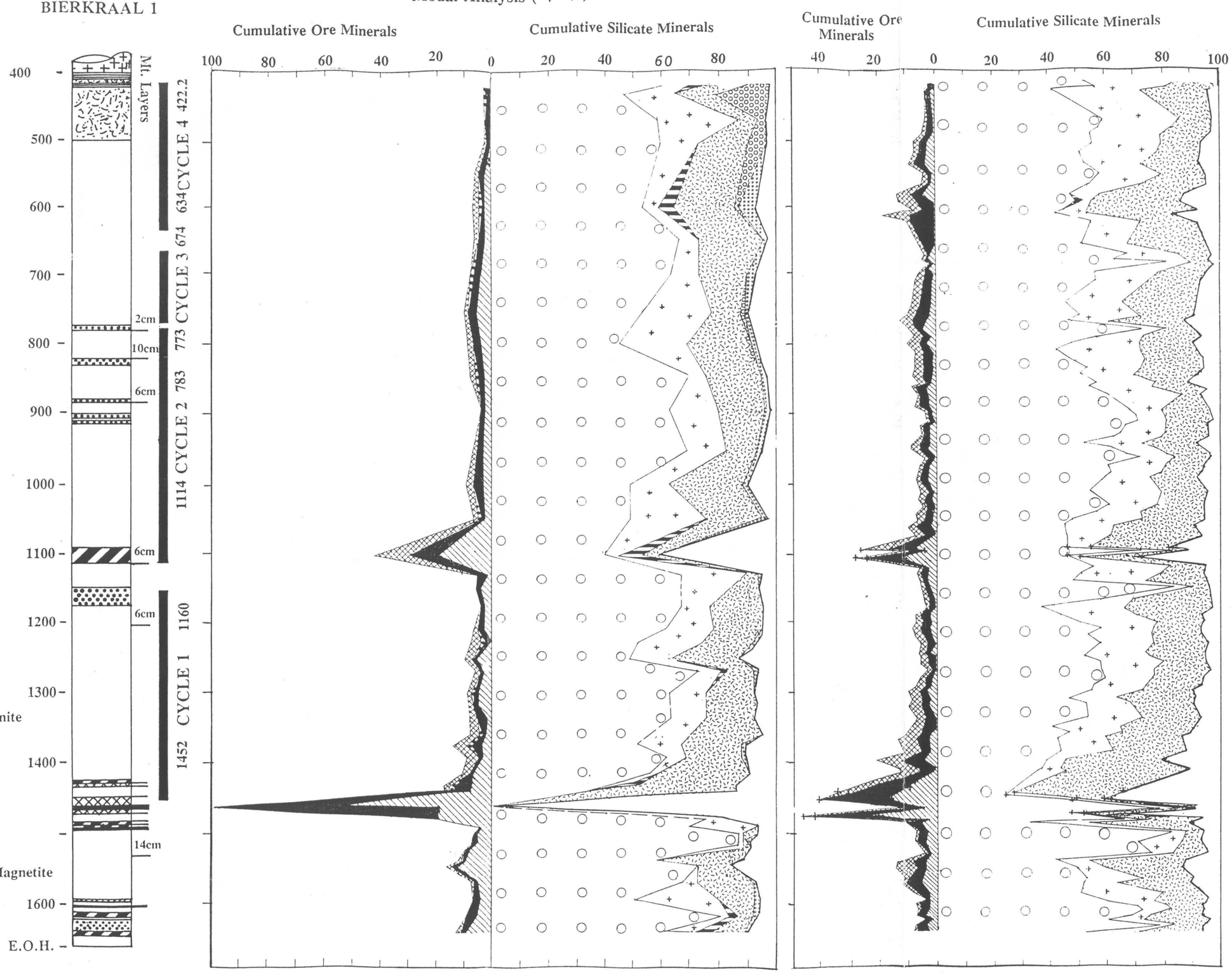

Figure 8: Modal analysis determined by point counting.

Figure 9: CIPW norms calculated from XRF data given in Appendix 8A.

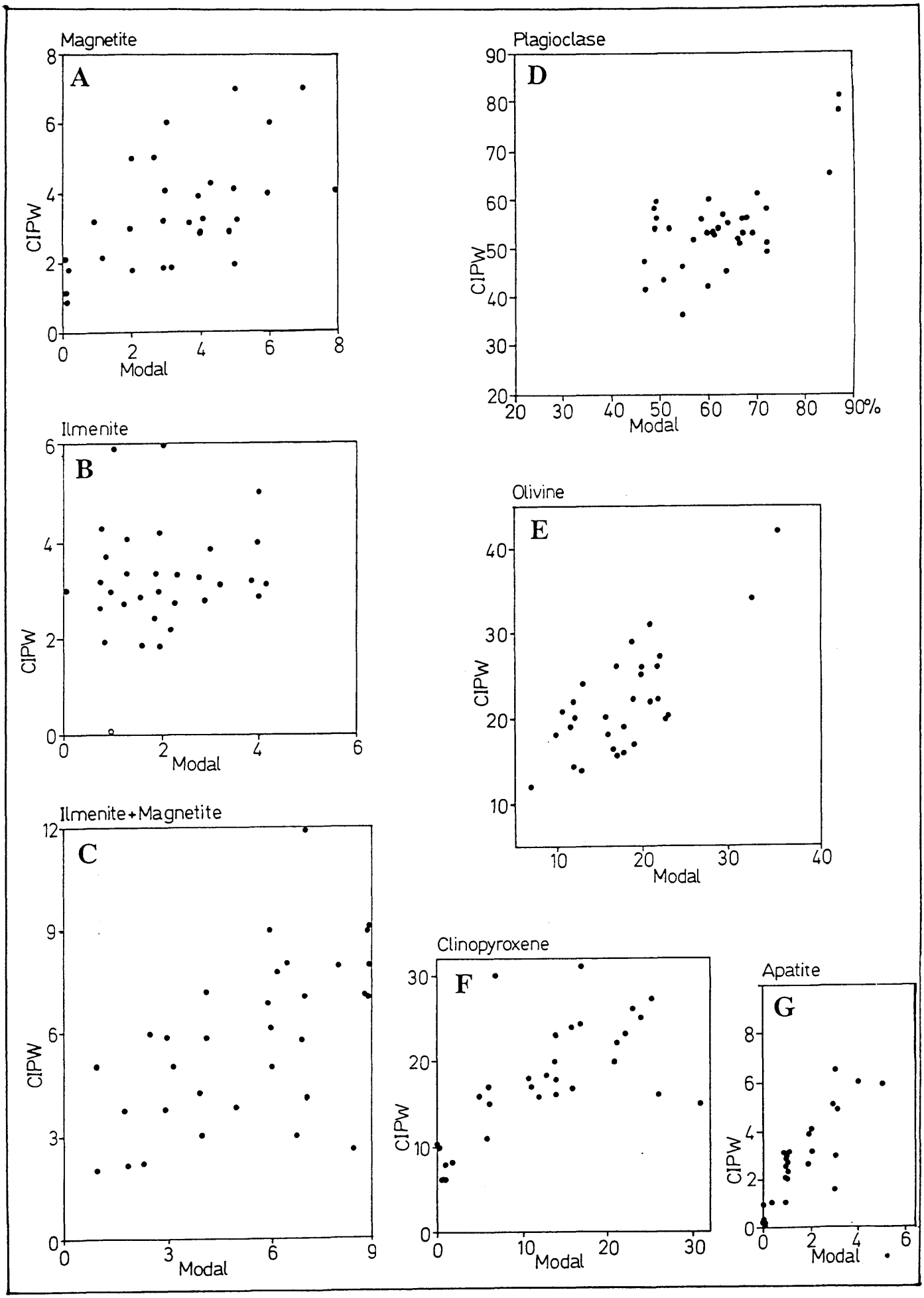

Figure 10: Comparison of modal and normative proportions in volume percent.

4.2 Olivine

Olivine is a major constituent of the silicates of Bk-1 with the exception of anorthosite which only contains trace amounts (1 486.7 and 1 498.7). The olivine content ranges from 15 to 30 percent for most of the borehole, while olivine-rich layers, containing up to 53 percent (1 447.3) are present. Unlike the Roossenekal section (Von Gruenewaldt, 1973), olivine is present directly below the roof contact in borehole Bk-1.

4.3 Pyroxene

The modal proportions of pyroxene was determined as ortho- and clino- pyroxene. Inverted pigeonite was included into the clinopyroxene group. Clinopyroxene predominates with only isolated samples containing more than 1 v % orthopyroxene (423, 601.5, 1 178.2, 1 270.4, 1 439, 1 508.4, 1 627.5, 1 649.8). Sample 1 100.8 is an exception in that it contains an unusual 10 v % orthopyroxene. Clinopyroxene is the most abundant ferromagnesian mineral in the Upper Zone of the eastern Bushveld (Von Gruenewaldt, 1973). In contrast, the olivine content of borehole Bk-1 from the western Bushveld rivals that of clinopyroxene.

4.4 Hornblende

Hornblende consistently comprises more than one v % of the diorite in the uppermost 180 m but can be as high as 20 v % (433). Traces of hornblende are present throughout the entire borehole.

4.5 Magnetite and Ilmenite

The magnetite content of the gabbro units of borehole Bk-1 is below 7 v %. The uppermost 350 m exhibits a steady decrease in magnetite content and ilmenite becomes dominant near the roof contact. Prominent magnetitite layers are often overlain by magnetite gabbro, with the upper contact of the magnetitite layers often gradational, as found in the eastern Bushveld (Von Gruenewaldt, 1973). Magnetite and ilmenite vary sympathetically throughout most of the borehole.

4.6 Apatite

Euhedral apatite crystals occur throughout borehole Bk-1 except for two intervals, from 1 465.5 to 1 530.8, and from 1 580 to 1 627.5 at the lower end of the borehole. The highest apatite concentrations are associated with magnetite rich horizons, where the highest content of 13 v % (1 100.8) occurs in a magnetite gabbro. This is similar to the situation in the Roossenekal district where the highest recorded apatite concentration of 8.5 v % is found immediately above magnetitite layer 21. Grades of apatite, as high as 10 v % over intervals of up to 40 m, are found in the Upper Zone (Von Gruenewaldt, 1994). The average apatite content in Bk-1 is below 3 v %.

4.7 Accessory Minerals

Biotite is the most common accessory mineral, often exceeding 1 v %. Modal proportions are not determined for the accessory minerals such as K- feldspar, quartz and zircon. Mineral separation indicates that they are only significant in the uppermost part of the borehole. Zircon for instance only appears in the apatite concentrate from the upper 130 m (Fig. 2).

5 MINERAL COMPOSITIONAL TRENDS

5.1 Oxides

The bulk TiO_2 content in the magnetitite layers increases from approximately 12 % at the base of the Upper Zone to approximately 20 % in the upper parts of the sequence (Von Gruenewaldt, 1971). Vanadium exhibits the opposite trend and decreases from approximately 2 % to 0.2 % toward the roof. Similar trends apply to magnetitite layers intersected in borehole Bk-1 (Reynolds, 1985b). The Al_2O_3 and Cr_2O_3 content of magnetite is low and variable, and no systematic trend was detected. Ilmenite shows little compositional change and has a composition close to that of end-member ilmenite (Reynolds, 1985b).

The Cr_2O_3 content of closely spaced samples across individual magnetitite layers of the eastern Bushveld show a dramatic depletion of chrome over short intervals, especially at the base of magnetitite layers (Cawthorn and MacCarthy, 1981). The Cr_2O_3 content then remains constant over large intervals after which sharp reversals in chrome content occurs. This holds for most of the eastern Bushveld magnetites, lateral exceptions occur (Elandsfontein) where the section has lower concentrations of chrome and exhibit erratic trends. Considerable lateral variations are noted by Klemm et al., (1985).

Klemm et al., (1985) compare the composition of magnetite in magnetitite layers to that in the host rocks of the eastern Bushveld. Magnetite in magnetitite layers is richer in TiO_2, MgO, Al_2O_3 and SiO_2 but lower in V_2O_5. V_2O_5, MgO, NiO and Cu show cyclic increases with abrupt changes, but the overall trend is a decrease, with an increase in stratigraphic height. TiO_2, ZnO and Cr_2O_3 increases with stratigraphic height. Magnetites from discordant magnetitite pipes have compositions broadly similar to that of magnetite at the same stratigraphic horizon in the layered sequence. These overall patterns are indicative of normal differentiation, with the exception of the Cr_2O_3 trend (Klemm et al., 1985).

Ternary variation diagrams of Cr_2O_3-(MgO + Al_2O_3)-V_2O_5 and V_2O_5-TiO_2-Cr_2O_3 show that each sub-zone of the Upper Zone of the eastern Bushveld can clearly be discerned (Klemm et al., 1985). Trends for subzone A, B and C show a (MgO + Al_2O_3) and TiO_2 enrichment respectively. Subzone D (excluding magnetitite layer 21), the Main Magnetite Layer and the strata just above the Main Magnetite Layer show the opposite trend (Fig. 11). The magnetite from the magnetitite pipes define a separate group in the ternary diagrams and no trends are evident (Klemm et al., 1985).

5.2 Olivine

Olivine compositions were determined by electron microprobe (Appendix 5) and supplemented by published data from Merkle and Von Gruenewaldt (1986) and Reynolds (1985a).

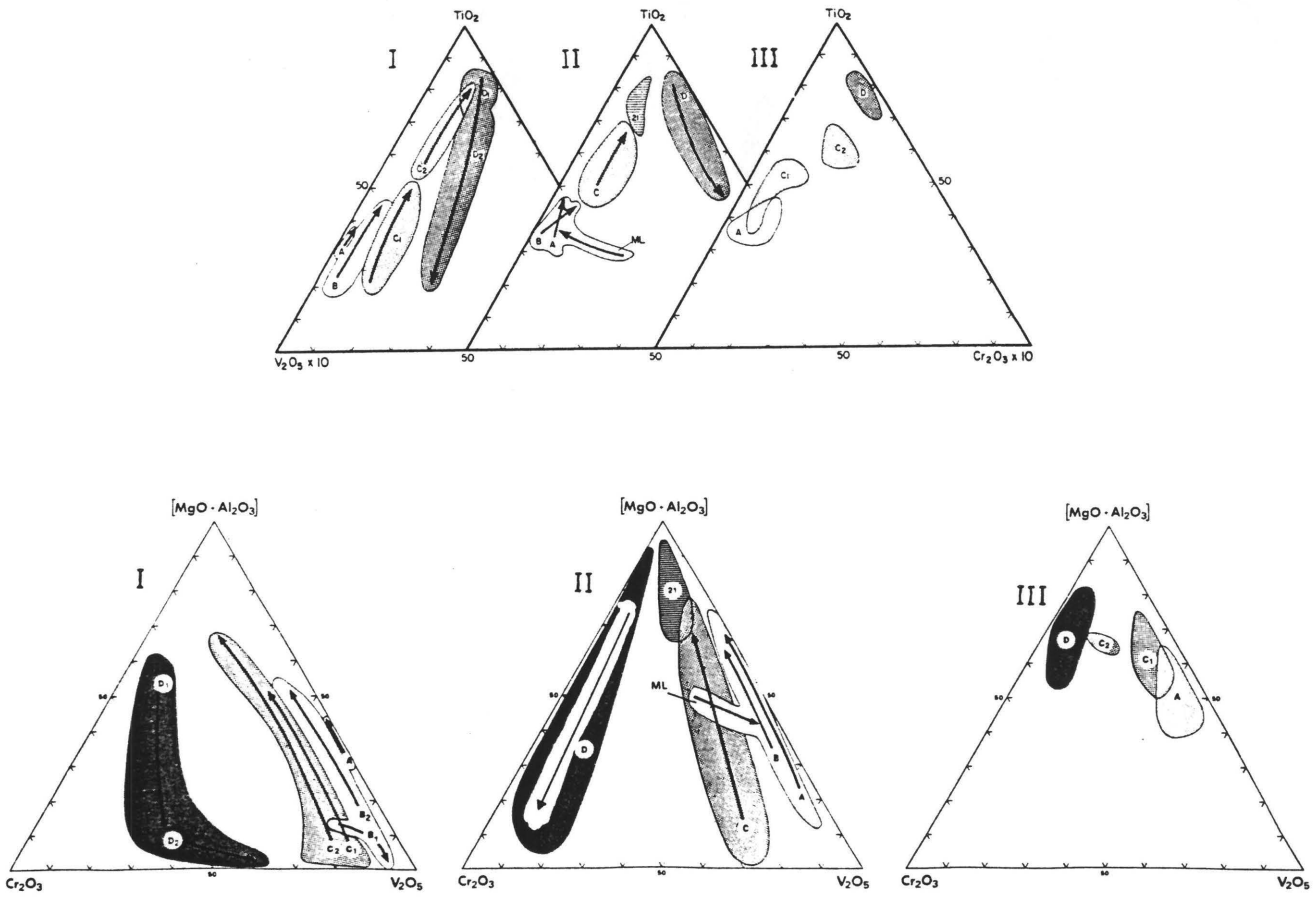

Figure 11: TiO2-V2O5-Cr2O3 and Cr2O3-(MgO+Al2O3)-V2O5 plots of magnetite from:
I - Host rocks,
II - Magnetitite layers and,
III - Magnetitite pipes of the various Subzones A, B, C and D.
Arrows indicate compostional trends from bottom to top of each subzone. Other trends which were specified were:
B1 - The sequence between the Main Magnetite Layer and magnetitite layer 6.
C1 - The sequence from the base of Subzone C to magnetitite layer 13.
C2 - the sequence from magnetitite layer 13 to the top of Subzone C.
D1 - The bottom of Subzone D to below magnetitite layer 17.
D2 - Between magnetitite layers 17 to 21.
ML - The Main Magnetite layer.
21 - Magnetite layer 21.
The figures were adapted from Klemm et al., (1985).

(Mg/Mg+Fe)

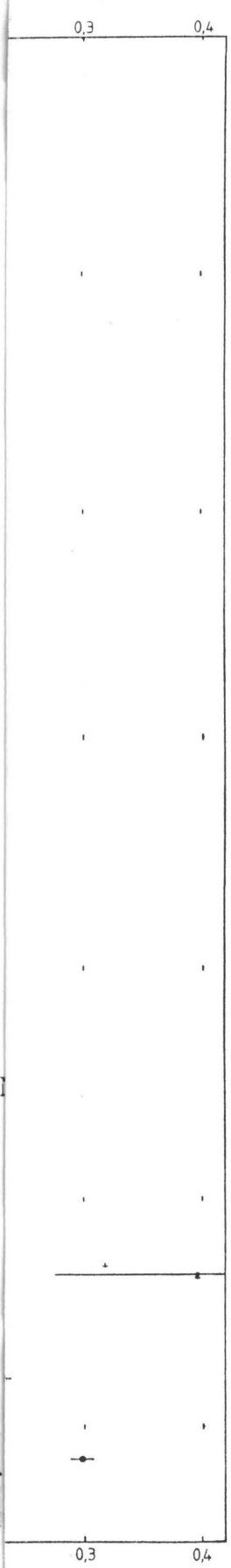

LEGE

gh Bk-1.

The composition of olivine in individual thin sections is remarkably consistent for most of the borehole. No zonation or inhomogeneity exceeding analytical uncertainty is evident, nor is any compositional dependence upon surrounding mineralogy indicated.

Olivine is extremely iron-rich and the compositional range is Fa_{46} (1 468.3) (Reynolds, 1985a) to Fa_{98} (474.5). In detail the magnesium number mirrors the MnO whole rock pattern. Highest magnesium numbers are within magnetitite horizons, eg. 1 465.5 and 1 100.8. Although an overall systematic increase in the iron content toward the roof is present, the detailed pattern is one of a cyclic iron enrichment (Fig. 12B). This pattern is reflected in a sympathetic enrichment in the MnO content and the magnesium number of the olivine.

5.3 Pyroxene

No pyroxene was analysed with the microprobe because both augite and inverted pigeonite, are characterized by very fine exsolution lamellae. These exsolution lamellae complicate the meaningful analysis by microprobe (see Kitamura et al., 1981).

5.4 Apatite

The compositional trends of cumulus apatite in borehole Bk-1 are investigated by microprobe. CaO, FeO, P_2O_5, Cl^- and F^- were determined. The F^- values are found to be constantly 0.50 % too high due to a P_2O_5 interference (Appendix 6).

Zoning, inhomogeneity or relationship between apatite composition and surrounding mineralogy is not significant within the 3 σ uncertainty range. The apatite is typically fluorapatite with F content of 2 mass percent (samples 1 396 and 601.5) to end-member fluorapatite composition (approximately 3.3 % F, sample 951). An extremely high fluorine content of the cumulus apatite of the Upper Zone is also observed by Boudreau et al., (1986). Although the apatite is enriched in F toward the roof (Fig. 13) the large error range associated with the F determinations makes the identification of real trends difficult. Due to small compositional variations, adjacent samples cannot be destinguised on the grounds of F content alone. Trends are only noticeable across several samples, with exceptions between samples 1 320 and 1 364; 551 and 601.5; 845 and 951. The Cl content almost perfectly mirrors the F trend and ranges from the lower limit of detection (less than 0.04%) to 0.72 mass percent.

Inclusions in apatite are abundant. Orientated inclusions were studied microscopically by Von Gruenewaldt (1971) who concludes that the inclusions are biotite or a green pleochroic mineral, possibly chlorite. Hornblende is mentioned as a possible, though unlikely inclusion mineral. Tiny grains of magnetite are also common as inclusions (Von Gruenewaldt, 1971) and can explain the variable FeO content found in the probe analyses (Appendix 6) and the partial loss of apatite during magnetic separation (Fig. 2).

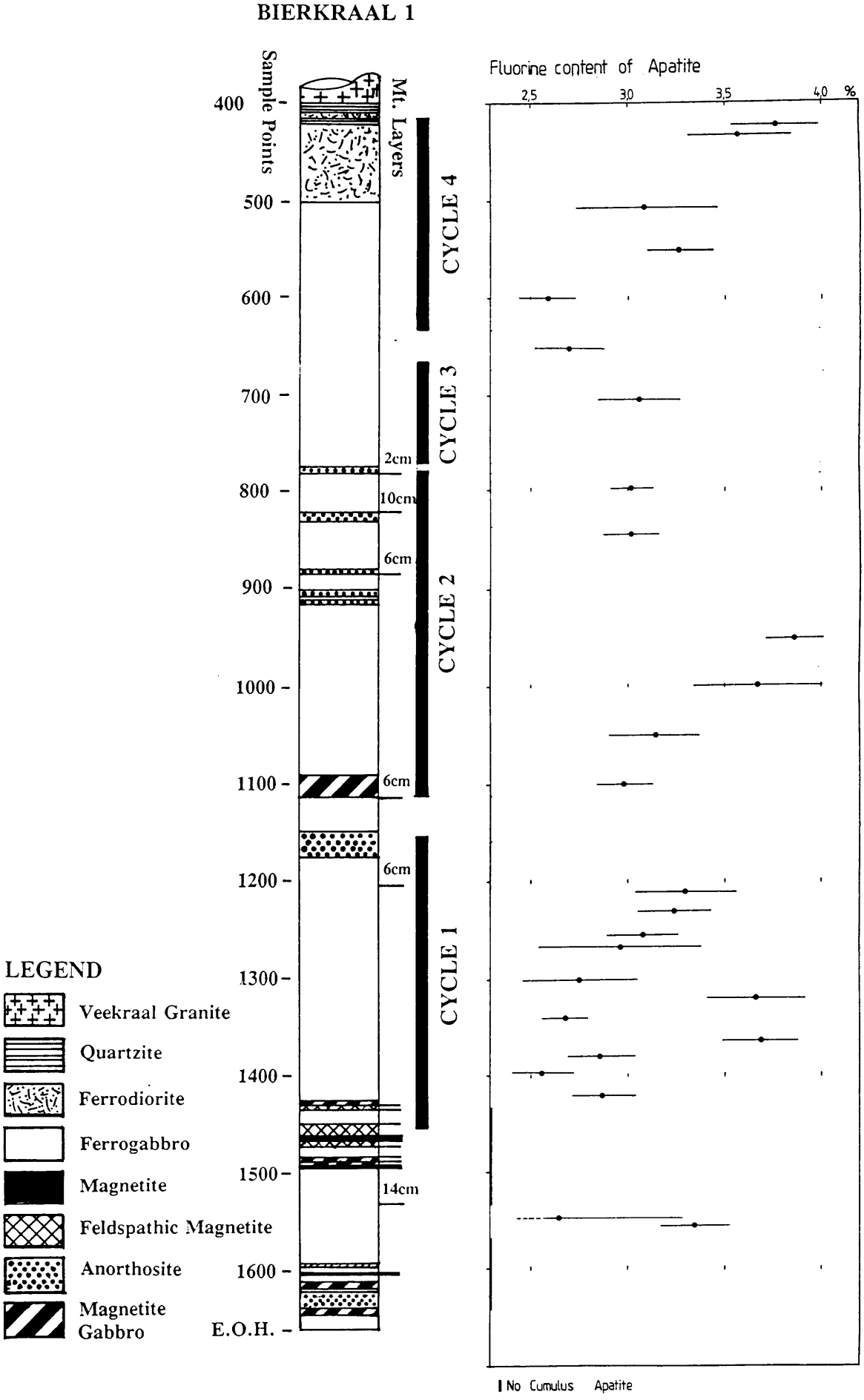

Figure 13: F-content in apatite in the Bk-1 borehole. Error bar represent analytical uncertainty (1σ).

The inclusions in the apatite prove too small for quantitative analysis by microprobe and are only qualitatively investigated with the aid of an energy dispersive analytical system. Up to four phases are identified in a single inclusion on the basis of textural and compositional differences. Based on the relative peak intensities, these phases are most likely alumino-silicates with 1) Mg and Fe or, 2) K or, 3) Na or 4) K and Fe as secondary elements. The phases can quite feasibly be: chlorite, orthoclase, plagioclase or biotite. Although this does not clarify the situation any further than the previous investigations do, it seems that the inclusions are polymineralic.

5.5 Plagioclase

The plagioclase composition was determined by microprobe. Five randomly chosen cumulus plagioclase crystals were analyzed at core and rim positions (Appendix 7).

No zoning of the plagioclase crystals is indicated to exceed the analytical error for any of the components analyzed viz.: Na_2O, SiO_2, CaO, FeO, Al_2O_3, MgO or K_2O nor was any compositional interdependence with surrounding mineralogy found. Butcher and Merkle (1991) demonstrate that reverse zoning occurs in the plagioclase associated with the magnetitite layers in the western Bushveld Complex. This reverse zoning is limited to the outermost 10 to 20 μm of the crystal and is not dependent on the adjacent mineralogy, nor is it necessarily developed along all boundaries.

As could be expected from normal differentiation processes, the average An content decreases with increasing stratigraphic height (Fig. 14). The compositional variation, at certain stratigraphic levels, is larger than that found across the entire borehole. The An composition of the plagioclase in borehole Bk-1, based on optical determinations, shows a gradational variation in the borehole with reasonably tight grouping of duplicate analyses (Walraven and Wolmarans, 1979). The optical determination seem to give a better reproducibility than the microprobe data. The larger scatter of the microprobe analyses is not an analytical artifact since the reproducibility of the analysis is 0.43 An % (3δ). An explanation for the compositional variation can be that plagioclase, in certain samples, is sub-microscopically polycomposite in nature (see D. Harney, 1991). The exact extent and reason for this submicroscopic variation is uncertain. It is inconclusive whether there is any relationship with rock type or even post magmatic processes.

5.6 Sulphides

The sulphides of borehole Bk-1 were extensively studied by Merkle and Von Gruenewaldt (1986). The sulphide mineralogy is predominantly pyrrhotite with lesser chalcopyrite and minor pentlandite. Sphalerite, molybdenite, loelliggite, safflorite, cobaltite, mackinawite, vallerite, marcasite, galena and cubanite are rare.

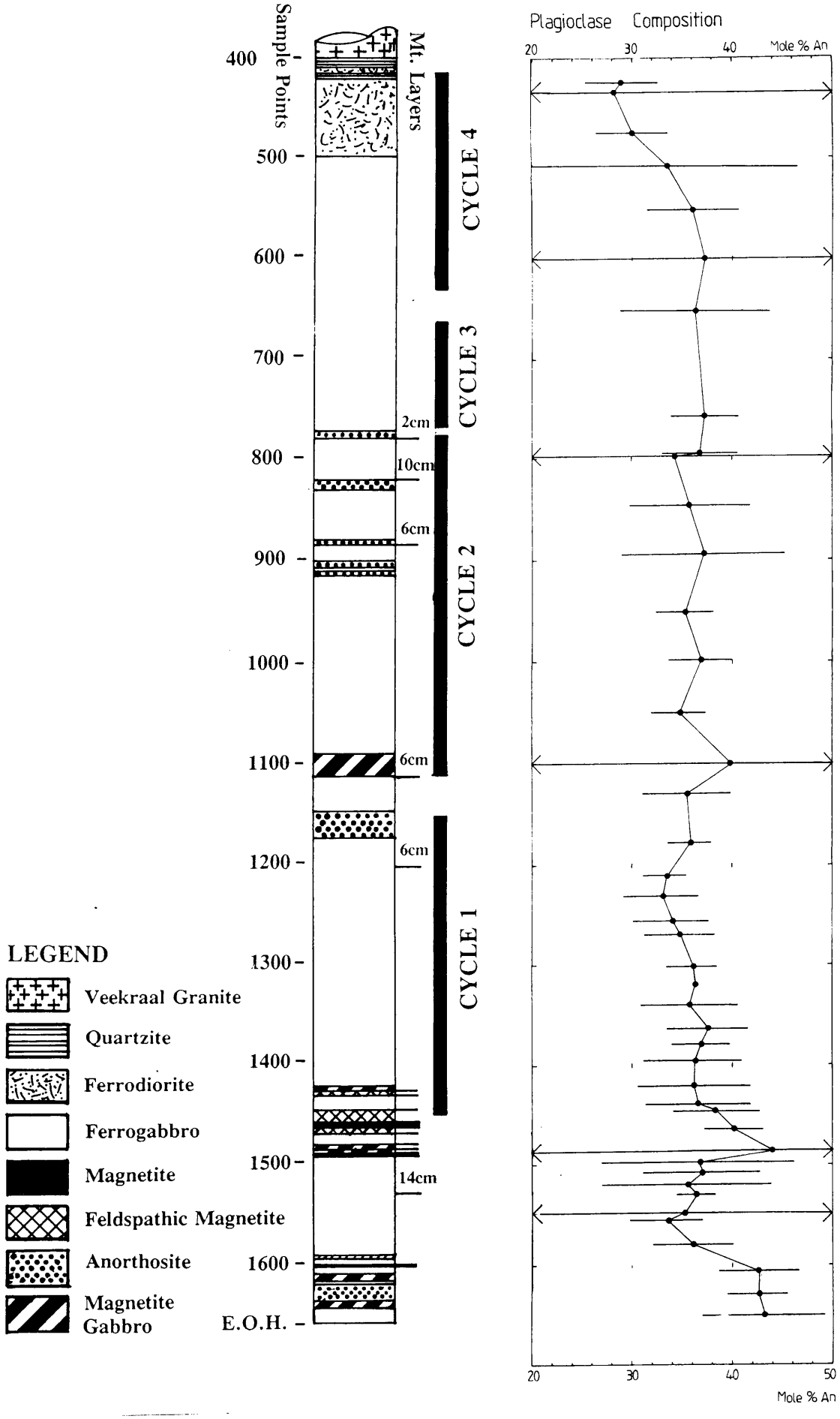

Figure 14: Microprobe analyses of plagioclase samples of the Bk-1 borehole. Mean values and variations (3σ) of plagioclase composition are given. Error bars with arrows indicate where the 3σ variation went off scale.

The enrichment of the magma in Zn, Mo, As and Pb by fractionation is reflected by the increase of sphalerite, molybdenite, arsenides and galena towards the roof. Modal proportions of pentlandite and chalcopyrite vary sympathetically with whole rock values of S, Co and Ni, while high Cu values are associated with magnetitite layers. The sulphides occur typically in intergranular spaces, but drop-like inclusions are also common in silicates and oxides.

Pentlandite occurs throughout borehole Bk-1, but because of the small size of grains in the upper parts of the borehole this section is not included in the detailed study by Merkle and Von Gruenewaldt (1986). Pentlandite contains a fairly high Co content and shows significant cyclic compositional changes.

Pyrrhotite found in the Bk-1 borehole consists of varying mixtures of the two end-member minerals, namely intermediate pyrrhotite and troilite. The lowest concentration of Co and Ni is associated with the troilite rich end-member, while the pyrrhotite end-member is also characterized by an enrichment of iron just above the magnetitite layers.

5.7 Accessory Minerals

Accessory minerals were not routinely analyzed as it is felt that little information relating to primary differentiation is forthcoming from such data.

6 WHOLE ROCK GEOCHEMISTRY

6.1 Introduction

A characteristic feature of the Upper Zone of the Bushveld is the presence of numerous magnetitite layers. Because of their economic importance they dominate the literature, while the associated anorthosites and host rocks are not extensively discussed. Notable exceptions to this approach are investigations by Molyneux (1970) and Von Gruenewaldt (1971) who discuss the petrography of the various rock types of the eastern Bushveld; Reynolds (1985a) who discusses the mineralogical and textural aspects of the Upper Zone in the western Bushveld as intersected by borehole Bk-1; Klemm et al., (1985) compare the composition of the magnetite in the magnetitite layers with that of the disseminated magnetite in the host rocks; Merkle and Von Gruenewaldt (1986) discuss the whole rock chemistry and sulphides of borehole Bk-1.

The objective of this chapter is to place some constraints on the possible formation mechanism of the magnetitite layers by geochemical modelling. Additional data is introduced to supplement the information available on the host rocks.

6.2 Detailed Geochemistry

Cawthorn and MacCarthy (1985) identify a systematic trend of incompatible trace elements across the entire Bk-1 borehole which they successfully modelled in terms of Rayleigh fractionation. Detailed sampling and geochemical analysis of borehole Bk-1 by Merkle and Von Gruenewaldt (1986) indicate the presence of rhythmic cycles. The base of each cycle roughly coincides with a magnetitite layer or magnetite gabbro. This does not hold where several magnetitite layers occur within a short interval, such as between 784 and 893 m collar depths. It will be demonstrated that this cyclicity can be modelled in terms of Rayleigh fractionation.

The calculation and interpretation of a Spearman correlation matrix (Merkle and Von Gruenewaldt, 1986) leads to the recognition of four groups of elements. Each group is characterized by sympathetic inter-element relationships.

These groups are (Fig. 15):

1) The silicate or lithophile component i.e. SiO_2, CaO, Na_2O, K_2O, Ba, Rb and Sr.
2) The titanium magnetite or oxide component: FeO, TiO_2, MnO, Nb, Zn and Zr. These components correlate negatively with group one.
3) The apatite group i.e. P and Y.
4) The sulphide or chalcophile group i.e. S, Cu, Co and Ni. These elements correlate positively with group 2.

BIERKRAAL 1

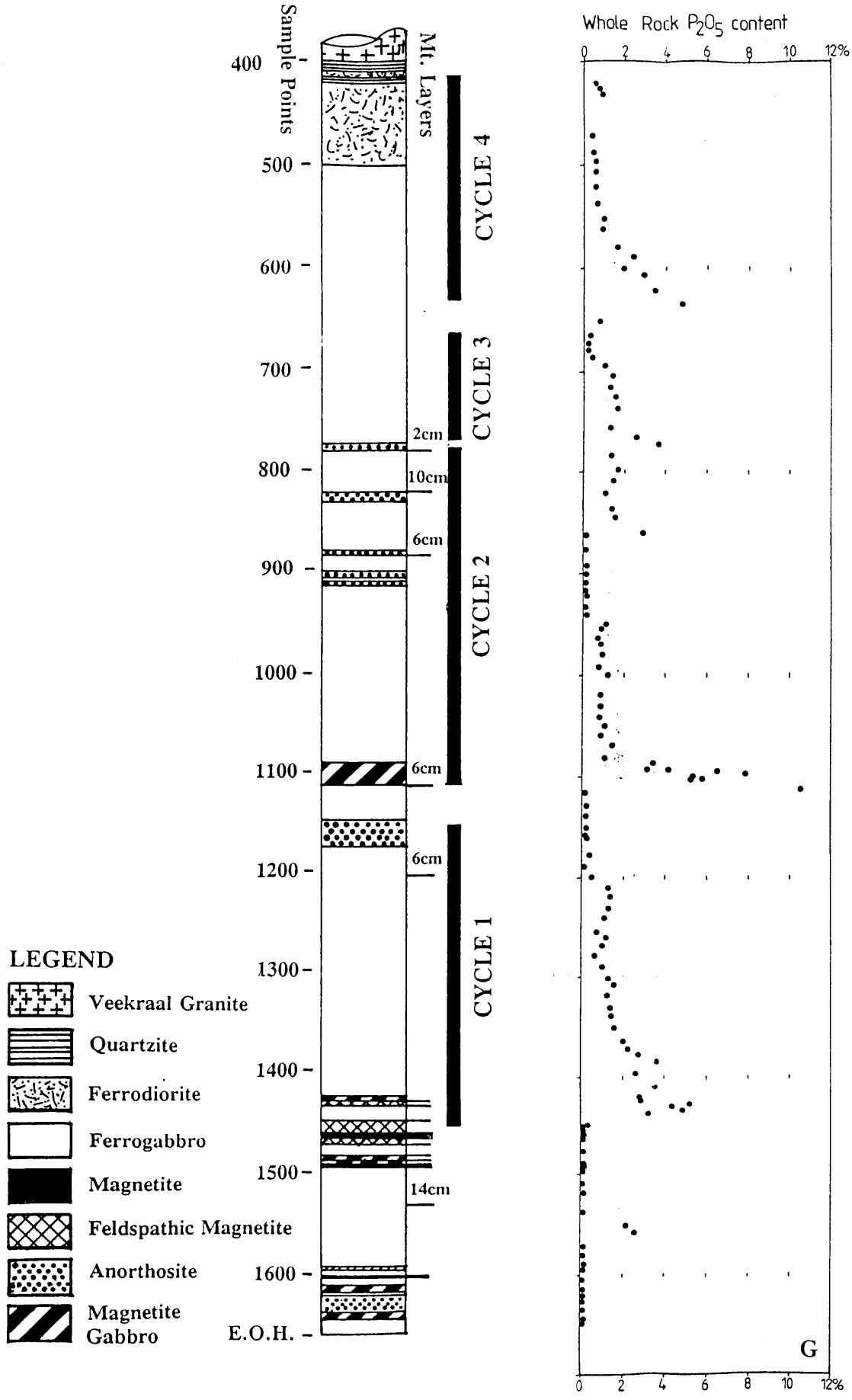

BIERKRAAL 1

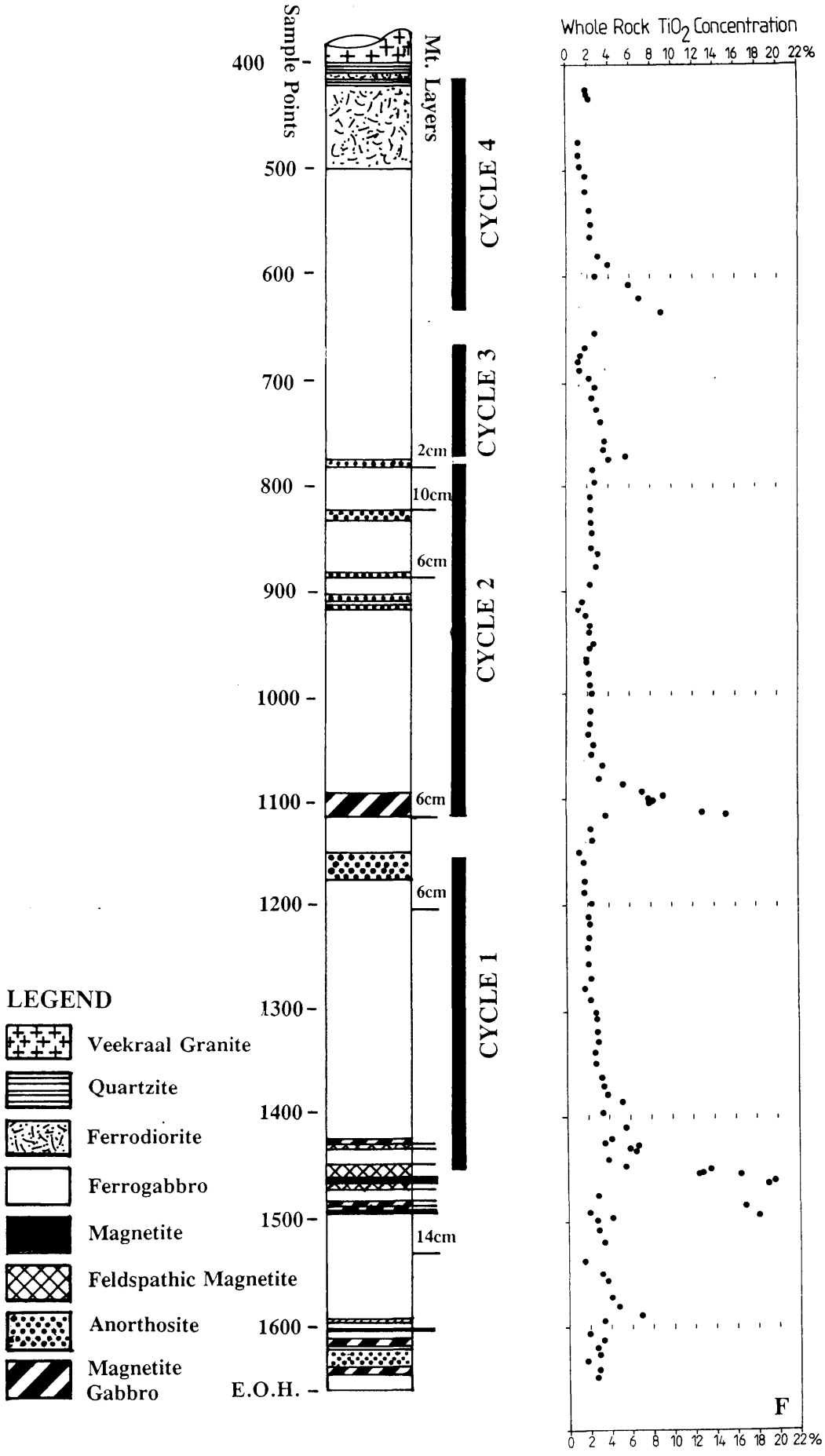

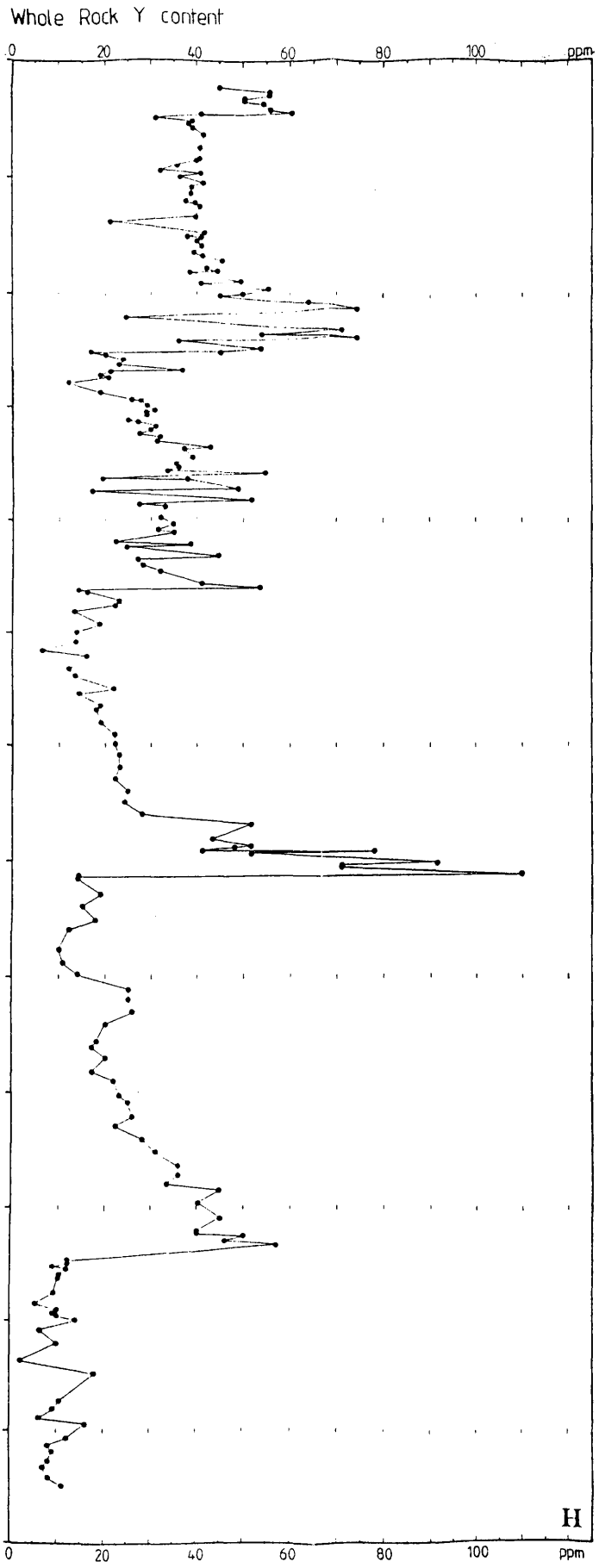

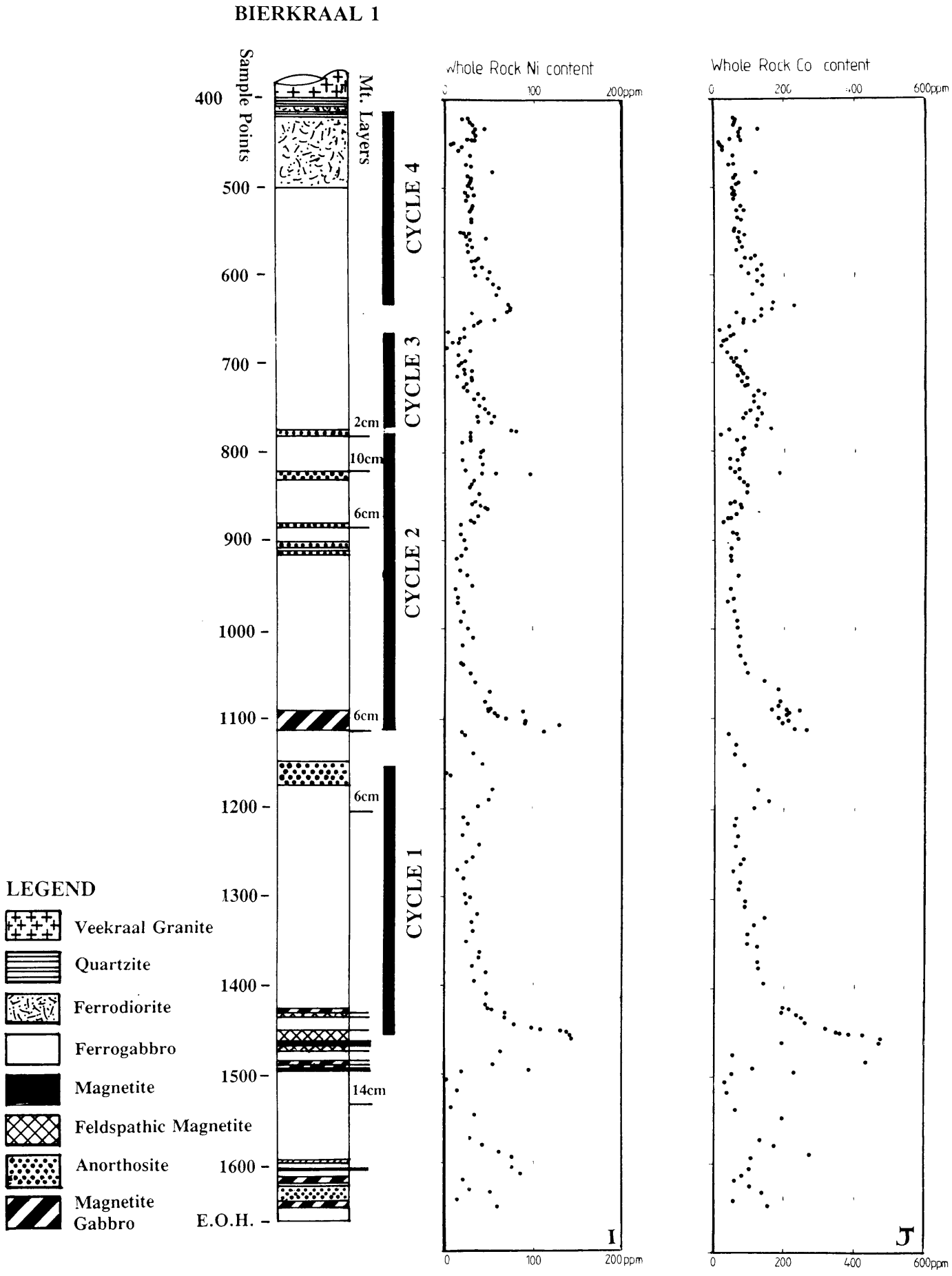

Figure 15: Variation in whole rock composition of the group 1 (A to E), group 2 (F), group 3 (G to H) and group 4 (I to J) elements. The cyclic patterns of the element trends are obvious in all plots.

6.3 Geochemical Fractionation Cycles.

In this study, cycles are defined by purely geochemical considerations regardless of the rock units. For the purpose of defining the cyclic units a short list of elements is selected that reflects the variations. At least one element from each group as suggested by Merkle and Von Gruenewaldt (1986) is included. The short list consistes of:

1) Silicate association: SiO_2, K_2O, Ba, Sr and Rb. (Discussed in Chapter 6.3.1)
2) Magnetite association: TiO_2. (Discussed in Chapter 6.3.2)
3) Apatite association: P_2O_5 and Y. (Discussed in Chapters 6.3.3 and 7)
4) Sulphide association: Ni and Co. (Discussed in Chapter 6.3.4)

A cycle is defined as a set of adjacent samples in which a recognizable systematic trend, without reversal, occurs. Stratigraphic intervals of the cycles are (Fig 15A to 15J):

Cycle 1) 1452	to	1160 m.
Cycle 2) 1113.5	to	783 m.
Cycle 3) 772.5	to	674 m.
Cycle 4) 633.8	to	422.2 m.

These cycles do not significantly differ from those identified by Merkle and Von Gruenewaldt (1986). They are merely quantitively defined in terms of collar depth. The intervals between cycles from 1 113.5 to 1 160 m; from 772.5 to 783 m, and from 633.8 to 674 m are reversals which cannot be attributed to simple fractional crystallization and are referred to as reverse cycles.

6.3.1 Group 1 - The Silicate Association

6.3.1.1 Rayleigh Fractionation.

Rayleigh fractionation processes are assumed for the trace elements trends such as Rb, Sr, Zr and Nb and are modelled by Cawthorn and MacCarthy (1985). They conclude that the upper 500 m of the layered suite as intersected by the Bk-1 borehole is derived from the differentiation of a single homogeneous magma with a trapped liquid content of 10 to 30 percent. The fractionation trend is largely calculated using the absolute concentration of Rb, since Zr, Y and Nb are greatly affected by modal proportions within the rocks. Zr is readily taken up in magnetite (Cawthorn and MacCarthy, 1985), while Y and Nb both have a large affinity for apatite (Watson and Green, 1981). The authors admit that individual samples vary greatly from the modelled trend, and ascribed this to fluctuations of trapped liquid contents. The more detailed sampling by Merkle and Von Gruenewaldt (1986) leads to the identification of four rhythmic cycles within the Bk-1 borehole section. These cycles can individually be modelled using Rayleigh fractionation processes.

Perfect fractionation is modelled by the Rayleigh fractionation equation (Gast, 1968):

$$C^i_x = C^i_0 . f^{(D-1)} \qquad ...(1)$$

where

C^i_x = concentration of element i in crystallizing phase x.

C^i_0 = concentration of element i in the parental magma.

f = mass proportion of residual magma.

D^i = distribution coefficient.

and

$$D^i = D^i_a / X_a \qquad ...(2)$$

where

$D^i a$ = distribution coefficient of element i in mineral a.

X_a = mass fraction of crystallizing mineral a (Gast, 1968).

6.3.1.1.1 Distribution Coefficients.

Extensive literature is available concerning distribution coefficients of various minerals and host melts. Few are specific to gabbro rock types. Distribution coefficients for several elements are documented by Paster et al. (1974) using samples obtained from the Skaergaard intrusion, while Mason (1972) determined minor and trace element distribution coefficients by analyzing mineral separates from the Muzzle River gabbro. These references are the major source of distribution coefficient values used in this investigation and are listed in Table 2. Where distribution coefficients of a given element into a specific mineral within a gabbro matrix composition are not available, values relevant to a basaltic or andesitic matrix are used (Ewart and Duncan, 1983; Ross, 1977; Paster et al., 1974; Goodman 1972; Mason 1972; and Philpotts and Schnetzler, 1970). Discrepancies are found within various literature sources and therefore minimum and maximum data sets are used. The resulting range of distribution coefficients is seen as an interval in which the distribution coefficient applicable for a gabbro will expectedly fall. The calculation of whole rock distribution coefficients according to Equation 2, therefore result in a minimum and maximum value.

The Rayleigh equation which assumes a closed uniform magma chamber undergoing continuous crystal fractionation, whereby the crystals are removed from the magma at formation (Cox et al., 1979). If a constant amount of trapped liquid is present in the crystal pile, the trapped liquid has the same composition as the overlying liquid. The effective distribution coefficient of such a trapped liquid is then equal to unity and the Equation 2 reduces to:-

Table 2:

The published distribution coefficients of several incompatible elements in various minerals.

	Elements		
Minerals	Ba	Rb	Sr
Magnetite	e:0.4000	----	----
Ilmenite	----	----	----
Plagioclase	a:1.21 b:0.6800	d: 0.50 c: 0.57 a:1.055	a:1.00
Apatite	a:0.0140	----	a:0.880
Olivine	b:0.0013 b:0.27	b:0.0023 b:0.1880	b:0.0012 b:0.1200
Clinopyroxene	----	a:0.0129 b:0.004	a:0.07 b:0.119
Orthopyroxene	a:0.0121 a:0.04	a:0.0287 a:0.148	a:0.04 a:0.0104
Biotite	a:3.8	f:3.06	a:0.53

a: Correspond to determinations on andesite.
(Mason, 1972; Paster et al., 1974)
b: Correspond to determinations on basalt.
(Mason, 1972; Paster et al., 1974)
c: Literature average.
d: Goodman, (1972).
e: Ross, (1977).
f: Philpotts and Schnetzler (1970).

Note. All values are taken from a compilation of distribution coefficients by Ewart and Duncan (1983).

$$D^i = (D^i_a/X_a) + t \qquad ...(3)$$

where

t = mass proportion trapped liquid.

D^i = effective distribution coefficient.

6.3.1.1.2 Calculation of f

The value f of Equation 1 is by definition the mass proportion of liquid remaining at a particular stage of crystal fractionation. For simplification, the f value (Equation 1) is assumed to have a linear relationship with collar height. This assumption implies that the magma chamber is a perfect geometrical cylinder and that isodensitic phases crystallize throughout. In nature, however, the f value does not necessarily have a linear relationship with stratigraphic height. The f value is affected by the mass ratio of crystallized magma to liquid remaining at that particular point in time. Thus the crystallization of dense magnetite or fayalite and less dense plagioclase, inevitably leads to a non-linear relationship between f and stratigraphic height.

The geometry of the magma chamber can cause a substantial deviation from a simple linear relationship between f and stratigraphic height. The geometric effect is impossible to evaluate for the Upper Zone since large sections of the Bushveld Complex are covered by younger rock types (eg. in the Bethal area; Buchanan 1972) or removed by erosion. The exact extent and shape of the original magma body is unknown. Detailed correlation between the Upper Zone rock types of the various lobes is not possible and the extent of mass exchange between these lobes is uncertain. The model is simplified by considering the Upper Zone as a system in which mass exchange is possible.

An estimate of f can be attempted with the aid of chemical data. This technique relies upon the monitoring of an incompatible element such as P in basaltic liquid (eg. Anderson and Green, 1969) and can only be applied to a totally closed system provided that no cumulus apatite is formed. It cannot be applied to the Bushveld Complex where magma addition and mixing events occur during crystallization of the Critical and Main Zones (Cawthorn and MacCarthy, 1981 and Hamer and Sharpe, 1985) and the presence of cumulus apatite. The use of least square evaluation using various trace elements is unsuccessful due to the inability to identify relevant end-point melt compositions i.e. daughter and parent pairs. This is largely caused by the effect of modal proportions upon the trace element distribution.

6.3.1.1.3 Solving the Rayleigh Equation

The successful application of the Rayleigh equation is largely dependent upon the recognition of suitable incompatible trace elements. The presence of incompatible trace elements during the late stages of differentiation are rare, particularly in the Upper Zone. The presence of orthoclase, apatite, zircon and sulphide practically excludes the use of many traditionally accepted incompatible trace elements such as the REEs, Y, Zr, Co, Ba, etc., as these elements have large distribution coefficients in these minerals. The absolute concentrations of these elements will

be controlled by the modal proportions of minor and trace minerals rather than by fractionation processes of the major minerals. The effect of trace minerals on these "incompatible" elements cannot be accurately determined by modal calculations due the statistical difficulties associated with determining of modal proportions of trace minerals.

Rb is chosen as the least problematic incompatible trace element. Distribution coefficients of Rb in the minerals of the Upper Zone are generally less than unity with the exception of plagioclase (0,50 - 1.05), biotite (3.06) and orthoclase.

The Rb distribution coefficient into biotite exceeds that of plagioclase (see Table 2). The modal proportions of both biotite and orthoclase are insignificant relative to plagioclase so that the Rb trends will be more dependent on modal proportions of plagioclase, than any other mineral. The modal proportions of plagioclase vary from approximately 50 v % to 80 v % and thus less than a two fold variation can be attributed to modal effects.

Texturally biotite is an interstitial phase in the Upper Zone rocks and therefore crystallized from the trapped liquid within the crystal pile. As a late phase it is disproportionately enriched in incompatible trace elements compared to plagioclase. Biotite could therefore not have dominate the fractionation pattern of Rb since it is effectively part of the trapped liquid component (Equation 3) and not the main differentiation process.

The least square regression technique is used for fitting the Rayleigh fractionation line to the Rb values within a logarithmic co-ordinate system. This technique utilizes the fact that C_x and f are linear in logarithmic co-ordinates (Fig. 16). Equation (10) then mathematically reduced to:-

$$C_x = C_0.f^{(D-1)} \qquad \ldots(1)$$

$$\ln C_x = \ln C_0 + (D-1).\ln f \qquad \ldots(4)$$

where

$\ln C_x$ = the y variable.
$\ln C_0$ = the y intercept.
$\ln f$ = the x variable.
$(D-1)$ = the gradient.

A simple linear regression of the values in logarithmic co-ordinates gives the best fit of the Rayleigh curve to the absolute Rb values.

The initial stage of Rb modelling is similar to that used by Cawthorn and MacCarthy (1985). A Rayleigh curve is fitted to the absolute Rb concentration covering all available values from borehole Bk-1. The base of borehole Bk-1 is

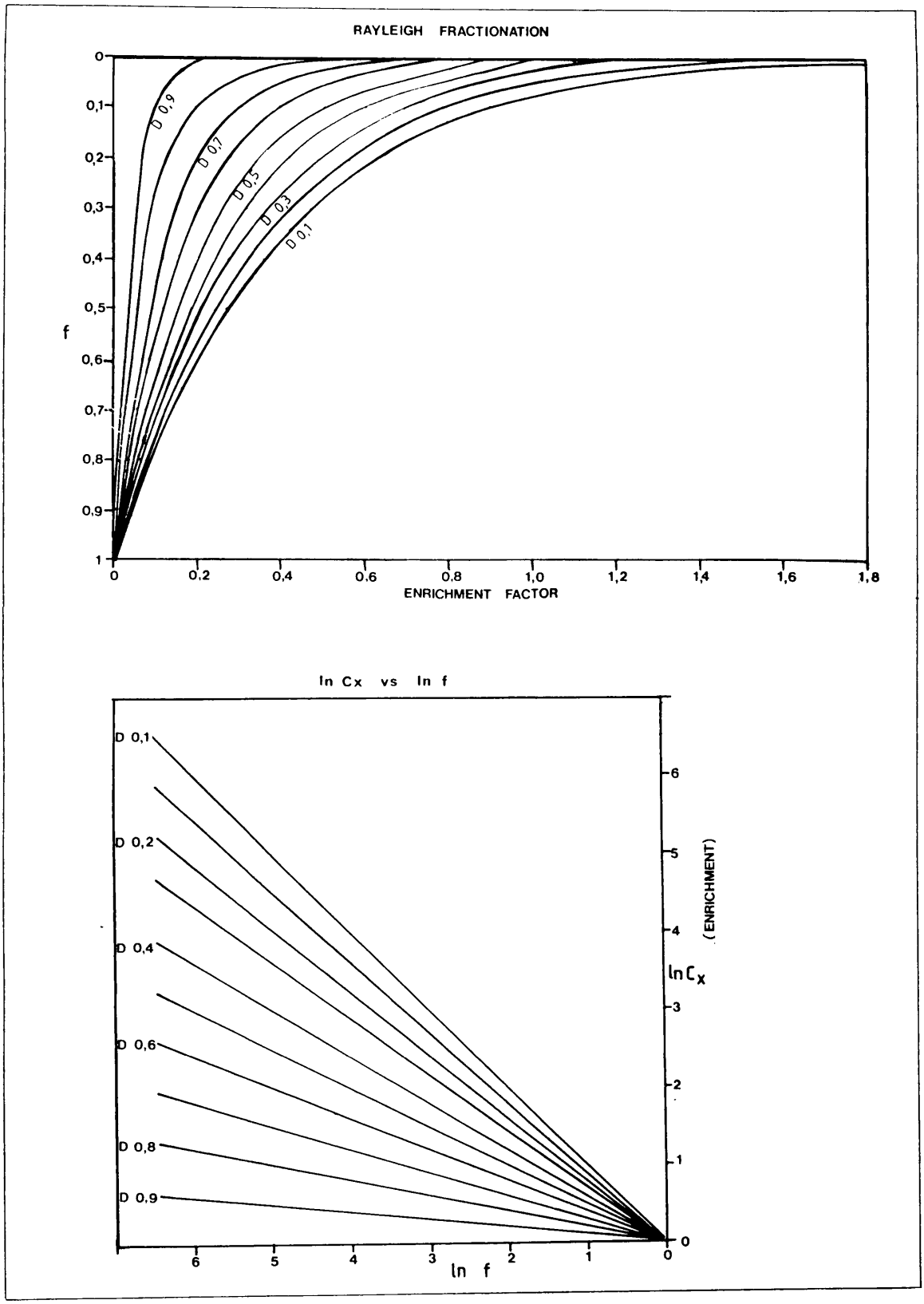

Figure 16: Rayleigh fractionation curves. These curves are linear within logarithmic co-ordinates (Cox et al., 1979).

arbitrarily assigned the value of f = 1 and the contact between the diorite and the Veekraal granite is taken as the end-point of crystallization. This contact is assigned the value f = 0 and the remaining values are calculated as a simple linear function of collar depth (Fig. 17).

Solving the Rayleigh equation for these conditions by regression gives an effective distribution coefficient of 0.70 and a parental magma composition of 11 ppm Rb. The effective distribution coefficients calculated using Equation (2) are given in Table (3) and plotted in Figure 14. The average Rb effective distribution coefficients of the modal data are: 0.33 (minimum) and 0.59 (maximum). The discrepancy between the distribution coefficient determined by the regression technique (0.70) and the modal data (0.33 and 0.59) is ascribed to the trapped liquid content (Equation 3). The absolute discrepancy or trapped liquid content is calculated as (Equation 3) 37 and 15 percent respectively. These values compare well with the values determined by Cawthorn and MacCarthy (1985) which are 10 to 30 percent trapped liquid.

This model is highly simplified and the deviations of observed Rb concentration from the model curve is substantial (Fig. 17). Cawthorn and MacCarthy (1985) attribute these deviations from the ideal curve to fluctuations in the trapped liquid content. Notwithstanding the scatter of the Rb data, this deviation seems systematic. If this interpretation is to be considered valid, a systematic variation of trapped liquid content is required, else an alternative fractionation model has to be developed.

These variations in the Rb concentration do not have an obvious correlation relative to the effective distribution coefficients (Figs. 18 and 15D) calculated by modal proportions (Equation 2). Fluctuating modal proportions have a definite effect on the concentration of Rb in the rock samples. To eliminate this effect the distribution pattern of Rb is smoothed by using moving averages of absolute Rb concentrations. The average of 2 adjacent samples is calculated to reveal the systematic variation in Rb (Fig. 19). The 4 cycles defined in Chapter 6.3 are clearly identified within the Rb trend. These cycles are characterized by an exponential increase of Rb concentration, which is reminiscent of the Rayleigh fractionation of incompatible trace elements. It is possible that these 4 cycles are produced by fractionation, which has been periodically interrupted by influxes of new magma and mixing events. It is not necessary to evoke a systematic variation in trapped liquid content to model the Rb trends.

6.3.1.1.4 Solving the Rayleigh Equation for Cycles 1-4

If the cycles are the product of fractionation, which has been periodically interrupted, each cycle can be fitted to the Rayleigh fractionation curves.

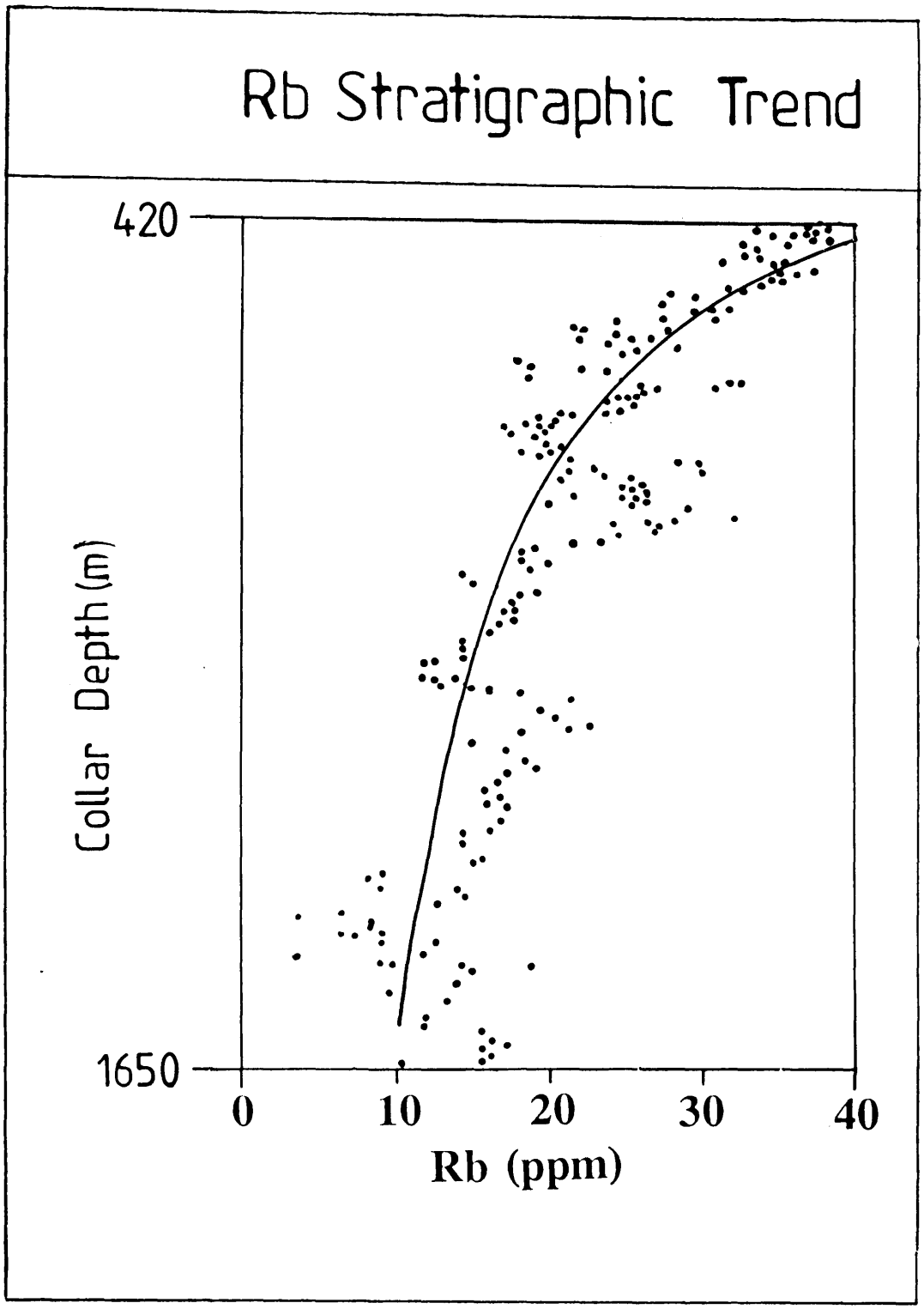

Figure 17: The whole rock Rb content plotted as the floating mean of two adjacent samples. This smoothing is done to minimize the effect of variable trapped liquid contents. The drawn curve represents the modelled Rayleigh fractionation trend of all the Rb data as one overall trend.

Table 3: Distribution coefficients calculated with the aid of modal proportions (Equation 2).

Sample	423	433	474	601	652	705	757	798	845
Rb Min.	0.297	0.225	0.300	0.451	0.370	0.294	0.298	0.238	0.346
Max.	0.580	0.445	0.565	0.725	0.690	0.580	0.544	0.461	0.666
Sr Min.	0.529	0.428	0.542	0.492	0.563	0.530	0.492	0.397	0.580
Max.	0.563	0.468	0.571	0.530	0.602	0.563	0.520	0.441	0.614
Ba Min.	0.533	0.427	0.549	0.484	0.561	0.525	0.676	0.582	0.500
Max.	0.563	0.460	0.571	0.521	0.598	0.555	0.958	0.848	0.866

Sample	893	951	999	1050	1100	1128	1178	1211	1231
Rb Min.	0.328	0.339	0.253	0.258	0.163	0.358	0.334	0.289	0.112
Max.	0.619	0.652	0.497	0.494	0.313	0.648	0.665	0.573	0.519
Sr Min.	0.533	0.611	0.415	0.427	0.375	0.594	0.582	0.523	0.464
Max.	0.570	0.637	0.462	0.471	0.389	0.616	0.616	0.559	0.505
Ba Min.	0.633	0.608	0.495	0.662	0.342	0.756	0.410	0.577	0.605
Max.	0.970	0.972	0.789	0.939	0.515	1.078	0.792	0.905	0.895

Sample	1256	1270	1302	1340	1379	1421	1439	1447	1498
Rb Min.	0.230	0.389	0.298	0.294	0.258	0.233	0.178	0.149	0.364
Max.	0.478	0.723	0.590	0.584	0.492	0.511	0.412	0.367	0.667
Sr Min.	0.436	0.644	0.541	0.537	0.434	0.424	0.327	0.279	0.652
Max.	0.479	0.669	0.573	0.573	0.472	0.476	0.383	0.351	0.667
Ba Min.	0.491	0.597	0.561	0.523	0.536	0.330	0.286	0.217	0.814
Max.	0.784	0.975	0.895	0.858	0.813	0.663	0.573	0.494	1.149

Sample	1508	1520	1548	1580	1606	1627	1649	Average
Rb Min.	0.462	0.561	0.261	0.333	0.283	0.472	0.314	0.32
Max.	0.853	0.959	0.559	0.643	0.502	0.849	0.586	0.55
Sr Min.	0.808	0.822	0.457	0.542	0.421	0.777	0.509	0.520
Max.	0.811	0.823	0.506	0.577	0.457	0.780	0.536	0.554
Ba Min.	0.601	0.726	0.347	0.517	0.769	0.638	0.573	0.565
Max.	1.031	1.156	0.700	0.871	1.019	1.048	0.887	0.887

Average = Average weighted according to sample spacing.

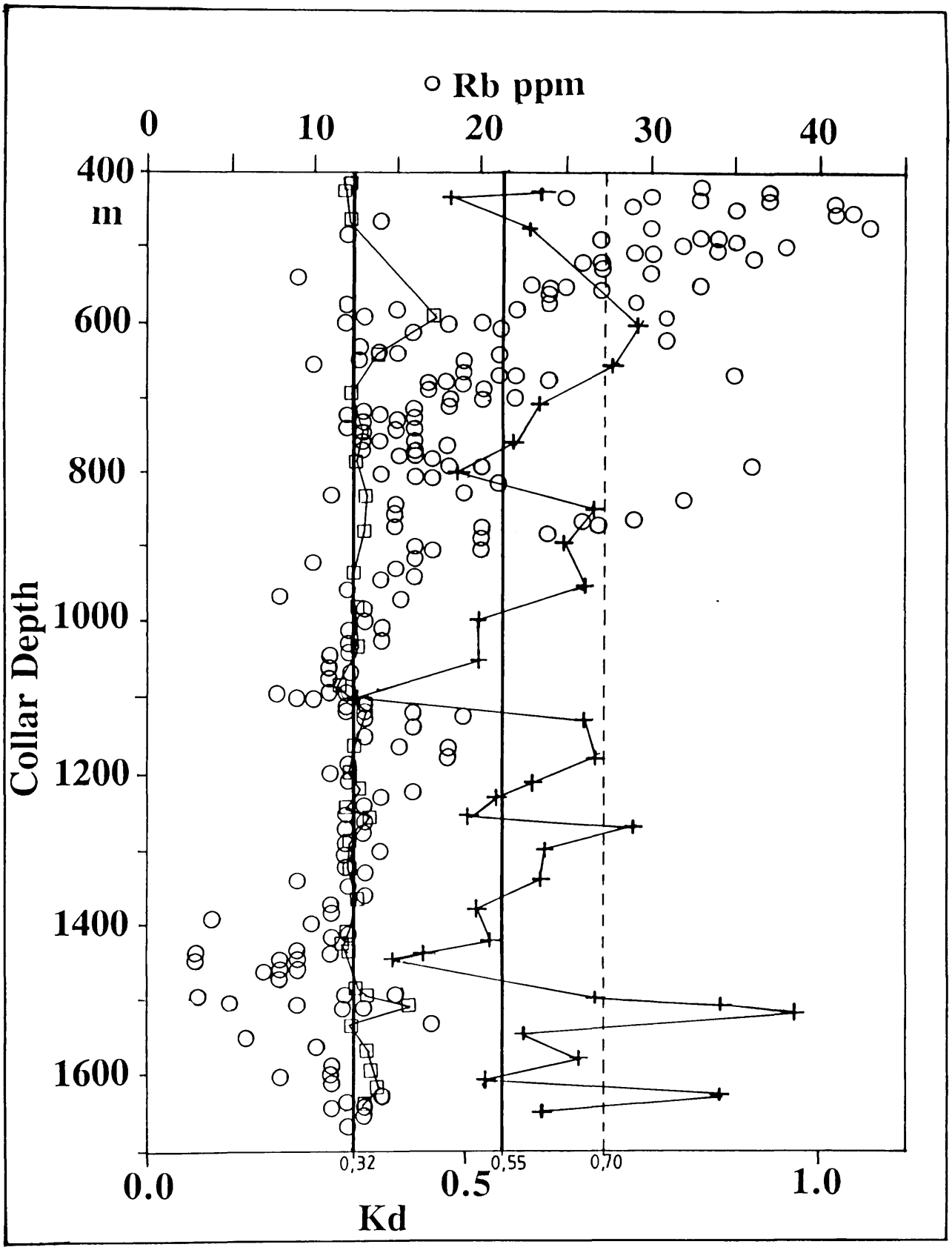

Figure 18: The Rb distribution coefficients calculated according to Equation 2, Chapter 6.3 (see table 3).

□ Min Kd Value

\+ Max Kd Value

○ Whole Rock Rb Content (ppm)

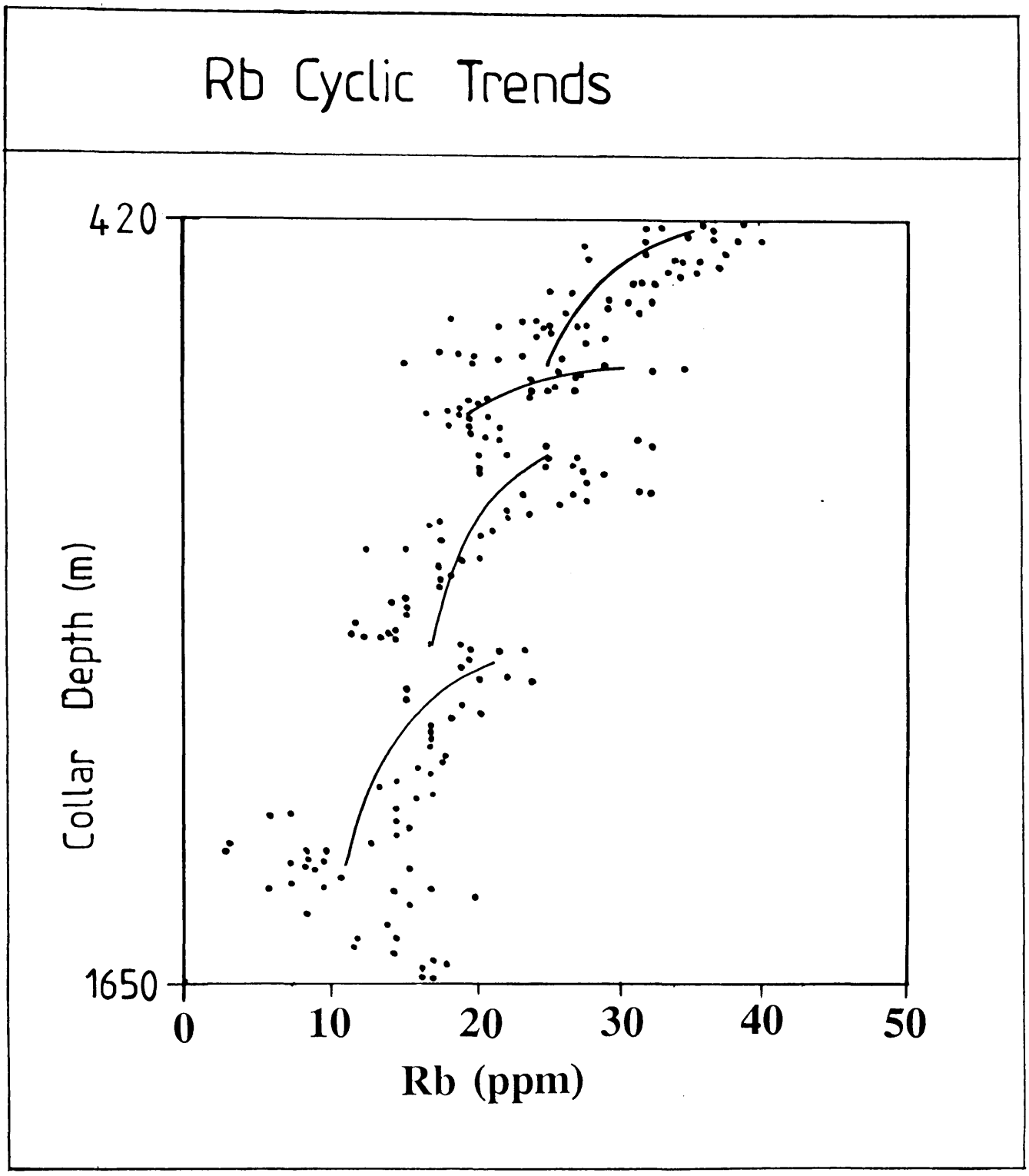

Figure 19: Cyclic trends of Rb values. The Rb values are plotted as the floating mean of two adjacent samples to minimize the effect of variable trapped liquid content. Drawn curves represent the Rayleigh fractionation modelled by treating the cycles independently. The uppermost cycle is not a very good fit, possibly due to the systematic increase in the trpped liquid content below the roof.

In order to fit a Rayleigh fractionation curve to each cycle as defined in the beginning of Chapter 6.3, f is chosen to cover the entire permissible range of 0 to 1 across each cycle. The calculated distribution coefficients according to the log-log least square technique are:

Cycle 1) 0.846;
Cycle 2) 0.850;
Cycle 3) 0.884;
Cycle 4) 0.836.

The trapped liquid content can be calculated by the application of Equation (3) in the form of:

D^i (determined by regression, Equation 4) = D^i (Modal Calculations, Equation 2) + Trapped liquid content.

or

Trapped liquid content = D^i (regression) - D^i (modal) ...(5)

The corresponding trapped liquid content, according to Equation (3), and the average effective bulk distribution coefficient for each cycle from Table (4) is:

Cycle 1) 0.81-0.31;
Cycle 2) 0.81-0.32;
Cycle 3) 0.84-0.32;
Cycle 4) 0.77-0.26.

The trapped liquid content of the first overall modelling approach is 0.15 to 0.37 (see Chapter 6.3.1.1.3)

The implied mass proportion of trapped liquid content within each cycle (Table 4) seems excessive and does not fall within the constraints implied by the first overall approach.

Ba and Sr are not ideal incompatible elements in this case study but, similar calculations are repeated for Sr (Table 5B) and Ba which confirm the result of the Rb modelling relating to the trapped liquid content. It is clear that the modelled Ba values associated with the lower distribution coefficients are illogical because a negative trapped liquid content is physically impossible. The trapped liquid content as calculated using the Sr values is fairly well constrained, which implies that the trapped liquid is too high.

Table 4:

Solutions to Rayleigh Equations of cycles 1 to 4.

	Effective distribution coefficient (by regression)	Effective distribution coefficient (Modal, Eq 2)		Implied trapped liquid (%)
Rb Cycle 1:	0.846	max.	0.538	31
		min.	0.137	81
Cycle 2:	0.850	max.	0.529	32
		min.	0.234	81
Cycle 3:	0.884	max.	0.562	32
		min.	0.254	84
Cycle 4:	0.836	max.	0.578	26
		min.	0.266	77
Sr Cycle 1:	0.840	max.	0.515	33
		min.	0.472	37
Cycle 2:	0.917	max.	0.512	41
		min.	0.477	44
Cycle 3:	0.911	max.	0.542	37
		min.	0.512	40
Cycle 4:	0.970	max.	0.534	44
		min.	0.498	47
Ba Cycle 1:	0.792	max.	0.787	1
		min.	0.467	33
Cycle 2:	0.808	max.	0.843	-4
		min.	0.548	26
Cycle 3:	0.806	max.	0.917	-11
		min.	0.611	20
Cycle 4:	0.816	max.	0.985	-17
		min.	0.688	13

Note: Effective Kd (Regression) =
Effective Kd (Modal) + Trapped liquid content
(see Equation 3)

Table 5a:
The f value of the rhythmic cycles (Rb).

End of cycle	Collar height	f (initial, overall approach) See Chapter 6.3.1.1.3 and Fig 17	f (cycles) See Chapter 6.3.1.1.4 and Fig 19	Fraction of reverse cycle relative to preceding cycle Chapter 6.3	Model
1	1160	0.7164	a:0.3375 b:0.2248 c:0.0570 d:-0.003	0.1592	3 3 2 2
2	783	0.3504	a:0.3374 b:0.2238 c:0.0634 d:-0.003	0.0318	3 3 3 2
3	674	0.2445	a:0.5124 b:0.3979 c:0.1491 d:-0.01	0.4081	1 1 2 2
4	422.2	0	a:0.3242 b:0.2082 c:0.0348 d:-0.005	0	1 1 1 2

Note: a: Values calculated by using the minimum mineral coefficients and minimum trapped liquid.
b: Values calculated by using the minimum mineral coefficients and maximum trapped liquid.
c: Values calculated by using the maximum mineral coefficients and minimum trapped liquid.
d: Values calculated by using the maximum mineral coefficients and maximum trapped liquid.
See text for description of models (Chapter 6.3.1.3)

Table: 5B

Comparison of f values for Sr

End of cycle	Collar height	f (initial, overall approach)	f (cycles)	Fraction of reverse cycle relative to preceding cycle	Model
1	1160	0.7164	a:0.0871 b:-0.0003 c:0.0632 d:-0.003	0.1592	2 2 2 2
2	783	0.3504	a:0.2404 b:0.0144 c:0.2090 d:0.0014	0.0318	3 2 3 2
3	674	0.2445	a:0.2904 b:0.0213 c:0.2569 d:-0.001	0.4081	1 2 1 2
4	422.2	0	a:0.6296 b:0.2895 c:0.5979 d:0.1828	0	1 1 1 1

Note: a: Values calculated by using the minimum mineral coefficients and minimum trapped liquid.
b: Values calculated by using the minimum mineral coefficients and maximum trapped liquid.
c: Values calculated by using the maximum mineral coefficients and minimum trapped liquid.
d: Values calculated by using the maximum mineral coefficients and maximum trapped liquid.
See text for description of models.
This table represents the same exercise as was done for Rb in Table 5A.

6.3.1.1.5 Discussion

The effective distribution coefficient of an element in a given matrix is a function of the trapped liquid content and the sum product of the mass fraction, times the distribution coefficients of each mineral component within the matrix (Equation 2). The excessive trapped liquid content can be the result of an over estimation of the effective distribution coefficient (i.e. the slope of the regression in the log-log co-ordinates is over estimated, Equation 4). Alternatively, the distribution coefficients used for each mineral constituent are too small (Equations 2).

The distribution coefficient for a given element, specific to each mineral (Equation 2), cannot be responsible for this discrepancy. Identical methods are used throughout the calculation, even in the first overall approach. In the log-log linear least square regression, the effective distribution coefficient is a function of the slope of the $\ln C_x$ vs. lnf plot (see Equation 4). The discrepancy can only reflect the incorrect definition of f, implying that the f value does not run the full permissible range (0-1) but rather a fraction thereof.

New f ranges are calculated for each cycle (Fig. 19) by confining the trapped liquid content to the range of 15 to 37 mass percent as is implied by the first overall approach. The first overall model assumes that one uninterrupted fractionation of the magma occurs (Fig. 17). Using Equation 4 and the linear relationship of f with collar depth, four possible f minima are calculated for each cycle. These four possible minima correspond to the various combinations of trapped liquid (i.e. 15 % to 37 %) and effective distribution coefficients (Table 4, 2nd column). The determined values of f at the end of each cycle are listed in Table 5A.

6.3.1.2 Crystallization Models

At least four crystallization models result when the f values calculated for each cycle are compared with the f value calculated in a similar manner by Cawthorn and MacCarthy (1985). For the simplification of the text, the calculations of f according to Cawthorn and MacCarthy (1985) model is referred to as the uninterrupted fractionation model.

6.3.1.3.1 Model 1

This model is characterized by the fact that the f calculated at the end of each cycle is greater than the f calculated for this point in the uninterrupted fractionation model. This simply implies that, a larger body of magma is required than assumed in the uninterrupted fractionation model.

This model can be adapted to the presented data if it were to be assumed that the magma chamber is conical in shape rather than perfectly cylindrical. Alternatively, it can be assumed that a substantial mass loss occurs in the roof of the chamber. Both alternatives have no indicators in the borehole profile unless the roof of each individual cycle is stratigraphically higher than the available geochemical data suggests.

It is therefore not possible to test this model and will be contrary to the closed system defined in the uninterrupted fractionation model. This model can only be considered as a mathematical solution.

6.3.1.3.2 Model 2

The f calculated for each cycle is less than f as calculated in the uninterrupted fractionation model. The newly calculated f is less than the mass ratio of the overlying reverse cycle (defined in Chapter 6.3) when compared to the cycle in question (Table 5a).

This model principally demonstrates that the magma remaining at the end of a specific cycle can be completely mixed with the reverse cycle above it.

6.3.1.3.3 Model 3

The f calculated, by limiting the trapped liquid to the 15 to 37 percent range, is less than the f calculated by the uninterrupted fractionation model but greater than the mass fraction of the reverse cycle above the cycle in question.

This model demonstrates that residual magma at the end of each cycle cannot be absorbed by the overlying reverse cycle but has to, at least partially, be absorbed elsewhere in the magma chamber or ejected from the magma chamber.

6.3.1.3.4 Model 4

Magma addition is theoretically possible at any point where the f calculated at the end of a cycle is less than the f calculated in the first approach.

6.3.1.4 Discussion

It cannot be expected that one model will fit all the cycles, since no reverse cycle is identified above cycle 4, nor will it seem possible that four very similar cycles are formed by radically different processes.

The conditions of Model 2 can be realized in various ways:
1) A normal cycle can represent the fractionation of a magma crystallizing dense phases such as olivine and magnetite, thus producing a less dense residual magma. The reverse cycle can represent the addition and mixing of less fractionated magma with the residual magma of the cycle. Fractionation of this fresh or new magma after mixing will form the next normal cycle. Cycle four will then represent the final crystallization of the magma.
2) The addition of the less fractionated magma is not necessarily a new magma influx but can simply represent density stratification of the magma chamber. The only physical criteria which is to be met by this new magma is that it is less dense than the magma layer from which the previous cycle crystallized. With

fractionation the residual liquid will decrease in density until mixing across the boundary of the two liquids is possible and a reverse cycle is created.

Model 3 will essentially represent the same process with the difference that the residual magma of the preceding cycle cannot be taken up in the reverse cycle alone and that the next normal cycle represents the fractionation of a mixture of the two magmas. This will require a relatively efficient homogenizing process.

Model 4 readily explains reverse cycles but will have to be tested using the REE data.

Note that the constraints of Model 2, 3 and 4 are adhered to during crystallization of density stratified magma.

6.3.2 Group 2: The Magnetite Association

The co-precipitation of Ti-magnetite and ilmenite is a common feature of late stages of crystallization of tholeitic magmas (Reynolds, 1985b). This co-precipitation explains the strong correlation between Ti and Fe in the whole rock analyses (Fig. 8). A similar correlation between TiO_2, MnO and Zn in the magnetite exists and the increase of these elements with stratigraphic height is a result of fractional crystallization (Klemm et al., 1985).

During crystallization, Zr and Nb partitions strongly into magnetite (Cawthorn and MacCarthy, 1985) while Mn preferentially partitions into ilmenite rather than into Ti-magnetite. Similar tendencies occur during sub-solidus re-equilibration (Reynolds, 1985b).

The strong positive correlation of these elements can be the result of the copious co-precipitation of ilmenite and magnetite during fractional crystallization.

6.3.3 Group 3: The Apatite Association

This group is extensively discussed in chapter 7.

The effect of modal proportions on the concentration of any group of elements is demonstrated by the relationship of modal apatite with Y (and the REEs). The distribution coefficients of the REEs and Y in apatite are approximately twenty times greater than that of clinopyroxene. Zircon has a great affinity for Y and the REEs, however, the modal proportions of zircon in the Upper Zone are not sufficient to markedly affect the REE trends.

The dependence of these element concentrations on modal apatite and distribution coefficients is illustrated in Figures 20 and 21. The variation in Y concentration, effective distribution coefficients and apatite modal content is plotted against collar depth (refer to Fig. 20 and 21). The effective coefficients, hence modal proportions (Equation 2), determine the concentration of the REEs in the crystal

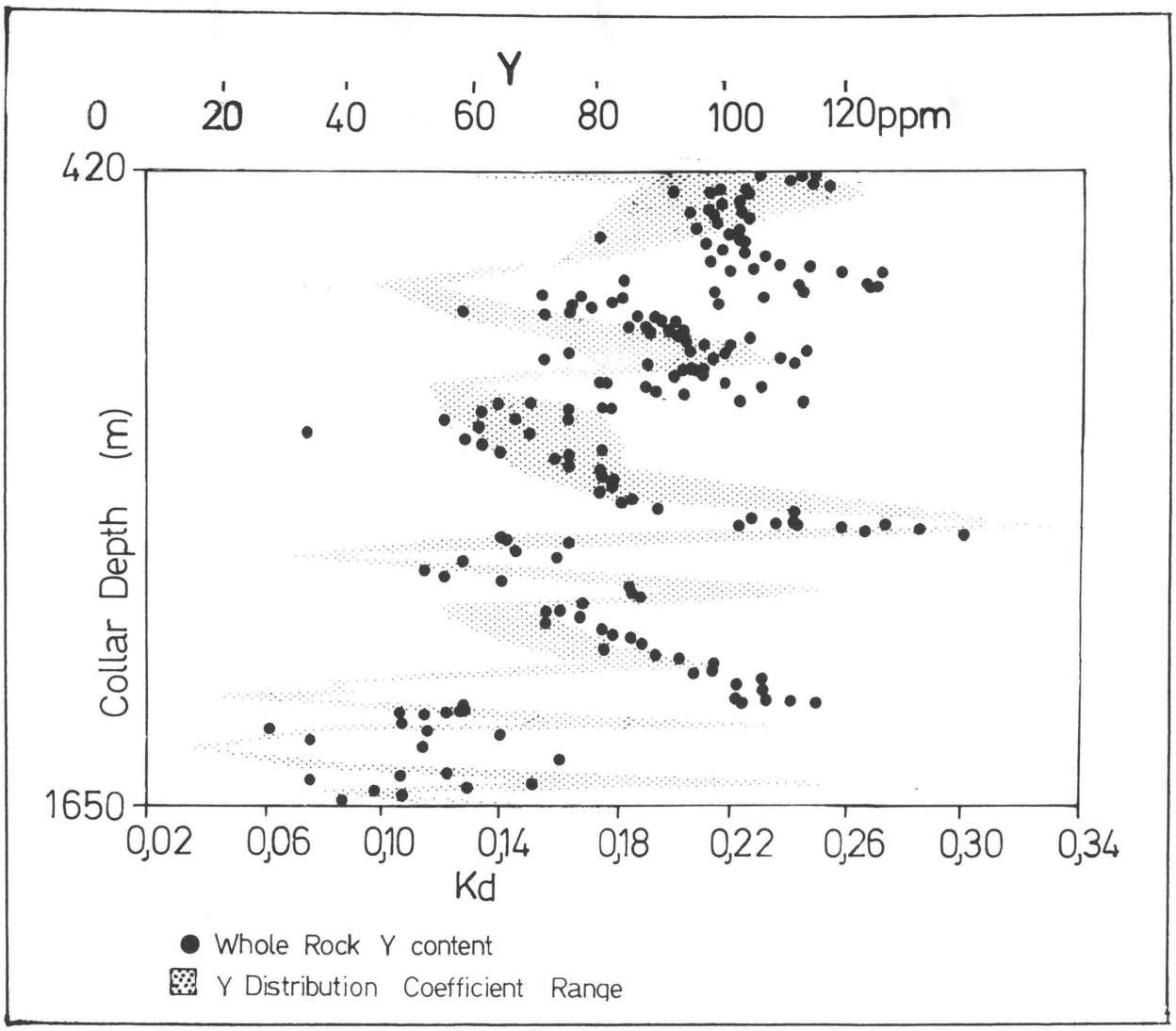

Figure 20: The whole rock Y content and the calculated distribution coefficients (Equation 2, Chapter 6.3.1.1).

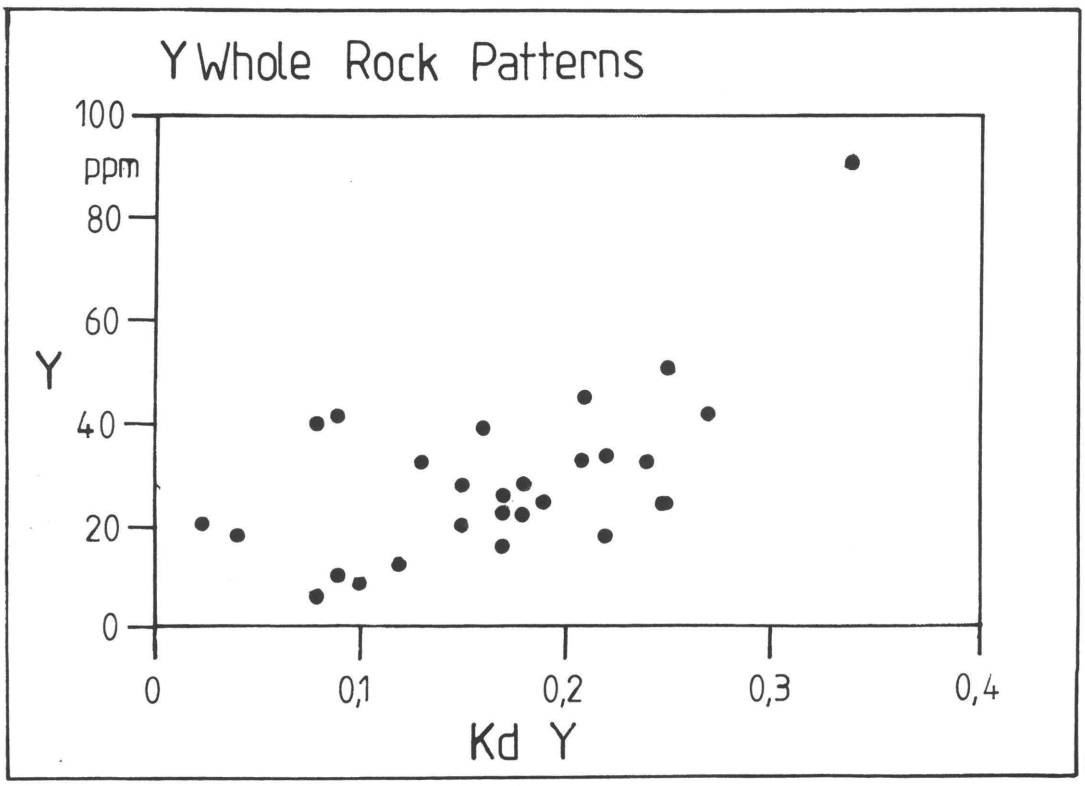

55

Figure 21: The whole rock Y content versus the calculated Y distribution coefficients. Note that a broad relationship exists.

pile, while the effects of fractionation and trapped liquid are completely obliterated by the presence of apatite. Notable exceptions to this rule are the uppermost two samples. The Y concentration continue to rise in this interval but, the effective distribution coefficient show a dramatic decrease. These samples represent the final stages of solidification of the Bushveld Complex. The trapped liquid content rises dramatically under such conditions and therefore alters the effective distribution coefficient according to Equation 3.

6.3.4 Group 4: The Sulphide Association

The behaviour of this group of elements is extensively discussed by Merkle and Von Gruenewaldt (1986). The effects of differentiation processes are seen in an increase in the Co/Ni ratio in the whole rock and in pentlandite. This trend is irregular across stratigraphic height. Continuous sulphide liquation by liquid-liquid immiscibility occurring during a differentiation process results in a smooth trend. The mechanism evoked to cause these reversals is the introduction and mixing of a less evolved magma. The separation of the sulphide liquid at this stage depletes the magma so rapidly in Ni relative to Co, that disequilibrium results. Due to the disequilibrium depletion of Ni, the Co is then taken up more rapidly in the immiscible sulphide liquid. This trend is further amplified by the ever decreasing amount of sulphide liquid separating from the magma and the resulting effect of the R factor (Merkle and Von Gruenewaldt, 1986).

The modal proportions of chalcopyrite associated with magnetitite layers is also explained by a mixing event. The enrichment of Cu in this association is ascribed to a higher R factor of the sulphides that separated during crystallization of the magnetitite layers. This increase in R factor can be attained by the adding of a magma relatively enriched in Cu, or simply increasing the extent of mixing within the liquid containing the immiscible sulphide liquid (Merkle and Von Gruenewaldt, 1986).

6.4 Summary

Cawthorn and MacCarthy (1985) identify one geochemical trend across the entire Bk-1 borehole. Four geochemical cycles are identified by means of closer sample spacing (Merkle and Von Gruenewaldt, 1986). The four geochemical cycles are quantified, which indicate that all geochemical groups reflect the defined cycles fairly accurately.

The silicate group trends for borehole Bk-1 can be modelled in terms of Rayleigh fractionation as one overall trend (Cawthorn and MacCarthy (1985). However, the four smaller geochemical cycles (Merkle and Von Gruenewaldt, 1986) can also be individually fitted to Rayleigh fractionation curves. Repeated cycles can be caused by introducing and mixing the melt with less evolved magma (Merkle and Von Gruenewaldt, 1986). Two mechanisms by which this might occur are: 1) influx of new or fresh magma resulting in mixing episodes, or 2) the repeated formation and disintegration of density stratiform layers.

The trend of the magnetite-ilmenite group is ascribed to the copious co-precipitation of Ti-magnetite and ilmenite due to late stage crystallization.

The trend of the apatite group (P_2O_5 and Y) is associated with the modal effects of apatite and the high affinity of apatite for Y.

The behaviour of the sulphide association is attributed to differentiation processes and the subsequent formation of immiscible sulphide liquid. Revers cycles are considred to have formed during the mixing events.

7 RARE EARTH ELEMENT DATA

7.1 Distribution Coefficients

Under ideal circumstances, the distribution coefficient of a given element is determined as the ratio between a specific mineral phenocryst and a volcanic glass or melt. Consequently, the calculation of distribution coefficients in a cumulate such as in the Upper Zone represented non-ideal conditions. These conditions are non-ideal because, a) bottom growth and crystal settling effectively isolates the cumulate from the liquid and, b) post cumulus effects take place in the crystal pile. Accessory phases, such as apatite in a gabbro, can dominate trends of trace elements and REEs rather than primary differentiation processes. This effect is demonstrated by calculations using the modal data from borehole Bk-1 to establish distribution coefficients.

Theoretical whole rock distribution coefficients are calculated using modal proportions and the distribution coefficients of each mineral according to Equation 2 (chapter 6.3.1.1). These coefficients exclude the 15 to 37 percent trapped liquid content estimated by the initial Rb modelling. Where trapped liquid is brought into consideration (Equation 3, chapter 6.3.1.1). the distribution coefficients of any trace element is elevated by an estimated 0,15 to 0,37.

Straightforward stratigraphic trends of the distribution coefficients of the REEs calculated according to Equation 2 (chapter 6.3.1.1) are exceptionally difficult to identify. These trends are however dominated by modal proportions of apatite. The whole rock distribution coefficients are high in the apatite-rich-zones and decrease sympathetically with P_2O_5 (Figure 22) or apatite content. As a further effect of modal proportions, Eu is selectively enriched or depleted relative to the other lanthanides. This selective change is brought about by the relative ratio of apatite to feldspar and this is illustrated in Figure 23, in which the effective REE distribution coefficients (calculated from the modal proportions of the whole rock samples), are plotted. Sample 1 100.8, contains 39 v % plagioclase and 18 v % apatite which indicates that the crystallization process at this point selectively enriches Eu in the melt relative to the other REEs. On the other hand, the composition of sample 893, containing 62 v % plagioclase and only 2 v % apatite, suggests that the crystallization processes result in a selective Eu depletion in the melt. The whole rock effective distribution coefficients in general, illustrates that the REEs are concentrated in the liquid. The coefficients are below unity except in the case of the apatite-magnetite rich zones such as sample 1 100,8.

In order to test whether apatite crystallizes near equilibrium conditions relative to the host whole rock the distribution coefficients of the REEs into apatite and the ratio of the REEs in apatite to that in the host whole rock (REE in [Apatite]/REE in [Whole Rock]) was compared. The variation of this ratio is extremely large with the majority of values ranging from 12 to 49. Extreme values are determined for sample 1 100.8 with an exceptionally low value of 5.8, and sample 893 with an exceptionally high value of 160.3 (Fig. 24). Unfortunately these values are greatly influenced by the modal proportion of apatite in the whole rock and do not approximate the phenocryst/groundmass ratio which a distribution coefficient should.

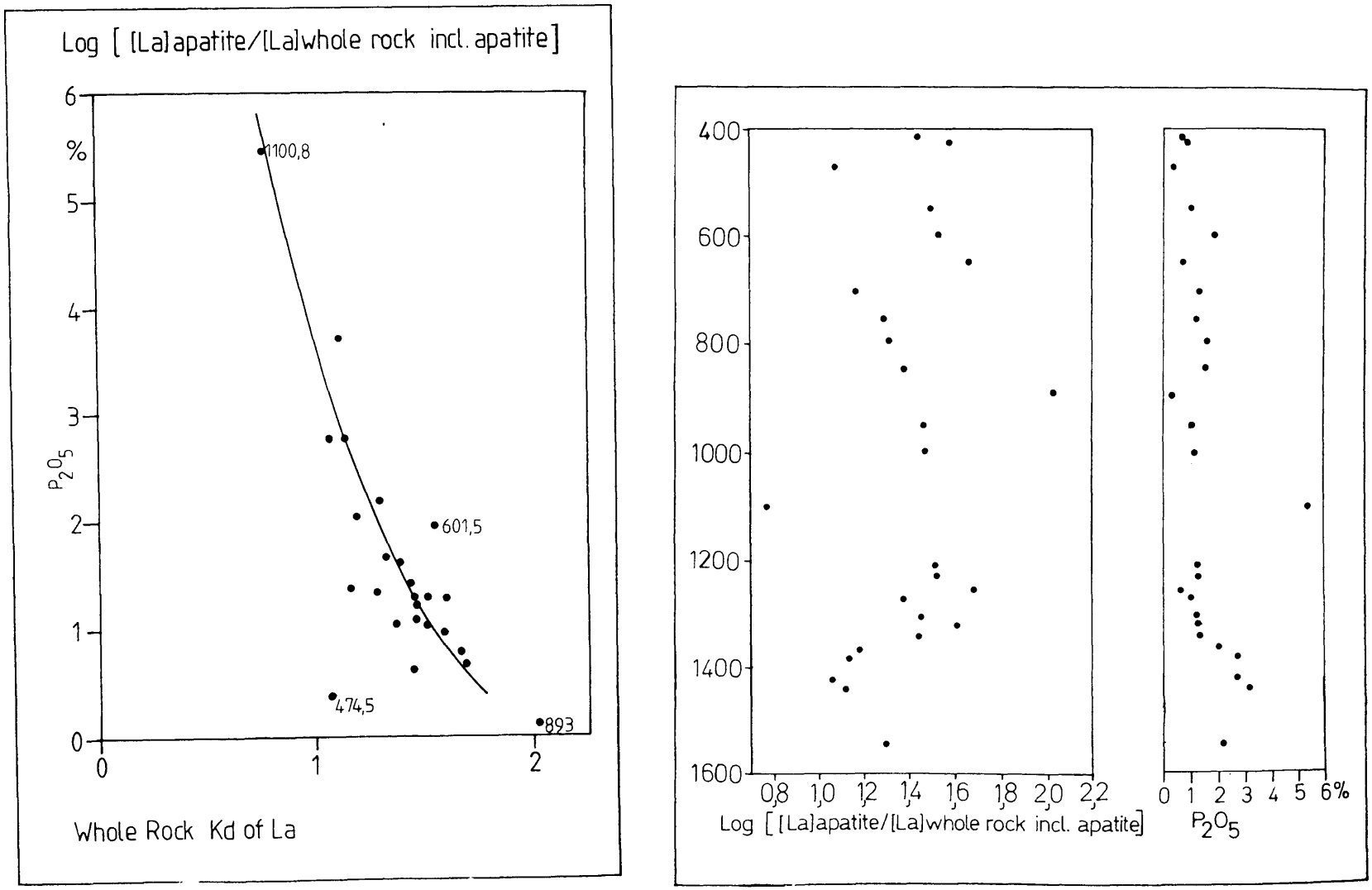

Figure 22: The relationship between REE content of apatite and of the host rock. Note the inverse relationship with P2O5 content.

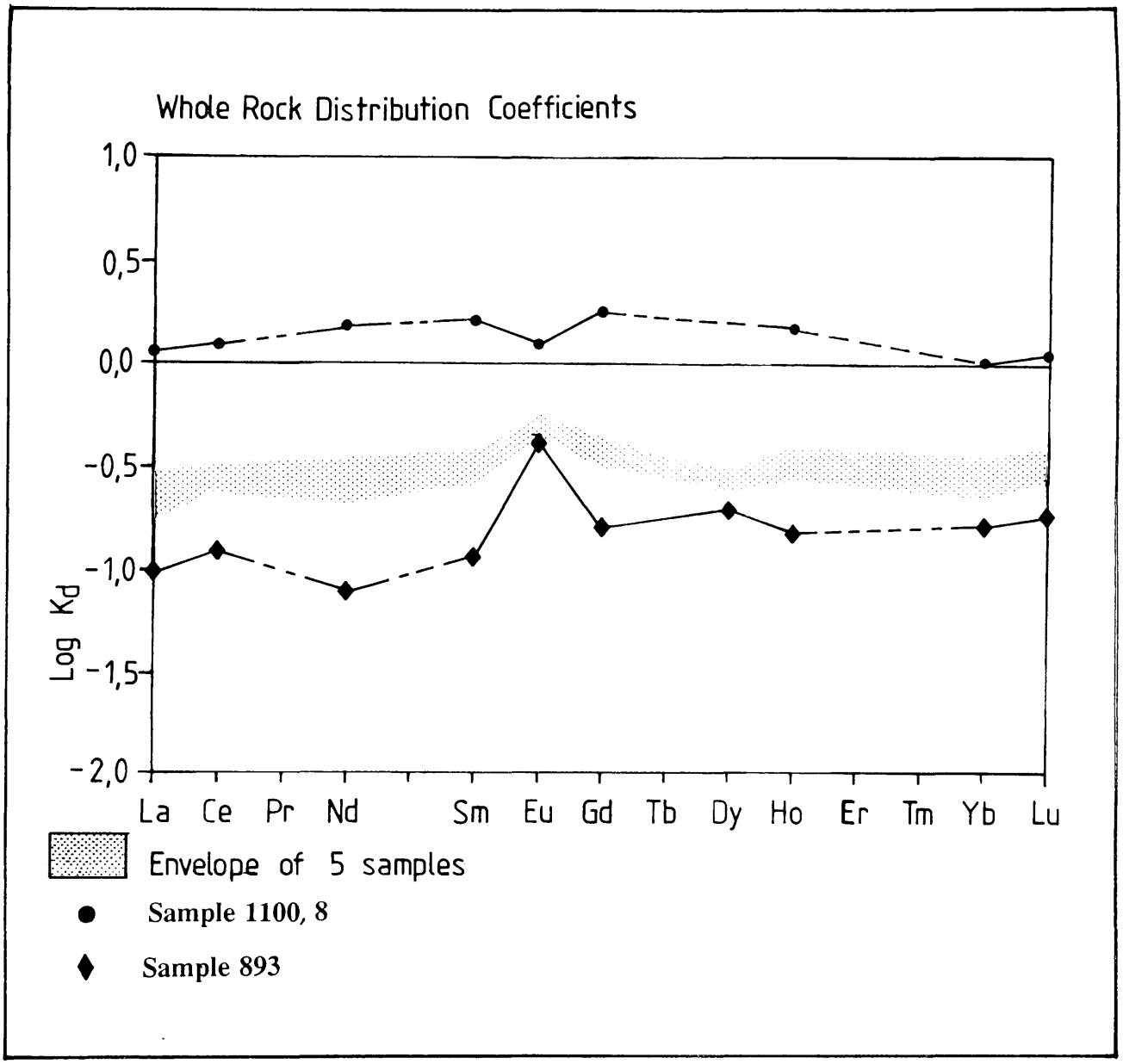

Figure 23: The calculated distribution coefficients (Equation 3, Chapter 6.3.1.1.1). Note that the apatite-rich sample 1100,8 is the only sample with a distribution coefficient above unity. The crystallization of apatite-rich zones therefore produced the only rock type which can cause a depletion in the REE content of co-existing melt.

The distribution coefficient pattern of both apatite and plagioclase have anomalous Eu levels when compared to the remaining REEs. Enrichment or depletion of the Eu, relative to the other REEs can be achieved by a change in the modal proportions of apatite and plagioclase.

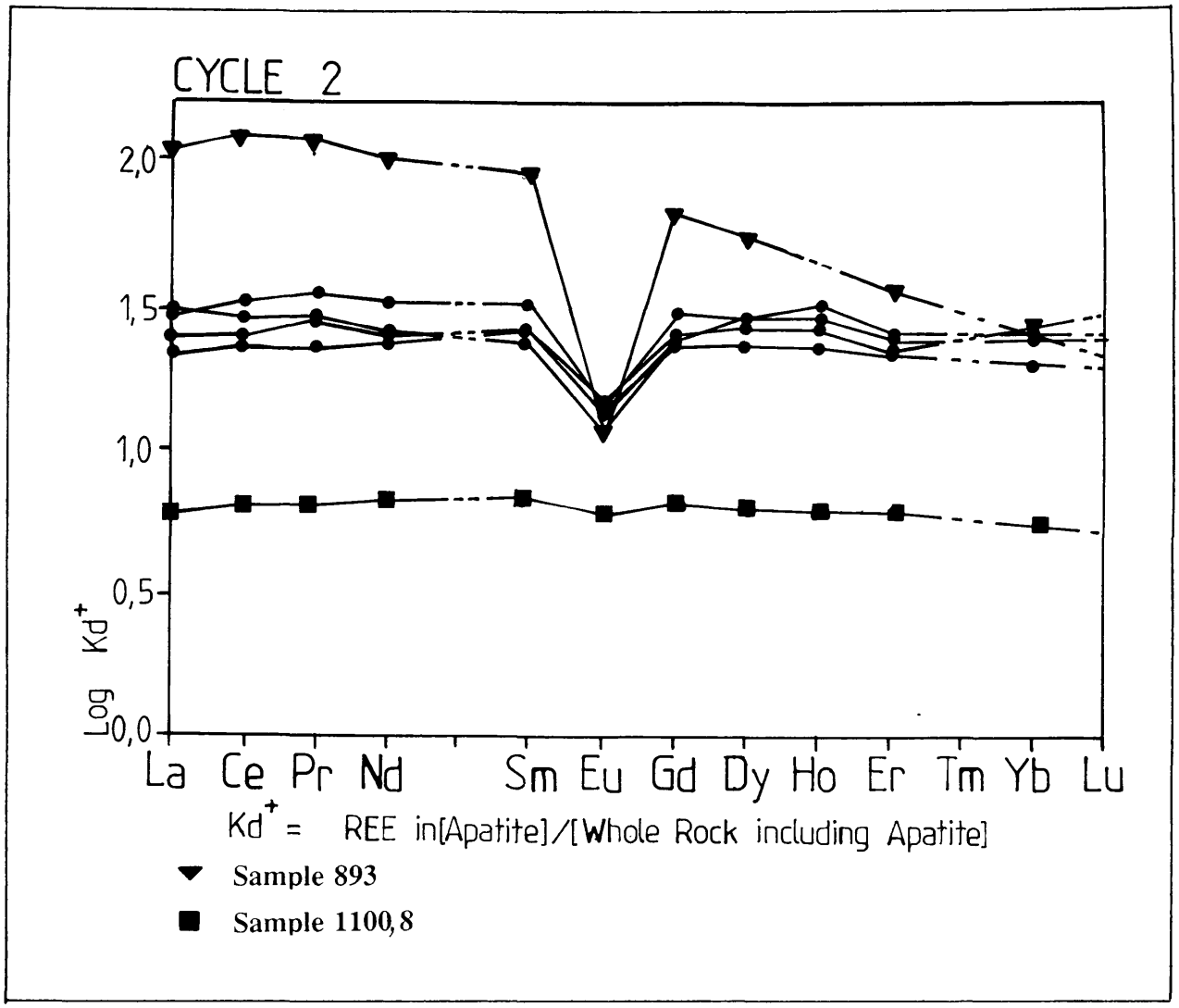

Figure 24: The apatite REE distribution coefficients as determined by the ratio of REE content in apatite to that in the whole rock of samples in cycle 2.

The whole rock REE content is corrected for the REE content of apatite. This correction is made by subtracting the REE content within the apatite, as determined on apatite concentrates, from the whole rock REE analyses. Modal data is used as a measure of apatite content in the whole rock. The resulting "ground mass" values are extremely low, resulting in even greater calculated distribution coefficient for apatite.

Occasionally the absolute lanthanide content of the apatite exceeds the whole rock content. This problem is caused firstly, by the large statistical error in determining accessory amounts of extremely REE rich apatite by modal analysis, and secondly, by analytical difficulties.

To compensate for the analytical difficulties, the whole rock data are corrected by the same factor by which the analyzed NIM L sample is depressed from the published standard value. Corrected REE ratios for samples 1 100.8 and 893 are approximately 17 and 36 respectively. While correcting the same samples by the factor suggested by the SY-3 standard results in partitioning ratios of approximately 38 and 77 respectively.

Fujimaki (1986) determined distribution coefficients for apatite in andesite and diorite. The ratio of La in apatite to ground mass was determined to be 28.2 (diorite) and 14.5 (andesite). As in the Bk-1 cumulates, these ratios do not represent true distribution coefficients but are elevated due to the early crystallization of minerals such as plagioclase. In the case of diorite, the early crystallization of feldspar can concentrate the lanthanides in the apatite by a factor of 4 (Fujimaki, 1986). The crystallization sequence of the Upper Zone gabbro is not straight forward. A large proportion of apatite occurs interstitially to the large silicate grains (Reynolds, 1985a). This texture implies that most of the silicates crystallizes before the apatite. Correcting for the four-fold factor as suggested by Fujimaki, (1986), the distribution ratios for the Bk-1 samples range from 2.23 (sample 474.5) to 32,84 (sample 1 320.8).

Distribution ratios of the lanthanides for apatite are largely exaggerated, implying that the apatite do not crystallize in equilibrium with its host rock. Samples 1 421, 1 379, 1 100.8 and 601.5 are the only samples from the three zones of high apatite, high Ti-magnetite identified by Reynolds (1985a. Please note that the collar depths in this article are reproduced incorrectly). Their corrected distribution ratios are:

Sample	K_d (NIM L)	K_d (Sy 3)	Apatite:Oxide volume ratio
1421	13	8	1:4,5
1379	37	23	1:3
1100.8	9	6	1:2,5
601.5	19	12	1:1

The equilibrium distribution coefficient of La into apatite in a gabbro matrix is approximately 5 (Roelandts and Duchesne, 1979). The distribution coefficient in the apatite-magnetite samples (eg. 1 100.8) approximate the equilibrium

conditions the best. These three zones represent the samples where a Fe-Ti-Mn-P-REE immiscible melt concentrated and can exist within late stage dioritic residue (Reynolds, 1985a). Sample 1 100.8 is also characterized by an apatite:oxide volume ratio of 1:2,5 which is very close to the 1:2 volume ratio suggested as a eutectic mixture at which immiscible Fe-Ti oxide apatite melts separates to form nelsonites (Philpotts, 1967).

7.2 Apatite Rare Earth Element Patterns

7.2.1 Apatite Rare Earth Element Patterns of Bk-1

The REE analyses of apatite from borehole Bk-1 are characterized by a total REE content which varies from 795 ppm at 1 548 m to 4 315 ppm at 423 m with approximately equal amounts of Nd and La (Appendix 4). The chondrite normalized trends are smooth except for marked negative Eu anomalies and, occasionally less distinct negative Ce anomalies (Fig. 25). The trends are typically LREE enriched with a Ce/Yb ratio in the range of 13 to 26. This LREE enrichment is typical of rocks which crystallize from a late-stage differentiate (Tikhonenkova and Udod, 1984). The REE patterns of the apatites (Fig. 26) are grouped according to the geochemical cycles identified in chapter 6.3. Within these groups the REEs form closely matched parallel patterns with fairly constant Ce/Yb ratios. The Ce/Yb ratios are:

Cycle 1: 19 to 37
Cycle 2: 26 to 61
Cycle 3: 25 to 29
Cycle 4: 36 to 45

There is a marked degree of overlap in REE concentrations amongst the cycles (Fig. 26). Average REE trends for each cycle show that the negative Eu anomaly increases with each successive cycle from cycle 1 to 4. The mean total REE content has a similar enrichment trend from cycle 1 to 4, with the exception of cycle 3 which has the lowest REE content (Fig. 26).

7.2.2 Apatite Rare Earth Trends - eastern Bushveld

The REE concentration in apatite samples from the eastern Bushveld, as in the western Bushveld, are also in the order of a thousand times enriched when compared to chondritic levels. Their LREE enriched nature is reflected by the Ce/Yb ratios with a range of 24 to 48. Apatite from the eastern Bushveld tends to have significant negative Eu anomalies (Fig. 27), with the exception of samples 11d and 9d which, unlike the remaining samples, have no significant Eu anomaly. A general enrichment in the REE content of apatite with stratigraphic height is evident.

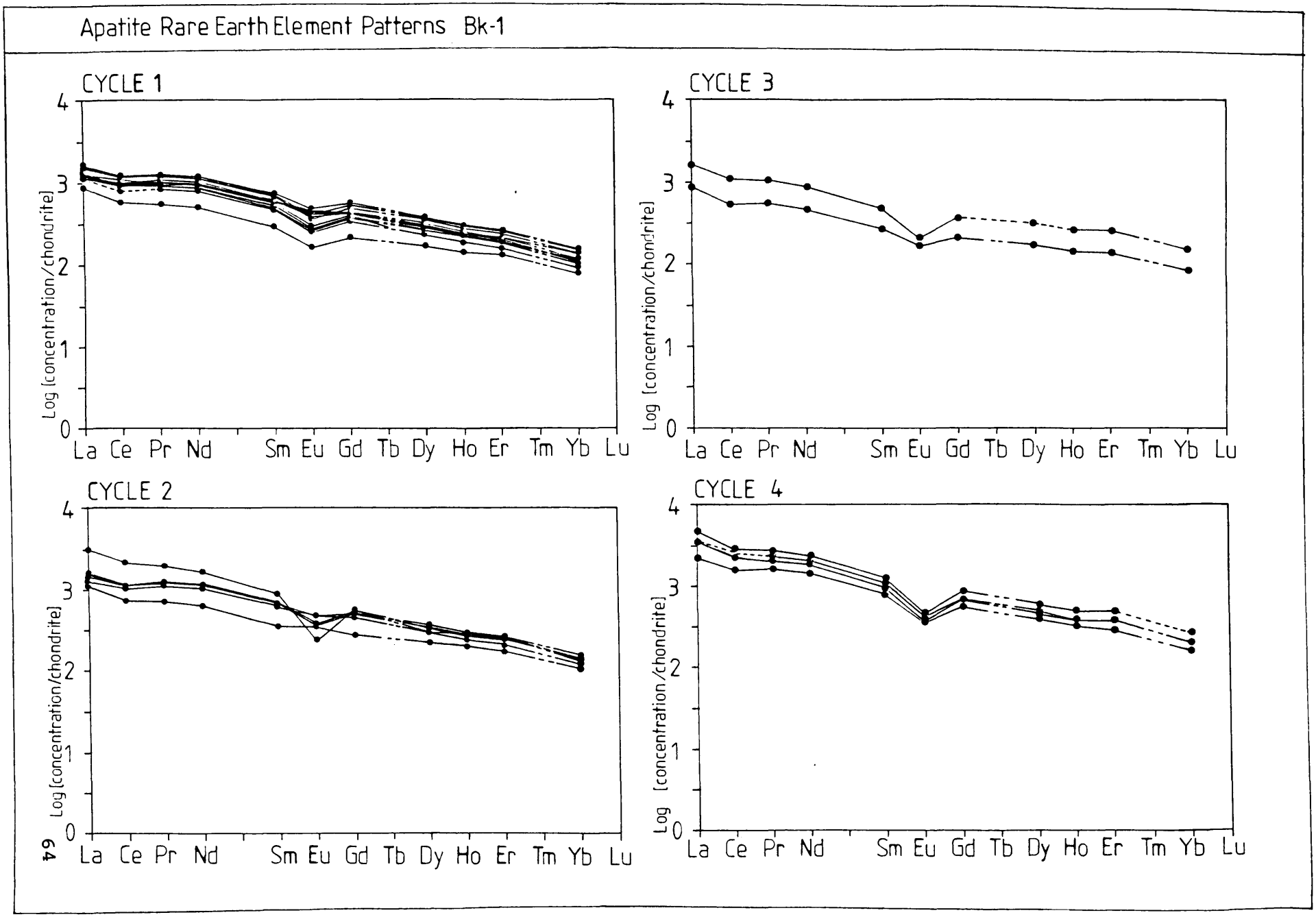

Figure 25: Chondrite normalized REE patterns of apatite in different cycles of the Bk-1 Borehole.

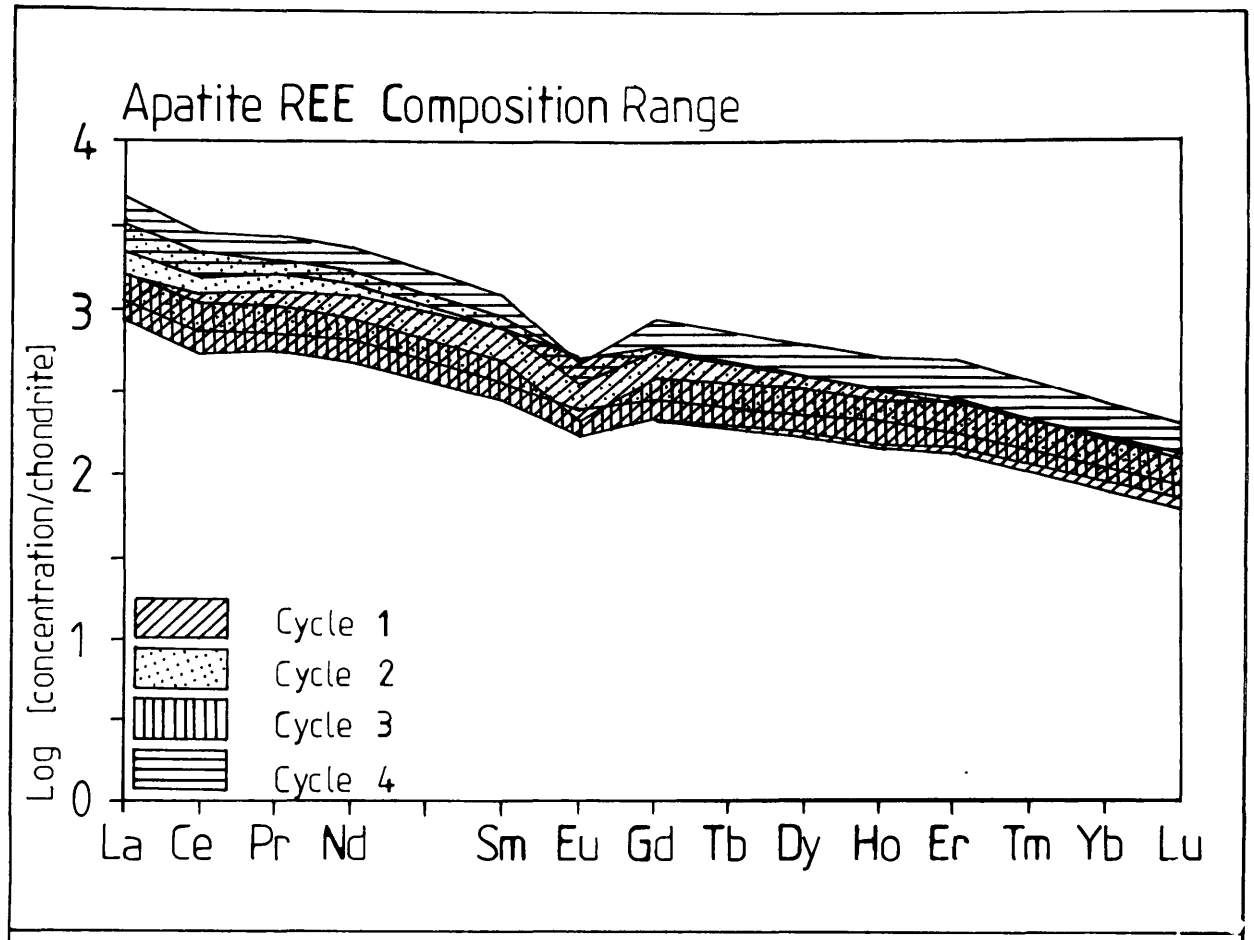

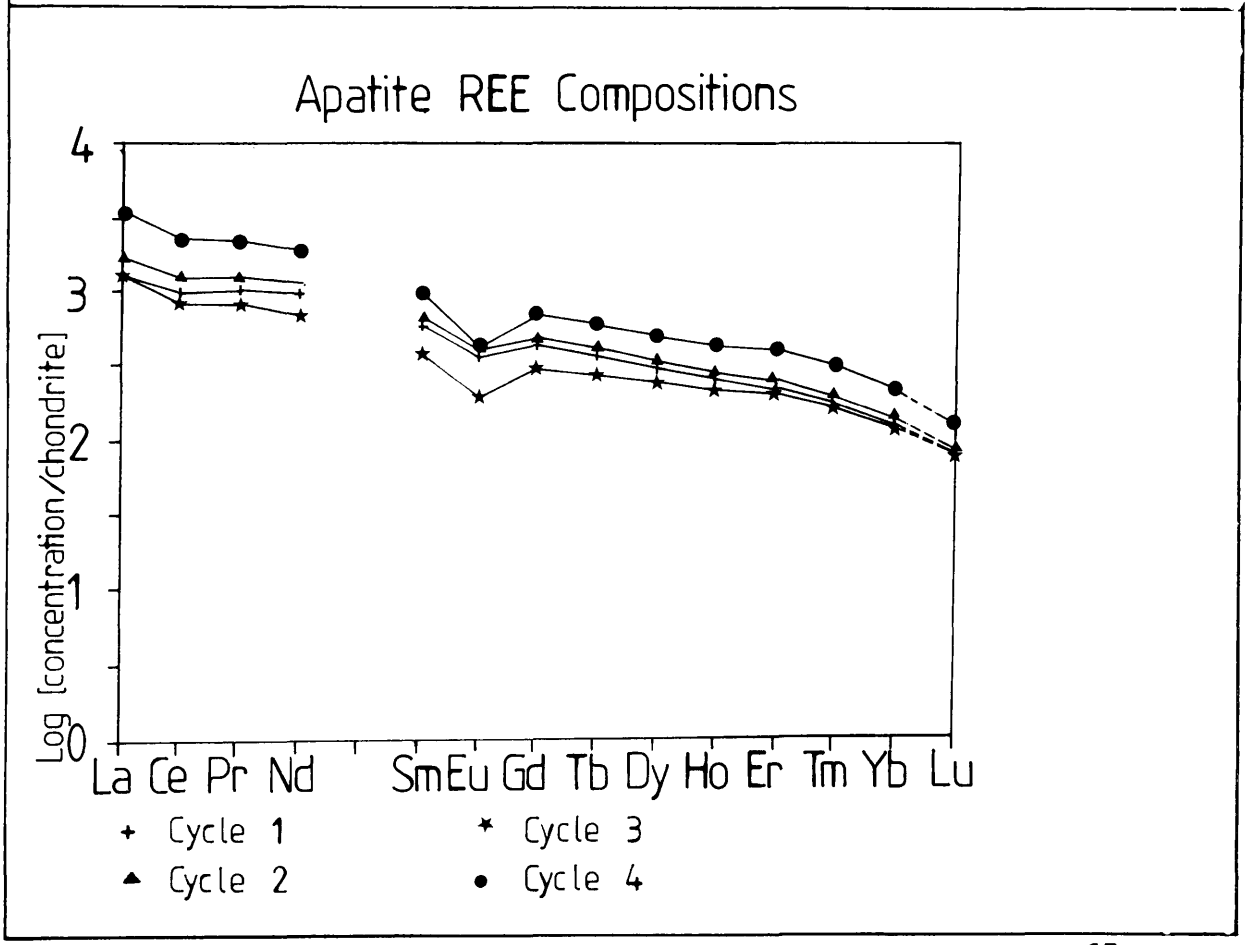

Figure 26: The mean REE composition of apatite in the 4 identified cycles.

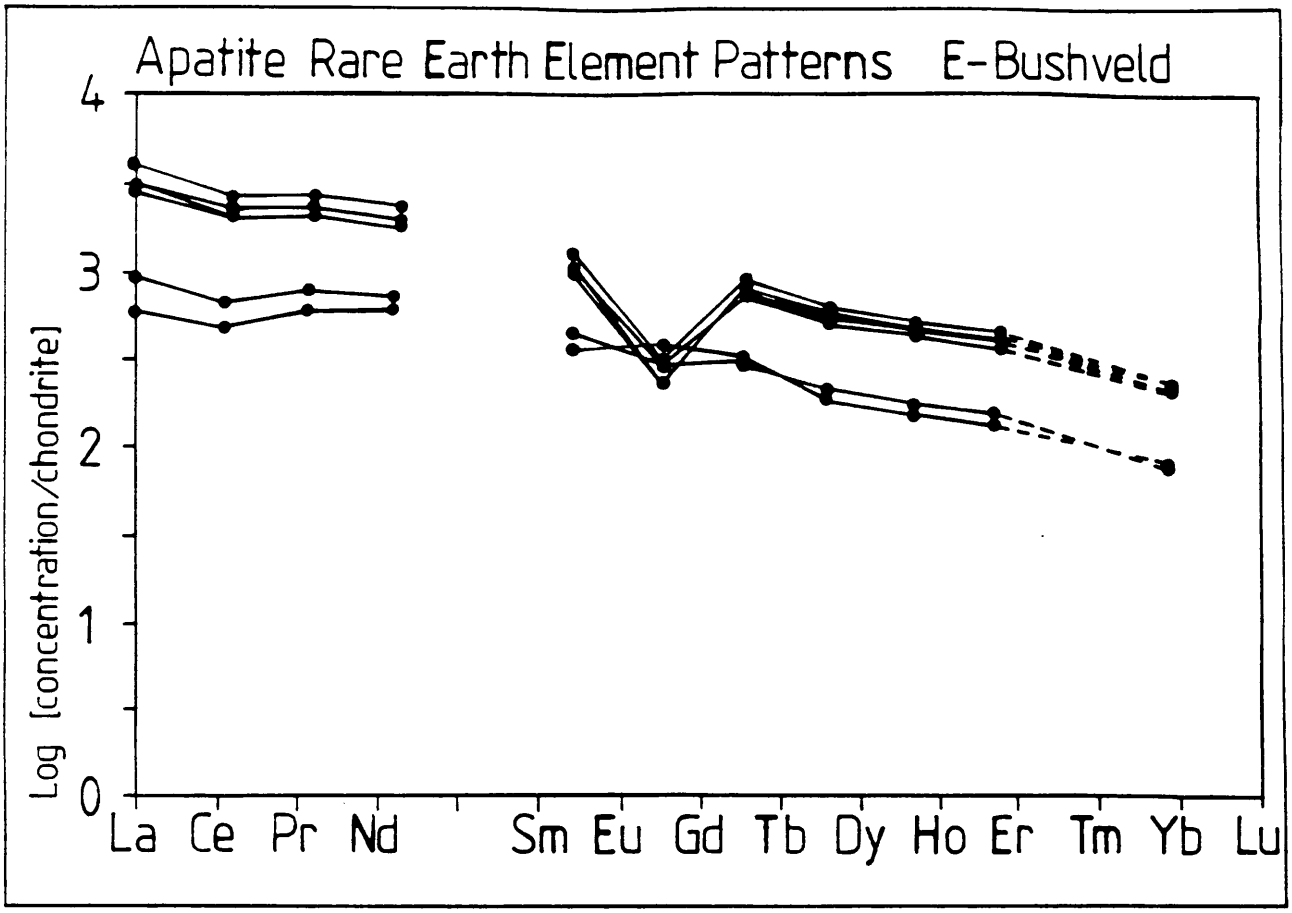

Figure 27: The chondrite normalized REE patterns of apatite from the Upper Zone in the Roossenekal district, eastern Bushveld.

7.2.3 Comparison of the Apatite Samples

The overall higher Ce/Yb ratios of the apatite samples from the eastern Bushveld indicate that they are slightly more LREE enriched than those from the Bk-1 section. This relative enrichment is evident in a ternary plot of the light, medium and heavy REEs (Fig. 28). Significant overlap of the eastern and western Bushveld samples is evident but, the eastern Bushveld samples are shown to be biased toward the LREE end point.

Fleischer (1983) determined various LREE ratios for apatites attained from various rock types. The data from the Bk-1 and the eastern Bushveld compare well with the field defined by granite, granodiorite, gabbro and syenite (see Figure 25). The Bushveld data is biased toward the apatite of sedimentary origin. The bias toward the sedimentary field can be indicative of assimilation of Transvaal rocks.

7.3 Whole Rock Rare Earth Element Patterns

7.3.1 Eastern Bushveld Whole Rock Samples

The whole rock chondrite normalized REE patterns of the eastern Bushveld (Fig. 30) are characterized by a marked degree of LREE enrichment with, a Ce/Yb ratio in the range 13 (Sample 17C) to 31 (Sample 20B). These patterns are further characterized by a substantial positive Eu anomaly which is especially pronounced in the stratigraphic uppermost samples (no. 2D, 3D) and samples from subzone B.

Slightly positive Er and Nd anomalies, which can possibly be the result of the analytical procedure, are present in the chondrite normalized patterns. The Ce value seems to be slightly depressed. Extensive overlapping of the REE patterns are found from subzone to subzone and therefore the patterns from the various subzones cannot be distinguished. Subzone D has a substantially higher REE content, which can be ascribed to the comparatively high modal proportion of apatite in the rocks.

7.3.2 The Bierkraal 1 Borehole Whole Rock Samples

The chondrite normalized pattern of the samples originating from the Bk-1 are LREE enriched with a Ce/Yb ratio ranging from 7 (1 128,7 m) to 31 (845,75 m). The whole rock REE patterns are grouped according to the cycles defined in chapter 6.3 (Fig. 31). The cycles cannot be distinguished by means of absolute REE content. Cycle 1 exhibits the greatest range in REE concentrations, while the average values for each cycle shows an enrichment of the REEs with increasing stratigraphic height, except in the case of cycle 3 (Fig. 32). As in the case of the apatite samples, the average REE pattern of cycle 3 lies below that of cycle 1.

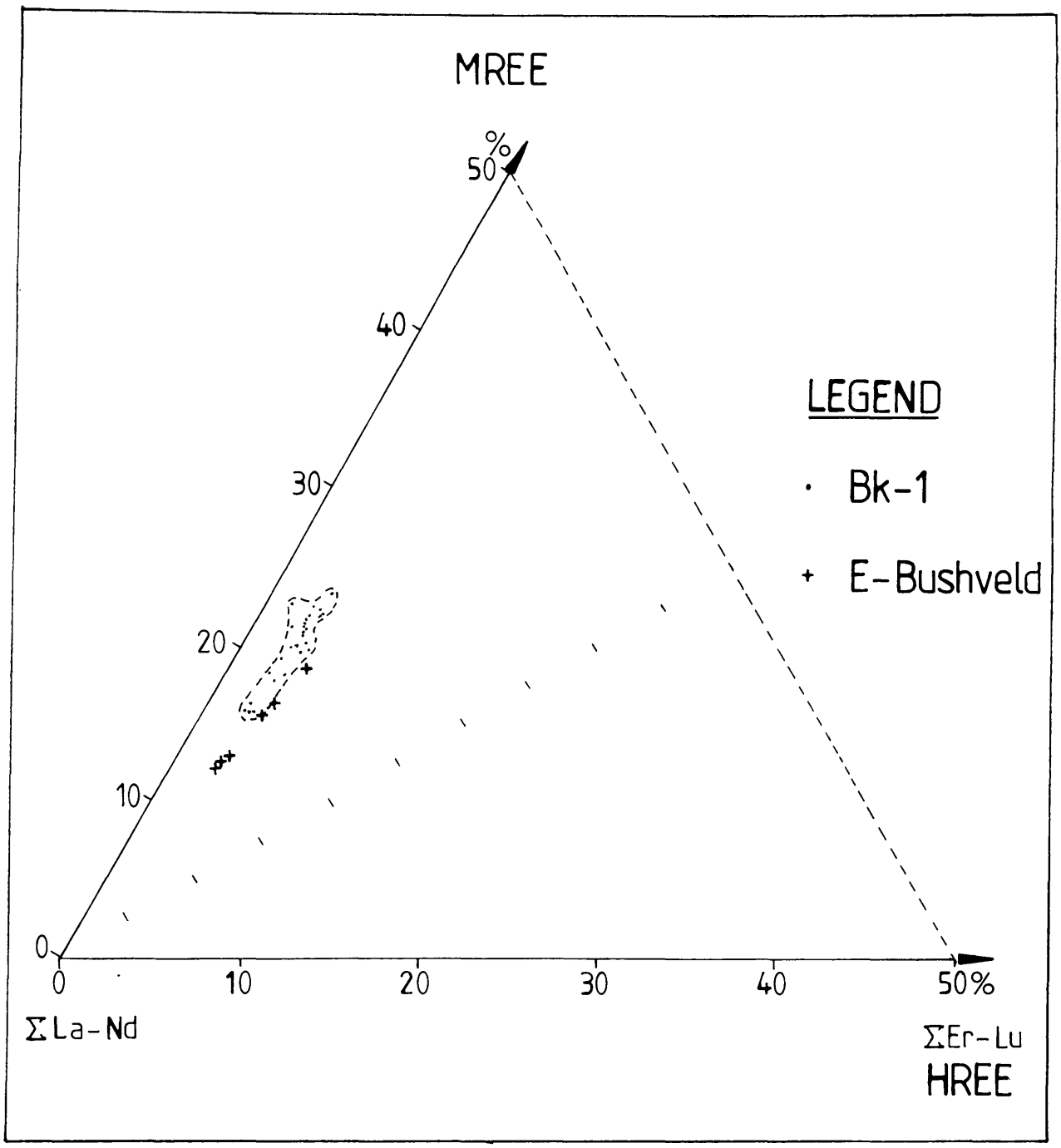

Figure 28: The ratios of LREEs, MREEs and HREEs in apatite. The points form an elongated field. This LREE enrichment is typical of fractionation where copious amounts of plagioclase have crystallized.

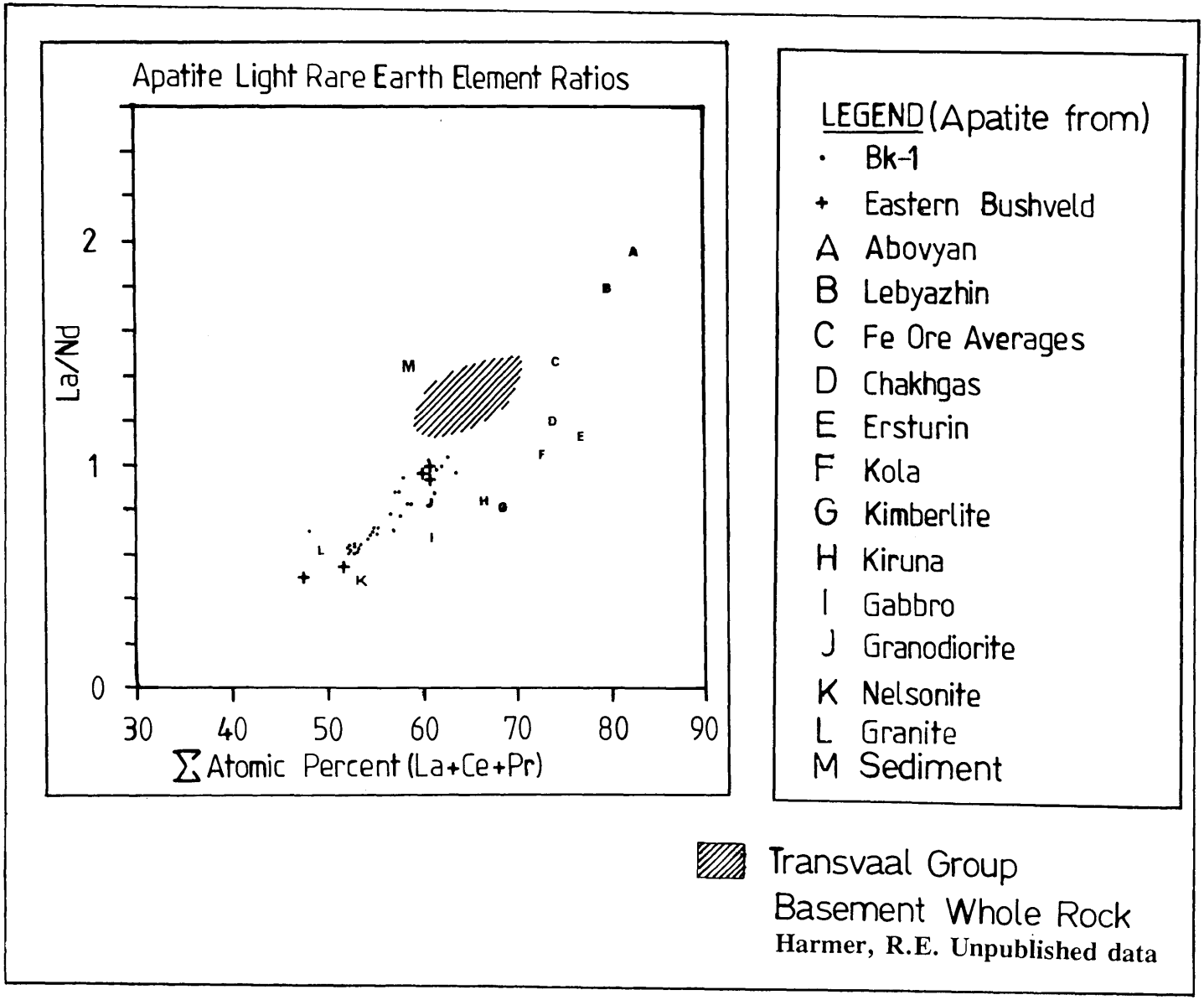

Figure 29: LREE ratios of apatite in various rock types. Note the position of the Bushveld apatite in relation to those from sedimentary rocks and to the whole rock composition of the Transvaal Group sediments.

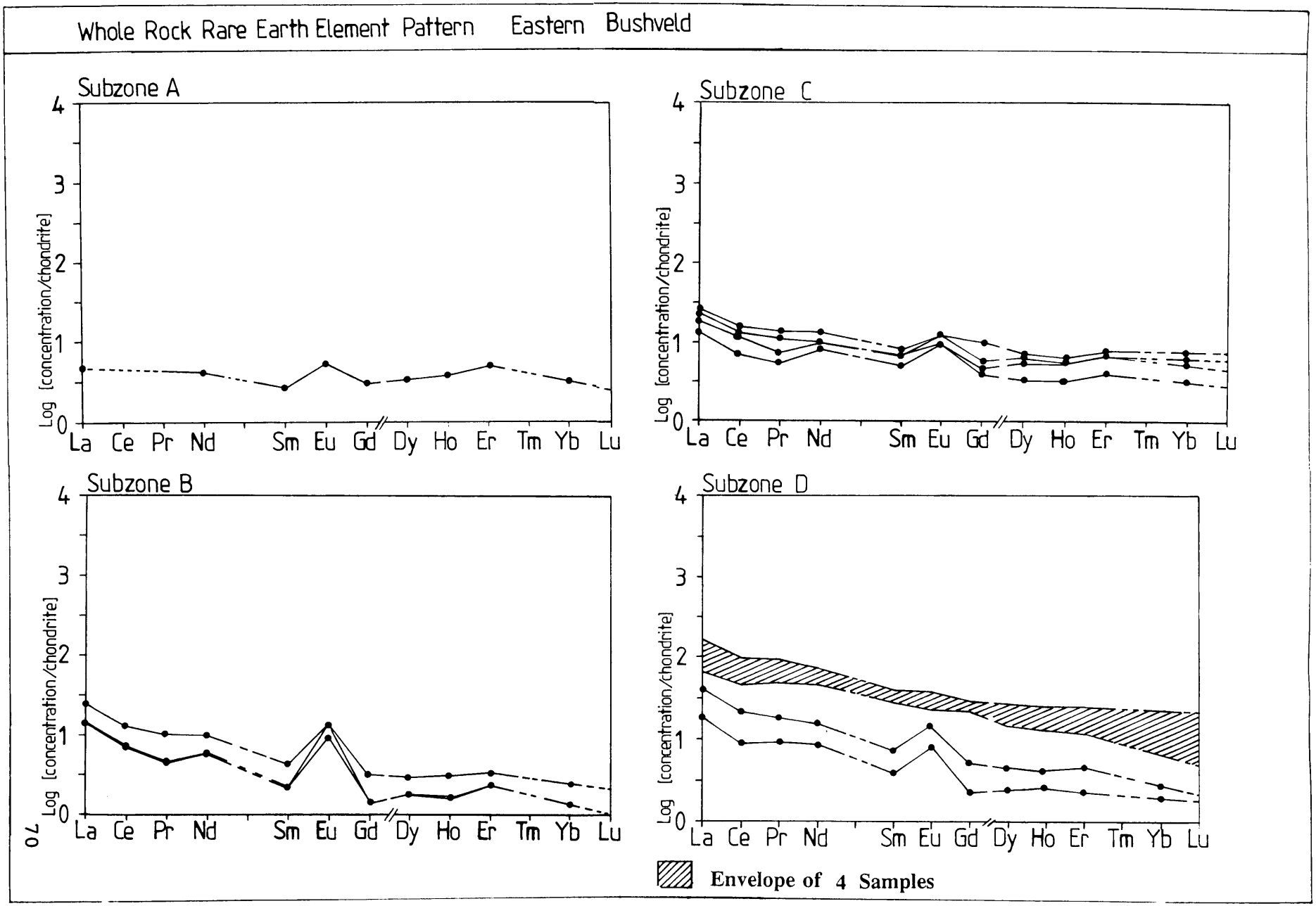

Figure 30: Whole rock chondrite normalized REE patterns, eastern Bushveld.

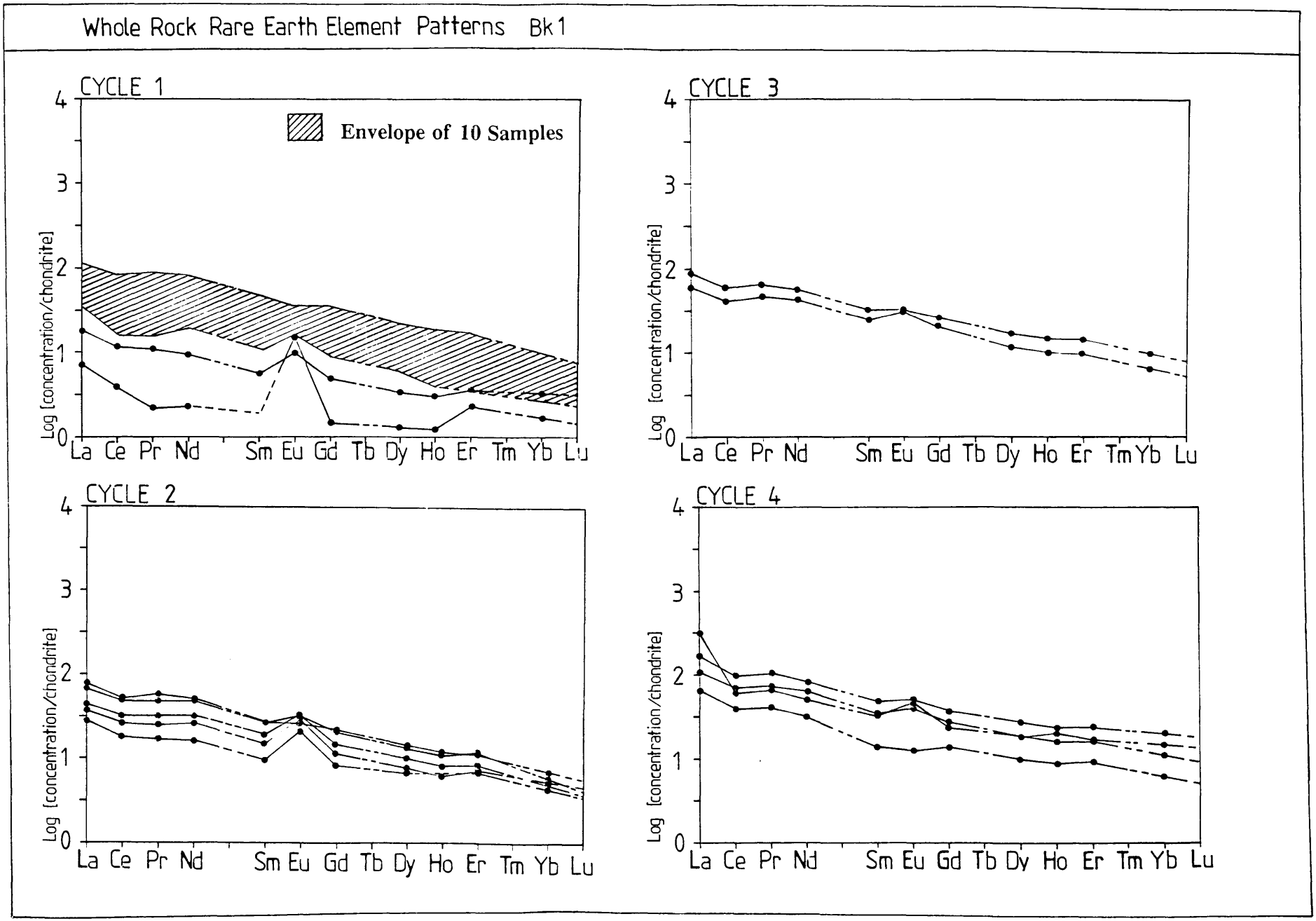

Figure 31: The whole rock chondrite normalized REE patterns from the 4 cycles in the Bk-1 borehole.

7.3.3 Modal Effects on Whole Rock Samples

The REE pattern of apatite is indicative of the high distribution ratio of the middle lanthanides and the low distribution ratio of divalent Eu (Fujimaki, 1988). High concentrations of the REEs in the whole rock samples of borehole Bk-1 are due to elevated apatite concentration. Whole rock patterns are dominated by the partitioning trends of the lanthanides in the apatite, with a relative depletion of Eu, La and Ce, especially where modal proportions of apatite are significant.

Conversely, the whole rock samples which have relatively low REE contents and low apatite contents, are characterized by a significant positive Eu anomalies and less significant negative La and Ce anomalies. Whole rock REE patterns, differ according to the absolute content of REEs. This effect is predominantly controlled by modal proportions, particularly that of apatite and plagioclase. Plagioclase favours the partitioning of the LREE over the HREE, while divalent Eu partitions strongly into the plagioclase (Fujimaki and Tatsumoto, 1984). Large positive Eu anomalies are associated with plagioclase-rich Upper Zone samples which have low absolute REE content and minimal apatite.

The LREE enrichment caused by the modal effects of plagioclase is, however countered by the selective partitioning of the MREE and HREE into clinopyroxene. Orthopyroxene has similar relative partitioning trends as the clinopyroxene. The absolute distribution coefficients are too small to have a significant effect on the whole rock patterns.

Olivine occurs in significant modal proportions in the Upper Zone. The distribution coefficients of the lanthanides are so small that olivine can be seen as an effective dilution agent of the REEs. The dilution by olivine has no effect on the REE patterns (Fujimaki and Tatsumoto, 1984).

7.3.4 Marginal Rocks

During the investigation of marginal rock types of the Bushveld Complex, at least two distinct parental magma types were identified by Irvine and Sharpe, (1986). These two magma types are referred to as the A and U melts, owing to plagioclase (anorthositic) and olivine (ultramafic) which are the liquidus minerals of the respective melts. In order to test whether the marginal rock can be the source melt of the Upper Zone rocks, the data in this investigation is compared to the composition of the marginal rock.

The REE composition of the two compositional end-member marginal rocks as reported by Hatton and Sharpe (1989), indicates that the marginal rocks are enriched in the LREE with a Ce/Yb ratio ranging from 10.9 to 35,8. The ultramafic marginal rocks, U type, are characterized by a slight enrichment of the LREE compared to the A (anorthositic) type. The A type marginal rocks are further distinguished from the U type by having a slight positive Eu anomaly (Figure 33).

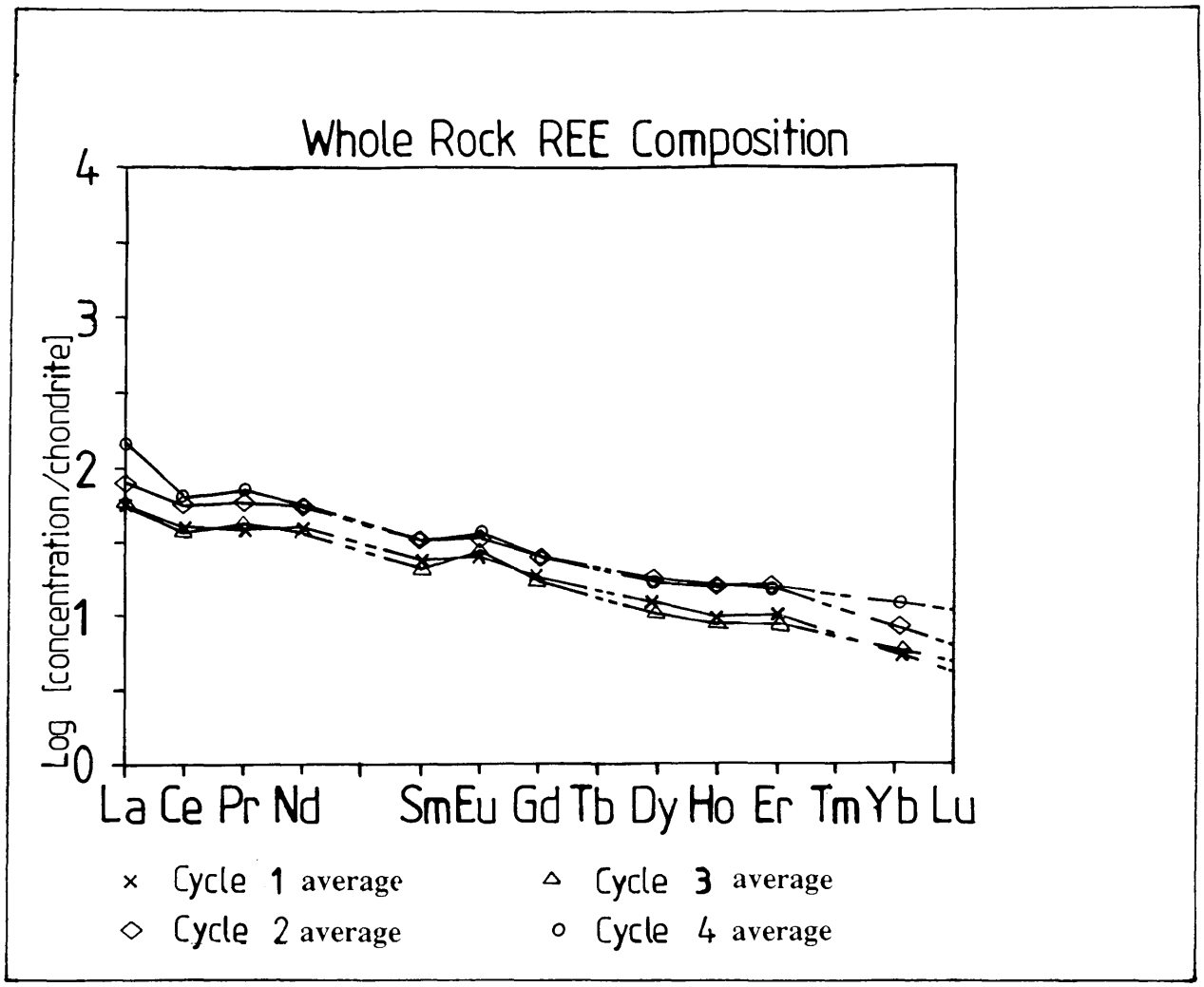

Figure 32: The mean chondrite normalized REE patterns of Bk-1. The mean REE contents were determined for cycle 1 to 4 and then normalized to chondrite.

To compare the Bk-1 and eastern Bushveld samples with the marginal rocks, the REE concentration of the whole rock samples are normalized to each of the two postulated parental magma types (Irvine and Sharpe, 1986). Samples CO045 and CO230 (Hatton and Sharpe, 1989) are taken as representative of the A and U magma types respectively.

The REE concentrations in the Upper Zone rock types are mostly of the same order as the marginal rocks. Only the apatite-rich layers are up to 10 times enrichment relative to the marginal rock types (Fig. 34). Similar trends are identified in the Skaergaard intrusion where the gabbros have very similar absolute and relative REE content to the marginal rocks. The uppermost gabbro samples, which have an enrichment of up to 10 times relative to the marginal rocks (Haskin and Haskin, 1968) are the exception. A disproportionate enrichment in the LREE relative to the marginal samples CO045 (A) and CO230 (U) (Hatton and Sharpe, 1989) is demonstrated by the Nd/Yb ratio. Such an enrichment is to be expected as a result of fractionation processes. The Ce and La values are, however, not as enriched as the remaining LREE. Although the apatite-rich samples are also enriched in TREE, they have a depressed Eu anomaly. This, in particular, is attributed to the modal effects of plagioclase and apatite.

The whole rock REE patterns are controlled by modal apatite and feldspar. Rocks sampled in this study can be the product of fractional processes of either the U or the A type magmas or mixtures thereof (Fig. 35). There are no indicators from the REE data that links the Upper Zone to the one or other magma types.

7.3.5 Biotite Rare Earth Element Patterns

The separation procedure for the biotite samples is generally ineffective (Fig. 2) and it is not possible to obtain sufficient material from the Bk-1 borehole. Three biotite samples from the Roossenekal district of the eastern Bushveld and supplied by G. von Gruenewaldt are included in the investigation. These samples originate from the subzones D and C of the Upper Zone.

The biotite in the Upper Zone is interstitial to the major silicate and oxide phases which indicates that it is a late crystallizing phase. Since the REEs are incompatible elements, the interstitial fluids will probably be rich in the REEs and any biotite crystallizing from these fluids will be enriched in such elements.

The biotite samples are 3 to 10 times more enriched in the REEs than chondrite (Fig. 36). Several biotite samples listed in Appendix 10 are discarded because the REE content is below the detection limit.

The modal proportions of biotite are rarely in the percent range and can therefore not play any significant role in influencing the REE trends of the Upper Zone.

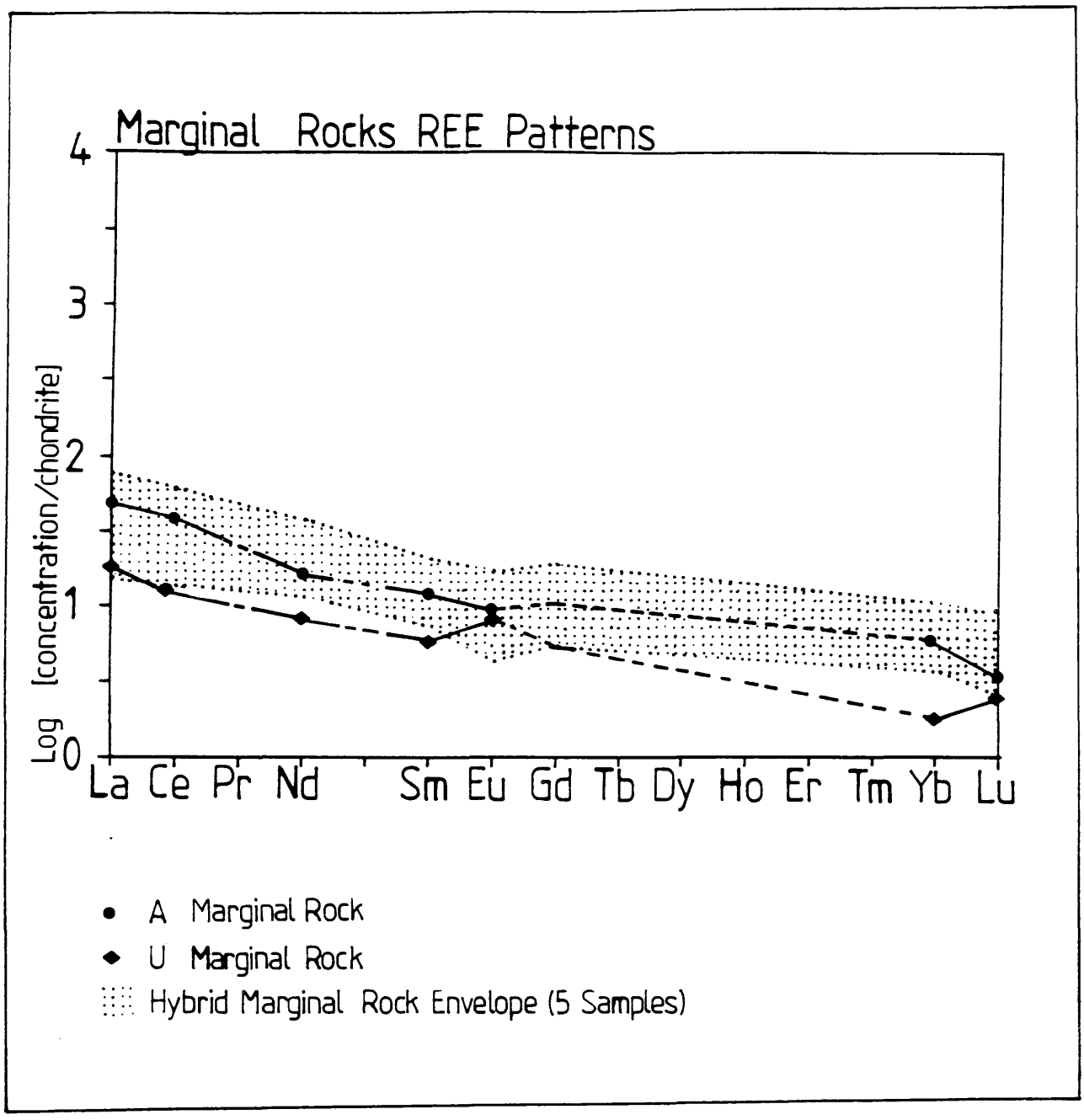

Figure 33: The chondrite normalized REE patterns of the marginal rocks of the Bushveld Complex (Hatton and Sharpe, 1989). Note the slight difference between the patterns of the A and U magma types.

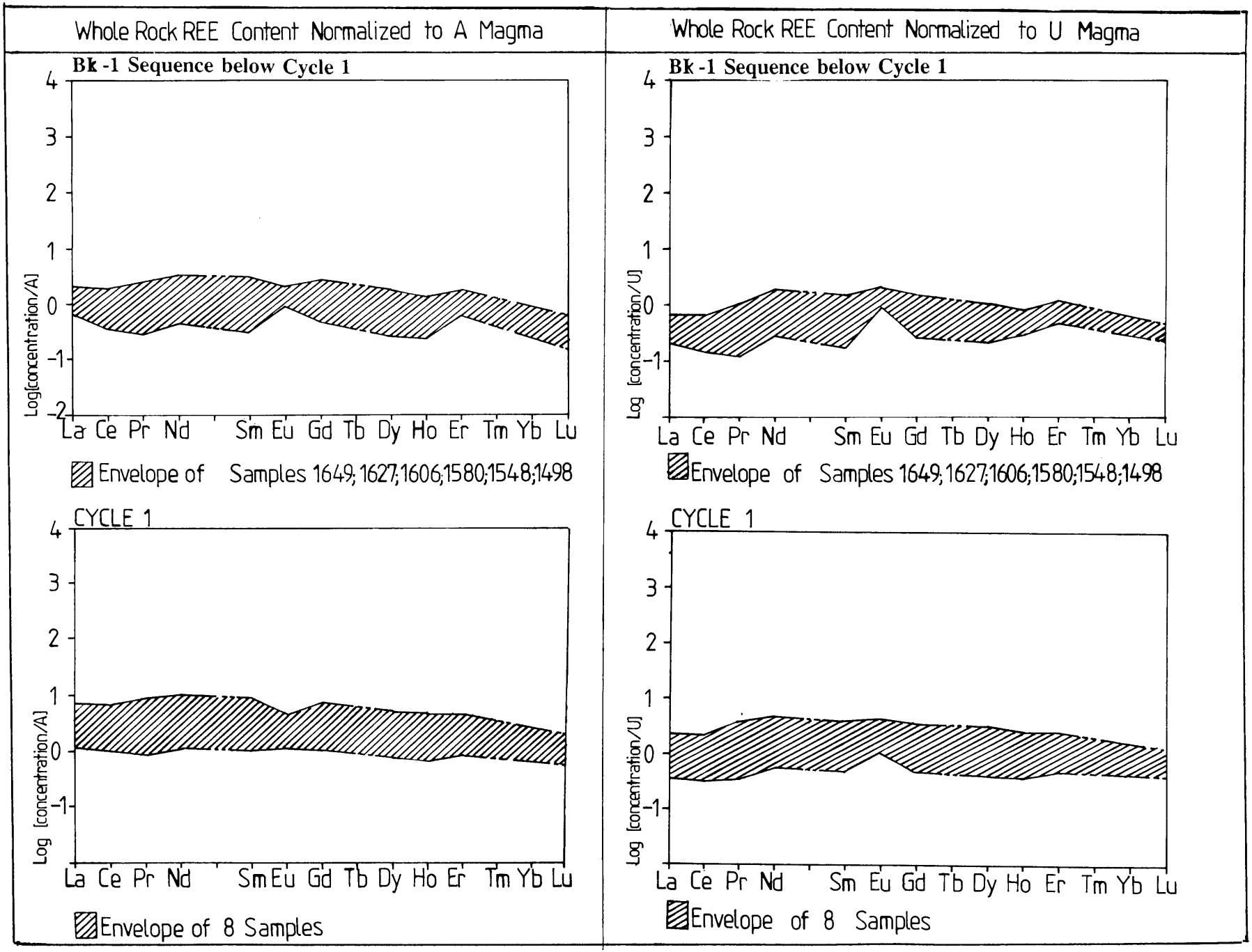

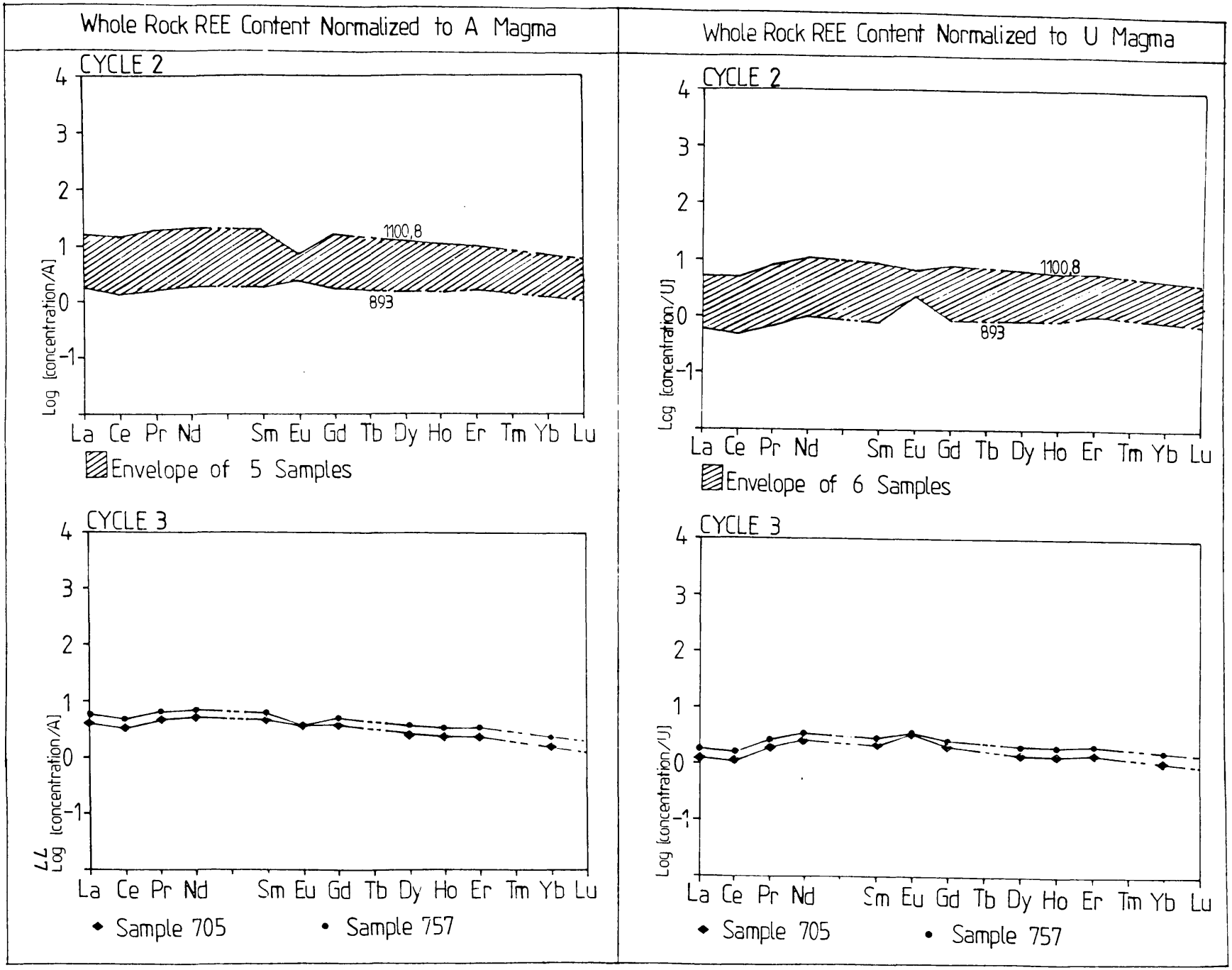

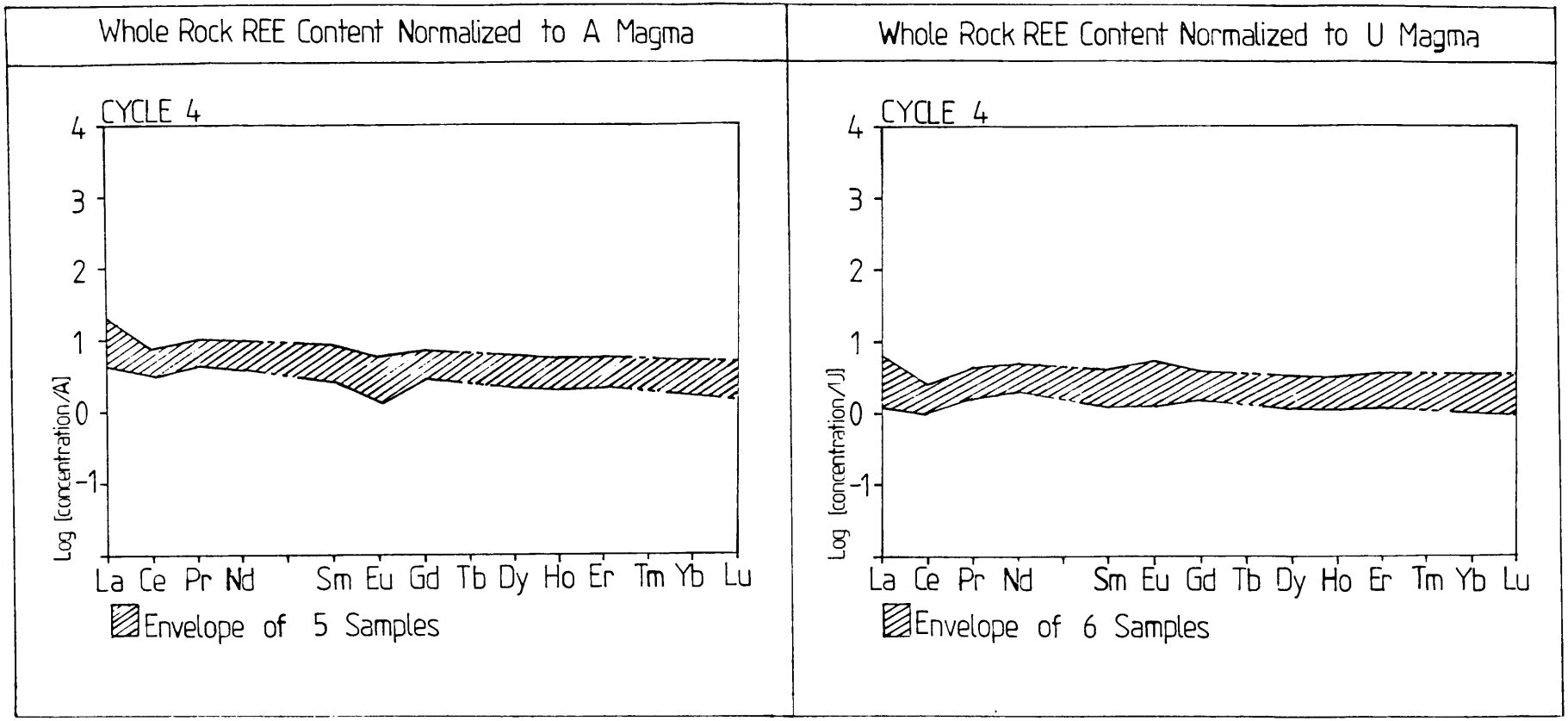

Figure 34: Whole rock REE contents normalized to the A and U magma types (Hatton and Sharpe, 1989). Note that the resulting two patterns are very similar. The distinguishing feature is the relative REE enrichment and the nature of the Eu anomaly. These plots cannot distinguish whether the A or U magma is the source magma for the Upper Zone.

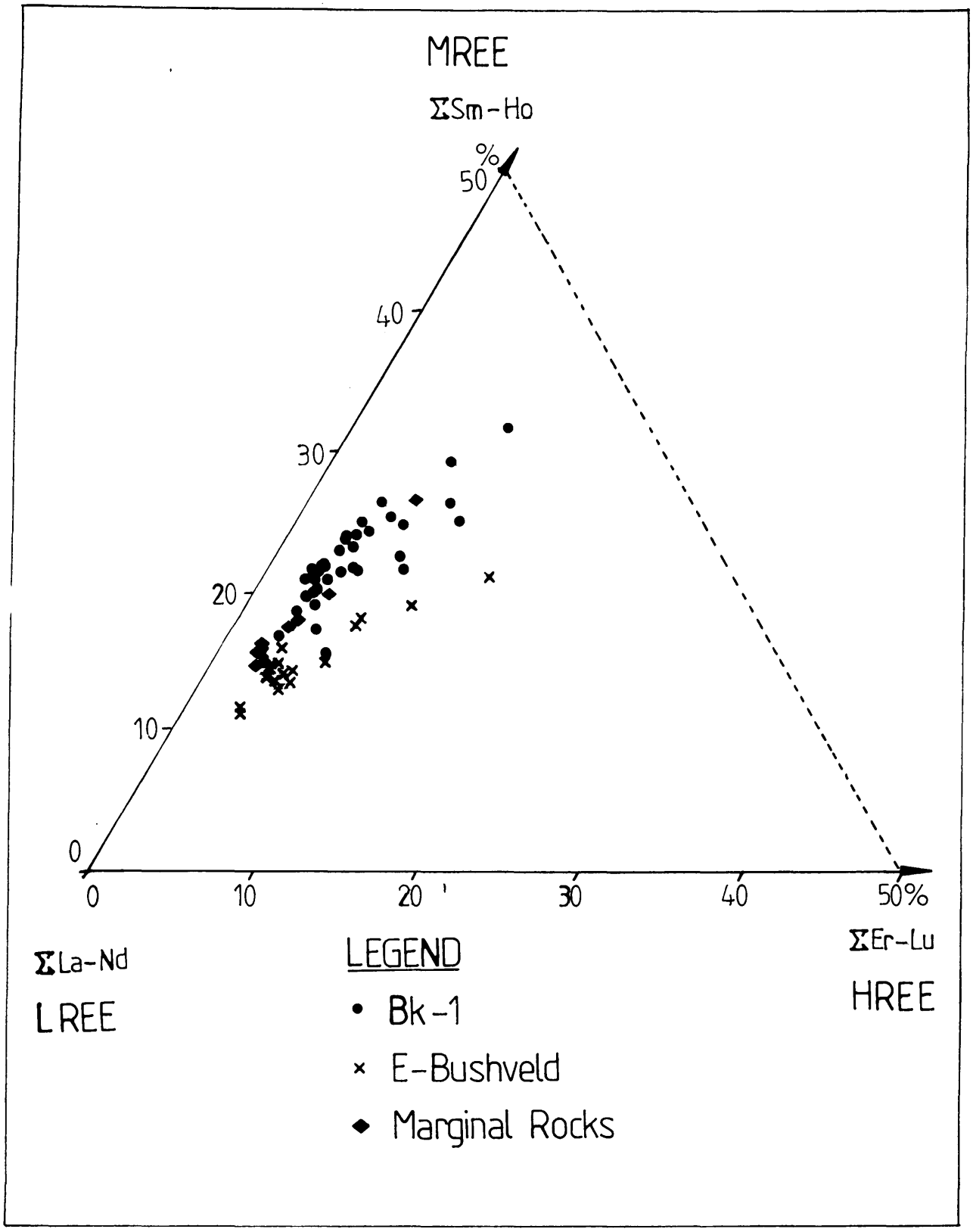

Figure 35: The LREE, MREE and HREE ratios of the whole rock samples. Note that the marginal rocks cannot be distinguished from the Upper Zone samples in this plot.

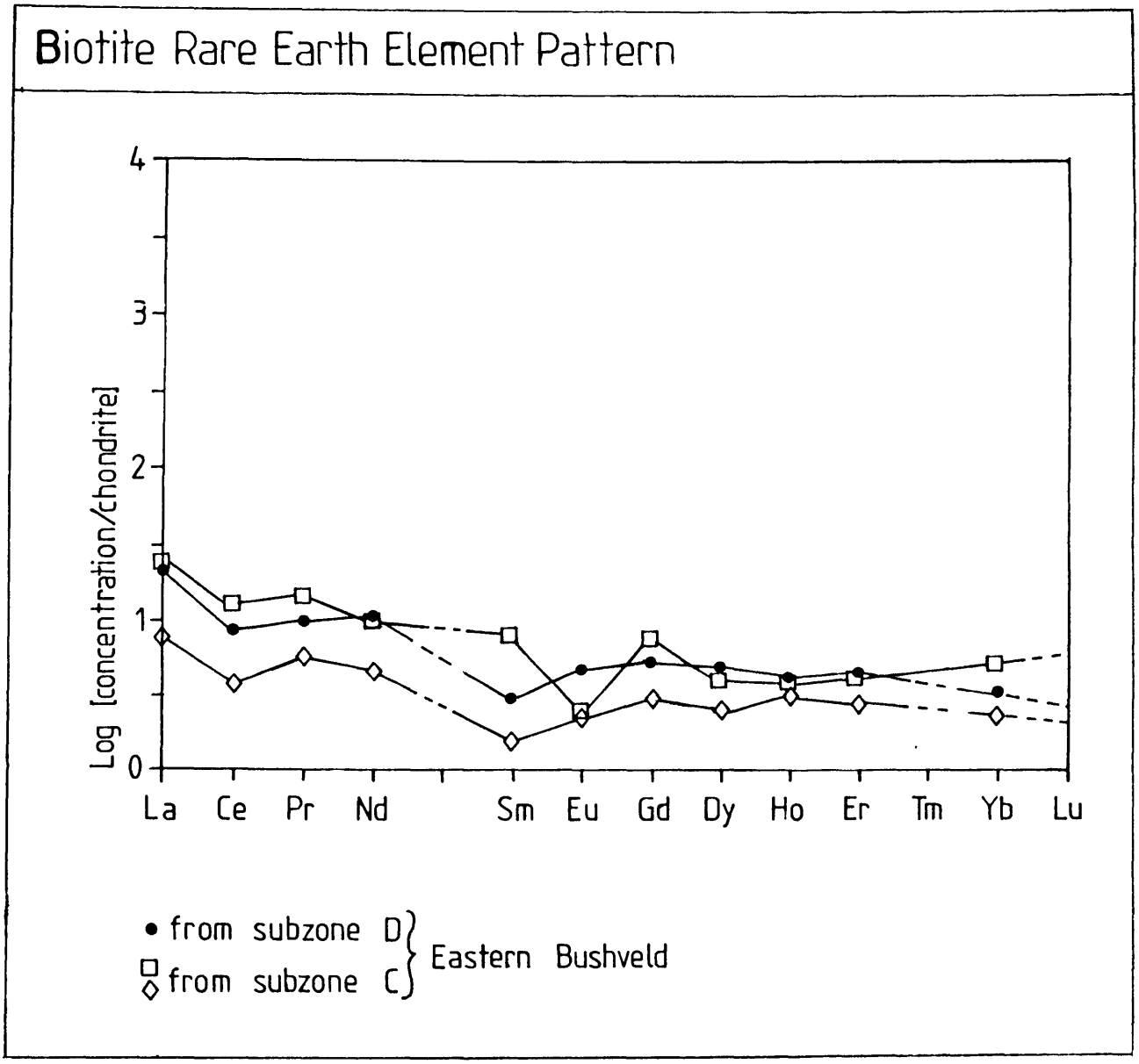

Figure 36: The chondrite normalized patterns of biotite from the Upper Zone in the Roossenekal district of the eastern Bushveld Complex.

7.3.6 Alteration and Metamorphism

Alteration processes and metamorphism seem to have little effect on REE patterns, except under extreme hydrothermal conditions (Giuliani et al., 1987). The mobility of the lanthanides depends upon the presence of complexing anions such as carbonate, phosphate, fluorine as well as high water to rock ratios (Giuliani et al., 1987). Chlorine complexing is an effective process which permits mobilization of the LREE (MacLean, 1988). Alteration can cause both the enrichment and depletion of the REEs in the host rock, while relative LREE (MacLean, 1988) and HREE (Giuliani et al., 1987) enrichment is also possible. MacLean (1988) reports that the alteration in the Phelps Dodge massive sulphide deposit is associated with constant REE ratios (i.e. smooth changes in the REE chondrite normalized patterns) which he ascribes to a dominant complexing agent responsible for the mobilization of all the REE. Giuliani et al., (1987) found that the REE patterns of the alteration zone of skarn deposits of central Morocco depend on the mineral phase precipitating from the hydrothermal fluids.

The possible effect of alteration in the Bk-1 samples is difficult to evaluate because of the lack of any significant evidence of alteration processes. There is no evidence for the large proportions of water-rich fluids which are required to mobilise the REEs. Boudreau et al., (1986) identified three types of apatite within the Skaergaard and Bushveld complexes: 1) Cumulus apatite (essentially fluorapatites); 2) Non-cumulus apatite and 3) Cl-rich apatites associated with the PGE-rich layers. Boudreau et al., (1986) argues that the crystallization of interstitial melt exsolves a Cl-rich fluid which will transport the lanthanides and alkali elements. Apatite can then equilibrate with the Cl-rich hydrothermal fluids and consequently, become enriched in the REEs and chloride.

The fluorapatite concentrates from the Bk-1 (Fig. 13) exhibit no substantial zoning. The lack of zonation can be a result of analytical difficulties, due to the large excitation area of the microprobe technique. If the lack of zonation is confirmed and not related to analytical difficulties, it can be assumed that chlorite-phosphate hydrothermal alteration is not significant in the Upper Zone of the western Bushveld.

7.4 Detailed Trends in Bierkraal 1 Borehole

All available data from borehole Bk-1 (including major, trace and REE analyses of whole rock samples; apatite REE analyses; compositional data of olivine, plagioclase and apatite; modal and CIPW norms) was used to calculate Spearman correlation matrices. Correlation matrices are used to identify geochemical tendencies and the interrelationships of the major and trace elements with the REE concentrations and trends. The data is re-organized into data sets corresponding to the cyclic units defined by whole rock geochemistry in Chapter 6.3. A further distinction between the various rock types within each cycle would have been desirable, however, insufficient data eliminates such an approach.

The Spearman correlation matrices are used to compare the effective trends and systematic element relationships within each cycle. Many of the trends and correlations can be ascribed to fractionation processes and modal effects. If it is assumed that the fractionation occurred in a systematic manner, such as bottom growth or crystal settling, it would follow that these trends should follow in an established stratigraphic sequence. These trends however, do not follow in an obvious stratigraphic sequence.

The crystallization of magnetitite layers are often compared to the formation of chromitite layers. The crystallization of the chromitite layers is ascribed to the mixing of different magma types, assimilation, or influxes and mixing of fresh magma with residual magma in the magma chamber after some fractional crystallization has taken place (Irvine, 1975; Irvine, 1977). Considering the possibility of magma mixing, the data relevant to cycle 1 is closely scrutinized to test such a hypothesis. Cycle 1 is chosen because it represents the cycle with the most comprehensive data set of all the identified cycles.

Several anomalies are identified with the Spearman correlation matrix for cycle 1. There is little correlation between the apatite Eu anomaly (AEua) and the apatite fluorine content. As a result of normal fractionation processes the fluorine content of apatite systematically increases with stratigraphic height (Fig. 13). Due to the copious co-precipitation of plagioclase, the apatite Eu anomaly (AEua) should have a systematic decrease with stratigraphic height. There ought to be a distinct positive correlation between AEua and F, however, the correlation is found to be very weak (Fig. 37A).

The plot of apatite Eu anomaly (AEUa) vs. apatite fluorine content (F), exhibits two trends (groups). The trends consist of samples 1 364; 1 320 and 1 211 on the one hand, and of samples 1 421, 1 379, 1 340, 1 302 and 1 270 respectively (Figure 33A). Samples 1 231 and 1 256 deviate from both trends but can conceivably be hybrids of the two trends. Note that the two trends each follow in stratigraphic order as will be expected from crystallization on the magma chamber floor.

The existence of a double trend within cycle 1 cannot be statistically substantiated with only this plot since, the error bars associated with the data are too large for successful discrimination. Similar double trends, which vary sympathetically with stratigraphy, are identified in numerous inter element plots. Although the trends generally overlap, grouping the analyses in the same sequence as in the AEua vs. F plot (Figure 37A) result in a systematic variation with stratigraphic height. To illustrate this point, the AEua vs. P_2O_5; AEua vs. OMgN; P_2O_5 vs. OMgN; TiO_2 vs. K_2O and OMn vs. OMgN plots (Fig. 37A to 37F) are presented (see the introduction chapter for the explanation of abbreviations). These inter-element plots are but a few of the numerous plots which show the same stratigraphic sympathetic twin trends. The fact that these twin trends are the result of fractionation processes is illustrated by the OMn vs. OMgN plot (Fig. 37F), from which it is seen that the Mn/Mg ratio of the olivine increases with stratigraphic height. Normal differentiation occurs within the individual trends as demonstrated by the olivine composition and the whole rock potassium content, which increases with increasing stratigraphic height (Fig. 37E).

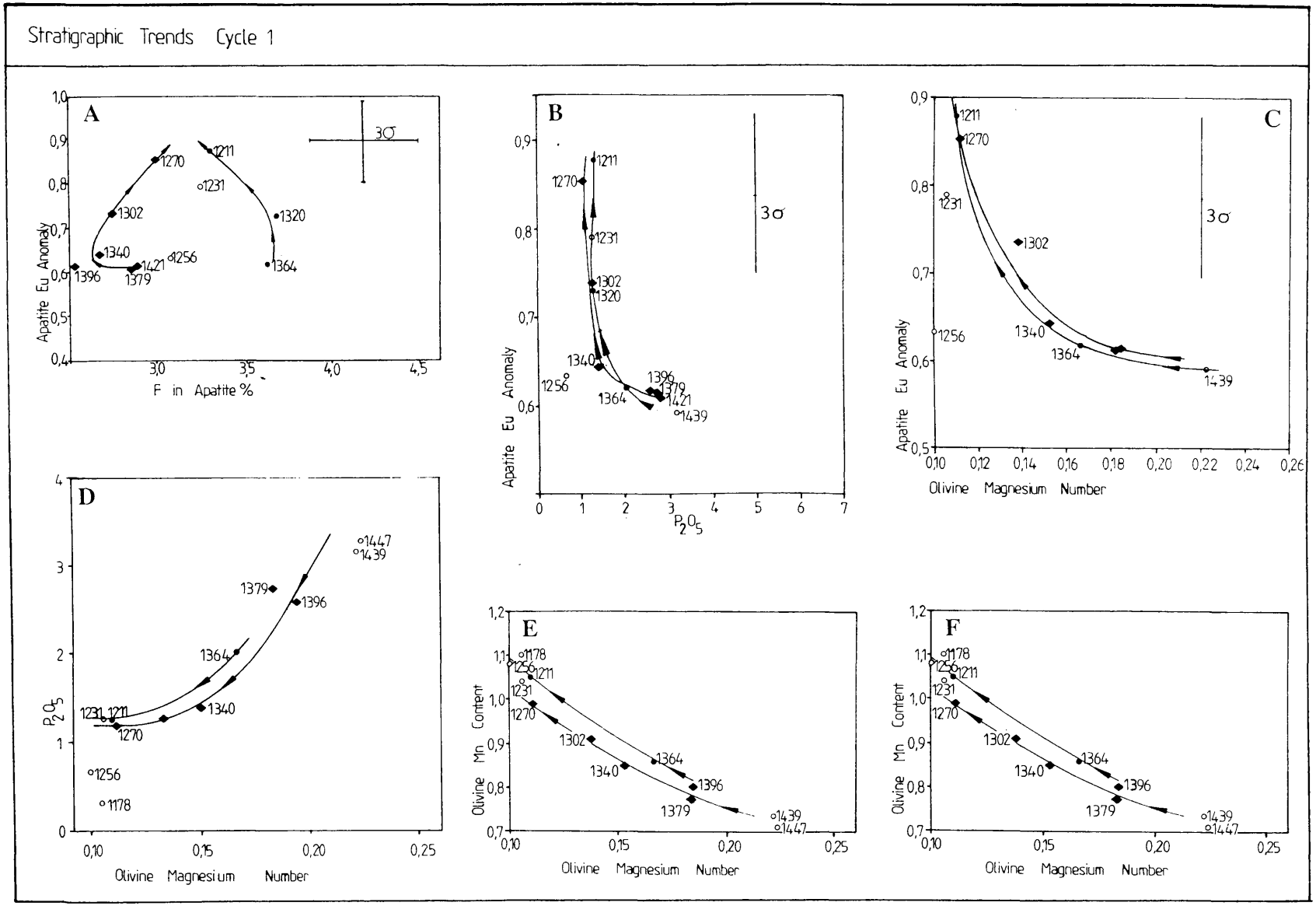

Figure 37: Whole rock and mineral geochemical trends in cycle 1. These inter-element plots are all arranged according to the grouping found in Fig 33A. The interwoven trends exist in each plot and follow in a stratigraphic sequence as indicated by the arrows.

The AEua vs. OMgN plot (Fig. 37C) indicates that the differentiation process is characterized by the smoothing of the negative Eu anomaly. A similar tendency is demonstrated by the apatite Eu anomaly vs. F content of apatite (Fig. 37A).

Sr compatibility and by analogy, the Eu^{+2} in apatite is not affected by the fluctuation in melt composition, temperature, pressure or water content of the melt (Watson and Green, 1981). The Eu anomaly cannot be directly caused by the selective partitioning of Eu^{+2} into apatite in the 7,5 to 20 Kbar pressure range. Melt composition does however have an effect on the partitioning of the trivalent REEs into apatite. An increase from 50 to 68 % SiO_2 at 950° C causes a 4 fold increase in the distribution coefficients, while an increase in the temperature from 950°C to 1 080°C lowers the distribution coefficients by a factor of two (Watson and Green, 1981). To alter the distribution coefficient of the trivalent REEs is a mechanism of altering the Eu anomaly in apatite.

The silica content in cycle 1 varies from 18 % in sample 1 450 to 50 % in sample 1 160 (Appendix 8A). Although this is a considerable variation the samples are comprised of cumulate phases and do not necessarily represent the liquid composition from which the apatite crystallized. The potential increase in the silica content of the magma can increase the partitioning of the trivalent REEs (Watson and Green, 1981) and, by having done so, increase the negative Eu anomaly. This should result in an increase of the Eu anomaly with increasing stratigraphic height. However, the opposite is observed for the Eu-anomaly.

A decrease in the partitioning of the trivalent REEs into apatite and the associated smoothing of the negative Eu-anomaly can be achieved by an increase in the crystallization temperature. This mechanism is inconsistent with the increase in fluorine content of apatite towards the roof contact. The increased iron content of olivine indicates a cooling toward the roof.

Smoothing of the negative Eu anomaly in apatite can also be achieved by a systematic increase in oxygen activity. An increase in oxygen activity can affect the Eu^{2+}/Eu^{3+} ratio and in turn the potential partitioning of Eu into apatite and especially Eu^{2+} into plagioclase. This seems an unlikely mechanism since the oxide minerals are concentrated at the lower parts of the cycles (Merkle and Von Gruenewaldt, 1986).

Plagioclase crystals can float in dense iron enriched basaltic liquids (Campbell et al., 1978) such as that from which the Upper Zone crystallized. The resorption of floating or pre-existing plagioclase will selectively increase the concentration of the Eu in the liquid and by doing so, smooth the Eu anomaly in the crystallizing apatite. The large range of plagioclase composition associated with several horizons can possibly be attributed to the partial resorption of plagioclase.

The detailed investigation of cycle 1 indicates that normal fractionation is at work with crystallization occurring at the floor of the magma chamber. Twin trends, both undergoing normal fractionation, can be identified within the cycle and are shown to be systematically interwoven in the stratigraphic sequence.

These twin trends (within a cycle) cannot be distinguished on any conventional geochemical grounds. Twin trends cannot be the result of fresh magma additions since this would cause reversals in the overall trends which would result in cyclic units. The twin trends are not only chemically similar but also follow identical trends, indicating that the mechanism which controls the crystallization are closely allied. The twin trends are also consistent with normal fractionation and bottom crystallization processes. These twin trends are interpreted to represent adjoining convection cells that oscillated laterally, and periodically dominated the bottom crystallization at a specific point. It is possible that seismic activity during the crystallization process could have been responsible for such a mechanism.

The Eu anomaly within the apatite indicates that normal fractionation and crystallization is accompanied by either an increase in the oxygen fugacity, or the resorption of pre-existing plagioclase crystals.

7.5 Bk-1 Cyclic Trends

Twin trends are identified in all 4 defined cycles of the Bk-1 samples, but due to the limited data base these trends can only been seen as highly speculative. The grouping of the remaining cycles are identified in a similar manner as that in cycle 1 and are included in the remaining plots for comparison.

Fleischer (1983) proposed a plot to distinguish various rock types on the basis of LREE ratios (Fig. 29). Although not demonstrated, both trends within cycle 1 seem to move from the gabbro and gabbro diorite field toward the granite point with increasing stratigraphic height. Cycles 2 and 4 trend in the opposite direction and fractionate toward the syenite point. Cycle 3 is only represented by two points, but their relative stratigraphic positions indicate a similar trend to cycle 1.

The ternary plot LREE, MREE and HREE of apatite (Fig. 38) indicates that the HREE content remains below five percent in all cycles. Both twin trends in cycle 1 are enriched in the MREEs. The two points in cycle 3 suggest a similar trend relative to stratigraphic height. The selective enrichment of the MREE in cycle 1 and 3 can be related to the preference of apatite for the MREE. The selective nature of apatite can be seen in the distribution coefficient pattern of apatite (Fujimaki, 1988). Early crystallization of plagioclase can increase the relative MREE content of the liquid and enhanced the MREE enrichment of apatite crystallizing from such a liquid.

A systematic enrichment of the LREE occurs in cycles 2 and 4 with increasing stratigraphic height. The preferential LREE enrichment of cycles 2 and 4 reflects differentiation of the primary magma (Tikhonenkova and Udod, 1984).

The expected evolutionary trend of apatite composition will include the accumulation of fluorine and the total REEs (Fig. 39). This phenomenon is observed on a large scale (TREE in cycle 4 apatite is greater than that of cycle 1) but, the increase is rather erratic.

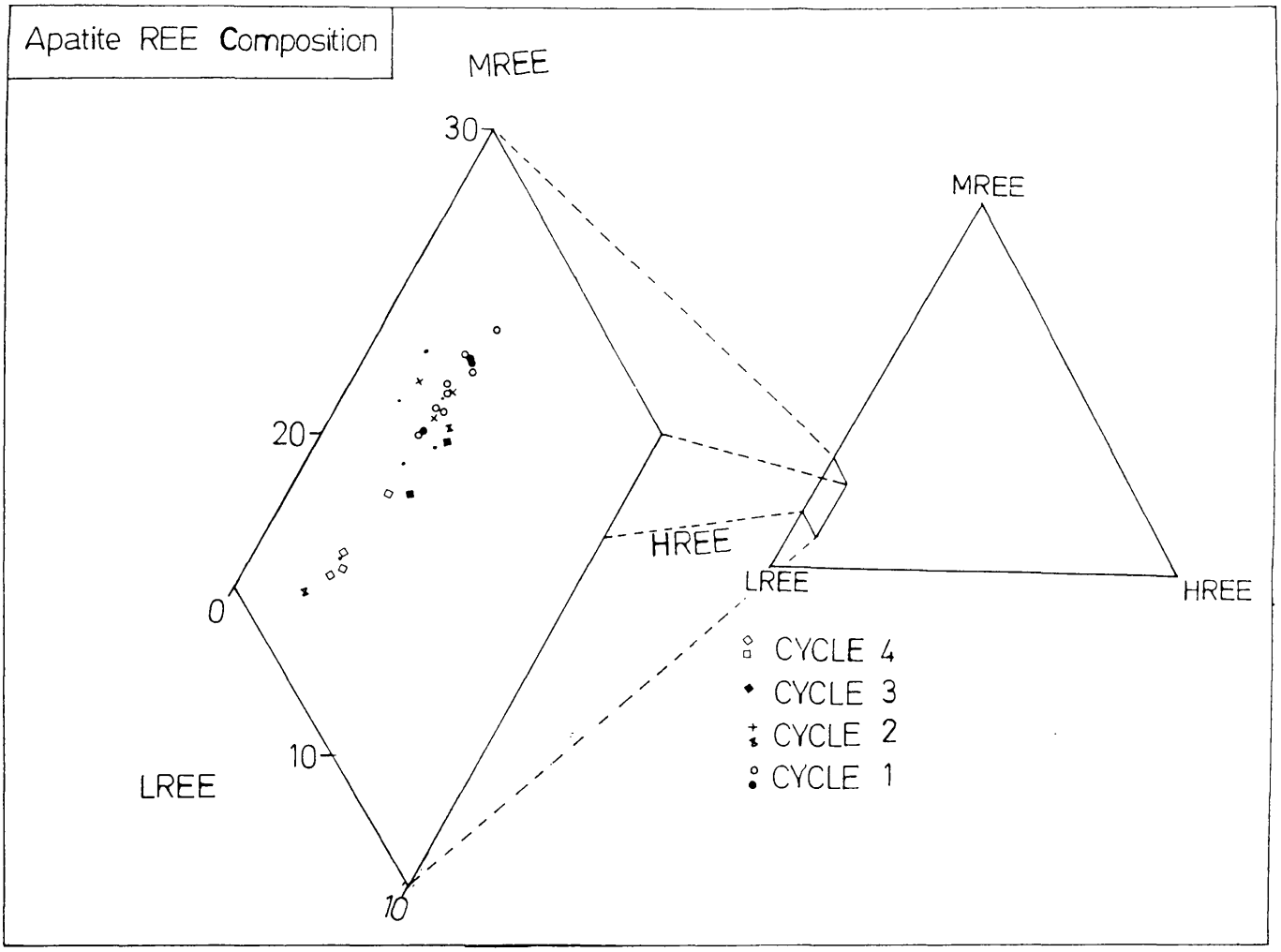

Figure 38: The LREE, MREE and HREE ratios of apatite from the various cycles. The symbols distiunguish between interwoven trends of each cycle.

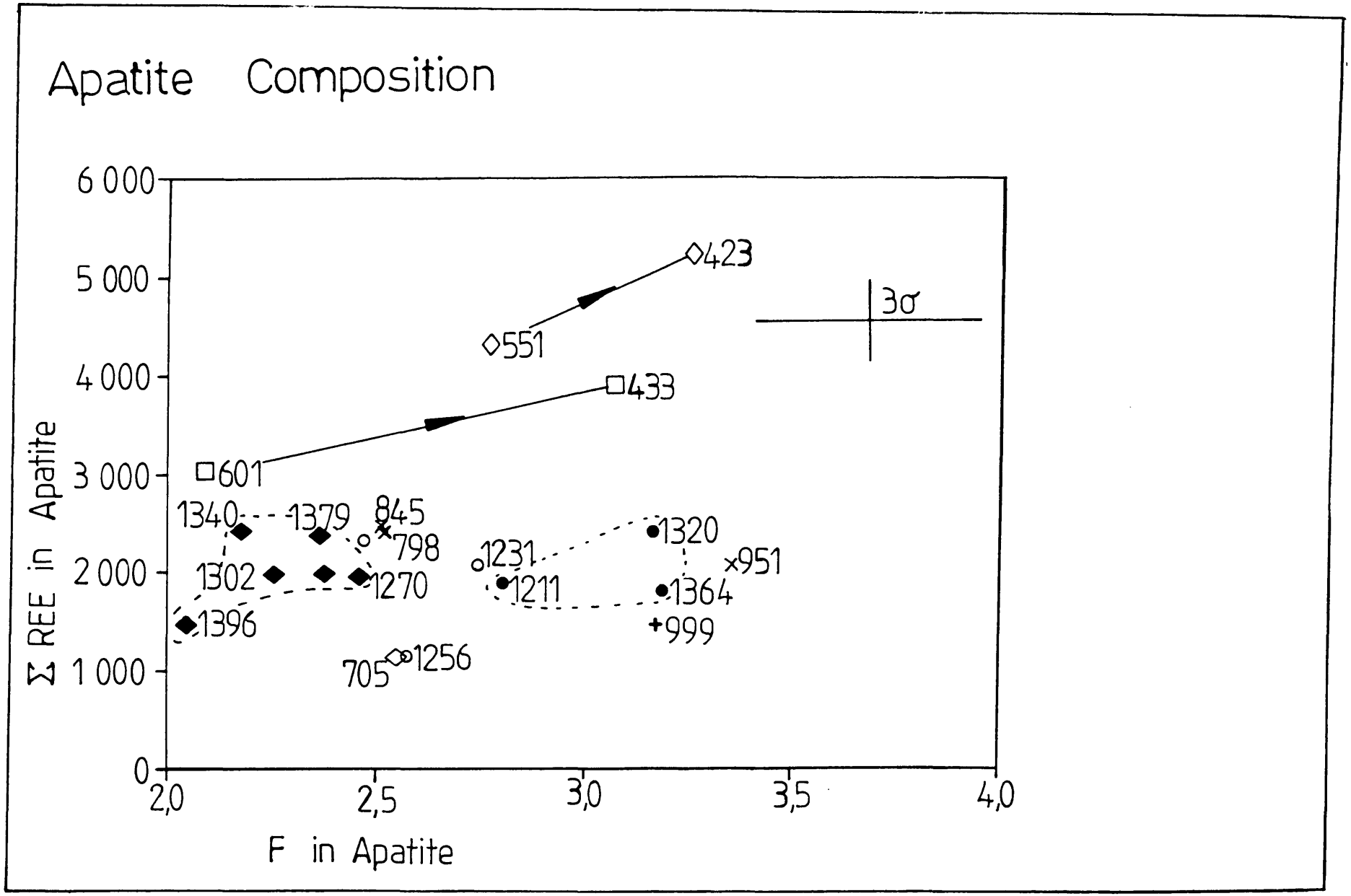

Figure 39: Apatite composition of the Bk-1 borehole. The TREE contents of apatite are plotted against the F contents of apatite to illustrate the various interwoven trends within each cycle. See Figure 34 for legend.

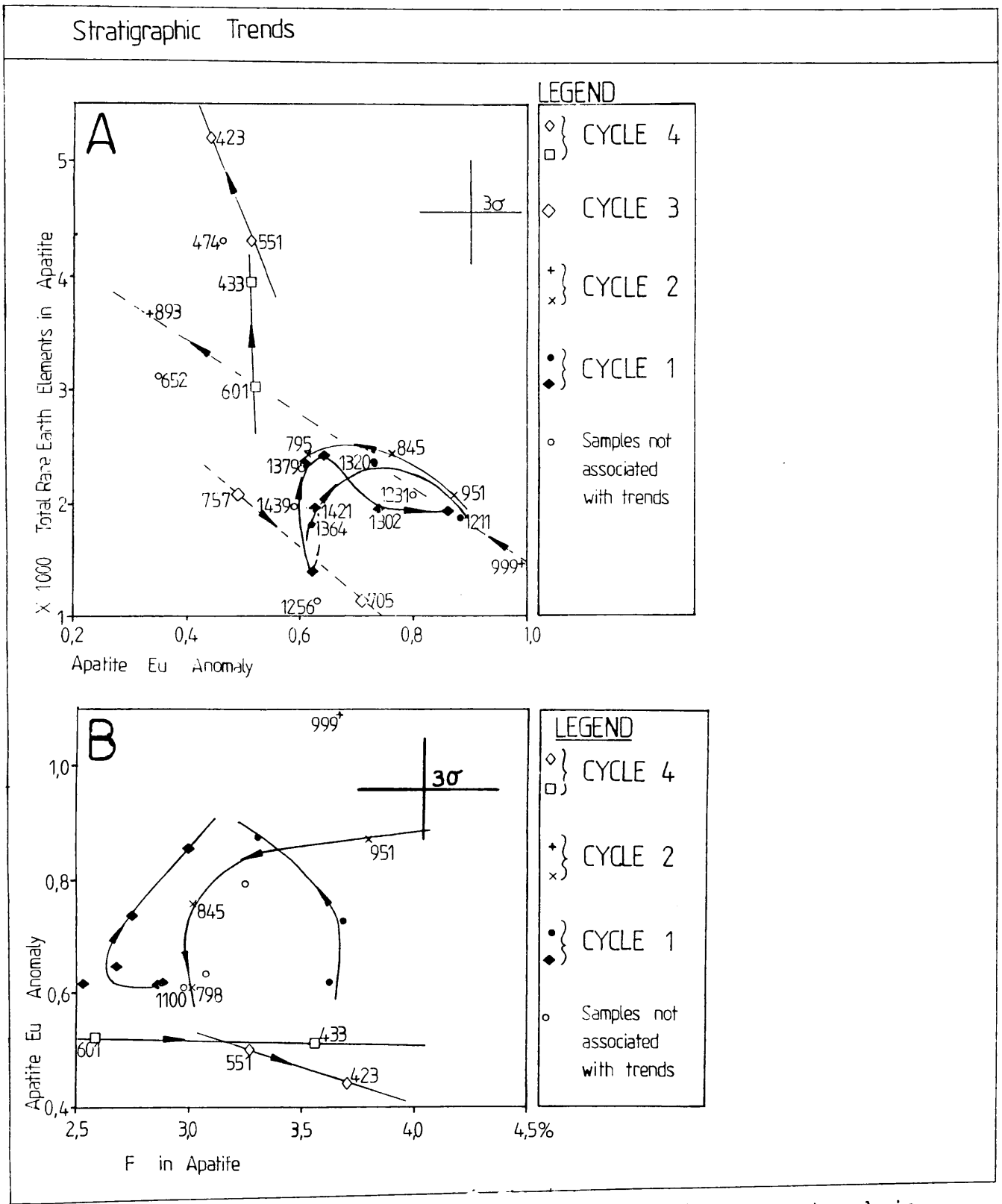

Figure 40: Stratigraphic twin trends. In these plots two interwoven trends in apatite composition can be identified within each of the cycles.

The twin trends within cycle 1 do not follow a systematic pattern, but are clearly grouped in fluorine-rich and fluorine-poor populations. These population correspond to the twin trends already identified (eg Fig. 37A). The two trends in cycle 4 show a sympathetic increase in the total REE and fluorine content of apatite with increasing stratigraphic height. Fluorine data from the remaining cycles is not available and no conclusion can be drawn for the trends in cycles 2 and 3.

The variation of the apatite Eu anomaly with the TREE content of apatite (Fig. 40A) indicates that cycle 1 (possibly cycle 3) has a tendency toward lower REE content and a smaller negative Eu anomaly while cycle 2, and to a limited extent cycle 4, has trends in the opposite direction. During fractional crystallization, where plagioclase is an important constituent, the negative Eu anomaly should increase with the TREE content within apatite (Roelandts and Duchesne, 1979). As is the case in cycles 2 and 4. The REE distribution coefficients in apatite are substantially larger that those in plagioclase, and favour the enrichment of Eu over the remaining REEs in the melt. If sufficient apatite crystallizes and substantially enriches the melt in Eu, the proportion of Eu incorporated into the subsequent apatite will be increased (relative to the remaining REEs) and the negative Eu anomaly will decrease while the total REEs are depleted. The copious crystallization of apatite can conceivably contribute to the effects in cycle 1 and 3.

8 SUMMARY AND CONCLUSIONS

Mineralogically, the silicate phases of borehole Bk-1 consist of 50 to 70 v % plagioclase. The anorthosite layers consist of up to 87 v % plagioclase while, magnetitite layers consist of up to 97 percent titaniferous magnetite and ilmenite.

Olivine occurs throughout borehole Bk-1 and the rocks contain between 15 and 30 v % olivine. Pyroxene is generally well below 10 v %, with hornblende only being significant in the upper part of the borehole.

Apatite is the most important REE bearing mineral in the Upper Zone. Usually in the low percent range, it may reach up to 13 v %. Apatite is typically fluorapatite with F content of 2 to 3,3 percent.

The total REE content of apatite is 1 548 to 4 315 ppm, which is in the order of 1 000 times enriched over chondrite levels. The apatite is LREE enriched, which is typical for late differentiation products. The apatite from the eastern Bushveld is more LREE enriched than borehole Bk-1 samples.

Accessory minerals are biotite as well as K-feldspar, quartz and zircon which are concentrated to the uppermost parts of the sequence.

The olivine composition is iron-rich and ranges in composition from Fa_{46} to Fa_{98}. Four cycles of upward Fe enrichment are identified. Plagioclase composition ranges from An_{28} to An_{44} but extreme variation in composition are found within several individual samples.

Whole rock geochemical data indicates an overall enrichment of incompatible elements. At least 4 smaller cycles of enrichment can be identified within the overall trend. Cycles within the geochemical trends reflect normal fractionation.

Modelling of the overall whole rock Rb contents, according to the Rayleigh fractionation, indicates that an overall enrichment in the residual melt occurs throughout borehole Bk-1. Trapped liquid content is calculated at 15 to 37 percent.

The overall upward enrichment of Rb in the Bk-1 can be subdivided into four cycles of enrichment, separated by reversals. These cycles undergo crystallization in a system where residual liquid has escaped and most likely mixed with overlying melt.

Four cycles corresponding to the whole rock geochemistry are evident in the REE content of apatite and whole rock samples. The REE trends are shown to be largely dominated by modal proportions (especially by apatite and plagioclase) and by normal fractionation.

Whole rock REE patterns are similar in all four cycles and do not give a clear indication whether crystallization occurs from an A or U type magma. The replenishment by a less fractionated magma, rather than the introduction of new magma, is considered responsible for the cyclic trends.

Distribution coefficients are calculated by the ratio of REE content of apatite to REE content of host matrix. These ratios indicate that the apatite associated with the magnetite-apatite zones crystallize under conditions nearer to equilibrium (approximately $K_d = 5$), than apatite in any other rock unit. This supports the theory that the magnetite-apatite rich zones develop due to the formation of Fe-P_2O_5-rich immiscible melts.

Biotite is shown to be insignificant at affecting the REE patterns and is not excessively enriched even though it occurs as a common interstitial mineral.

Twin trends following in stratigraphic sequence are identified in some cycles. These are found to be similar in behaviour and to be interwoven. These trends are the result of normal fractionation processes. The presence of interwoven trends are ascribed to crystallization being alternatively dominated by adjacent convection cells within the same magma strata.

9 ACKNOWLEDGMENTS

It is with sincere gratitude that I would hereby like to express my thanks by acknowledging the considerable assistance given me during the preparation of this dissertation by the following:

a) Ion Exchange Procedure
- Dr S Weinert for assisting in the development of the cation exchange procedure.
- Dr Baldwin of the National Chemical Research Laboratory, CSIR for making a laboratory available for the preparation of the REE concentrate.

b) XRF Investigation
- The Geological Survey of South Africa for making an XRF available for the initial XRF investigation.
- Prof A. Wilson for investigating the final XRF procedure at the University of Natal, Pietermaritzburg.

c) I.C.P. Analysis
- Dr D.H. Cornell for making the ICP at the University of Stellenbosch available for the final REE analysis.

d) Samples and Data
- Geological Survey of South Africa for making samples available from the Bk-1 borehole.
- Dr R.K.W. Merkle for making substantial XRF data available from borehole Bk-1.
- Prof G. Von Gruenewaldt for making data and samples available from the Roossenekal district.
- Dr H.E. Hörsch for setting up all electron micro-probe techniques employed.

e) Financial
- Foundation for Research Development for grants.

f) Discussions
- Valuable comments given by Drs A.H. Victor and F.W.E. Strelow of the CSIR concerning the cation exchange procedure.
- Members of the Institute for Geological Research on the Bushveld Complex, especially Prof G. von Gruenewaldt, Dr R.K.W. Merkle, Dr C.J. Hatton and Dr F.J. Reichardt for numerous valuable comments and recommendations.

g) Supervision
- The project was initiated due to the numerous suggestions made by Prof M.R. Sharpe. The project was finalized under the valued supervision of Prof G. von Gruenewaldt and Dr R.K.W. Merkle.

10 REFERENCES

Anderson, A.T. and Green, L.P., (1969)
Phosphorous fractionation diagram as a quantative indicator of crystallization and differentiation of basaltic liquids.
Geochimica et Cosmochimica Acta., Vol. 33, pp493-505.

Atkins, F.B., (1969)
Pyroxenes of the Bushveld Intrusion, South Africa.
Journal of Petrology., Vol. 10., pp222-249.

Belcher, C.B., (1963)
Sodium peroxide as a flux in refractory and mineral analysis.
Talanta, Vol. 10, pp75-81.

Boudraeu, A.E., Mathez, E.A. and McCullum, I.S., (1986)
Halogen geochemistry of the Stillwater and Bushveld Complexes: Evidence of transport of the platinum group elements by Cl-rich fluids.
Journal of Petrology., Vol. 27, Part 4, pp967-986.

Buchanan, D.L., (1972)
The petrology of rocks of the Bushveld Complex of the type intersected by boreholes in the Bethal area. Unpubl. MSc thesis, University of Pretoria, Pretoria, P86.

Butcher, A.R. and Merkle, R.K.W., (1991)
Unusual textures and structures associated with the Mangetitite layer in the Bushveld Complex: A contribution to the adcumulus debate. Mineralogical Magazine. Vol. 55, pp465-477.

Campbell, I.H., Roeder, P.L. and Dixon, J.M. (1978)
Plagioclase buoyancy in basaltic liquids as determined with a centrifuge furnace.
Contributions to Mineralogy and Petrology. Vol. 67, pp369-377

Campbell, W.J., Spano, E.F. and Green, T.E. (1966)
Micro and trace analysis by combination of ion exchange resin loaded papers and X-ray spectrography.
Analytical Chemistry, Vol. 38, No. 8, pp987-996.

Cawthorn, R.G. and MacCarthy. T.S., (1981)
Bottom crystallization and diffusion control in layered complexes: Evidence from Cr distribution in magnetite from the Bushveld Complex.
Transactions of the Geological Society of South Africa. Vol. 84, pp41-50.

Cawthorn, R.G. and MacCarthy, T.S., (1985)
Incompatible trace element behavior in the Bushveld Complex.
Economic Geology. Vol. 80, pp1016-1026.

Cantrell, K.J. and Bryne, R.H., (1987)
Rare earth element complexation by carbonate and oxalate ions.
Geochimica et Cosmochimica Acta. Vol. 51, pp597-605.

Cornell, D.H., Walters, P.E. and Schade, J., (1988)
Rare earth analysis by ICP-AES at Stellenboch.
Geocongress 1988, 22nd Congress of the Geological Society of South Africa, Extended Abstracts. pp763-766

Cox, K.G., Bell, J.D. and Pankhurst, R.J., (1979)
THE INTERPRETATION OF IGNEOUS ROCKS. George Allen and Unwin.
London, P450.

Eby, G.N., (1972)
Determination of rare earth, yttrium and scandium abundances in rocks and minerals by ion exchange X-ray fluorescence procedure.
Analytical Chemistry. Vol. 44, pp2137-2143.

Evensen, N.M., Hamilton, P.J. and O'Nions, R.K., (1978)
Rare earth abundances in Chondrite meteorites.
Geochimica et Cosmochimca Acta. Vol. 42, pp1199-1212.

Ewart, A and Duncan, A.R. (1983)
A compilation of distribution coefficients.
Unpublished data. Universities of Queensland and Cape Town.

Fleicher, M. (1983)
Distribution of the lanthanides and yttrium in apatites from iron ores and its bearing on the genesis of ores of the Kiruna type.
Economic Geology. Vol. 78, pp1007-1010.

Fujimaki, H., (1986)
Partition coefficients of Hf, Zr and rare earth elements between zircon, apatite and liquid. Contributions Mineral Petrology. Vol. 94, pp42-45.

Fujimaki, H. and Tatsumoto, M., (1984)
Partition coefficients of Hf, Zr and REE between phenocrysts and groundmass.
Journal of Geophysical Research. Vol. 89, Supplement, ppB662-B672.

Gast, P.W., (1968)
Trace element fractionation and the origin of tholeiitic and alkaline magma types.
Geochimica et Cosmochimica Acta. Vol. 32, pp1057-1086.

Giuliani, G., Cheeilletz, A. and Mechiche, M., (1987)
Behaviour of rare earth elements during thermal metamorphism and hydrothermal infiltration associated with skarn and vein-type tungsten ore bodies in central Morocco. Chemical Geology. Vol. 64., pp279-294.

Goodman, R.J., (1972)
Distribution of Ga and Rb in co-existing ground mass and phenocrysts of the some basic volcanic rocks.
Geochimica et Cosmochimica Acta. Vol.36, pp303-317.

Harmer, R.E. and Sharpe, M.R., (1985)
Field relations and strontium isotope systematics of the marginal rocks of the eastern Bushveld Complex.
Economic Geology. Vol. 80, pp813-837.

Harney, D.M.W., (1991)
Mineralogy of the lower part of the Upper Zone, eastern Bushveld Complex: Implications for ore-forming processes.
Unpubl. PhD. Thesis., University of Pretoria. Pretoria, P153.

Haskin, L.A. and Haskin, M.A., (1968)
Rare earth elements in the Skaergaard Intrusion.
Geochimica et Cosmochimica Acta. Vol. 32, pp433-447.

Hatton, C. and Sharpe, M.R., (1989)
Significance and origin of boninite-like rocks associated with the Bushveld Complex, in BONINITES AND RELATED ROCKS (A.J. Crawford, ed.), Unwin and Hyman Ltd., pp174-207

Henderson, P., (1984)
RARE EARTH ELEMENT GEOCHEMISTRY. Elsevier, Amsterdam, P510.

Hutchison, C.S., (1974)
LABORATORY HANDBOOK OF PETROGRAPHIC TECHNIQUES.
John Wiley and Sons Inc., New York, P527.

Irvine, T.N., (1977)
Crystallization sequence in the Muskox Intrusion and other layered intrusions-origin of chromitite layers and similar deposits of other magmatic ores. Geochimica et Cosmochimica Acta. Vol. 39, pp991-1020.

Irvine, T.N., (1977)
Origin of chromitite layers in the Muskox intrusion and other layered intrusions. Geology. Vol. 5, pp273-277.

Irvine, T.N. and Sharpe, M.R. (1986)
Magma mixing and the origin of stratiform oxide ore zones in the Bushveld Complex. Geocongress 1986, 21st Congress Geological Society of South Africa, Extended Abstracts, pp599-602.

Jackson, P.F.S. and Strelow, F.W.E., (1975)
The rare-earth contents of the six international geological reference materials of Southern African origin.
Chemical Geology. Vol. 15, pp303-307.

Jeffrey, P.G. and Hutchison, D., (1981)
CHEMICAL METHODS OF ROCK ANALYSIS.
Pergamon Press, Oxford, P379.

Kitamura, M., Yasudo, M. and Morimoto, N., (1981)
A study of fine textures of Bushveld augite by 200 kV analytical electron microscopy.
Bulletin of Mineralogy. Vol. 104, pp278-284

Klemm, D.D., Henckel, J., Dehm, R. and von Gruenewaldt, G., (1985)
The geochemistry of titanomagnetite in magnetite layers and their host rocks of the eastern Bushveld Complex.
Economic Geology. Vol. 80, pp1075-1088.

Kruger, F.J., Cawthorn, R.G. and Walsh, K.L., (1987)
Strontium isotopic evidence against magma addition in the Upper Zone of the Bushveld Complex.
Earth and Planetary Science Letters. Vol. 84, pp55-58.

Lambert, D.D. and Simmons, E.C., (1987)
Magma evolution in the Stillwater Complex, Montana:I. Rare-earth element evidence for the formation of the ultramafic series.
American Journal of Science. Vol. 287, pp1-32.

Langmyhr, F.J. and Sveen, S., (1965)
Decomposability in hydrofluoric acid of the main and some minor and trace minerals of silicate rocks.
Analytical Chimica Acta. Vol. 32, pp1-7.

MacLean, W.H., (1988)
Rare earth element mobility at constant inter-rare earth element ratios in the alteration in the alteration zone at the Phelps Dodge sulphide deposit. Matagami, Quebec.
Mineral Deposita. Vol. 23, pp231-238.

Mason, B., (1972)
Minor and trace element distribution in minerals of the Muzzle river Gabbro, N.Z.. Journal of Geology and Geophysics. Vol. 15, pp465-475.
Markgraaf, J., (1979)
Pyroxenes of the western Bushveld Complex, South Africa Transactions of the Geological Society of South Africa, pp217-224.
Merkle, R.K.W. and Von Gruenewaldt, G., (1986)
Compositional variation of the Co-rich pentlandite: Relation to the evolution of the Upper Zone of the western Bushveld Complex, South Africa.
Canadian Mineralogist. Vol. 24, pp529-546.
Molyneux, T.G., (1970)
The geology and structure of the area in the vicinity of Magnetite Heights, eastern Transvaal, with special reference to the magnetic iron ore.
Geological Society of South Africa. Special Publication 1, pp228-241.
Morse, S.A., (1981)
Kiglapait Geochemistry III: Potassium and rubidium.
Geochimica et Cosmochimica Acta. Vol. 45, pp163-180.
Morse, S.A. and Nolan, K.M., (1985)
Kiglapait geochemistry VII: Yttrium and the rare earth elements.
Geochimica et Cosmochimica Acta. Vol. 49, pp1621-1644.
Paster, T.P., Schauwecker, D.S. and Haskin, L.A., (1974)
The behaviour of some trace elements during solidification of the Skaergaard layered series.
Geochimica et Cosmochimica Acta. Vol. 38., pp1549-1577.
Philpotts, J.A. (1967)
Silicate liquid immiscibility: Its probable extent and petrogenetic significance.
American Journal of Science. Vol. 276, pp1147-1177.
Rafter, T.A., (1950)
Sodium peroxide decomposition of minerals in platinum vessels. Analyst. Vol. 75, pp485-492.
Philpotts, J.A. and Schnetzler, C.C., (1970)
Partition coefficients of rare earth elements between igneous matrix material and rock forming mineral phenocrysts-II.
Geochimica et Cosmochimica Acta. Vol. 34, pp331-340.
Reynolds, I.M., (1985a)
Contrasted mineralogy and textural relationships in the uppermost titaniferous magnetite of the Bushveld Complex in the Bierkraal area north of Rustenburg.
Economic Geology. Vol. 80, pp1027-1048.
Reynolds, I.M., (1985b)
The nature and origin of titaniferous magnetite rich layers in the Upper Zone of the Bushveld Complex: A review and synthesis.
Economic Geology. Vol. 80, pp1089-1108.
Reeves, R.d. and Brooks, R.R., (1978)
TRACE ELEMENT ANALYSIS OF GEOLOGICAL MATERIALS.
Wiley and Sons Inc., New York, P421.
Robinson, P., Higgens, N.C. and Jenner, G.A., (1986)
Determination of rare earth elements, yttrium and scandium in rocks by and ion exchange X-ray fluorescence technique.
Chemical Geology. Vol. 55, pp120-137.

Roeder, P.L., MacArthur, D., Ma, X. and Palmer, G.R., (1987)
Cathodoluminescence and microprobe study of rare-earth elements in apatite. American Mineralogist. Vol.72, pp801-811

Roelandts, I and Duchesne, J.C., (1979)
Rare earth elements in apatite from layered norites and iron titanium oxide ore-bodies related to anothosites (Rogaland, S.W., Norway). in ORIGIN AND DISTRIBUTION OF THE ELEMENTS. (Editor Ahrens, L.H.), Pergamon, pp199-212

Schoeller, W.R. and Powell, A.R., (1985)
THE ANALYSIS OF MINERALS AND ORES OF THE RARER ELEMENTS. Charles Grifin Ltd., London, P408.

Seelye, F.T. and Rafter, T.A. (1950)
Low temperature decomposition of rocks, ores and minerals by sodium peroxide using platinum vessels.
Nature. Vol. 165, pp317.

South Africa Committee for Stratigraphy, (1980)
STRATIGRAPHY OF SOUTH AFRICA. Handbook 8.
Geological Survey of South Africa. P690.

Strelow, F.W.E. (1960)
An ion exchange selectivity scale of cations based on equilibrium distribution coefficients.
Analytical Chemistry. Vol. 32, pp1185-1188.

Strelow, F.W.E. (1973)
Application of ion exchange to element separation and analysis in ion exchange and solvent extraction. (Editors: Marinsky, J.A. and Marcus, Y., Marcel Dekker Inc., New York, Vol. 5, Chapter 2, P278.

Strelow, F.W.E., Liebenberg, C.J. and von S. Toerien, F., (1969)
Separation of aluminium from other elements by anion exchange chromatography in oxalic-hydrochloric acid mixtures and its application to silicate analysis.
Analytical Chemistry. Vol. 41, pp2058-2060.

Strelow, F.W.E., Rethmeyer, R. and Bothma, C.J.C., (1965)
Ion exchange selectivity scales for cations in nitric acid media with a sulfonated polystyrene resin.
Analytical Chemistry. Vol. 37, pp106-110.

Strelow, F.W.E., and van der Walt, T.N., (1982)
Cation exchange in tartaric acid-nitric acid and in tartaric acid-ammonium tartrate solution.
Analytical Chemistry. Vol. 54, pp457-462.

Strelow, F.W.E., and van der Walt, T.N., (1984)
Cation exchange separation of Magnesium from large amounts of aluminium, in oxalic acid medium.
South African Journal of Chemistry. Vol. 37, pp149-152.

Strelow, F.W.E., Victor, A.H., van Zyl, C.R. and Eloff, C., (1971)
Distribution coefficients and cation exchange behaviour of elements in hydrochloric acid-acetone. Analytical Chemistry. Vol. 43, pp870-876.

Tikonenkova, R.P. and Udod, N.I, (1984)
Rare earth elements in apatite in Gremyakha-Vyrmes intrusion in the Kola peninsular. Geochemistry International. pp28-34.
(Translated from Geokhimiya, 1984, No. 1, pp113-119)

Von Gruenewaldt, G., (1994)
Ilmenite-apatite enrichment in the Upper Zone of the Bushveld Complex: a major titanium-rock phosphate resource. International Geological Review, Vol. 35 (In Press).

Von Gruenewaldt, G., (1971)
Petrographic and mineralogical investigation of the rock of the Bushveld Complex of the eastern Transvaal. Unpubl. PhD. thesis, University of Pretoria. Pretoria.

Von Gruenewaldt, G., (1973)
The Main and Upper Zone of the Bushveld Complex in the Roossenekal area, eastern Transvaal.
Transactions of the Geological Society of South Africa. Vol.76, pp207-227

Walraven, F. and Wolmarans, L.G., (1979)
Stratigraphy of the Upper Part of the Rustenburg layered Suite, Bushveld Complex in western Transvaal.
Annals of the Geological Survey Survey of South Africa. Vol.13, pp103-114

Watson, E.B. and Green, T.H. (1981)
Apatite/liquid partition coefficients for the rare earth elements and strontium. Earth and Planetary Science Letters. Vol. 56, pp405-421.

Young, E.J., Myers, A.T., Munson, E.L. and Conklin, N.M. (1969)
Mineralogy and geochemistry of fluorapatite from Cerro de Mercado, Durango, Mexico. United States Geological Survey., Professional Paper 650-D, D84-93.

APPENDIX

Appendix 1

THE DISSOLUTION PROCEDURE OF SAMPLES.

1 Preparation

Taking into account the anticipated REE content, samples of 0,25 - 3 g, were massed out and transferred to teflon beakers. The samples were moistened before acid was added so as to prevent over heating and resulting spluttering (Jeffrey and Hutchison, 1981).

Ten milliliters of 48 percent hydrofluoric acid was added per gram of sample, after which 5 ml concentrated hydrochloric acid and 5 ml concentrated perchloric acid was added respectively. The beaker was then placed on a hot plate and the temperature gradually raised to 200° C. Silicon and fluorine were then removed by fuming the perchloric acid for approximately ten minutes (Langmyhr and Sveen, 1965). A hydrofluoric-sulphuric acid mixture would have been more effective at removing the fluorine. The use of sulphuric acid would however, have led to a barium sulfate precipitation in barium rich samples (Eby, 1972; Jeffrey and Hutchison, 1981) such as feldspar separates.

After removing the beaker and cooling it, the edge of the beaker was rinsed to remove any fluorine present. Ten milliliters concentrated hydrochloric acid was added and the solution was brought to fuming for approximately 10 minutes. This step was repeated three times, allowing the solution to almost dry out during the third fuming.

After allowing the solution to cool, approximately 20 ml de-ionised water and 2-3 drops 30 % hydrogen peroxide were added to the beaker. The solution re-heated until all the salts were dissolved. The addition of hydrogen peroxide was necessary to stabilize titanium as a peroxide complex and to prevent the partial reduction of iron on the column (pers. commun. Victor, A.H.).

The solution was transferred to a glass beaker and the volume was increased to approximately 100 ml. While cooling a further 2-3 drops 30 % hydrogen peroxide was added and the solution was filtered using a 7 cm diameter slow to medium flow rate filter paper. If a precipitate was present a slow flow rate filter paper was used and the solution was passed through the filter paper twice.

2 Fusion

The hydrofluoric acid decomposition technique was unsuccessful in decomposing zircon (Jeffrey and Hutchison, 1981) while magnetite required a lengthy treatment (Langmyhr and Sveen, 1965). Zircon contained a relatively high concentration of REEs. The residues of the samples containing zircon were fused with sodium peroxide at a low furnace temperature in platinum crucibles (Seelye and Rafter, 1950; Belcher, 1963).

Filter paper which contained either zircon residue, precipitate or both residue and precipitate, was dried and heated in a platinum crucible at 800° C for approximately 10 minutes. Anhydrous sodium peroxide was used as flux and added to the crucible at a ratio of one to four mass parts sample to sodium peroxide respectively (Seelye and Rafter, 1950). One hundred milligrams sodium peroxide was considered sufficient when zircon was the only filtrate. If a precipitate had formed the appropriate amount of sodium peroxide was added while taking care that the cation exchange column was not overloaded. The platinum crucible was returned to the muffle furnace at 200° C and the temperature was gradually raised to 480° C. Heating lasted for approximately 10 minutes. Platinum crucibles could have been eroded by sodium peroxide above a temperature of 500° C (Belcher, 1963). Special care would have had to be taken when copious sulfides were present since they reacted strongly exothermally with the sodium peroxide (Seelye and Rafter, 1950). The exothermic reaction could have substantially elevate the temperature within the crucible. This problem could have been overcome by fusing a layer of sodium carbonate in the crucible prior to the sodium peroxide fusion. The sodium carbonate would then protect the platinum crucible if the final fusion was executed below the melting point of the sodium carbonate (Belcher, 1963).

After cooling the crucibles, 5 ml de-ionised water and 5 ml concentrated hydrochloric acid was added. The precipitation of insoluble salts was prevented by adding the acids rapidly (Rafter, 1950). The dissolution reaction was fairly violent so the crucibles were covered while adding the acids. After the residue was dissolved it was added to the appropriate solution of the original sample. The volume of combined sample solution was increased to 200 ml and the hydrochloric acid concentration adjusted to 0.1 M.

Sodium peroxide sintering would have been quite rapid and more effective than the hydrofluoric-perchloric acid decomposition (Robinson et al., 1986). The sodium peroxide sintering had a major drawback in that a large quantity of sodium would have been added in the process. This would have required larger columns, more reagents and time. The sodium peroxide would have been a major source of impurities and contaminants including alkali, alkali earth and transiotion elements (Belcher, 1963).

Appendix 2A

CATION EXCHANGE PROCEDURES

1 Cation Exchange Column Procedure

The behaviour of elements in an ion exchange column were given as:

$$V = K_d.X \text{ (mass [g] of dry resin)} \quad ...(A1)$$

where V represented the volume of the eluent (ml) required to elute the maximum of the elution peak. Kd was known as the equilibrium distribution coefficient and represented the value:

$$K_d = \frac{\text{amount of ion on resin}}{\text{amount of ion in aqueous phase}} \cdot \frac{\text{volume of aqueous phase [ml]}}{\text{mass of dry resin [g]}} \quad ...(A2)$$

(Note that 1 ml water is equivalent to 1 g water.)

The equilibrium distribution coefficient was affected by:
a) the composition and concentration of the aqueous phase;
b) resin type;
c) ratio of cation amount to capacity, known as q and;
d) to a lesser extent the temperature and pressure (Strelow, 1960).

The columns in this instance consisted of borosilicate glass tubes with an inner diameter of 21 mm, sealed at the bottom with fused-in sintered glass filters and fitted with buret taps. Separation funnels fitted to the columns by ground-glass joints were used as reservoirs.

Ten gram (dry) Bio-Rad AG 50W-X8, 200-400 mesh polystyrene resin was used and considered sufficient to absorb approximately 0.5 g of the proposed geological sample. The sample was comparitively large since the silicon was removed by the hydrofluoric-perchloric acid decomposition prior to absorption on the cation exchange column.

The samples in this study generally contained large quantities of iron, aluminium, alkali and alkali-earth elements. In order to achieve effective concentration, the REE were separated from as much of the matrix cations as possible. Ba was removed since it interfered specrographically with the determination of cerium (Robinson et al., 1986) using XRF analysis.

Using published distribution coefficients in Equation (A1), a simplified one-column procedure was used instead of a two-column procedure as described by Eby, (1972) and Robinson et al., (1986). The sample was absorbed onto the column as a 200 ml solution of 0.1 M hydrochloric acid + 0,3 % hydrogen peroxide (Fig. 2, Chapter 2.2.3). The solution was allowed to drain through the column. The reservoir and column was rinsed three times with a 10 ml solution

of 0,1 M hydrochloric acid 0,3 % hydrogen peroxide. The rinsing solution was allowed to drain below the resin bed surface.

According to Equation (A1), the 0,1 M hydrochloric absorption procedure allowed, amongst others, Zr, (Hf), Th, the REE, Ba, Al, Fe and Ti to be absorbed very strongly on the resin. The lighter alkali-earth elements were partially leached (Strelow, 1960). Iron was leached from the column using a 130 ml solution consisting of 90 % acetone, 10 % 1 M hydrochloric acid containing 0,3 % hydrogen peroxide (Defined as 0.1m HCl-90 % acetone by Strelow et al., 1971). During equilibrium conditions this would have removed all ferric cations present on the column. The solution was once again allowed to drain below the resin bed surface before adding the the next eluting agent.

The barium, alkali, alkali-earth and the majority of the aluminium was stripped using 220 ml 2 M nitric acid, 0,3 % hydrogen peroxide. The distribution coefficient (Strelow et al., 1965) suggested that all aluminium was removed. Excessive aluminium resulted in non-equilibrium conditions which caused the extensive tailing of aluminium itself (Strelow, 1960). Aluminium did not constitute a spectrographic interference during REE analysis by XRF. Aluminium was removed from the final aliquot which could have prevented the overloading of the cation exchange filter paper to the detriment of the absorption of the REE.

The nitric acid solution was drained and a small portion of water was added and drained into the column[1]. The REE, Hf, Th and Zr were leached using 300 ml 5 M hydrochloric acid (Strelow, 1960). The water portion was included in the final hydrochloric acid aliquot.

The column was shaken up in water and drained. Another 100 ml water was added and passed through the column. The column was then re-used for further samples.

2 Ion Exchange Loaded Filter Paper

The hydrochloric acid REE solution was dried on a water bath and then re-dissolved in 1 ml concentrated hydrochloric acid. Water was added to give a 100 ml 0,1 M hydrochloric acid solution. Discs, 29,5 mm in diameter were cut by punch from

---

1 * An aliquot of water was added so that the nitric-hydrochloric acid interface was separated. A dilute aqua-regia could have formed at this interface which would have damaged the column.

Whatman SA-2 cation exchange loaded filter paper. One disc was added to each sample solution which was then gently shaken for one day on a shaking table. The solution was then set aside for a further two days. Eby (1972) used 0,01 M HCl during this procedure and found that 95-97 percent of the ions in solution were absorbed during the first day if overloading had not occurred [2]. After two days 99 % had been absorbed and after the third day all ions were absorbed. A 0,1 M HCl solution was used during this study but, similar results were to be expected when considering the strong adsorption characteristics of the Amberlite IR-120 resin used in the paper.

2* Whatman SA-2 was withdrawn from the international market and the specifications were not readily available. The approximate exchange capacity of the paper was given as 1.9-2.0 meq/g by Campbell et al., (1966) and determined under working condition (Appendix 2B). The size of the paper was determined by the size of the XRF equipment window and the expected REE content of the sample.

Appendix 2B

CAPACITY OF ION EXCHANGE PAPER

Determination of the absorption capacity of the ion exchange loaded filter paper

The Whatman SA-2 ion exchange resin loaded filter paper (formerly known as Reeve angle 2) was cut into 29,5 mm diameter discs using a customized punch to achieve the maximum cutting accuracy. To determine the operative absorption capacity of the ion exchange loaded filter paper, a disc was placed in 100 ml, 0,1 M HCl solution containing excess La. The paper was shaken in the solution on a sieve table for a period of twenty four hours. This period would have been sufficient to absorb 95-97 % of the proposed ions if overloading was not approached (Eby, 1972). The paper was air dried and burnt off in a Pt crucible at 1000° C using a muffle furnace. The remaining La_2O_3 was massed and the capacity of the disc calculated. The capacity of the 29,5 mm disc was found to be 0.287 meq.

Calculation

Mass of paper (air dry): 0,1053 g

Pt crucible + La_2O_3: 23,2775 g
Pt crucible: - 23,2619 g
La_2O_3: 0,0156 g

0,0156 g La_2O_3 = 0,0156 g/ 325,82 $g.mol^{-1}$
= 0,0478 mmol La_2O_3
x2 = 0,0956 La^{+3}

therefore the capacity of the disc: 0,0956 La^{+3} x 3 (charge/atom)
= 0,287 meq

Normalized capacity of paper: 0,287 meq/0,1053 g
= 2,73 $meq.g^{-1}$

Appendix 3

X-RAY FLUORESCENCE SPECTROSCOPY

Thin Film X-Ray Fluorescence Spectroscopy

In thin film XRF spectroscopy, the composition of a sample is determined as a direct proportion to the intensity of the relative X-ray lines. The matrix absorption and fluorescence must be negligibly small and the sample infinitely thin. Sample homogeneity was a prerequisite. This was achieved in this study by removing the matrix material chemically by cation exchange columns and by absorbing the trace amounts of REEs into Whatman SA-2 cation resin loaded paper.

Extensive mass absorption calculations by Eby, (1972) showed that the absorption effect was negligible up to a total REE + Y + Sc content of 500 μg in Whatman SA-2 paper of 4,5 cm^2. The absorption effect was approximately 10 percent for a total REE + Y + Sc content of 1200 μg using the same paper (Eby, 1972). These REE levels translated to an area concentration of 111.1 $\mu g/cm^2$ and 266.7 $\mu g/cm^2$ respectively. This would have implied that the total permissible content of REE, Y and Sc in the 29,5 mm diameter disc was 759 μg and 1823 μg respectively. Above the higher value a correction would have been necessary for mass absorption effects and the procedure would not, strictly, have been a thin film technique any more.

Calibration Standards

REE stock solutions were prepared from Spex HiPure oxides and titrated by E.D.T.A. solution. The E.D.T.A. was standardized by lead carbonate solution. The Y, Sc, Ba, Fe, Ni, Cr, Mn, and Pb stock solutions were prepared from high grade analytical reagents. Various levels of element standard papers were prepared by pipetting stock solutions. The standardized papers were prepared in the same manner as the real samples. A complete list of prepared standards were given in Table (A 3.1). These standardized discs were used for this investigation as calibration standards and to determine inter-element corrections.

Table A3.1

The Standards for XRF Calibration
(values given in μg)

La	1.834, 4.584, 9.168, 18.34, 45.84, 183.4, 458.4, 916.8, 1375.
Ce	1.945, 4.862, 9.723, 48.62, 97.23, 486.2, 972.3, 2431.
Pr	1.940, 4.851, 9.701, 29.10, 48.51, 97.01, 145.5.
Nd	1.847, 4.617, 9.233, 18.47, 46.17, 92.33,461.7, 923.3.
Sm	2.048, 5.120, 10.24, 20.48, 51.20, 81.91, 122.87.
Eu	1.996, 4.991, 7.986, 9.982, 14.97, 19.96.
Gd	2.117, 5.292, 10.58, 21.17, 42.33, 84.66.
Tb	2.001, 5.002, 8.003, 10.00, 15.01, 30.01.
Dy	2.459, 6.148, 12.30, 24.59, 49.18, 98.37, 122.96.
Ho	2.029, 5.072, 10.14, 20.29, 40.58, 50.72, 101.44.
Er	2.149, 5.374, 10.75, 16.12, 32.24, 53.73, 85.96.
Tm	2.535, 6.337, 10.14, 12.67, 19.01, 25.35.
Yb	2.000, 5.001, 10.00, 20.00, 40.01, 100.02.
Lu	2.659, 6.648, 10.64, 13.30, 19.94, 26.59.

R.E.E. 1, 10.

Interference Standards

Fe	5, 10, 20, 50, 100, 200, 500, 1 000, 2 000.
Y	2, 5, 10, 20, 50, 100, 200, 1 000, 2 000.
Sc	2, 5, 10, 20, 50, 100, 200.
Ba	2, 5, 10, 20, 50, 100, 150, 500, 1000.
Ti	5, 10, 20, 50.
Hf	5, 10, 20, 50, 100, 200, 250, 500, 1 000.
Pb	5, 10, 20, 50, 100, 500, 1 000.

Sample Homogeneity

The REE concentrate was absorbed from a 100 ml 0.1 M HCl solution using the Whatman SA-2 resin loaded paper. The characteristics of the final sample were largely dependent upon the nature of the paper.

The paper consisted of approximately 50 mass percent alpha cellulose and ion exchange resin respectively (Campbell et al., 1966). The resin used in the Whatman SA-2 was Amberlite IR-120. According to product specification this was a strong acid cation styrene exchange resin with a sulphate functional group and was effective in the entire pH range. The alpha cellulose on the other hand was unable to absorb the REE at a low pH. The ions would have been absorbed exclusively by the resin particles and homogeneity would dependent upon the distribution of the resin particles.

The sample homogeneity was investigated by analyzing two traverses with a point spacing of approximately 50 microns across a 2500 μg La standard paper using an electron microprobe. The beam size was 50 microns and the results were illustrated in Figure A3.1. The sample was clearly heterogeneous on this scale. This was attributed to two factors: firstly, the electron beam was unable to penetrate or excite the entire paper depth of approximately 0.29 mm thick; secondly, the paper consisted of relatively large resin particles interspaced by barren alpha cellulose fibres. Figure A3.1 represented a limited depth of paper and La-rich resin beads alternating with La poor Alpha-cellulose fibre. The sample homogeneity could only have been realistically tested by XRF. The averaging of several adjacent points across the traverse in Figure A3.1 brought about a marked improvement in apparent homogeneity. This apparent improvement in homogeneity supported the opinion that inhomogeneity was caused by the two component nature of the paper. Inhomogeneity was probably not caused by the absorption procedure or the irregular absorption of the sample on a larger scale.

Sample homogeneity was tested during the analysis by analyzing the paper on both sides. Those samples which had a larger deviation in analytical values from one side to the other, than suggested by the random statistical error, had to be reprepared.

XRF Investigation

The aim of the initial XRF investigation was to equal the detection limits as were given by Robinson et al., (1986) and to investigate the feasibility of using the Philips PW 1404 XRF spectrometer at the Department of Geology, University of Natal, Pietermaritzburg. For comparative reasons, it was attempted to keep the operating conditions the same as used by Robinson et al., (1986):

Au target X-ray tube.
50 kV, 50 mA.

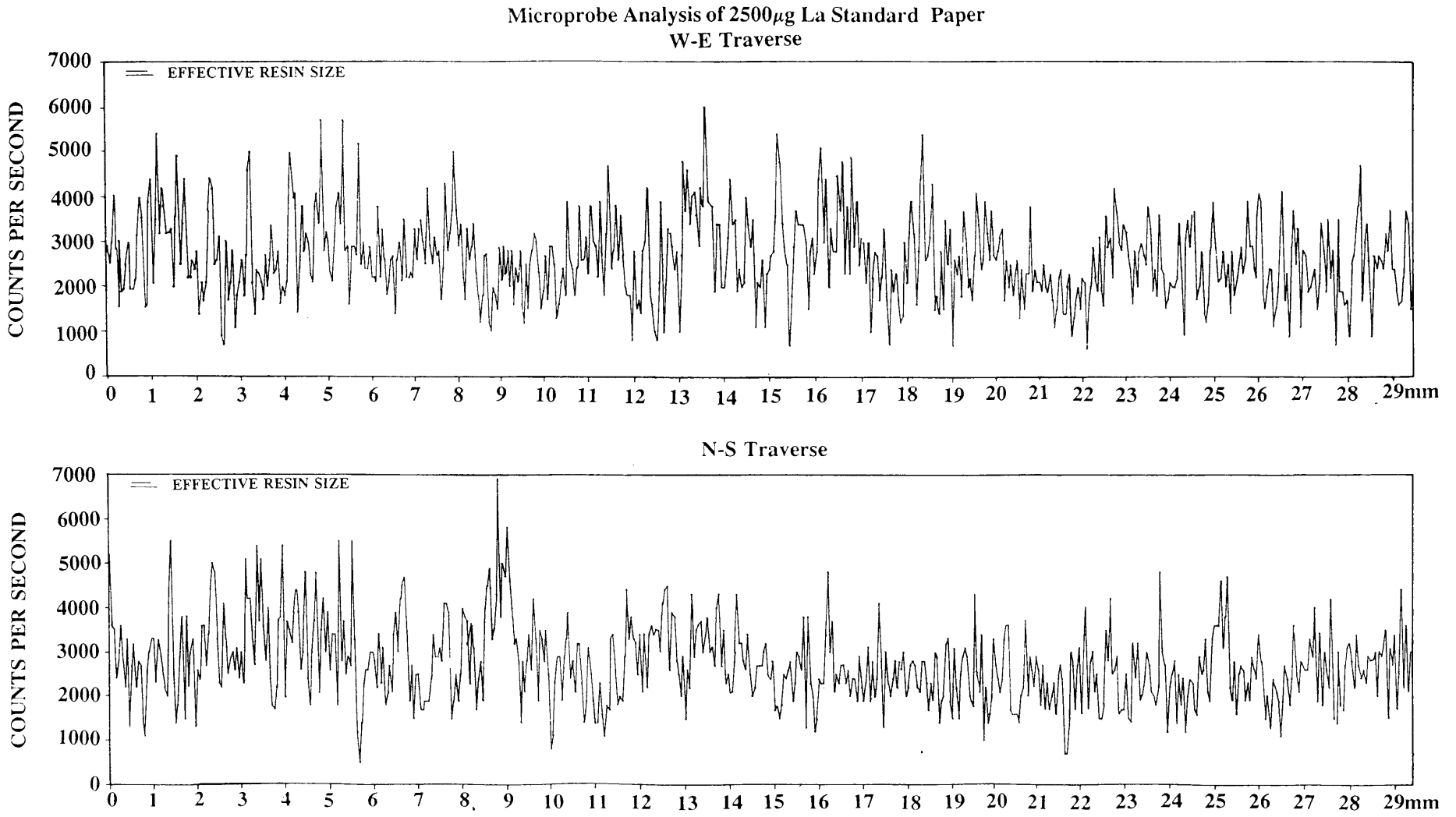

Figure A3.1: Microprobe step scan across a 2 500μg La standard resin loaded ion exchange filter paper. Although the resin loaded paper is definitely not homogenous on such a small scale, a sufficient homogeneity is indicated by XRF this film techniques.

LiF 200 crystal.
Fine collimator.
Gas-flow proportional + scintillation counter.
Vacuum.
Counting time 20 seconds, except where otherwise specified.
Mask diameter 26 mm.

Parameters such as pulse-height analyzer, mask material and sample holder inners were varied. The spectrometer was peaked up on the same characteristic lines as those used by Robinson et al., (1986) and the background positions adjusted in accordance.

The most critical factor in the initial stages of investigation was to determine whether the lower limits of detection (lld) using this technique were sufficiently sensitive. The most frequently used definition of the lower limit of detection in XRF spectroscopy was:

$$lld = {}^{6}/_{m}\sqrt{{}^{Rb}/_{T}}$$

m = count per second per microgram (intensity).
Rb = count per second on background.
T = counting time.

The lower limit of detection was effected by intensity, background level and time. Time only affects the accuracy of the counting statistics. The real variables affected by machine conditions were intensity and background count rate.

The lower limit of detection was proportional to the square root of the background count rate. A low background was of cardinal importance to a good lower limit of detection. The source of background was investigated using a fairly open pulse height analyzer setting of 32-80 percent. The bulk of the background was due to the scatter effect of the paper (Table A3.2), while the brass inner had contributed substantially. It was clear that some of the background levels were unacceptably high when compared to those implied by the Robinson et al., (1986) data. To eliminate the scatter effect of the inner material, a pure wax backstop was placed behind the paper in a similar manner as that used by Eby (1972). This attempt proved to be counter productive since the background increased dramatically due to the wax.

Al, Au and Cu/Te masking materials were tested but no significant difference in the background levels were noted. Unfortunately the masks differed in absolute thickness and slight variations could have been caused by material thickness. For practical reasons the Cu/Te masks were chosen as the final masking material.

Table A3.2

Source of Background.

Angle 2Θ	Robinson* Back-ground	Sample Holder T=20s	Sample Holder +Brass inner T=20s	Sample Holder +Brass inner +SA2 Blank T=20s	Sample Hold. +Brass inner +SA-2 Blank +Wax Back Stop T=20s
87.185	30.3	2.7	5.4	33.2	74.3
82.925	36.6	2.6	3.1	41.0	160.0
81.020	-	3.0	3.0	83.2	332.6
79.055	47.8	2.5	3.7	66.7	177.2
75.445	53.8	3.2	3.9	51.7	127.2
72.145	72.7	3.3	4.7	63.5	155.0
69.370	244.3	5.7	7.0	101.1	255.3
66.240	117.2	5.3	7.3	128.0	-
63.615	131.8	6.2	7.5	115.8	-
62.950	212.7	8.7	10.8	149.0	-
62.200	-	5.3	8.6	133.2	-
61.100	169.0	5.4	7.1	138.7	-
58.805	209.1	7.1	8.7	176.2	-
57.520	2846.9	101.0	150.3	1435.6	-
56.605	234.8	7.1	8.7	196.3	-
55.300	-	5.7	7.7	209.1	-
54.555	287.6	6.9	9.5	215.1	-
52.630	1408.7	6.7	10.3	247.7	-
50.810	360.6	7.2	10.0	264.7	-
49.095	452.1	13.7	20.3	329.1	-
48.000	-	7.6	15.7	313.2	-
47.425	423.2	7.9	17.2	329.1	-

* This data is implied in Robinson et al., (1986) and represents equivalent lines rather than the identical angles.

-Count rate in counts per second. (c.p.s.)
-Pulse height analyzer set at 32-80 percent.

Different materials were tried in making sample holder inners. The purpose of an inner cup in the sample holder was to flatten the paper sample flush with the mask, prevent the paper from being pulled through the mask window by the vacuum and to centralize the paper over the mask window. The inner had to be weighty enough to flatten the paper and fit tightly for effective centralization. Ideally it would not contribute to higher background levels.

Table (A3.2) showed that the inner material contributed to the background. The contribution of the inner material to the background was minimal when compared to that of the blank paper. The Fe K_{α} line at angle 57.52° showed a substantial rise when using the brass inner and a plastic replica was substituted. The background levels of a blank paper, were compared in Table (A3.3), but there was no improvement, not even in the Fe $K_{\alpha 1}$ line. The plastic inner was used since it was the cheaper and easier to manufacture.

A detailed scrutiny of the pulse height distribution of both the scintillation and gas flow proportional counters revealed that the 32-80 percent window was too large. The wide window was the cause of the high background levels of the first run. The final window setting included the entire proportional gas flow counter peak which was more symmetrical and intense than the scintillation peak. Ideal windows vary from element to element but, a uniform setting of 43-61 percent was finally chosen for all the elements. The background levels were dramatically reduced and the lower limit of detections when recalculated for 80 seconds counting time (Table A3.4), were in the same order of magnitude as those given by Robinson et al., (1986). The background count rate was simply taken as the count rate of the blank paper at the same angle.

The linearity of the count rate verses the content (or concentration per area) was tested using the Nd standards. For this purpose the background readings were taken as the count rate of the line on the blank paper. The paper was analyzed on both sides of the paper and the average of the two readings taken. The relationship was linear, as seen in Figure A3.2. A linear relationship existed but, the 500 μg point was off the calibration line. All Nd papers where prepared from the same stock solution and in the same manner. An error in preparation seemed unlikely. This paper was further characterized by a high deviation of count rate from one side of the paper to the other. This would have implied that the one side of the paper contained more Nd than the other. This explanation seemed improbable since, in thin film XRF spectroscopy, the sample approximated an infinitely thin film. A detectable concentration gradient from one side to the other would not have been possible.

The same difficulty was present in the Robinson et al., (1986) work and no systematic differences from one side of the paper to the other were noted. The only alternative was to discard any data where a discrepancy in count rate from one side of the paper to the other, was greater than that suggested by the count rate statistics (at 3 sigma level).

The choice of large or small channel mask was tested using Ce, Eu, Yb as representative samples. The large channel mask produced substantially higher

Table A3.3

The effect of the brass and plastic inners on background levels.

Line	Angle 2Θ	Brass Inner +Blank (c.p.s.)	σ^1	Plastic Inner +Blank (c.p.s.)	σ^1
Ba	87.185	18.9	0.97	19.4	0.98
La	82.925	22.0	1.0	22.7	1.1
B_1	81.020	25.3	1.1	28.3	1.2
Ce	79.055	33.2	1.3	34.1	1.3
Pr	75.445	37.6	1.4	34.9	1.3
Nd	72.145	46.4	1.5	49.0	1.6
Cr	69.370	72.5	1.9	71.9	1.9
Sm	66.240	70.9	1.9	73.9	1.9
Eu	63.615	88.8	2.1	90.8	2.1
Mn	62.950	122.5	2.5	122.8	2.5
B_2	62.200	98.2	2.2	103.3	2.3
Gd	61.100	103.5	2.3	106.9	2.3
Tb	58.805	134.5	2.6	136.2	2.6
Fe	57.520	1181.4	7.6	1183.0	7.7
Dy	56.605	149.0	2.7	154.2	2.8
B_3	55.300	155.7	2.8	160.5	2.8
Ho	54.555	172.2	2.9	168.6	2.9
Er	52.630	202.8	3.2	193.9	3.1
Tm	50.810	198.9	3.2	208.3	3.2
Yb	49.095	244.9	3.5	284.0	3.8
B_4	48.000	236.3	3.4	241.3	3.5
Lu	47.425	247.0	3.5	245.7	3.5

counting time = 20s.
Cu/Te masks.

Table A3.4

Lower Limits of Detection (l.l.d.)

Line	Angle 2θ	Std level (μg)	Count Rate T=20s	Back-ground *	Back-ground T=20s	Inten-sity *	Inten sity	- l.l.d. ~	l.l.d. *
Ba	87.185	500	3298.2	18.9	30.3	6.6	10.0	0.44	0.37
La	82.925	1000	5422.0	22.0	36.6	5.4	11.6	0.58	0.35
B_1	81.020	-	-	25.3	-	-	-	-	-
Ce	79.055	2500	12651	33.2	47.8	5.0	14.1	0.77	0.33
Pr	75.445	150	2113.9	37.6	53.8	13.8	15.9	0.30	0.31
Nd	72.145	1000	1049.1	46.4	72.7	10.1	22.0	0.45	0.26
Cr	69.370	-	-	72.5	244.3	-	-	-	-
Sm	66.240	120	1993.3	70.9	117.2	16.0	31.6	0.14	0.23
Eu	63.615	20	471.7	88.8	131.8	19.2	35.0	0.33	0.22
Mn	62.950	-	-	122.5	212.7	-	-	-	-
B_2	62.200	-	-	98.2	-	-	-	-	-
Gd	61.100	80	2388.2	103.5	169.0	28.6	43.6	0.23	0.20
Tb	58.805	30	704.3	134.5	209.1	19.0	48.5	0.41	0.20
Fe	57.520	-	-	1181	2847	-	-	-	-
Dy	56.605	100	4262.2	149.0	234.8	41.1	54.1	0.20	0.19
B_3	55.300	-	-	155.7	-	-	-	-	-
Ho	54.555	100	3631.8	172.2	287.6	34.6	63.2	0.25	0.18
Er	52.630	80	3028.0	202.8	335.7	35.3	72.3	0.27	0.17
Tm	50.810	20	1097.4	198.9	360.6	44.9	74.9	0.21	0.17
Yb	49.095	100	3805.3	244.9	452.1	35.6	83.9	0.29	0.17
B_4	48.000	-	-	236.3	-	-	-	-	-
Lu	47.425	20	1460.1	24.7	423.2	60.7	92.0	0.17	0.15

* Robinson et al., (1986).
l.l.d. lower limit of detection.
~ l.l.d. recalculated to 80 seconds.
Count rate in counts per second (c.p.s.)
Pulse height analyzer 43-61 percent.

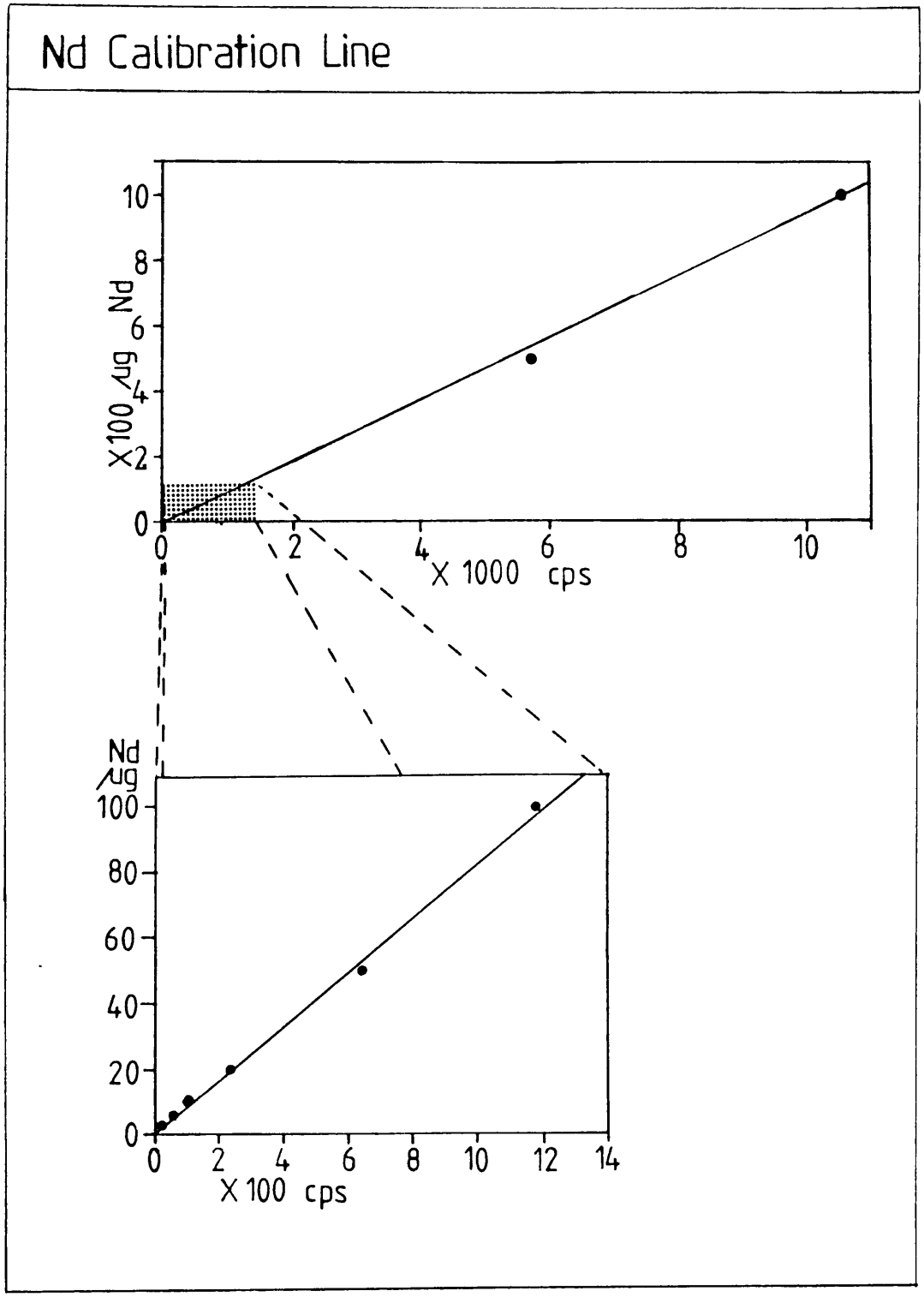

Figure A3.2: The Nd calibration line of standard solutions absorbed onto Whatman SA-2 cation exchange loaded filter paper.

intensities but, was associated with a larger deviation of count rate from one side of the paper to the other. The elevated background values eroded any advantage gained by a higher intensity to such an extent that the lld was extensively raised (Table A3.5). The small channel mask seemed the better option. The background levels not only critically effected the lld but also the accuracy of the technique. Robinson et al., (1986) simply used the intensities measured on blank papers as the background levels. Blank papers had to be used during the determination of the inter-element correction factors because the chosen backgrounds (B_{1-4}) could not be used due to inter-element interferences. This approach was used to calculate the interference correction factor of Pr on B_3 (Table A3.6). The coefficients cannot statistically be distinguished but, the associated error on the coefficients seemed excessive. Rather than use this method it was decided to calculate the background at position B_{1-4} and the REE lines by using psuedo-backgrounds. These psuedo-backgrounds were chosen on either side of the B_{1-4} positions (backgrounds) and on either side of the element under investigation. These psuedo-background positions were chosen, with a spectral calculator, to be as close to the background to be calculated as possible while staying in an interference-free position.

The interference corrections of a specific element on the background was then calculated using the psuedo-backgrounds. The determined correction factors had unacceptably high associated count rate errors (Table A3.2). The calculated count rate backgrounds at positions (B1-4) were often higher than the actual count rate at these positions (B_{1-4}). The likely reasons were: 1) To find interference free positions the psuedo-background was chosen too far from the background to be calculated; and 2) the psuedo-backgrounds were not interference-free. The interference was not necessarily due to the element under investigation but could have been due to acid or tube impurities. To investigate these factors a step scan was done across positions B_3 and the Pr line. The step scan showed the interference effect of Pr on B_3, and the irregular nature of the background. Psuedo-background on either side of B_3 and the Pr peak were chosen as indicated in Figure A3.3. Forty second counts were taken at these psuedo-backgrounds, B_3 and the Pr peak using both sides of the 100 μg and 150 μg Pr papers. The interference correction factors were all within expected counting statistic variations and were reproduced in Table A3.8 .

Coefficients determined by using blank level count rates as background levels were represented in Table (A3.6) while, Table (A3.8) represented coefficients determined by employing psuedo-backgrounds to calculate the background levels. The coefficients in Table (A3.8) had a substantially smaller standard deviation than those in Table (A3.6) which, implied that using psuedo-backgrounds to calculate backgrounds was a better technique. The data accumulated represented a small population. The techniques would have had to have been repeated several times before the results would have been conclusive.

Table A3.5

The effect of small or large channel mask on intensity, background level and lower limit of detection.

	Blank (c.p.s.)		Line Count Rate (c.p.s.)		Intensity (c.p.s.μg^{-1})			lld (μg^{-1})		
	s	l	s	l	s	l	*	s	l	*
Ce	32.9	84.2	12584.5	17469.3	5.02	6.95	14.95	0.64	0.96	0.33
B_2	119.7	232.1	-	-	-	-	-	-	-	-
Eu	93.2	216.1	496.6	743.4	20.17	26.37	35.00	0.32	0.37	0.22
B_3	158.1	397.0	-	-	-	-	-	-	-	-
Yb	285.1	760.6	3925.5	6094.6	36.40	53.34	83.90	0.31	0.35	0.17

Ce standard 2500 μg
Eu standard 20 μg
Yb standard 100 μg
l - large channel mask
s - small channel mask
* - Robinson et al., (1986)
l.l.d. - lower limit of detection

$$\text{l.l.d.} = 6/m\sqrt{Rb/T}$$

m - intensity
Rb - background count rate (c.p.s)
T - 80s

Table A3.6

Calculation of interference factor of Pr on B_3 according to the Robinson et al., (1986), method.

Line	Angle 2Θ	Std Sample	Blank	$Intensity_{cor}$	Ratio
B_3	55.330	201.1	161.7	39.4	
Pr_{100}	75.430	1459.0	35.1	1429.3	0.0277
					+-0.0021
B_3	55.330	191.2	161.7	29.5	
Pr_{100}	75.430	1116.6	35.1	1081.5	0.0273
					+-0.0028
B_3	55.330	185.0	161.7	23.3	
Pr_{50}	75.430	664.7	35.1	629.6	0.0370
					+-0.0047
B_3	55.330	179.6	161.7	17.9	
Pr_{50}	75.430	585.0	35.1	559.9	0.0320
					+-0.0052

+- refers to σ^1 value.
$Intensity_{cor}$ = Sample line - Blank line
Ratio = $Intensity_{(cor\ Blank)}/Intensity_{(cor\ sample)}$.
Average ratio = 0.0310
Θ^1=0.0045
c.o.v.=14.6%

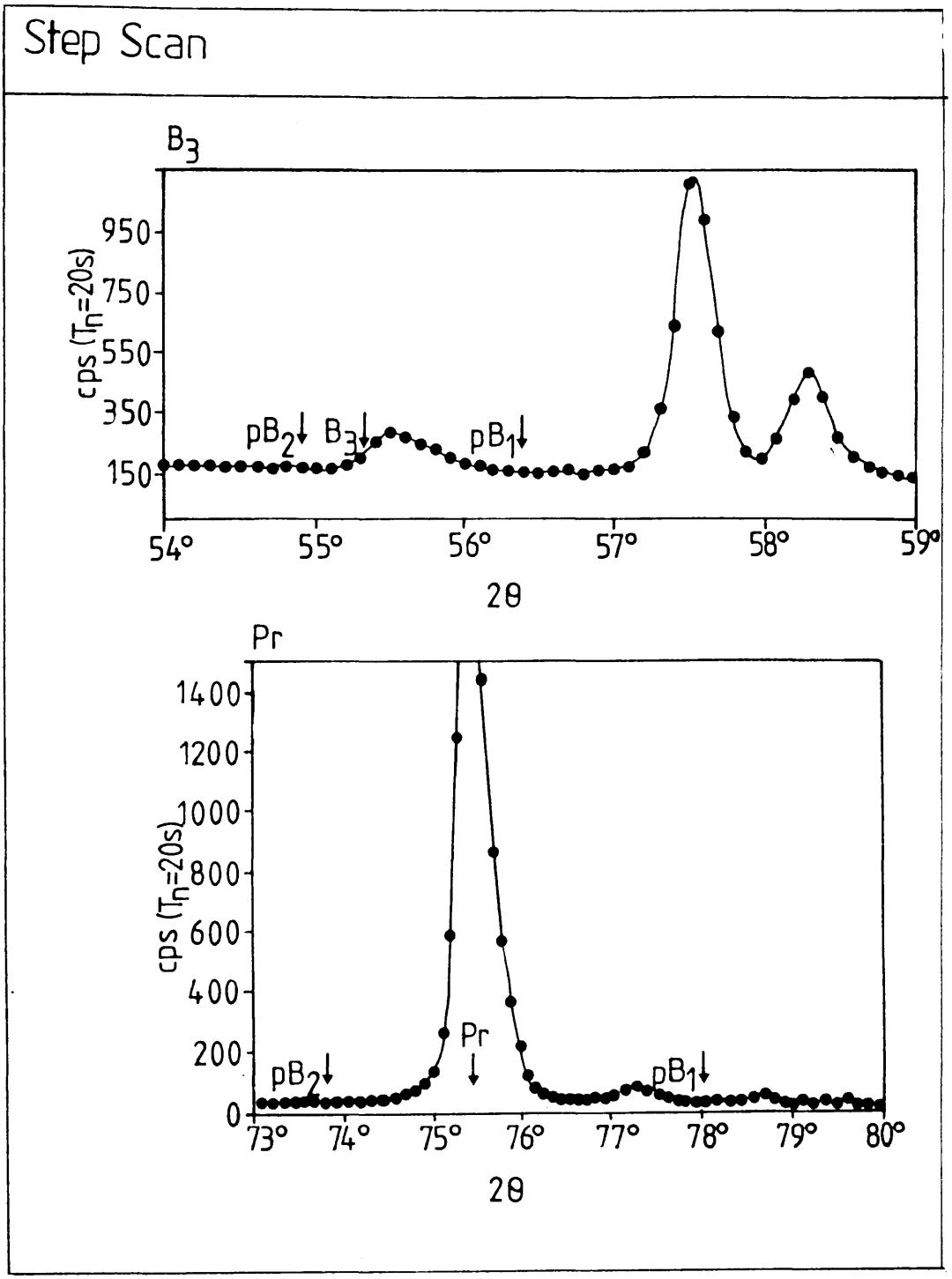

Figure A3.3: XRF srep scan across the Pr peak and background B_3. Note the interference on B_3.

Table A3.7

Calculation of interference correction of Pr on B_3 using psuedo-backgrounds determined by spectral calculator.

Line	Angle	Intensity	B_{calc}	B_{cor}	Ratio
pB_2	47.150	287.4			
B_3	55.330	201.1	187.5	13.6	
pB_1	60.400	119.9			
					0.0096
pB_2	73.900	45.6			+-0.0028
Pr_{100}	75.425	1459.0	42.1	1416.9	
pB_1	80.700	30.1			
pB_2	47.150	271.1			
B_3	55.330	191.2	177.6	13.6	
pB_1	60.400	119.6			
					0.0126
pB_2	73.900	43.9			+-0.0035
Pr_{100}	75.425	1116.6	40.3	1076.3	
pB_1	80.700	27.9			
pB_2	47.150	289.3			
B_3	55.330	185.0	183.6	1.4	
B_1	60.400	118.1			
					0.0022
pB_2	73.900	42.8			+-0.0060
Pr_{100}	75.425	664.7	39.4	625.3	
pB_1	80.700	27.8			
pB_2	47.150	265.5			
B_3	55.330	179.6	174.4	5.2	
pB_1	60.400	117.9			
					0.0095
pB_2	73.900	42.1			+-0.0068
Pr_{100}	75.425	585.0	38.8	546.2	
pB_1	80.700	27.6			

+- refers to σ^1 value.

pB - psuedo-background.

$B_{calc} = \{[(pB_2-pB_1)/(\Theta_2-\Theta_1)] \times (\Theta_3-\Theta_1)\} + pB_1$

$B_{cor} = B_3 - B_{calc}$

Ratio = B_{corB3}/B_{corPr}

Table A3.8

Calculation of the interference correction of Pr on the B_3 after step scan.

Line	Angle 2Θ	Count Rate (c.p.s.)	B_{calc}*	Line Intensity	Ratio
pB_2	54.900	166.8			
B_3	55.330	205.8	161.3	44.5	
pB_1	56.400	147.7			
					0.0207
pB_2	73.800	46.8			+-0.0017
Pr_{150}	75.430	2192.7	42.6	2150.1	
pB_1	78.000	35.9			
pB_2	54.900	166.8			
B_3	55.330	204.7	162.1	42.6	
pB_1	56.400	150.4			
					0.0226
pB_2	73.800	45.5			+-0.0019
Pr_{150}	75.430	1922.7	41.4	1881.3	
pB_1	78.000	35.0			
.					
pB_2	54.900	173.3			
B_3	55.330	198.8	167.9	30.9	
pB_1	56.400	154.3			
					0.0217
pB_2	73.800	43.5			+-0.0025
Pr_{100}	75.430	1461.5	39.7	1421.8	
pB_1	78.000	33.6			
pB_2	54.900	167.6			
B_3	55.330	193.3	164.0	29.3	
pB_1	56.400	155.0			
					0.0263
pB_2	73.800	45.9			+-0.0032
Pr_{100}	75.430	1153.9	41.5	1112.4	
pB_1	78.000	34.6			

+- refers to σ^1 value.
$B_{calc} = [(pB_2-pB_1)/(\Theta_2-\Theta_1)]$ X $(x-pB_1)$.
Line Intensity = $x-B_{calc}$. Where x = B_3 or Pr_x.
Ratio = Line intensity of Pr_x /Line intensity of B_3.
Average ratio = 0.0228
σ^1=0.0024
c.o.v.=10.7%

Discussion

The investigation showed that the Philips PW 1404 was a viable instrument to use for REE thin film analysis and was capable of reproducing results comparable to those of Robinson et al., (1986). Count rates encountered in this method were relatively small and experimental conditions would have had to have been repeated exhaustively before a statistical improvement could have been shown. Step scans of all peak and background positions would have been necessary when calculating interference coefficients. Extreme machine time would have been used for the calibration of such a technique. The excessive time which would have been required to calibrate the XRF under optimum conditions precluded this technique for the purpose of this work. The samples were finally analyzed by ICP (Inductively Coupled Plasma).

Appendix 4A
The REE analysis results and 1σ coefficient of variation.

ppm	Evensen	,423	,423ap	,433	,433ap	,474.5
La	0.24	40.86	1137.38	21.66	839.58	76.00
Ce	0.64	60.53	1819.90	29.56	1347.92	38.77
Pr	0.10	10.10	263.59	5.70	200.00	6.30
Nd	0.47	39.43	1093.69	23.58	837.50	24.27
Sm	0.15	7.29	184.95	4.52	132.29	4.94
Eu	0.06	2.96	26.21	1.57	21.88	2.70
Gd	0.20	7.52	170.39	4.34	127.08	4.90
Tb*	0.37	12.00	267.06	6.95	200.91	7.81
Dy	0.25	6.93	150.48	4.03	114.58	4.50
Ho	0.06	1.34	28.16	0.76	22.92	1.13
Er	0.17	3.95	82.52	2.18	65.63	2.82
Tm*	0.03	0.55	9.87	0.30	7.73	0.40
Yb	0.17	3.22	45.15	1.70	34.38	2.36
Lu*	0.03	0.44	4.10	0.23	2.91	0.33

cov	,423	,423ap	,433	,433ap	,474.5
La	5.28	6.72	6.92	11.45	4.00
Ce	6.78	8.26	9.20	13.68	8.63
Pr	7.21	9.40	9.18	15.82	9.41
Nd	6.14	7.76	7.59	12.99	8.07
Sm	7.07	9.37	8.74	15.82	8.76
Eu	2.99	6.66	3.87	10.82	3.22
Gd	11.12	15.56	14.01	26.37	14.21
Tb*					
Dy	6.95	10.13	8.90	17.04	8.79
Ho	11.61	17.18	15.03	28.24	13.00
Er	13.13	19.11	16.95	31.37	16.04
Tm*					
Yb	8.68	15.50	11.52	26.28	10.41
lu*					

* These values were calculated using the linear extrapolation of the chondrite normalized patterns.
cov - 1σ coefficient of variation expressed in percent.
Evensen - The chondite value (Evensen et al., 1978)

ppm	,474.5ap	,551.5	,551.5ap	,601.5	,601.5ap	,652
La	908.70	26.15	852.33	15.87	553.95	12.19
Ce	1486.09	44.72	1488.89	25.79	1011.40	20.58
Pr	201.74	7.17	244.44	4.02	159.53	3.52
Nd	924.35	30.20	964.44	15.29	671.00	14.58
Sm	152.17	5.31	158.89	2.36	117.59	2.65
Eu	22.61	2.27	25.56	0.72	19.77	1.35
Gd	143.48	5.60	141.11	2.85	112.91	2.86
Tb*	226.35	8.60	216.95	4.48	178.76	4.29
Dy	128.70	4.70	118.89	2.54	102.14	2.26
Ho	21.74	0.91	22.22	0.50	18.86	0.43
Er	63.48	2.62	63.33	1.56	49.03	1.37
Tm*	7.53	0.34	7.47	0.20	5.92	0.18
Yb	33.91	1.79	33.33	1.03	27.53	0.97
Lu*	2.97	0.21	2.85	0.12	2.60	0.12

cov	,474.5ap	,551.5	,551.5ap	,601.5	,601.5ap	,652
La	10.06	6.75	11.73	8.00	2.53	9.00
Ce	12.02	8.11	13.46	9.81	2.94	10.84
Pr	14.38	8.88	14.77	11.03	3.17	11.72
Nd	11.29	7.27	12.50	9.51	2.60	9.69
Sm	13.59	8.51	14.94	12.08	3.13	10.94
Eu	9.70	3.54	10.24	5.82	2.02	4.24
Gd	22.67	13.36	25.85	17.43	5.01	17.32
Tb*						
Dy	14.65	8.66	17.23	10.76	3.23	11.28
Ho	26.01	14.51	29.20	17.82	5.52	18.90
Er	29.16	16.71	33.04	20.14	6.52	21.44
Tm*						
Yb	24.12	11.98	27.25	14.60	5.22	15.00
lu*						

* These values were calculated using the linear extrapolation of the chondrite normalized patterns.
cov - 1σ coefficient of variation expressed in percent.
Evensen - The chondite value (Evensen et al., 1978)

ppm	,652ap	,705.5	,705.5ap	,757.7	,757.7ap	,798
La	582.58	14.51	215.67	21.61	419.81	18.91
Ce	1043.44	26.27	352.74	38.00	696.02	33.18
Pr	157.47	4.51	53.98	6.26	101.66	5.56
Nd	699.10	20.06	228.72	26.76	409.55	24.15
Sm	125.57	3.75	41.95	5.04	73.21	4.23
Eu	14.25	1.78	10.01	1.88	12.03	1.57
Gd	117.42	4.08	44.07	5.22	75.66	4.55
Tb*	181.14	5.91	72.64	7.92	125.74	6.97
Dy	99.77	2.95	43.76	4.25	76.53	3.80
Ho	19.00	0.57	8.42	0.84	14.60	0.70
Er	53.62	1.64	23.49	2.38	41.18	1.91
Tm*	6.22	0.20	2.90	0.30	5.02	0.24
Yb	26.92	0.99	14.08	1.49	23.83	1.15
Lu*	2.11	0.10	1.45	0.16	2.35	0.12

cov	,652ap	,705.5	,705.5ap	,757.7	,757.7ap	,798
La	6.41	8.27	4.16	6.84	3.15	7.29
Ce	7.46	9.65	5.11	8.11	3.85	8.65
Pr	8.30	10.33	5.61	8.74	4.31	9.29
Nd	6.62	8.23	4.58	7.11	3.61	7.49
Sm	7.80	9.30	5.37	8.06	4.30	8.77
Eu	6.19	3.68	2.92	3.58	2.82	3.92
Gd	12.79	14.45	8.25	12.74	6.65	13.66
Tb*						
Dy	8.49	9.96	5.07	8.40	4.05	8.85
Ho	14.33	16.68	8.49	13.92	6.81	15.16
Er	16.19	19.51	9.69	16.16	7.72	18.04
Tm*						
Yb	13.74	14.79	7.51	12.10	6.09	13.76
lu*						

ppm	,798ap	,845.75	,845.75ap	,893	,893ap	,951
La	399.13	16.66	404.25	7.06	748.07	10.98
Ce	748.05	30.45	760.02	11.40	1344.21	20.44
Pr	124.66	4.65	126.45	1.63	186.70	3.12
Nd	554.22	22.86	553.97	7.84	774.68	15.58
Sm	105.82	4.20	109.24	1.51	134.76	3.12
Eu	21.20	1.90	27.52	1.26	13.73	2.03
Gd	103.89	4.34	108.49	1.75	114.16	3.15
Tb*	159.41	6.53	167.13	2.93	175.16	4.88
Dy	87.10	3.47	91.86	1.80	95.71	2.70
Ho	15.77	0.64	16.98	1.02	16.74	0.48
Er	40.46	2.04	43.79	1.25	43.78	1.48
Tm*	4.89	0.23	5.40	0.16	5.07	0.18
Yb	22.77	0.97	26.06	0.88	21.89	0.83
Lu*	2.16	0.07	2.66	0.11	1.70	0.08

cov	,798ap	,845.75	,845.75ap	,893	,893ap	,951
La	3.23	7.47	3.21	12.02	7.73	9.69
Ce	3.71	8.89	3.68	14.49	9.16	11.04
Pr	3.89	9.78	3.86	17.13	10.44	12.38
Nd	3.10	7.54	3.10	13.13	8.69	9.19
Sm	3.57	8.73	3.51	14.56	10.69	10.31
Eu	2.12	3.54	1.86	4.38	8.73	3.44
Gd	5.67	13.67	5.55	22.04	17.88	16.38
Tb*						
Dy	3.79	9.30	3.69	13.32	12.31	10.83
Ho	6.55	15.55	6.31	13.00	21.27	18.83
Er	7.78	17.44	7.48	22.28	24.60	20.51
Tm*						
Yb	6.23	14.93	5.82	16.00	21.67	16.44
lu*						
Er	16.19	19.51	9.69	16.16	7.72	18.04
Tm*						
Yb	13.74	14.79	7.51	12.10	6.09	13.76
lu*						

ppm	,951ap	,999.8	,999.8ap	,1050.2	,1100.8	,1100.8ap
La	318.58	9.14	268.94	12.01	61.73	368.92
Ce	646.23	16.87	471.21	19.90	114.97	732.77
Pr	106.98	2.42	68.56	3.07	18.56	115.34
Nd	491.20	12.51	305.16	15.92	82.60	547.46
Sm	98.38	2.35	54.59	3.10	15.79	106.24
Eu	27.81	1.77	20.08	1.63	3.61	21.46
Gd	93.93	2.40	56.77	3.14	16.29	106.11
Tb*	142.43	3.73	94.95	4.96	24.95	159.64
Dy	76.45	2.08	58.24	2.83	13.59	84.66
Ho	13.77	0.36	11.32	0.52	2.55	15.86
Er	34.95	1.18	29.78	4.65	6.77	40.96
Tm*	4.22	0.15	3.70	0.43	0.84	4.89
Yb	19.68	0.73	18.04	0.88	4.09	22.37
Lu*	1.87	0.08	1.88	0.00	0.43	2.03

cov	,951ap	,999.8	,999.8ap	,1050.2	,1100.8	,1100.8ap
La	3.59	10.61	4.28	9.29	4.13	6.06
Ce	4.06	12.09	5.20	11.20	4.76	6.88
Pr	4.18	14.06	5.72	12.50	5.08	7.31
Nd	3.31	10.22	4.60	9.11	4.04	5.69
Sm	3.85	11.84	5.64	10.35	4.65	6.69
Eu	1.87	3.70	2.41	3.85	2.59	3.85
Gd	5.98	18.82	8.42	16.45	7.21	10.21
Tb*						
Dy	4.17	12.37	5.24	10.61	4.84	7.21
Ho	7.14	21.83	8.63	18.19	8.20	12.09
Er	8.36	23.01	9.92	19.43	9.58	14.03
Tm*						
Yb	6.93	17.51	7.94	15.96	7.41	11.81
lu*						

ppm	,1128.7	,1151.3	,1178.2	,1211	,1211ap	,1231.2
La	1.68	4.28	1.80	8.59	280.53	9.39
Ce	4.71	8.10	2.53	15.93	574.70	19.11
Pr	0.65	0.84	0.21	2.36	96.31	3.03
Nd	4.31	5.79	1.08	12.44	453.90	17.41
Sm	0.88	0.90	0.13	2.48	91.81	3.59
Eu	1.22	1.03	0.84	1.45	25.99	1.80
Gd	0.95	1.26	0.31	2.63	86.84	3.44
Tb*	1.70	2.13	0.53	4.08	133.51	5.25
Dy	1.12	1.32	0.34	2.27	73.16	2.85
Ho	0.20	0.22	0.07	0.39	13.16	0.48
Er	0.95	0.99	0.39	1.18	32.46	1.58
Tm*	0.13	0.13	0.05	0.14	4.00	0.19
Yb	0.70	0.69	0.28	0.69	19.34	0.84
Lu*	0.09	0.08	0.03	0.07	1.98	0.07

cov	,1128.7	,1151.3	,1178.2	,1211	,1211ap	,1231.2
La	16.47	12.74	22.77	10.93	3.99	9.53
Ce	18.80	15.58	26.90	12.42	4.49	10.96
Pr	22.05	20.13	48.34	14.27	4.59	11.91
Nd	16.13	14.23	29.85	10.25	3.59	8.60
Sm	17.11	16.91	37.80	11.53	4.15	9.39
Eu	4.42	4.81	6.35	4.08	2.01	3.63
Gd	27.32	24.20	52.49	17.98	6.48	15.26
Tb*						
Dy	15.50	14.47	30.56	11.85	4.45	10.20
Ho	25.01	24.49	48.17	21.11	7.61	17.65
Er	25.55	25.07	39.90	22.96	9.05	19.85
Tm*						
Yb	17.46	17.54	28.35	18.07	7.29	15.94
lu*						

ppm	,1231.2ap	1256.3	,1256.3ap	1270.4	,1270.4ap	1302.8
La	310.65	4.37	213.44	12.71	300.45	10.69
Ce	644.93	9.74	366.18	10.60	608.12	20.82
Pr	108.00	1.48	53.09	1.53	98.11	3.20
Nd	505.07	8.99	242.22	8.87	464.87	16.69
Sm	93.58	1.63	45.49	1.57	91.30	3.03
Eu	24.36	1.46	9.42	0.88	25.19	1.53
Gd	91.80	1.72	44.19	1.67	86.25	2.96
Tb*	142.72	2.67	72.11	2.58	132.63	4.61
Dy	79.50	1.48	42.89	1.43	72.71	2.58
Ho	14.21	0.31	8.24	0.20	13.17	0.44
Er	34.41	1.07	22.31	0.90	32.01	1.40
Tm*	4.19	0.12	2.77	0.10	3.88	0.16
Yb	19.76	0.49	13.48	0.39	18.18	0.73
Lu*	1.93	0.03	1.40	0.02	1.75	0.06

cov	,1231.2ap	1256.3	,1256.3ap	1270.4	,1270.4ap	1302.8
La	3.36	12.64	4.39	8.40	3.77	9.04
Ce	3.76	14.50	5.38	14.04	4.27	10.55
Pr	3.84	16.19	5.93	16.01	4.45	11.62
Nd	3.01	11.69	4.71	11.78	3.47	8.77
Sm	3.64	13.33	5.64	13.59	4.07	10.15
Eu	1.84	4.02	3.20	5.17	2.00	3.94
Gd	5.58	21.04	8.71	21.34	6.36	16.40
Tb*						
Dy	3.78	13.72	5.57	13.97	4.37	10.68
Ho	6.49	23.69	9.22	25.13	7.44	18.43
Er	7.78	24.02	10.46	26.25	8.91	21.03
Tm*						
Yb	6.39	20.67	8.38	22.86	7.36	17.04
lu*						

ppm	,1302.8ap	1320.8	,1320ap	,1340.1	,1340.1ap	1364.1
La	302.18	9.19	370.34	13.71	386.33	20.26
Ce	598.36	19.09	739.26	26.64	766.55	38.08
Pr	92.73	2.84	118.02	4.09	120.08	6.12
Nd	466.55	15.95	570.26	20.12	559.22	27.79
Sm	95.82	2.99	113.93	3.68	110.08	5.57
Eu	22.36	1.46	27.46	1.69	23.10	1.74
Gd	86.91	3.05	113.06	3.87	107.55	5.51
Tb*	135.81	4.75	173.09	5.99	166.31	8.50
Dy	76.20	2.65	94.26	3.32	91.92	4.68
Ho	13.82	0.44	17.31	0.59	17.18	0.84
Er	36.73	1.64	43.59	2.41	41.71	2.26
Tm*	4.64	0.20	5.36	0.27	5.18	0.27
Yb	23.27	0.90	25.81	1.04	25.33	1.29
Lu*	2.56	0.08	2.62	0.06	2.65	0.12

cov	,1302.8ap	1320.8	,1320ap	,1340.1	,1340.1ap	1364.1
La	7.92	9.61	4.71	8.13	3.19	7.16
Ce	8.94	10.96	5.35	9.45	3.65	8.18
Pr	9.64	12.27	5.62	10.38	3.86	8.83
Nd	7.29	8.96	4.34	8.01	3.03	6.91
Sm	8.30	10.22	5.04	9.29	3.56	7.77
Eu	4.47	4.03	2.65	3.74	2.00	3.71
Gd	13.34	16.15	7.69	14.42	5.46	12.37
Tb*						
Dy	8.98	10.55	5.31	9.48	3.72	8.23
Ho	15.31	18.33	8.98	16.17	6.25	14.31
Er	17.49	19.44	10.57	16.05	7.48	16.58
Tm*						
Yb	13.70	15.49	8.55	14.34	5.98	13.14
lu*						

ppm	,1364.1ap	,1379.1	,1379.1ap	,1396ap	,1421	,1421ap
La	314.99	27.21	376.74	259.93	26.33	308.76
Ce	587.35	51.48	752.55	297.19	48.46	681.77
Pr	88.24	8.50	116.71	79.52	7.67	95.48
Nd	403.79	38.74	543.13	368.51	35.57	439.92
Sm	75.38	7.45	105.83	69.61	6.92	85.70
Eu	15.35	2.14	20.95	13.89	1.85	17.05
Gd	74.29	7.20	101.35	66.60	6.80	81.73
Tb*	117.88	11.21	157.60	103.59	10.21	126.48
Dy	67.57	6.26	87.81	57.74	5.40	69.98
Ho	12.73	1.08	16.20	10.77	1.06	13.05
Er	31.63	3.10	40.12	26.65	2.86	32.30
Tm*	3.81	0.37	4.86	3.21	0.35	3.92
Yb	17.65	1.65	22.80	14.90	1.63	18.39
Lu*	1.65	0.14	2.19	1.40	0.16	1.77

cov	,1364.1ap	,1379.1	,1379.1ap	,1396ap	,1421	,1421ap
La	3.65	5.99	3.27	3.96	6.30	3.64
Ce	4.31	6.97	3.73	4.53	7.28	3.95
Pr	4.65	7.36	3.96	4.82	7.90	4.42
Nd	3.69	5.85	3.11	3.80	6.13	3.49
Sm	4.44	6.66	3.67	4.55	7.00	4.11
Eu	2.54	3.34	2.13	2.63	3.61	2.38
Gd	6.79	10.72	5.69	7.06	11.16	6.39
Tb*						
Dy	4.49	7.02	3.85	4.78	7.32	4.36
Ho	7.50	12.22	6.51	8.03	12.70	7.32
Er	8.88	14.18	7.72	9.52	14.72	8.68
Tm*						
Yb	7.40	11.52	6.37	7.92	11.73	7.16
lu*						

ppm	,1439.1	,1439.1ap	,1447.3	,1498.9	,1508.2	,1520.4
La	25.41	341.64	4.46	3.21	5.46	8.13
Ce	47.08	661.75	7.28	4.93	6.77	12.54
Pr	7.72	99.88	1.05	0.53	0.52	1.69
Nd	35.15	441.49	4.45	4.32	4.25	7.30
Sm	6.60	78.61	0.86	0.96	0.51	1.16
Eu	1.79	15.23	0.59	0.82	1.15	1.32
Gd	6.89	76.78	1.02	1.03	0.48	0.98
Tb*	10.46	122.42	1.57	1.80	0.90	1.63
Dy	5.63	70.63	0.86	1.16	0.63	0.99
Ho	1.06	13.21	0.17	0.23	0.12	0.19
Er	2.82	32.92	0.59	0.95	0.74	0.65
Tm*	0.34	3.92	0.09	0.11	0.08	0.08
Yb	1.54	17.76	0.52	0.53	0.30	0.37
Lu*	0.14	1.58	0.07	0.05	0.01	0.04

cov	,1439.1	,1439.1ap	,1447.3	,1498.9	,1508.2	,1520.4
La	6.41	3.45	14.97	17.50	13.61	11.23
Ce	7.38	3.99	17.67	20.47	17.97	13.76
Pr	7.88	4.30	21.27	29.96	30.49	16.85
Nd	6.17	3.47	16.61	17.70	17.83	13.62
Sm	7.16	4.27	18.89	18.90	23.58	16.48
Eu	3.67	2.51	6.39	5.43	4.58	4.28
Gd	11.10	6.57	28.74	28.67	42.07	29.41
Tb*						
Dy	7.52	4.32	19.20	16.55	22.41	17.98
Ho	12.73	7.24	32.26	27.36	37.93	29.99
Er	14.85	8.56	32.48	25.57	29.10	31.07
Tm*						
Yb	12.09	7.26	20.73	20.65	27.18	24.52
lu*						

ppm	,1548.4	,1548.4ap	1556.6ap,	1580.5	,1606.2	,1627.5
La	7.99	162.84	176.30	2.57	2.81	2.67
Ce	15.95	323.22	350.54	6.52	3.67	3.07
Pr	2.52	51.14	55.52	0.59	0.37 ,	
Nd	13.92	257.59	275.71	2.18	2.75	2.01
Sm	2.62	50.82	55.20	0.31	0.46	0.28
Eu	1.08	14.26	14.89	0.60	0.48	0.68
Gd	2.89	51.10	54.88	0.94	0.57 ,	
Tb*	4.21	76.21	82.73	1.18	1.17	0.23
Dy	2.12	39.86	44.01	0.43	0.88	0.31
Ho	0.34	7.17	8.00	0.12	0.19	0.06
Er	1.29	17.68	19.67	0.52	0.82	0.45
Tm*	0.14	1.36	2.31	0.06	0.10	0.05
Yb	0.56		10.23	0.25	0.52	0.16
Lu*	0.03	-1.35	0.86	0.02	0.06	0.00

cov	,1548	,1548ap	,1556,6ap	1580.5	,1606.2	,1627.5
La	10.16	5.05	4.85	19.44	18.63	19.09
Ce	11.85	5.75	5.53	18.29	22.90	24.41
Pr	12.92	6.08	5.83	28.63	36.11	ERR
Nd	9.55	4.59	4.44	24.96	22.22	25.98
Sm	10.84	5.37	5.15	28.69	24.69	35.18
Eu	4.69	2.62	2.56	6.32	7.07	5.94
Gd	16.58	8.14	7.86	30.04	38.43	ERR
Tb*						
Dy	11.69	5.81	5.53	27.22	19.05	32.09
Ho	20.50	9.94	9.40	37.40	30.02	46.78
Er	21.93	11.80	11.19	34.71	27.53	37.01
Tm*						
Yb	19.36	10.17	9.67	29.84	20.80	37.09
lu*						

ppm	,1649.5
La	3.47
Ce	4.79
Pr	0.29
Nd	3.00
Sm	0.47
Eu	0.51
Gd	0.51
Tb*	1.08
Dy	0.83
Ho	0.15
Er	0.81
Tm*	0.10
Yb	0.45
Lu*	0.04

cov	,1649.5
La	16.91
Ce	20.69
Pr	40.76
Nd	21.26
Sm	24.43
Eu	6.85
Gd	40.82
Tb*	
Dy	19.57
Ho	34.34
Er	27.67
Tm*	
Yb	22.43
lu*	

Appendix 4B
The REE analysis results - eastern Bushveld.

	,eb1d	,eb2d	,eb2dap	,eb3d	,eb3dap	,eb4dap	,eb5d
La	39.72	32.15	1156.67	31.37	896.09	903.53	26.47
Ce	63.19	54.19	2061.32	53.77	1581.96	1596.77	42.70
Pr	9.10	8.56	319.96	8.21	248.45	247.75	6.17
Nd	35.10	31.67	1322.47	33.47	1022.66	1016.48	25.72
Sm	6.10	6.18	238.14	6.30	187.97	186.94	4.55
Eu	1.62	2.25	20.77	2.15	19.25	15.96	1.60
Gd	5.82	6.03	219.87	6.17	180.97	176.76	4.41
Dy	6.81	5.74	186.66	6.22	162.50	156.88	4.78
Ho	1.43	1.16	34.56	1.22	30.24	29.04	0.97
Er	4.25	3.18	87.74	3.42	77.98	73.94	2.90
Yb	3.62	2.31	43.15	2.45	43.19	39.47	2.22

,c.o.v.,eb1d	,eb2d	,eb2dap	,eb3d	,eb3dap	,eb4dap	,eb5d
La 5.08	5.67	2.86	5.76	2.05	1.71	6.25
Ce 6.29	6.81	3.37	6.86	2.43	2.03	7.65
Pr 7.19	7.45	3.66	7.63	2.62	2.20	8.80
Nd 6.16	6.31	3.03	6.36	2.17	1.83	7.24
Sm 7.38	7.36	3.59	7.33	2.56	2.15	8.58
Eu 3.78	3.23	3.23	3.32	2.11	1.95	3.83
Gd 11.97	11.80	5.88	11.72	4.09	3.47	13.85
Dy 6.77	7.41	3.91	7.15	2.64	2.25	8.15
Ho 10.85	12.10	6.67	11.86	4.50	3.85	13.27
Er 11.99	13.91	7.97	13.48	5.33	4.59	14.63
Yb 7.80	9.80	6.82	9.56	4.30	3.77	10.03

cov - 1σ coefficient of variation expressed as a percent

	,eb7dap	,eb8d	,eb9d	,eb9dap	,eb10d	,eb11d
La	569.28	4.27	0.68	186.28	16.91	9.33
Ce	935.59	5.43	1.25	378.77	29.77	13.91
Pr	144.11	0.88	lld	71.49	4.76	1.80
Nd	588.80	4.08	0.68	343.66	21.89	7.55
Sm	109.93	0.58	lld	71.68	4.31	1.14
Eu	19.56	0.46	0.02	25.86	1.33	0.82
Gd	107.64	0.47	lld	73.76	4.46	1.08
Dy	93.95	0.62	lld	59.82	3.74	1.14
Ho	17.27	0.15	lld	10.83	0.71	0.23
Er	45.50	0.56	0.38	27.05	1.98	0.77
Yb	27.36	0.32	0.21	15.74	1.06	0.45

,c.o.v.	,eb7dap	,eb8d	,eb9d	,eb9dap	,eb10d	,eb11d
La	1.94	14.94	30.88	3.35		10.51
Ce	2.38	18.71	37.99	3.70		13.14
Pr	2.59	23.19		3.65		16.33
Nd	2.16	18.16	44.72	2.80		13.41
Sm	2.51	22.37	75.81	3.08		16.58
Eu	1.58	6.97	19.58	1.36		5.42
Gd	3.99	42.41		4.77		28.02
Dy	2.62	22.57		3.25		16.72
Ho	4.48	34.28		5.60		27.62
Er	5.26	33.50	40.46	6.75		28.49
Yb	4.07	26.55	32.97	5.31		22.26

	,eb11dap	,eb12c	,eb13c	,eb14c	,eb15c	,eb16c	,eb17c
La	268.58	4.52	3.29	5.70	6.43	6.89	5.96
Ce	516.22	7.22	4.50	8.46	9.77	9.62	8.54
Pr	90.85	0.71	0.51	1.06	1.28	1.08	1.03
Nd	417.12	4.68	3.86	4.77	6.11	5.27	5.36
Sm	83.12	1.04	0.77	0.78	1.20	0.80	1.02
Eu	21.15	0.72	0.54	0.66	0.62	0.77	0.67
Gd	83.06	1.19	0.93	0.78	1.84	0.80	0.88
Dy	67.03	1.63	1.39	0.82	1.69	0.95	1.21
Ho	12.04	0.31	0.29	0.17	0.33	0.20	0.25
Er	30.23	1.18	1.10	0.65	1.20	0.77	0.97
Yb	16.00	0.86	1.22	0.55	0.90	0.50	0.64

,c.o.v.	,eb11dap	,eb12c	,eb13c	,eb14c	,eb15c	,eb16c	,eb17c
La	3.77	14.89	17.32	13.32	12.59	12.18	13.05
Ce	4.27	17.77	21.21	16.35	15.38	15.49	16.29
Pr	4.36	25.92	30.56	21.26	19.35	21.06	21.55
Nd	3.42	16.26	18.73	16.83	14.89	16.04	15.88
Sm	3.86	17.32	19.73	19.63	16.20	19.48	18.38
Eu	2.03	5.79	6.67	6.05	6.25	5.61	6.02
Gd	6.07	26.75	30.16	33.04	21.45	32.67	31.11
Dy	4.14	13.96	15.14	19.68	13.74	18.31	16.22
Ho	7.17	23.45	24.48	31.99	22.86	29.39	26.25
Er	8.62	22.95	23.80	30.93	22.74	28.38	25.37
Yb	7.11	16.13	13.55	20.13	15.79	21.13	18.69

	,eb18b	,eb19b?	,eb20b	,eb21b	,eb22a	,a6/hd484	,ap10/g26
La	3.45	20.37	5.86	4.54	1.11	190.33	288.93
Ce	4.46	37.26	8.41	6.24	1.02	294.58	530.87
Pr	0.42	5.56	1.04	1.02	,	41.92	88.30
Nd	2.73	24.48	4.86	4.17	1.91	169.89	385.96
Sm	0.33	4.67	0.66	0.62	0.41	26.28	74.00
Eu	0.78	2.31	0.56	0.57	0.31	5.76	16.21
Gd	0.29	4.30	0.56	0.65	0.61	27.85	75.20
Dy	0.46	4.20	0.72	0.76	0.85	27.50	64.55
Ho	0.09	0.80	0.14	0.18	0.21	5.13	11.74
Er	0.39	2.22	0.56	0.57	0.80	13.84	29.67
Yb	0.22	1.77	0.27	0.39	0.52	6.92	16.29

,c.o.v.	,eb18b	,eb19b?	,eb20b	,eb21b	,eb22a	,ap6/hd48	,ap10/g26
La	16.90	7.12	13.17	14.86	28.09	3.36	2.86
Ce	21.25	8.40	16.43	18.59	33.35	4.25	3.32
Pr	33.71	9.23	21.51	21.73	ERR	4.83	3.48
Nd	22.26	7.46	16.70	17.99	26.68	4.03	2.80
Sm	28.14	8.81	21.13	21.76	25.64	5.15	3.22
Eu	5.57	3.26	6.55	6.53	8.79	2.92	1.82
Gd	54.47	14.07	38.95	36.25	37.42	7.88	5.02
Dy	26.22	8.97	21.04	20.47	19.40	4.85	3.32
Ho	44.50	14.89	35.16	31.14	28.75	8.26	5.71
Er	39.97	16.70	33.45	33.17	27.83	9.57	6.85
Yb	31.59	11.65	28.89	24.09	20.70	8.12	5.54

	,eb5d
La	26.47
Ce	42.70
Pr	6.17
Nd	25.72
Sm	4.55
Eu	1.60
Gd	4.41
Dy	4.78
Ho	0.97
Er	2.90
Yb	2.22

,c.o.v.	,eb5d
La	6.25
Ce	7.65
Pr	8.80
Nd	7.24
Sm	8.58
Eu	3.83
Gd	13.85
Dy	8.15
Ho	13.27
Er	14.63
Yb	10.03

Appendix 4C
REE analysis results of Biotites from the eastern Bushveld

	,eb5dbt	,eb7dbt	,eb15c	,eb15cbt	,eb16c	,eb16cbt
La	5.28	1.Ø4	6.43	1.86	6.89	5.68
Ce	5.48	,	9.77	2.39	9.62	8.Ø4
Pr	Ø.95	,	1.28	Ø.55	1.Ø8	1.35
Nd	5.13	1.Ø4	6.11	2.21	5.27	4.86
Sm	Ø.47	,	1.2Ø	Ø.24	Ø.8Ø	1.24
Eu	Ø.28	Ø.11	Ø.62	Ø.13	Ø.77	Ø.13
Gd	1.1Ø	Ø.5Ø	1.84	Ø.62	Ø.8Ø	1.55
Dy	1.26	,	1.69	Ø.64	Ø.95	1.Ø2
Ho	Ø.24	,	Ø.33	Ø.18	Ø.2Ø	Ø.22
Er	Ø.75	,	1.2Ø	Ø.46	Ø.77	Ø.73
Yb	Ø.55	,	Ø.9Ø	Ø.38	Ø.5Ø	Ø.86

,c.o.v.	,eb5dbt	,eb7dbt	,eb15c	,eb15cbt	,eb16c	,eb16cbt
La	27.93	5Ø.32	12.59	35.33	12.18	2Ø.16
Ce	32.84	5Ø.96	15.38	35.Ø7	15.49	23.89
Pr	44.Ø7	ERR	19.35	43.94	21.Ø6	27.8Ø
Nd	32.36	54.Ø7	14.89	37.Ø1	16.Ø4	24.9Ø
	ERR	ERR	ERR	ERR	ERR	ERR
Sm	4Ø.23	ERR	16.2Ø	4Ø.96	19.48	23.56
Eu	18.62	22.73	6.25	2Ø.87	5.61	2Ø.55
Gd	55.22	62.38	21.45	55.Ø5	32.67	34.82
Dy	32.6Ø	ERR	13.74	34.2Ø	18.31	27.21
Ho	55.Ø5	ERR	22.86	47.25	29.39	42.26
Er	57.17	ERR	22.74	54.31	28.38	43.27
	ERR	ERR	ERR	ERR	ERR	ERR
Yb	4Ø.69	ERR	15.79	37.27	21.13	24.77

c.o.v. - 1σ coefficient of variation expressed as a percentage of the mean value.
Note, the same samples were used by Von Gruenewaldt, (1971) and kindly supplied by him. However, the samples were renumbered and a listing of the previous and new numbers are given in Appendix 1Ø.

Appendix 5

Olivine Composition

The olivine composition was determined by a Jeol 733 Superprobe set at 20 kV. SiO2, MgO, FeO, MnO, CaO, Ni and Cr were analyzed but the Ni, CaO and Cr proved to be mostly below the detection limits. Reported values were calculated from 10 points, then analyzed as pairs of core and rim points of euhedral olivine.

M: Mean
SD: Standard Deviation (1σ)
Max: Maximum value
Min: Minimum value

	Sample	SiO2	Al2O3	Na2O	MgO	FeO	MnO	NiO
M	423.0	28.591	0.000	0.003	1.166	68.790	1.703	0.000
SD		0.127	0.000	0.006	0.178	0.722	0.082	0.000
Max		28.731	0.000	0.015	1.358	69.338	1.844	0.000
Min		28.437	0.000	0.000	0.873	67.579	1.626	0.000
M	474.5	28.751	0.065	0.011	0.617	69.014	1.673	0.016
SD		0.550	0.054	0.008	0.149	0.506	0.098	0.011
Max		29.693	0.159	0.026	0.746	69.521	1.829	0.029
Min		28.002	0.027	0.000	0.411	68.183	1.566	0.000
M	507.5	28.242	0.000	0.001	2.167	66.707	1.401	0.000
SD		0.870	0.000	0.004	0.100	1.171	0.051	0.002
Max		29.100	0.000	0.013	2.270	67.677	1.448	0.008
Min		26.115	0.000	0.000	1.898	63.744	1.316	0.000
M	551.5	29.196	0.000	0.000	3.946	64.810	1.155	0.003
SD		0.271	0.000	0.000	0.121	0.594	0.023	0.007
Max		29.730	0.000	0.000	4.097	65.480	1.184	0.019
Min		28.976	0.000	0.000	3.782	64.064	1.113	0.000
M	601.5	29.856	0.000	0.002	7.849	60.392	0.956	0.000
SD		0.325	0.000	0.002	0.370	0.358	0.051	0.000
Max		30.224	0.000	0.006	8.385	60.863	1.027	0.000
Min		29.233	0.000	0.000	7.270	59.732	0.862	0.000
M	652.0	29.876	0.000	0.003	7.990	60.934	0.978	0.015
SD		0.172	0.000	0.000	0.445	0.311	0.037	0.009
Max		30.183	0.000	0.000	8.330	61.634	1.034	0.029
Min		29.657	0.000	0.000	6.985	60.695	0.912	0.000
M	705.5	29.937	0.010	0.002	7.290	61.563	0.972	0.002
SD		0.650	0.017	0.003	0.218	0.546	0.039	0.002
Max		30.720	0.049	0.009	7.583	62.519	1.021	0.005
Min		29.282	0.000	0.000	6.928	60.918	0.913	0.000
M	752	30.116	0.000	0.000	7.767	59.043	0.988	0.000
SD		0.246	0.000	0.000	0.476	0.519	0.036	0.000
Max		30.505	0.000	0.000	8.145	59.859	1.047	0.000
Min		29.687	0.000	0.000	6.638	58.214	0.947	0.000
M	757.7	30.302	0.000	0.000	8.003	59.163	0.970	0.000
SD		0.178	0.000	0.000	0.102	0.370	0.017	0.000
Max		30.505	0.000	0.000	8.146	59.557	0.988	0.000
Min		30.109	0.000	0.000	7.926	58.672	0.946	0.000
M	798.0	30.684	0.000	0.007	10.418	57.984	0.914	0.000
SD		0.229	0.000	0.007	0.113	0.515	0.018	0.000
Max		31.020	0.000	0.020	10.523	58.480	0.942	0.000
Min		30.474	0.000	0.000	10.240	57.422	0.893	0.000

	Sample	SiO2	Al2O3	Na2O	MgO	FeO	MnO	NiO
M	845.8	30.586	0.000	0.000	10.661	56.680	0.900	0.001
SD		1.234	0.000	0.000	0.158	1.192	0.035	0.003
Max		30.885	0.000	0.000	10.858	57.758	0.945	0.095
Min		27.296	0.000	0.000	10.376	53.570	0.845	0.000
M	893.0	30.414	0.000	0.002	9.330	58.168	0.883	0.002
SD		0.126	0.000	0.004	0.716	0.548	0.032	0.001
Max		30.625	0.000	0.014	10.232	59.168	0.929	0.000
Min		30.265	0.000	0.000	8.149	57.661	0.837	0.000
M	951	29.917	0.000	0.012	6.687	63.234	1.055	0.001
SD		0.403	0.000	0.010	0.143	0.354	0.049	0.002
Max		30.378	0.000	0.026	6.912	63.850	1.100	0.006
Min		29.251	0.000	0.000	6.472	62.688	1.031	0.000
M	999.8	30.159	0.000	0.000	6.273	62.740	1.109	0.000
SD		0.324	0.000	0.001	0.071	0.496	0.044	0.000
Max		30.604	0.000	0.004	6.384	63.271	1.181	0.001
Min		29.482	0.000	0.000	6.192	61.521	1.076	0.000
M	1050.2	29.700	0.000	0.004	6.312	62.700	1.075	0.001
SD		0.291	0.000	0.006	0.092	0.468	0.057	0.004
Max		30.153	0.000	0.018	6.418	63.559	1.158	0.012
Min		29.348	0.000	0.000	6.155	62.141	1.013	0.000
M	1100.8	31.448	0.000	0.009	12.110	54.599	0.859	0.002
SD		0.322	0.000	0.008	0.345	0.665	0.026	0.001
Max		31.997	0.000	0.022	12.931	55.434	0.910	0.014
Min		31.065	0.000	0.000	11.726	53.579	0.821	0.000
M	1128.7	30.074	0.000	0.010	7.471	60.619	0.915	0.004
SD		0.712	0.000	0.014	0.266	0.861	0.038	0.006
Max		31.511	0.000	0.043	7.945	62.019	0.952	0.018
Min		28.944	0.000	0.000	7.030	58.939	0.845	0.000
M	1178.2	30.042	0.000	0.005	7.285	61.758	1.106	0.000
SD		1.362	0.024	0.014	0.919	3.628	0.119	0.000
Max		32.929	0.072	0.047	9.653	62.147	1.134	0.000
Min		28.008	0.000	0.000	6.740	50.065	0.718	0.000
M	1211.0	28.796	0.009	0.002	7.744	62.699	1.050	0.002
SD		0.730	0.013	0.012	0.919	0.502	0.050	0.003
Max		30.206	0.043	0.042	7.854	63.463	1.090	0.011
Min		28.022	0.000	0.000	7.616	61.641	0.951	0.000
M	1231.2	30.447	0.004	0.008	7.306	61.696	1.083	0.022
SD		0.354	0.012	0.008	0.178	0.599	0.028	0.008
Max		30.666	0.033	0.026	7.463	62.789	1.108	0.032
Min		29.626	0.000	0.000	6.865	60.940	1.020	0.011
M	1256.3	30.103	0.000	0.001	7.692	61.728	0.989	0.000
SD		0.146	0.000	0.009	0.155	0.302	0.031	0.000
Max		30.285	0.000	0.022	7.206	63.217	1.133	0.000
Min		29.830	0.000	0.000	6.638	62.230	1.035	0.000
M	1302.8	30.187	0.000	0.001	9.552	59.453	0.903	0.010
SD		0.562	0.000	0.011	0.174	0.478	0.032	0.010
Max		31.065	0.000	0.037	9.654	60.380	0.959	0.022
Min		29.111	0.000	0.000	9.224	58.836	0.846	0.000
M	1320.6	30.775	0.000	0.026	9.677	57.998	0.857	0.000
SD		0.265	0.000	0.011	0.223	0.725	0.020	0.000
Max		31.118	0.000	0.038	10.000	59.036	0.888	0.000
Min		30.300	0.000	0.001	9.238	56.240	0.824	0.000

	Sample	SiO2	Al2O3	Na2O	MgO	FeO	MnO	NiO
M	1340.1	31.070	0.000	0.001	10.330	57.246	0.853	0.001
SD		0.323	0.000	0.003	0.168	0.522	0.043	0.005
Max		31.709	0.000	0.009	10.525	58.104	0.942	0.018
Min		30.574	0.000	0.000	10.079	56.364	0.799	0.000
M	1364.0	30.408	0.000	0.006	11.255	56.388	0.865	0.000
SD		1.997	0.241	0.019	0.498	1.012	0.017	0.001
Max		31.516	0.764	0.032	11.469	56.550	0.875	0.004
Min		27.532	0.000	0.000	9.727	53.462	0.833	0.000
M	1379.1	30.980	0.000	0.009	12.423	55.497	0.774	0.000
SD		0.305	0.000	0.006	0.179	0.326	0.025	0.000
Max		31.153	0.000	0.016	12.505	55.284	0.831	0.000
Min		30.309	0.000	0.000	11.974	54.292	0.763	0.000
M	1396.0	30.816	0.029	0.018	12.350	54.937	0.812	0.001
SD		0.391	0.089	0.026	0.499	1.641	0.056	0.003
Max		31.239	0.267	0.036	12.504	55.283	0.830	0.011
Min		30.308	0.000	0.000	11.827	50.928	0.762	0.000
M	1439.1	31.704	0.000	0.010	15.193	53.199	0.745	0.004
SD		0.300	0.000	0.014	0.121	0.553	0.022	0.005
Max		32.090	0.000	0.037	15.405	53.386	0.775	0.015
Min		30.931	0.000	0.000	15.008	51.467	0.704	0.000
M	1447.3	31.628	0.000	0.002	15.330	52.989	0.701	0.004
SD		0.411	0.013	0.003	0.178	0.360	0.029	0.006
Max		32.417	0.037	0.009	15.386	53.782	0.730	0.016
Min		31.158	0.000	0.000	14.892	52.706	0.641	0.000
M	1465.5	35.239	0.044	0.002	25.992	39.936	0.468	0.000
SD		0.951	0.040	0.004	2.525	5.120	0.072	0.000
Max		38.148	0.101	0.013	33.616	46.005	0.519	0.000
Min		34.681	0.000	0.000	24.928	37.966	0.296	0.000
M	1508.2	47.552	0.366	0.014	9.225	39.944	0.645	0.000
SD		0.213	0.035	0.013	0.946	0.990	0.046	0.000
Max		47.775	0.438	0.028	9.612	41.888	0.708	0.000
Min		47.362	0.352	0.000	7.505	39.611	0.603	0.000
M	1548	31.676	0.000	0.000	15.848	52.223	0.726	0.007
SD		0.601	0.000	0.000	0.272	0.434	0.031	0.006
Max		32.418	0.000	0.000	16.481	52.784	0.757	0.018
Min		30.541	0.000	0.000	15.614	51.456	0.672	0.000
M	1556	32.282	0.000	0.000	16.080	50.570	0.667	0.000
SD		0.384	0.000	0.000	0.209	0.516	0.026	0.001
Max		32.781	0.000	0.000	16.420	51.161	0.713	0.005
Min		31.489	0.000	0.000	15.830	49.644	0.623	0.000
M	1580	31.915	0.000	0.006	14.809	53.457	0.664	0.000
SD		0.340	0.000	0.007	0.148	0.345	0.023	0.001
Max		32.308	0.000	0.020	15.133	53.886	0.706	0.003
Min		31.595	0.000	0.000	14.502	52.999	0.623	0.000
M	1627	33.201	0.000	0.001	18.416	49.028	0.546	0.000
SD		0.315	0.000	0.003	0.447	0.745	0.042	0.000
Max		33.791	0.000	0.009	19.136	49.903	0.590	0.000
Min		32.704	0.000	0.000	17.738	47.859	0.543	0.000

Appendix 6

Apatite Composition

The compositional trend of the cumulus apatite in the Bk-1 borehole was investigated using a Jeol Superprobe to determine CaO, FeO, P_2O_5, Cl and F content. Fluoride, tugtupite and natural hematite served as standards for F, Cl and FeO respectively. The Durago 1 apatite standard was used as a standard for P_2O_5 and CaO determinations and for evaluating the precision (Table A6.1).

Table A6.1

Comparison of the Durago 1 apatite standard

Element	Microprobe (Roeder et al., 1987)	Young et al., (1969)	Present det.	Standard deviation (1σ)
CaO	54.05	54.02	54.15	1.49
FeO	0.028	0.005	0.020	0.02
P2O5	40.90	40.78	41.72	2.22
Cl	0.36	0.41	0.37	0.035
F	3.53	3.53	4.03	0.253
Total	98.87	98.75	101.27	

Counting time on the F, Cl, CaO and FeO was 50 s on peak and 10 s on background. The phosphorous peak was counted for 20 seconds. Microprobe settings were: acceleration potential 15 kV; beam current $2x10^{-8}$ A and defocused beam of 10 um. The fluorine peak was discriminated from the phosphorous peak by using a pulse height setting, the gain at 4.3 and the window width at 1 V lower level. The analysis of the Durgo 1 apatite (Table 1) clearly showed that the F analyzed approximately 0.50 percent too high. This raised value was attributable to the phosphorous interference which had not been completely separated from the F peak by the pulse height analyzer. The fluorine determinations had good reproducibility and were used to define trends accurately. The resulting lower limits of detection were: F = 0.12 mass percent; Cl = 0.03 mass percent, and FeO = 0.04 mass percent. Ten points per thin section were analyzed as pairs of core and "rim" analyses per apatite grain.

M - Mean
SD - Standard deviation (1σ)
Min - Minimum value
Max - Maximum value

	Sample	CaO	FeO	P2O5	Cl-	F-
M	423.0	55.981	0.167	41.398	0.045	3.757
SD		0.1754	0.165	1.476	0.046	0.224
Max		57.436	0.236	43.218	0.131	4.102
Min		55.244	0.026	39.114	0.000	3.508

	Sample	CaO	FeO	P2O5	Cl-	F-
M	433.0	55.901	0.059	41.709	0.092	3.573
SD		1.324	0.059	1.933	0.038	0.262
Max		57.562	0.162	43.969	0.169	4.111
Min		53.718	0.000	38.803	0.051	3.343
M	507.5	56.311	0.238	41.805	0.227	3.093
SD		0.930	0.316	1.811	0.257	0.368
Max		57.823	1.112	48.396	0.713	3.784
Min		55.180	0.055	38.797	0.012	2.487
M	551.5	54.284	0.084	39.891	0.261	3.272
SD		1.118	0.216	1.840	0.032	0.168
Max		56.150	0.695	43.061	0.306	3.497
Min		52.357	0.000	37.826	0.213	3.018
M	601.5	53.679	0.035	38.230	0.715	2.591
SD		1.957	0.036	1.960	0.094	0.141
Max		56.111	0.100	40.093	0.836	2.891
Min		50.256	0.000	34.710	0.560	2.486
M	652.0	55.605	0.007	40.842	0.713	2.698
SD		1.168	0.017	1.056	0.108	0.179
Max		57.388	0.053	42.779	0.912	2.889
Min		53.851	0.000	39.436	0.565	2.379
M	705.5	54.526	0.156	39.820	0.512	3.059
SD		1.245	0.058	1.745	0.085	0.215
MAx		55.740	0.289	41.807	0.669	2.758
Min		52.686	0.097	36.902	0.385	3.069
M	798	52.641	0.243	39.081	0.671	3.022
SD		1.270	0.182	1.431	0.069	0.108
Max		54.888	0.567	41.298	0.759	3.316
Min		50.163	0.110	36.978	0.570	2.918
M	845.8	54.249	0.044	40.909	0.554	3.016
SD		0.749	0.051	1.271	0.010	0.143
Max		55.141	0.155	42.270	0.567	2.826
Min		52.911	0.000	39.734	0.540	3.195
M	951.0	56.957	0.159	39.383	0.439	3.859
SD		1.385	0.164	0.980	0.039	0.154
Max		58.528	0.508	41.871	0.506	4.031
Min		54.409	0.010	38.142	0.403	3.726
M	999.8	53.842	0.317	37.971	0.491	3.673
SD		2.208	0.137	1.319	0.035	0.337
Max		58.432	0.672	40.839	0.568	4.125
Min		51.502	0.117	37.212	0.456	3.194
M	1050.2	55.512	0.143	40.931	0.483	3.137
SD		1.176	0.196	1.337	0.080	0.237
Max		56.816	0.664	42.787	0.568	3.756
Min		53.540	0.000	38.154	0.319	2.885
M	1100.8	55.562	0.223	40.567	0.505	2.978
SD		1.496	0.244	1.293	0.065	0.135
Max		57.136	0.904	43.096	0.592	3.158
Min		52.416	0.114	38.703	0.391	2.756
M	1211.0	55.813	0.099	39.073	0.370	3.302
SD		0.880	0.075	1.214	0.022	0.259
Max		56.800	0.213	41.074	0.400	3.663
Min		54.129	0.000	37.061	0.343	2.964

	Sample	CaO	FeO	P2O5	Cl-	F-
M	1231.2	54.942	0.148	42.542	0.448	3.241
SD		0.733	0.096	1.426	0.037	0.191
Max		56.145	0.338	44.414	0.506	3.549
Min		54.549	0.031	39.445	0.395	2.942
M	1256.3	55.088	0.072	42.359	0.355	3.076
SD		0.697	0.060	1.307	0.022	0.184
Max		56.191	0.148	43.531	0.396	3.076
Min		53.773	0.000	41.943	0.321	2.757
M	1270.4	55.679	0.316	40.207	0.372	2.958
SD		1.887	0.345	1.568	0.031	0.421
Max		57.256	0.477	38.532	0.395	3.780
Min		53.113	0.111	43.736	0.345	2.443
M	1302.8	55.293	0.038	38.246	0.513	2.753
SD		0.965	0.063	0.965	0.096	0.293
Max		56.775	0.190	39.292	0.569	3.260
Min		54.610	0.000	37.179	0.457	2.614
M	1320.8	55.864	0.132	40.547	0.464	3.664
SD		0.926	0.146	1.505	0.030	0.259
Max		57.967	0.360	42.266	0.537	4.185
Min		54.941	0.033	35.232	0.419	3.333
M	1340.1	55.176	0.211	40.029	0.498	2.679
SD		1.028	0.164	1.125	0.054	0.117
Max		56.426	0.404	41.540	0.562	2.810
Min		52.836	0.009	37.363	0.426	2.558
M	1364.0	53.706	0.068	38.378	0.537	3.687
SD		0.594	0.049	1.139	0.017	0.201
Max		54.354	0.170	40.460	0.551	3.993
Min		52.328	0.000	36.724	0.500	3.305
M	1379.1	54.934	0.084	40.578	0.536	2.863
SD		1.073	0.049	1.850	0.027	0.176
Max		56.429	0.163	43.732	0.572	3.107
Min		53.772	0.020	37.030	0.485	2.583
M	1396.0	54.995	0.292	39.855	0.523	2.525
SD		1.662	0.320	1.709	0.038	0.194
Max		57.762	1.124	42.748	0.600	2.907
Min		52.703	0.022	37.121	0.487	2.165
M	1421.1	55.024	0.167	39.788	0.563	2.874
SD		1.252	0.038	2.301	0.030	0.167
Max		56.432	0.275	41.441	0.597	3.048
Min		53.393	0.101	36.372	0.504	2.698
M	1548.4	57.303	0.127	42.059	0.164	2.642
SD		0.833	0.120	1.690	0.042	0.643
Max		58.339	0.403	45.004	0.227	3.703
Min		56.091	0.000	39.906	0.113	2.117
M	1556.6	55.268	0.194	41.453	0.364	3.350
SD		0.747	0.045	2.056	0.015	0.180
Max		56.472	0.264	44.127	0.392	3.598
Min		55.348	0.114	37.627	0.358	3.116

Appendix 7

Plagioclase composition of samples from the Bk-1 borehole

The plagioclase composition was determined by microprobe. Eleven points were analyzed per thin section. The first point was duplicated and the remaining points represented core and "rim" analyses of 5 randomly chosen cumulus plagioclase crystals. The rim was arbitrarily defined as the area nearest to the edge of the plagioclase crystals without causing significant fluorescence of adjacent minerals ie., the center of the beam was at least 20 um from the crystal edge. Analysis conditions were, beam width 10 um; acceleration potential 15 kV; and defocused beam of size 20 um.

M: Mean
SD: Standard deviation (1σ)
Max: Maximum value
Min: Minimum value

Plagiocalse Composition

	Sample	SiO2	Al2O3	Na2O	MgO	FeO	K2O	CaO
M	423.0	57.870	26.270	7.036	0.002	0.132	0.157	8.395
SD		1.029	0.548	0.330	0.003	0.858	0.040	0.548
Max		59.914	26.797	7.813	0.014	3.231	0.216	8.979
Min		56.074	24.919	6.690	0.000	0.056	0.098	7.128
M	433.0	58.966	25.750	6.827	0.003	0.169	0.305	7.966
SD		1.845	3.478	2.216	0.009	0.066	5.417	3.379
Max		63.394	26.737	7.888	0.035	0.350	13.42	8.352
Min		57.853	17.512	1.799	0.000	0.087	0.167	0.122
M	474.5	58.422	26.34	6.827	0.008	0.167	0.231	8.623
SD		1.953	0.536	0.321	0.010	0.177	0.054	0.547
Max		58.760	26.595	7.548	0.040	0.792	0.418	9.011
Min		52.355	24.718	6.262	0.000	0.076	0.132	7.278
M	507.5	57.814	27.110	6.197	0.000	0.147	0.277	9.301
SD		2.443	0.878	0.353	0.000	0.261	0.032	0.579
Max		59.402	27.347	7.102	0.000	1.079	0.352	9.673
Min		52.835	24.551	6.097	0.000	0.105	0.251	8.000
M	551.5	56.110	27.64	5.748	0.000	0.231	0.298	10.210
SD		0.683	0.514	0.258	0.015	0.345	0.046	0.493
Max		57.659	26.918	6.521	0.056	1.411	0.409	10.464
Min		55.037	25.106	5.703	0.000	0.113	0.242	8.691
M	601.5	54.944	27.640	5.748	0.000	0.231	0.298	10.210
SD		2.635	2.310	0.771	0.043	3.087	2.021	1.883
Max		57.009	27.666	6.102	0.114	10.283	7.318	10.367
Min		46.566	19.600	3.182	0.000	0.161	0.255	3.703
M	652.0	55.609	27.72	5.762	0.000	0.187	0.377	9.880
SD		0.699	0.464	0.340	0.000	0.448	0.072	0.599
Max		57.373	28.853	6.546	0.000	1.782	0.424	10.897
Min		54.830	27.047	5.166	0.000	0.108	0.148	8.603
M	757.7	55.385	27.480	5.610	0.000	0.193	0.370	10.070
SD		0.394	0.165	0.203	0.005	0.063	0.035	0.328
Max		56.760	27.746	6.216	0.019	0.354	0.454	10.479
Min		55.211	27.138	5.355	0.000	0.113	0.327	9.055
M	798.0	56.205	26.760	5.338	0.003	0.214	1.288	9.362
SD		1.096	0.865	0.395	0.008	0.060	1.221	0.899
Max		58.351	27.908	5.936	0.023	0.346	4.784	10.499
Min		53.473	24.455	4.283	0.000	0.136	0.215	6.960

	Sample	SiO2	Al2O3	Na2O	MgO	FeO	K2O	CaO
M	845.8	56.769	27.35	5.793	0.000	0.238	0.326	9.667
SD		1.117	0.609	0.251	0.004	0.125	0.049	0.528
Max		57.777	27.931	6.189	0.019	0.734	0.424	10.951
Min		52.866	24.952	5.270	0.000	0.115	0.240	9.123
M	893.0	55.639	27.07	5.807	0.000	0.157	0.260	10.21
SD		4.977	1.740	1.158	0.000	0.066	0.096	2.076
Max		61.552	32.560	6.536	0.000	0.358	0.401	17.616
Min		41.110	25.184	1.743	0.000	0.116	0.036	9.588
M	951.0	56.939	27.35	5.966	0.000	0.241	0.424	9.854
SD		0.300	0.167	0.091	0.000	0.040	0.043	0.244
Max		57.672	27.619	6.237	0.000	0.309	0.510	10.034
Min		56.508	27.017	5.880	0.000	0.185	0.368	9.162
M	999.8	55.865	26.860	5.620	0.000	0.257	0.511	10.173
SD		0.710	0.354	0.151	0.002	0.080	0.043	0.392
Max		56.848	27.685	5.870	0.007	0.467	0.568	10.857
Min		54.984	26.227	5.400	0.000	0.181	0.435	9.550
M	1050.2	56.742	27.08	6.040	0.002	0.184	0.369	9.662
SD		0.572	0.263	0.152	0.002	0.059	0.042	0.340
Max		58.029	27.516	6.311	0.005	0.319	0.431	10.353
Min		55.709	26.620	5.731	0.000	0.115	0.311	8.969
M	1100.8	54.618	28.03	5.548	0.010	0.161	0.303	11.010
SD		1.091	1.602	1.113	0.009	0.069	0.116	2.059
Max		55.700	31.518	6.277	0.021	0.317	0.372	14.882
Min		49.558	27.161	3.265	0.000	0.137	0.045	9.528
M	1178.2	56.612	27.35	6.005	0.000	0.187	0.325	9.874
SD		0.772	0.383	0.093	0.000	0.312	0.063	0.119
Max		57.580	27.554	5.797	0.000	1.049	0.515	10.176
Min		55.662	26.530	5.558	0.000	0.206	0.339	9.821
M	1211.0	57.200	27.070	6.043	0.000	0.195	0.496	9.238
SD		0.350	0.528	0.230	0.000	0.313	0.049	0.477
Max		57.436	27.456	6.597	0.000	0.962	0.541	9.691
Min		56.471	25.961	5.911	0.000	0.124	0.388	8.367
M	1231.2	57.220	26.27	5.928	0.000	0.112	0.430	8.864
SD		0.846	0.448	0.337	0.004	0.036	0.078	0.713
Max		56.879	28.026	6.013	0.010	0.191	0.473	9.874
Min		54.666	26.746	5.145	0.000	0.097	0.289	7.826
M	1256.3	56.386	27.270	5.935	0.003	0.184	0.553	9.425
SD		2.421	1.647	1.055	0.006	0.048	0.153	2.111
Max		56.504	31.196	6.190	0.017	0.262	0.615	14.286
Min		50.347	26.820	3.486	0.000	0.118	0.189	8.851
M	1270.4	56.978	26.74	5.928	0.000	0.225	0.510	9.679
SD		2.316	1.061	0.283	0.000	0.111	0.070	0.550
Max		62.395	29.353	6.522	0.000	0.595	0.588	11.036
Min		56.412	26.484	5.798	0.000	0.278	0.390	9.435
M	1302.8	56.349	27.28	5.827	0.003	0.107	0.434	9.979
SD		0.739	0.173	0.173	0.003	0.052	0.057	0.421
Max		56.492	27.737	5.908	0.009	0.244	0.445	11.040
Min		54.533	27.322	5.408	0.000	0.096	0.312	9.961
M	1320.8	55.832	28.330	5.373	0.000	0.201	0.426	9.589
SD		0.708	0.693	0.307	0.000	0.048	0.062	0.580
Max		56.353	29.329	5.422	0.000	0.340	0.573	9.859
Min		54.509	27.478	4.676	0.000	0.219	0.410	8.448

	Sample	SiO2	Al2O3	Na2O	MgO	FeO	K2O	CaO
M	1340.1	56.190	27.540	5.683	0.008	0.201	0.426	9.589
SD		0.467	0.158	0.187	0.014	0.095	0.066	0.453
Max		56.876	28.087	5.860	0.040	0.430	0.507	10.262
Min		55.397	27.564	5.277	0.000	0.097	0.255	8.825
M	1364.0	55.336	27.280	5.769	0.004	0.169	0.324	10.430
SD		2.068	1.171	0.528	0.087	1.171	0.062	0.814
Max		55.567	30.037	5.958	0.319	4.393	0.370	12.347
Min		48.807	26.453	4.051	0.000	0.128	0.135	8.975
M	1379.1	55.848	27.680	5.744	0.000	0.205	0.350	10.110
SD		0.611	0.379	0.241	0.004	0.066	0.039	0.622
Max		56.862	28.690	5.916	0.018	0.359	0.392	11.557
Min		54.387	27.428	5.097	0.000	0.139	0.277	9.530
M	1396.0	56.029	27.470	5.841	0.014	0.230	0.369	9.971
SD		0.828	0.778	0.294	0.047	0.766	0.039	0.641
Max		57.015	28.823	6.078	0.163	2.953	0.419	11.621
Min		53.813	25.308	4.841	0.000	0.080	0.297	8.789
M	1421.1	57.302	27.160	5.649	0.000	0.186	0.364	9.651
SD		0.926	0.547	0.311	0.001	0.068	0.058	0.630
Max		58.769	28.321	6.021	0.004	0.363	0.453	11.294
Min		55.186	26.514	4.804	0.000	0.154	0.253	8.938
M	1439.1	55.914	27.380	5.762	0.000	0.150	0.377	10.000
SD		0.500	0.309	0.179	0.000	0.043	0.041	0.578
Max		56.356	28.126	5.990	0.000	0.226	0.418	11.034
Min		54.641	26.830	5.333	0.000	0.106	0.289	8.933
M	1447.3	55.384	27.99	5.677	0.000	0.280	0.348	10.280
SD		0.488	0.353	0.132	0.000	0.101	0.049	0.300
Max		56.349	28.505	5.914	0.000	0.445	0.458	10.716
Min		54.889	27.143	5.474	0.000	0.148	0.291	9.727
M	1465.5	54.989	27.920	5.547	0.000	0.033	0.078	10.860
SD		0.348	0.160	0.101	0.000	0.026	0.027	0.260
Max		55.628	28.149	5.716	0.000	0.092	0.165	11.172
Min		54.437	27.694	5.423	0.000	0.001	0.060	10.245
M	1498.9	55.996	27.810	5.739	0.000	0.231	0.402	10.030
SD		0.352	0.250	0.141	0.000	0.051	0.043	0.281
Max		56.755	28.265	6.101	0.000	0.334	0.458	10.535
Min		55.606	27.441	5.590	0.000	0.156	0.346	9.610
M	1508.2	55.685	27.270	5.796	0.002	0.160	0.389	10.280
SD		1.437	0.287	0.194	0.003	0.488	0.112	0.618
Max		56.652	27.607	6.083	0.010	1.938	0.755	10.848
Min		51.070	26.568	5.526	0.000	0.120	0.323	8.819
M	1530.8	56.065	27.19	5.673	0.006	0.191	0.400	9.853
SD		0.741	0.374	0.183	0.013	0.039	0.035	0.181
Max		56.470	27.634	6.171	0.038	0.276	0.456	10.045
Min		53.666	26.163	5.496	0.000	0.142	0.346	9.531
M	1556.6	56.567	26.920	6.143	0.000	0.182	0.500	9.400
SD		1.983	0.452	0.185	0.019	0.360	0.094	0.363
Max		57.170	27.526	6.284	0.061	1.798	0.834	10.435
Min		47.511	25.332	5.651	0.000	0.136	0.355	9.066
M	1580.5	57.259	27.420	5.930	0.000	0.135	0.296	10.010
SD		0.365	0.213	0.107	0.000	0.089	0.041	0.300
Max		57.838	28.149	6.095	0.000	0.351	0.355	10.689
Min		56.418	27.394	5.723	0.000	0.096	0.233	9.848

	Sample	SiO2	Al2O3	Na2O	MgO	FeO	K2O	CaO
M	1606.2	54.597	28.590	5.142	0.001	0.207	0.235	11.400
SD		0.612	0.263	0.131	0.004	0.026	0.069	0.309
Max		55.602	29.053	5.249	0.015	0.264	0.323	11.819
Min		53.243	28.224	4.811	0.000	0.161	0.078	10.901
M	1627.5	54.695	28.42	5.049	0.002	0.196	0.333	11.290
SD		0.898	0.154	0.137	0.004	0.033	0.052	0.163
Max		55.046	28.601	5.124	0.016	0.259	0.403	11.600
Min		52.238	28.151	4.609	0.000	0.150	0.245	10.986
M	1649.8	54.527	28.000	5.203	0.000	0.155	0.299	11.86
SD		0.879	0.606	0.102	0.046	0.483	0.029	0.532
Max		54.814	28.274	5.355	0.167	1.896	0.339	12.191
Min		52.492	26.600	4.972	0.000	0.087	0.242	10.258

Appendix 8A

XRF Major Element Analyses of Bierkraal 1.

- Unpublished analytical results on Bk-1 whole rock samples (values in %), courtesy of R.K.W., Merkle.

Sample	SiO2	TiO	Al2O3	Fe2O3	FeO	MnO	MgO
423.0	47.17	1.97	11.54	25.33	23.80	0.47	1.32
428.5	45.91	2.01	12.01	23.65	23.38	0.41	2.70
433.0	44.25	2.25	11.34	26.09	22.09	0.44	2.89
474.5	48.84	1.59	13.24	22.49	20.37	0.43	0.81
487.5	47.48	1.56	12.58	24.56	22.82	0.46	0.87
496.5	47.24	1.69	12.55	25.27	23.05	0.40	1.85
507.5	44.63	1.96	12.85	24.46	18.65	0.43	1.61
521.0	41.26	1.85	11.34	25.76	19.78	0.45	1.52
538.0	44.19	2.24	12.50	27.25	20.56	0.44	2.17
551.5	44.66	2.41	13.23	23.56	21.06	0.36	2.01
563.5	43.64	2.26	12.90	24.61	20.91	0.35	3.77
581.0	37.45	2.98	10.78	30.21	22.50	0.42	4.57
589.5	35.49	3.95	10.17	32.84	38.25	0.45	2.76
601.5	36.96	2.65	10.21	31.94	37.45	0.47	3.59
607.5	31.23	5.87	11.49	31.33	40.17	0.37	2.85
620.5	35.54	6.93	15.72	30.27	34.92	0.26	0.99
633.8	22.18	8.99	6.14	44.93	24.55	0.46	5.08
652.0	39.18	2.64	12.39	30.34	27.32	0.41	2.81
667.8	47.22	1.17	16.50	20.13	17.01	0.31	2.09
674.5	49.80	1.28	15.55	15.97	11.80	0.26	2.03
680.0	49.58	1.08	18.54	14.91	13.76	0.23	1.15
688.0	47.51	1.24	18.22	16.82	12.66	0.26	2.92
695.0	42.30	2.21	14.25	22.42	20.11	0.32	3.27
705.5	41.69	2.66	14.56	24.71	21.55	0.36	2.16
715.0	41.99	2.43	14.43	24.41	20.61	0.35	2.31
726.0	40.96	2.75	13.56	26.48	19.21	0.35	3.24
738.7	39.82	3.06	11.92	29.80	26.00	0.39	4.35
757.7	41.18	3.58	13.85	25.77	20.91	0.32	4.00
765.0	36.70	3.46	12.89	31.00	25.40	0.38	3.43
772.5	29.69	5.66	11.63	31.01	24.26	0.29	2.21
776.0	43.81	3.92	19.45	18.78	12.77	0.18	1.27
785.5	39.88	2.51	14.22	23.45	20.81	0.28	3.28
798.0	38.07	2.60	11.97	25.35	20.58	0.33	4.55
810.5	44.76	2.34	11.31	22.69	19.36	0.34	4.40
822.8	42.62	2.26	12.96	23.20	19.26	0.32	3.36
835.3	40.16	2.42	14.00	24.35	21.74	0.29	4.08
845.8	34.81	2.42	12.46	23.21	20.40	0.27	3.70
859.3	40.82	2.26	14.33	17.64	14.73	0.22	3.20
863.7	45.33	2.59	14.48	23.92	17.83	0.30	4.54
876.5	45.76	2.84	15.68	17.07	13.27	0.21	3.31
893.0	42.27	2.07	13.93	19.68	13.20	0.26	4.79
899.0	43.86	1.54	17.39	20.70	17.76	0.27	2.65
909.0	47.40	1.39	18.42	19.66	16.56	0.30	2.48
917.0	45.84	1.08	17.87	20.07	19.52	0.30	2.45
922.0	45.99	1.80	17.53	19.30	15.26	0.28	2.64
933.8	45.46	2.09	17.01	20.52	16.59	0.29	3.30
940.1	44.44	2.10	16.02	23.38	18.63	0.33	3.19
951.0	42.11	2.37	14.46	24.72	15.93	0.34	3.52
955.0	44.00	2.11	16.46	21.00	14.84	0.30	2.57
965.1	44.04	1.95	17.20	19.56	17.17	0.29	2.03
968.9	45.15	1.95	17.82	17.92	15.53	0.25	1.39
980.8	44.91	2.14	15.90	22.62	18.13	0.31	2.47
992.0	42.89	2.17	15.67	22.17	17.11	0.32	2.64
999.8	43.28	2.36	15.53	24.06	17.75	0.34	2.72
1009.6	29.06	5.20	9.59	35.94	19.79	0.41	3.94
1019.8	43.49	2.30	15.97	23.05	20.48	0.33	2.77
1030.0	44.02	2.24	15.58	23.56	20.06	0.33	2.73
1040.2	42.38	2.03	15.21	21.02	21.00	0.32	2.93
1050.2	41.87	2.54	14.64	25.86	22.77	0.36	3.26
1060.3	40.89	2.25	12.30	27.95	24.06	0.43	3.48
1068.9	36.83	3.41	11.95	34.05	28.67	0.48	3.01

Sample	SiO2	TiO	Al2O3	Fe2O3	FeO	MnO	MgO
1082.2	37.89	2.99	12.09	35.41	31.87	0.47	3.54
1086.7	27.40	5.42	8.44	39.94	26.93	0.49	3.38
1089.8	25.76	6.05	8.75	37.32	29.87	0.41	3.87
1091.0	27.58	6.07	8.53	41.63	30.95	0.47	4.31
1091.6	23.60	6.69	0.84	47.77	41.68	0.65	7.38
1092.8	25.20	7.19	7.92	42.61	34.80	0.46	4.70
1096.3	19.03	9.21	4.80	42.72	33.60	0.40	4.93
1100.8	22.10	7.77	6.75	43.30	28.05	0.44	4.34
1103.7	18.51	8.10	6.49	38.55	26.03	0.36	3.81
1104.9	21.77	7.95	7.34	41.17	12.50	0.38	4.31
1112.0	7.61	13.01	3.73	46.75	28.52	0.28	2.63
1113.5	17.96	15.24	8.29	52.06	31.82	0.32	2.99
1114.7	43.79	3.69	21.34	15.25	5.98	0.11	1.89
1128.7	44.99	2.28	14.33	20.55	16.20	0.29	3.74
1139.1	45.72	2.38	13.89	22.07	14.67	0.32	3.73
1151.3	38.13	1.22	11.81	23.67	16.50	0.38	3.44
1160.0	49.65	1.57	23.33	9.04	4.04	0.10	1.05
1161.5	48.69	1.56	22.68	10.33	2.96	0.13	1.32
1178.2	37.71	1.68	13.04	29.13	28.00	0.43	2.54
1189.8	41.21	1.71	9.10	37.14	33.22	0.61	3.49
1199.0	42.04	2.38	11.43	31.78	24.12	0.49	3.16
1211.0	38.82	2.04	13.19	20.63	17.32	0.28	3.51
1219.1	44.21	2.28	15.73	21.93	16.78	0.30	3.41
1231.2	42.60	2.15	13.79	23.25	18.93	0.32	3.57
1241.5	42.12	2.12	15.47	21.88	21.62	0.30	3.95
1256.3	41.41	2.10	13.35	25.97	21.46	0.37	2.99
1260.8	39.90	2.18	13.27	24.78	22.13	0.37	3.25
1270.4	40.70	2.31	14.81	18.99	17.10	0.25	3.24
1280.5	45.41	1.69	15.40	22.80	20.46	0.33	4.47
1289.7	44.18	2.26	15.67	22.23	18.80	0.29	4.07
1302.8	41.94	2.70	14.44	24.91	20.52	0.31	3.83
1308.6	42.19	2.78	14.67	24.51	16.89	0.32	4.12
1320.8	38.71	2.87	11.92	32.59	26.97	0.41	3.91
1329.2	40.20	2.87	13.21	28.83	23.08	0.36	3.67
1340.0	41.83	2.70	14.52	24.87	19.41	0.29	3.83
1350.6	40.57	2.79	13.86	24.45	23.42	0.29	3.86
1364.0	33.38	3.28	10.23	26.64	24.55	0.33	4.43
1371.9	38.55	3.39	12.84	28.56	23.20	0.32	4.79
1379.1	34.59	3.84	11.64	30.42	24.65	0.33	4.17
1385.0	28.96	6.19	9.36	38.68	28.75	0.36	5.31
1396.0	37.01	3.35	12.29	29.14	24.39	0.32	5.27
1410.2	30.49	5.70	10.43	35.50	27.72	0.33	5.01
1421.1	31.07	4.12	9.15	37.42	47.70	0.40	4.52
1424.3	30.63	3.55	8.73	35.89	31.90	0.41	5.50
1427.4	24.84	6.79	8.30	40.25	30.17	0.36	3.60
1430.3	25.59	5.87	6.69	42.17	33.92	0.40	4.36
1433.3	21.64	6.49	5.61	43.59	33.67	0.41	4.51
1439.1	29.43	3.94	7.56	40.86	34.00	0.45	6.35
1447.3	28.67	5.45	6.95	47.30	37.80	0.48	5.70
1450.1	18.81	13.58	5.40	55.15	39.62	0.40	5.08
1452.8	17.93	12.52	6.49	57.78	39.55	0.41	4.67
1453.3	17.49	12.90	5.84	56.84	39.15	0.40	4.62
1454.4	10.36	16.37	4.33	63.18	41.22	0.39	2.48
1459.6	4.73	19.66	4.27	70.26	39.05	0.37	1.10
1462.7	4.87	19.16	4.88	69.52	33.40	0.36	1.30
1476.2	44.08	2.89	21.78	14.97	9.48	0.10	0.70
1485.9	5.78	16.81	5.29	68.58	32.72	0.32	1.81
1491.0	44.34	2.29	17.62	21.19	16.56	0.23	4.60
1494.0	0.75	18.08	3.33	73.20	32.32	0.33	1.14
1496.0	34.72	4.06	8.68	36.42	26.82	0.40	6.25
1498.9	46.46	2.74	16.45	16.26	10.13	0.18	3.63
1508.2	47.03	2.87	22.66	12.58	5.78	0.07	0.38
1520.4	45.39	3.45	22.22	14.56	8.06	0.07	0.95
1538.1	45.68	1.45	19.48	15.40	10.71	0.16	2.66
1548.4	35.10	3.19	11.44	32.72	22.58	0.35	5.44
1556.6	35.20	3.70	13.24	29.33	22.39	0.27	4.34
1573.1	39.03	4.14	13.99	25.74	17.93	0.08	4.31
1580.5	36.14	4.80	14.17	30.82	20.70	0.27	3.83

Sample	SiO2	TiO2	Al2O3	Fe2O3	FeO	MnO	MgO
1589.1	29.39	7.01	10.78	43.01	29.80	0.36	5.11
1594.2	41.02	3.38	13.26	21.89	16.61	0.23	4.51
1606.2	46.28	1.75	14.41	19.77	14.10	0.26	6.14
1612.9	41.84	3.25	21.09	18.41	9.00	0.10	1.81
1620.4	42.70	2.74	21.38	15.36	7.62	0.09	2.36
1627.5	42.20	2.97	19.62	19.12	7.78	0.14	3.14
1633.7	41.20	1.73	16.60	21.19	17.36	0.19	6.18
1642.5	43.88	2.95	22.69	14.58	6.50	0.07	0.86
1649.8	39.25	2.75	14.38	23.79	17.35	0.22	5.88

Appendix 8B

XRF Major Element Analyses of Bierkraal 1.

-Unpublished analytical results on Bk-1 whole rock samples (values in %), courtesy of R.K.W. Merkle.

Sample	CaO	Na2O	K2O	P2O5	Cr3O4	NiO	L.O.II
423.0	8.89	4.97	1.17	0.62	0.08	18.00	-1.34
428.5	8.39	5.08	0.95	0.84	0.07	31.00	0.3
433.0	8.56	5.02	0.82	0.96	0.05	33.00	-1.50
474.5	9.16	5.24	0.93	0.39	0.05	.	-1.04
487.5	8.94	4.92	0.82	0.42	0.06	29.00	-1.58
496.5	8.88	4.80	0.74	0.51	0.09	26.00	-1.41
507.5	8.71	5.03	0.73	0.59	0.07	32.00	-1.38
521.0	8.43	5.13	0.62	0.58	0.06	31.00	-1.90
538.0	8.39	5.05	0.58	0.72	0.07	30.00	-1.90
551.5	8.84	5.18	0.72	1.02	0.08	21.00	-1.40
563.5	8.59	5.02	0.58	0.96	0.05	26.00	-1.63
581.0	8.32	5.04	0.36	1.67	0.09	.	-2.08
589.5	8.18	1.81	0.37	2.44	0.08	42.00	0.11
601.5	7.62	4.64	0.40	1.96	0.08	48.00	-1.99
607.5	9.61	5.26	0.40	3.77	0.09	55.00	-1.29
620.5	6.36	5.47	0.74	0.53	0.16	57.00	-0.56
633.8	8.64	3.93	0.28	4.82	0.17	.	-2.54
652.0	6.85	4.90	0.34	0.78	0.06	39.00	-2.14
667.8	8.15	5.18	0.48	0.25	0.05	23.00	-1.16
674.5	11.02	5.32	0.52	0.16	0.06	9.00	-0.63
680.0	8.65	5.44	0.67	0.18	0.05	0.00	-0.78
688.0	8.87	5.45	0.77	0.42	0.05	16.00	-0.92
695.0	9.24	5.26	0.40	1.06	0.07	24.00	-1.53
705.5	9.41	5.27	0.38	1.36	0.08	31.00	-1.50
715.0	9.27	5.20	0.36	1.31	0.05	31.00	-1.56
726.0	9.65	5.20	0.30	1.60	0.00	23.00	-1.62
738.7	9.37	5.01	0.31	1.68	0.08	34.00	-1.90
757.7	9.74	5.24	0.35	1.32	0.07	37.00	-1.44
765.0	8.71	5.01	0.28	2.61	0.08	53.00	-3.19
772.5	9.70	5.47	0.32	3.71	0.09	76.00	-1.84
776.0	8.03	5.47	0.48	0.22	0.08	29.00	-0.44
785.5	8.62	5.13	0.38	1.26	0.05	30.00	-1.46
798.0	9.77	5.03	0.29	1.65	0.06	44.00	-0.67
810.5	12.15	5.07	0.39	1.49	0.08	44.00	-0.96
822.8	10.35	5.05	0.37	1.10	0.07	43.00	-1.30
835.3	9.01	5.28	0.30	1.37	0.06	31.00	-1.55
845.8	8.70	5.18	0.26	1.60	0.06	40.00	-1.55
859.3	11.98	5.38	0.50	2.92	0.04	41.00	-0.69
863.7	9.45	5.15	0.32	0.09	0.08	50.00	-4.41
876.5	10.29	5.43	0.49	0.11	0.06	33.00	-0.55
893.0	9.05	5.22	0.37	0.11	0.04	25.00	-1.07
899.0	7.18	5.31	0.61	0.07	0.05	23.00	-1.35
909.0	8.01	5.32	0.45	0.05	0.06	24.00	-1.21
917.0	7.40	5.34	0.42	0.05	0.06	19.00	-1.50
922.0	8.93	5.29	0.35	0.39	0.06	13.00	-0.46
933.8	8.37	5.59	0.36	0.04	0.08	17.00	-1.31
940.1	8.14	5.45	0.42	0.23	0.07	26.00	-1.56
951.0	9.31	5.30	0.27	1.07	0.06	32.00	-1.65
955.0	9.09	5.64	0.40	0.89	0.06	12.00	0.48
965.1	9.00	5.62	0.35	0.73	0.03	15.00	-1.20
968.9	9.39	5.67	0.38	0.71	0.04	16.00	-1.70
980.8	9.84	5.47	0.32	0.91	0.07	22.00	-2.20
992.0	9.41	5.51	0.31	0.79	0.07	19.00	-1.46
999.8	9.47	5.34	0.30	1.20	0.09	26.00	-1.48
1009.6	8.86	5.35	0.17	3.65	0.09	32.00	-1.60
1019.8	9.15	5.41	0.33	0.94	0.06	20.00	-1.38
1030.0	9.29	4.96	0.33	0.86	0.07	18.00	-1.63
1040.2	9.41	5.19	0.41	0.83	0.05	22.00	-1.72
1050.2	9.08	4.91	0.29	1.15	0.07	30.00	-2.07
1060.3	9.46	4.73	0.24	0.91	0.07	36.00	-3.77
1068.9	7.64	5.10	0.23	1.48	0.10	52.00	-2.66

Sample	CaO	Na2O	K2O	P2O5	Cr3O4	NiO	L.O.I.
1082.2	6.78	5.09	0.22	1.14	0.09	45.00	-3.01
1086.7	7.32	5.28	0.14	3.04	0.10	52.00	-0.91
1089.8	7.80	5.17	0.14	3.55	0.11	51.00	4.66
1091.0	7.34	5.13	0.14	3.05	0.10	51.00	-2.93
1091.6	10.45	4.78	0.02	6.46	0.14	69.00	-3.25
1092.8	8.42	5.41	0.15	4.20	0.10	57.00	-2.61
1096.3	14.13	5.60	0.07	7.87	0.11	61.00	-2.80
1100.8	9.52	6.14	0.12	5.42	0.11	71.00	-2.02
1103.7	10.27	5.94	0.13	5.29	0.09	100.00	-1.45
1104.9	10.65	5.67	0.12	5.89	0.10	99.00	-1.00
1112.0	15.19	6.57	0.05	10.60	0.12	130.00	-0.41
1113.5	3.96	6.18	0.13	0.12	0.19	115.00	-2.35
1114.7	8.74	5.91	0.47	0.22	0.08	20.00	-0.53
1128.7	9.76	5.43	0.31	0.08	0.06	24.00	-0.98
1139.1	10.11	5.46	0.28	0.04	0.07	33.00	-1.04
1151.3	8.10	4.89	0.22	0.18	0.05	43.00	-1.51
1160.0	9.29	6.00	0.63	0.12	0.05	0.00	-0.18
1161.5	8.63	5.90	0.63	0.17	0.07	7.00	-0.11
1178.2	5.47	4.97	0.31	0.31	0.07	54.00	-2.42
1189.8	7.96	4.48	0.28	0.00	0.10	45.00	-2.88
1199.0	8.65	5.12	0.31	0.46	0.09	37.00	-2.25
1211.0	9.59	5.60	0.41	1.27	0.06	21.00	-0.20
1219.1	10.14	5.54	0.31	1.37	0.07	26.00	-1.35
1231.2	10.04	5.38	0.27	1.27	0.06	21.00	-1.35
1241.5	9.43	5.37	0.34	1.06	0.05	39.00	-1.35
1256.3	8.37	5.27	0.27	0.66	0.04	31.00	-1.78
1260.8	9.39	5.36	0.30	1.07	0.05	24.00	-1.67
1270.4	9.76	5.66	0.31	1.04	0.04	15.00	-1.10
1280.5	9.08	5.34	0.33	0.59	0.05	21.00	-1.50
1289.7	9.39	5.42	0.27	0.95	0.07	21.00	-1.23
1302.8	9.20	5.47	0.29	1.29	0.06	27.00	-1.47
1308.6	9.66	5.47	0.27	1.47	0.07	24.00	-1.59
1320.8	7.75	4.88	0.23	1.28	0.06	36.00	-2.24
1329.2	8.57	4.94	0.24	1.37	0.05	30.00	-2.12
1340.0	9.37	5.21	0.24	1.40	0.07	.	-1.68
1350.6	9.99	5.18	0.23	1.64	0.06	24.00	-1.57
1364.0	9.65	5.05	0.16	2.01	0.06	38.00	-1.84
1371.9	9.88	5.18	0.21	2.30	0.09	37.00	-1.92
1379.1	9.58	5.07	0.19	2.76	0.08	30.00	-2.10
1385.0	9.12	5.30	0.20	3.67	0.11	45.00	-2.36
1396.0	9.80	4.97	0.28	2.58	0.08	32.00	-1.65
1410.2	9.52	5.32	0.22	3.61	0.09	46.00	-2.40
1421.1	8.18	4.71	0.13	2.78	0.10	53.00	-2.61
1424.3	8.23	4.66	0.15	2.91	0.09	45.00	-2.41
1427.4	10.27	5.28	0.13	5.17	0.10	48.00	-2.28
1430.3	9.39	4.93	0.10	4.43	0.11	53.00	-2.59
1433.3	9.04	4.93	0.09	4.88	0.07	68.00	-2.35
1439.1	7.23	4.42	0.11	3.17	0.10	68.00	-2.80
1447.3	3.07	4.23	0.09	0.34	0.11	78.00	-3.38
1450.1	2.58	5.45	0.07	0.03	0.16	98.00	-3.33
1452.8	2.05	5.28	0.08	0.06	0.13	109.00	-3.28
1453.3	2.17	5.13	0.21	0.08	0.17	131.00	-3.10
1454.4	1.76	5.99	0.04	0.13	0.20	138.00	-3.80
1459.6	0.73	6.40	0.06	0.06	0.20	141.00	-3.00
1462.7	0.81	6.43	0.08	0.05	0.19	.	-2.53
1476.2	9.11	5.51	0.42	0.09	0.07	62.00	0.03
1485.9	1.13	6.17	0.05	0.03	0.35	233.00	-2.70
1491.0	7.12	4.74	0.30	0.03	0.06	54.00	-0.26
1494.0	0.19	6.25	0.00	0.04	0.49	220.00	-2.21
1496.0	5.95	4.14	0.12	0.03	0.07	.	-1.41
1498.9	10.72	5.56	0.30	0.01	0.06	19.00	-0.58
1508.2	8.64	5.96	0.44	0.05	0.06	1.00	-0.33
1520.4	8.35	6.05	0.45	0.06	0.05	14.00	-0.29
1538.1	7.84	5.35	0.37	0.10	0.07	7.00	-0.65
1548.4	7.24	4.90	0.22	2.19	0.08	35.00	-2.01
1556.6	8.35	5.26	0.24	2.61	0.07	.	-1.70
1573.1	7.68	5.35	0.23	0.02	0.06	28.00	-1.33
1580.5	5.92	5.15	0.26	0.02	0.08	41.00	-1.50

Sample	CaO	Na2O	K2O	P2O5	Cr3O4	NiO	L.O.I
1589.1	3.78	5.00	0.15	0.02	0.11	60.00	-2.57
1594.2	10.02	5.05	0.16	0.01	0.06	76.00	-0.55
1606.2	7.83	4.57	0.18	0.00	0.00	75.00	-0.63
1612.9	9.27	5.40	0.34	0.01	0.06	86.00	-0.03
1620.4	9.44	5.50	0.32	0.01	0.07	19.00	-0.17
1627.5	8.12	5.32	0.26	0.00	0.05	27.00	-0.60
1633.7	7.10	5.49	0.22	0.01	0.06	49.00	-1.17
1642.5	9.18	4.80	0.34	0.05	0.08	15.00	-0.06
1649.8	8.07	4.60	0.23	0.03	0.07	59.00	-0.98

Appendix 9A

XRF Trace Element Analyses of Bierkraal 1 samples.

- Unpublished analytical results on Bk-1 whole rock samples, courtesy of R.K.W. Merkle.
  Values given in ppm.

Sample	GRAPHITE	C	S	Ba	Co	Cu	Mo
423.0	76	182	2443	346	63	49	3
428.5	81	147	2399	423	60	38	8
433.0	48	160	2922	322	78	49	7
434.9	.	174	3599	263	128	19	8
437.8	.	267	2945	365	77	45	8
441.4	.	405	3027	450	77	59	11
444.8	.	422	1643	502	49	48	11
446.6	.	112	776	299	78	30	9
449.3	.	204	914	472	15	37	10
452.4	.	503	1019	550	20	39	9
454.8	.	278	1060	524	27	44	11
457.8	.	449	951	478	25	36	10
464.1	.	374	1548	423	53	40	11
474.5	70	79	1820	.	.	.	.
475.1	.	182	1994	361	56	45	10
475.5	.	79	1820	356	42	32	8
483.4	.	190	1860	369	121	30	7
486.4	.	283	2160	385	63	45	10
487.5	.	78	1816	410	55	47	10
489.4	.	400	2290	325	62	35	6
493.5	.	178	1560	304	72	39	10
496.5	.	52	1887	199	65	55	11
499.4	.	258	1300	279	56	18	8
504.7	.	355	1534	359	58	39	10
507.5	47	122	1793	341	54	31	8
507.8	.	334	1815	353	61	45	10
515.1	.	178	1943	637	55	51	10
521.0	56	68	1773	246	75	27	7
522.5	.	265	2356	308	64	32	8
525.7	.	164	3292	348	83	59	10
534.0	.	288	1975	315	68	21	8
538.0	34	60	1719	297	79	51	1
549.0	.	289	1988	389	58	50	10
551.5	42	150	2174	265	57	31	0
551.7	.	373	2357	267	73	32	5
554.7	.	237	2062	302	83	56	10
559.0	.	661	2352	273	66	34	7
563.5	47	110	1939	294	73	55	8
568.0	.	459	2720	262	81	37	8
571.5	.	481	3019	301	65	42	7
579.0	.	203	2687	173	117	36	7
581.3	.	77	3575	195	107	66	6
582.4	.	538	2158	332	90	58	10
589.5	36	76	3355	123	136	50	7
591.5	.	371	2046	259	78	32	8
594.8	.	248	2950	175	121	56	7
599.5	.	280	4336	199	98	66	7
601.5	68	73	3592	101	140	64	6
607.5	206	215	3226	191	121	57	9
611.9	.	352	3871	209	136	79	10
620.5	160	666	1539	337	110	38	8
631.7	.	287	3205	108	166	40	7
633.7	.	421	2790	158	228	64	9
633.8	347	340	2808	.	.	.	.
638.1	.	356	3543	167	162	49	9
638.2	.	212	5180	191	142	67	8
641.4	.	281	568	290	65	27	8
647.3	.	397	429	216	135	29	10
651.0	.	276	432	196	85	7	5
652.0	43	117	334	86	114	7	0

Sample	GRAPHITE C	S	Ba	Co	Cu	Mo
654.7	. 112	458	256	82	28	9
659.0	. 284	510	304	45	11	6
663.3	. 347	555	387	18	33	8
667.8	37 66	655	282	57	37	8
669.3	. 320	713	319	48	37	7
673.3	. 202	352	266	32	6	5
674.5	36 102	471	317	27	23	7
680.0	. 59	485	277	20	25	0
686.6	. 399	492	165	91	12	7
688.0	31 99	419	255	37	8	5
695.0	38 119	1307	172	62	32	5
695.5	. 255	1577	228	48	25	5
700.0	. 304	1566	265	56	53	8
704.4	. 192	1989	250	67	57	9
705.5	60 137	2130	191	75	48	7
709.0	. 278	2078	206	79	50	9
713.7	. 238	2071	132	82	39	4
715.0	31 108	2256	154	68	49	7
718.0	. 336	3206	154	97	57	7
722.0	. 191	2685	216	80	64	9
726.0	24 101	3017	149	96	71	4
727.5	. 269	3421	186	88	77	8
732.0	. 258	3419	93	128	50	7
736.5	. 310	3568	102	147	63	7
738.7	19 90	3296	168	115	91	8
744.8	. 197	4612	178	119	77	6
751.1	. 378	4943	127	129	84	7
754.8	. 259	3174	156	102	67	7
757.7	39 79	3322	228	92	99	9
759.8	. 200	3730	87	139	55	7
763.7	. 592	1170	168	84	7	6
765.0	42 63	2581	79	127	52	6
772.5	54 69	3897	182	121	73	7
773.8	. 218	2275	107	162	47	6
776.0	171 511	461	293	44	24	6
783.2	. 785	2262	368	18	51	15
785.5	30 62	1883	239	87	64	9
787.7	. 174	1749	259	66	63	8
798.0	42 97	2576	155	89	57	5
798.2	. 272	2491	185	81	45	6
804.0	. 196	1137	264	81	41	9
808.5	. 268	645	326	46	41	8
810.5	58 113	2192	204	67	43	6
820.0	. 219	1358	329	47	54	9
822.8	49 78	1930	242	70	72	9
823.4	. 258	3270	193	60	68	7
824.0	. 351	3314	28	187	56	7
830.8	. 287	2494	331	73	35	8
835.3	28 102	1802	161	87	54	6
839.6	. 471	2111	188	93	68	8
845.8	39 83	2888	196	93	85	7
857.7	. 434	795	251	54	34	9
859.3	. 308	802	238	46	12	7
862.0	. 225	332	203	76	8	7
863.7	71 197	307	179	80	4	6
872.0	. 342	308	295	60	30	9
876.3	. 149	302	226	41	9	5
876.5	59 114	302	249	40	6	7
880.5	. 521	287	328	23	15	6
892.5	. 344	478	277	56	29	8
893.0	54 245	367	169	63	11	6
899.0	62 427	85	217	67	28	8
909.0	110 283	166	234	47	7	5
917.0	43 86	223	149	49	1	0
922.0	137 814	759	223	49	42	7
933.8	43 68	141	231	56	23	7
940.1	43 98	189	165	69	3	6
951.0	48 63	2105	145	72	49	5

Sample	GRAPHITE	C	S	Ba	Co	Cu	Mo
955.0	47	102	1770	155	54	52	0
965.1	.	163	1429	233	51	55	8
968.9	38	48	1578	249	38	56	7
980.8	38	42	1672	165	59	43	6
992.0	33	43	1627	200	64	67	7
999.8	25	72	1365	218	65	51	8
1009.6	25	70	2233	144	72	46	6
1019.8	35	160	1821	208	71	60	8
1030.0	7	57	1753	190	74	52	2
1040.2	21	61	2382	180	88	61	7
1050.2	46	45	1541	102	95	26	5
1060.3	37	56	1898	130	142	51	8
1068.9	42	71	2031	64	181	46	8
1082.2	45	86	2383	32	185	45	5
1086.7	.	98	2972	64	181	46	8
1089.8	.	86	3185	65	164	42	6
1091.6	66	722	3109	64	242	46	6
1092.8	48	53	2563	125	217	52	11
1096.3	99	121	3486	62	206	45	7
1100.8	73	184	2042	86	184	64	8
1103.7	105	96	4483	163	215	111	9
1104.9	68	70	3860	76	193	71	7
1112.0	.	415	4551	175	230	107	11
1113.5	88	96	627	154	263	22	9
1114.7	84	215	424	345	41	37	8
1128.7	66	89	641	268	62	41	8
1139.1	60	209	312	181	60	14	5
1151.3	74	180	750	169	87	48	8
1160.0	71	224	301	347	11	35	7
1161.5	64	286	341	289	7	20	4
1178.2	29	206	174	115	127	29	8
1189.8	28	71	67	29	156	0	5
1199.0	16	70	130	67	113	7	5
1211.0	88	1908	344	211	64	36	8
1219.1	46	214	1711	185	60	52	6
1231.2	14	248	1397	195	69	70	9
1241.5	48	102	1326	127	65	33	3
1256.3	36	81	3456	116	88	43	6
1260.8	23	124	2048	113	79	80	6
1270.4	29	98	115	191	56	26	5
1280.5	37	426	135	142	76	21	6
1289.7	34	62	1068	170	71	40	8
1302.8	30	361	2054	101	89	47	4
1308.6	36	171	2488	151	86	69	6
1320.8	24	505	2976	128	145	84	9
1329.2	42	129	2486	74	111	51	1
1340.1	.	55	2325	139	97	61	7
1350.6	.	110	2771	140	95	77	7
1364.0	.	71	3265	66	123	69	5
1371.9	.	48	3344	95	123	79	5
1379.1	21	102	3823	32	128	88	0
1385.0	.	332	3420	72	200	91	7
1396.0	.	221	2740	128	141	89	9
1410.2	.	265	3500	74	170	75	6
1421.1	.	268	3400	59	198	104	9
1424.3	.	282	3860	66	213	91	6
1427.4	.	155	3430	0	194	72	0
1430.3	.	343	3670	37	236	101	0
1433.3	.	299	3690	0	250	58	5
1439.1	.	163	4480	40	260	105	6
1447.3	.	113	3180	0	320	78	5
1450.1	.	206	3110	158	349	88	10
1452.8	.	98	5230	54	360	108	6
1453.3	.	384	5450	170	384	129	9
1454.4	58	204	2600	219	425	78	8
1459.6	.	85	5150	278	471	141	8
1462.7	.	168	2420	240	470	60	9
1476.2	.	307	2770	211	53	97	4

Sample	GRAPHITE	C	S	Ba	Co	Cu	Mo
1485.9	.	205	2810	.	432	2	0
1491.0	.	383	652	162	111	26	6
1494.0	.	456	4370	64	519	78	4
1496.1	.	190	167	49	228	20	6
1498.9	.	343	72	204	52	25	6
1508.2	.	431	46	249	28	20	0
1520.4	.	262	91	259	39	22	8
1545.6	.	290	200	98	62	11	0
1548.4	.	240	2390	30	196	85	4
1556.6	.	149	2640	.	.	.	.
1573.1	.	164	2460	104	133	99	5
1580.5	.	576	2870	35	177	111	6
1589.1	.	81	4650	0	277	148	4
1594.2	.	294	2000	123	108	127	5
1606.2	.	368	1540	123	104	423	6
1612.9	.	229	1750	167	83	305	7
1620.4	.	198	148	191	66	30	5
1627.5	.	122	422	181	102	34	7
1633.7	.	203	284	108	141	29	6
1642.5	.	156	229	182	58	7	6
1649.8	.	116	2300	105	156	104	4

Appendix 9B

Trace Element Analysis continued.

- Values given in ppm.
- Unpublished analytical results on Bierkraal 1 whole samples, courtesy R.K.W. Merkle.

Sample	Nb	Ni	Rb	Sr	V	Y	Zn	Zr
422.2	19	26	45	330	0	57	192	196
423.0	13	18	33	291	1	45	194	151
426.0	17	28	37	332	0	54	185	163
428.5	16	31	37	322	0	54	165	158
433.0	15	33	30	285	0	51	167	149
434.9	15	44	25	233	0	51	182	125
437.8	15	32	33	295	0	54	180	172
441.4	16	34	37	290	0	57	178	144
444.8	15	24	41	336	0	61	167	155
446.6	18	31	29	262	0	42	188	126
449.3	14	10	35	530	0	31	167	190
452.4	19	9	35	464	0	38	200	151
454.8	15	19	42	475	0	36	168	115
457.8	13	15	41	416	0	38	183	153
464.1	14	29	14	333	0	43	175	135
475.1	13	24	30	334	0	41	164	136
475.5	13	29	43	353	0	38	148	133
483.4	13	52	12	309	0	41	177	90
486.4	13	26	33	299	0	39	167	123
487.5	13	29	34	332	0	36	153	143
489.4	12	29	27	308	0	36	172	129
493.5	13	28	35	293	0	33	156	110
496.5	12	26	32	286	0	42	177	120
499.4	13	30	38	273	0	37	157	131
504.7	12	23	34	298	0	43	181	136
507.5	13	32	29	366	0	37	147	107
507.8	13	26	30	356	0	38	167	93
515.1	13	23	36	326	0	37	152	116
521.0	12	31	26	300	0	34	151	106
522.5	13	30	27	329	0	39	151	114
525.7	13	28	27	290	0	41	163	116
534.0	12	29	30	315	0	39	158	118
538.0	8	30	9	295	0	22	120	52
549.0	13	18	33	356	0	43	177	95
551.5	9	21	23	319	0	35	149	107
551.7	12	28	25	312	0	42	161	88
554.7	13	24	27	314	0	40	199	115
559.0	12	28	24	336	0	42	164	101
563.5	11	26	24	324	0	38	159	95
568.0	12	31	24	313	0	42	155	107
571.5	14	26	29	348	0	46	165	125
579.0	13	38	12	305	0	43	171	99
581.3	11	36	15	283	0	44	175	97
582.4	13	29	22	342	0	36	203	94
589.5	12	42	13	258	0	49	167	95
591.5	13	33	31	311	0	41	169	131
594.8	13	52	12	309	0	56	177	90
599.5	11	34	20	300	0	44	165	98
601.5	10	48	18	246	0	39	156	88
607.5	14	55	21	280	0	64	170	115
611.9	13	61	16	247	0	76	185	126
620.5	15	57	31	366	0	24	177	113
631.7	12	72	13	220	0	71	151	93
633.7	13	74	13	152	0	53	195	104
638.1	14	73	15	204	0	75	198	111
638.2	13	71	14	226	0	72	184	106

Sample	Nb	Ni	Rb	Sr	V	Y	Zn	Zr
641.4	12	31	21	353	0	36	122	86
647.3	12	52	19	251	0	54	142	97
651.0	11	41	13	215	0	45	110	91
652.0	8	39	10	271	0	17	106	67
654.7	11	33	19	297	0	20	110	87
659.0	11	23	28	335	0	24	110	98
663.3	11	3	35	508	0	23	111	79
667.8	10	23	21	425	0	37	113	76
669.3	10	18	22	417	0	21	124	87
673.3	10	17	18	344	0	19	111	81
674.5	10	9	24	383	0	21	90	72
680.0	5	0	19	405	0	12	92	59
686.6	11	30	17	342	0	17	129	79
688.0	9	16	20	452	0	19	95	65
695.0	10	24	17	373	0	26	116	70
695.5	9	19	22	364	0	28	111	72
700.0	11	16	20	405	0	29	133	70
704.4	11	22	18	365	0	31	134	74
705.5	10	31	18	354	0	28	127	72
709.0	11	24	18	356	0	28	125	73
713.7	9	24	13	317	0	25	130	70
715.0	10	31	16	348	0	27	124	71
718.0	10	32	14	316	0	31	134	71
722.0	11	24	16	345	0	30	132	67
726.0	8	23	12	305	0	27	129	62
727.5	11	26	15	319	0	32	135	65
736.5	11	45	13	263	0	43	140	75
738.7	10	34	15	274	0	32	145	72
744.8	11	40	16	290	0	39	141	80
751.1	11	46	13	273	0	35	137	79
754.8	12	50	14	270	0	36	172	91
757.7	12	37	18	321	0	33	153	80
759.8	11	56	13	270	0	55	128	72
763.7	12	39	16	279	0	19	141	82
765.0	10	53	13	307	0	38	136	69
772.5	12	76	16	298	0	49	124	86
773.8	11	81	15	232	0	37	147	87
776.0	11	29	17	450	0	17	145	82
783.2	17	30	36	396	0	52	161	71
785.5	11	30	20	366	0	27	123	71
787.7	11	20	18	395	0	33	115	67
798.0	10	44	14	298	0	32	126	72
798.2	10	41	16	323	0	34	120	74
804.0	12	40	17	295	0	35	153	92
808.5	11	20	21	329	0	31	135	80
810.5	11	44	21	279	0	35	122	86
820.0	11	23	19	449	0	22	109	72
822.8	11	43	19	319	0	29	121	74
823.4	10	59	19	314	0	39	100	79
824.0	11	98	11	155	0	22	131	82
830.8	13	34	32	289	0	45	159	127
835.3	10	31	15	325	0	27	115	68
839.6	10	29	15	311	0	28	130	67
845.8	10	40	15	345	0	32	134	60
857.7	11	32	29	321	0	41	118	95
859.3	11	41	26	379	0	54	93	81
862.0	10	48	27	374	0	14	104	69
863.7	10	50	15	328	0	16	107	65
872.0	12	38	20	296	0	23	139	84
876.3	10	31	20	321	0	22	118	86
876.5	10	33	24	379	0	19	109	75
880.5	10	18	20	520	0	13	96	71
892.5	11	18	20	353	0	19	116	75
893.0	10	25	16	326	0	15	115	71
899.0	10	23	17	396	0	11	92	61
909.0	9	24	16	434	0	13	118	69

Sample	Nb	Ni	Rb	Sr	V	Y	Zn	Zr
917.0	6	19	10	399	0	6	107	48
922.0	10	13	15	410	0	16	129	60
933.8	10	17	16	403	0	12	121	59
940.1	9	26	14	371	0	13	114	61
951.0	9	32	12	353	0	22	126	60
955.0	6	12	8	376	0	14	107	42
965.1	10	15	15	434	0	19	122	54
968.9	10	16	15	461	0	18	111	52
980.8	9	22	13	397	0	19	113	54
992.0	10	19	13	384	0	22	128	57
999.8	10	26	14	405	0	22	129	56
1009.6	9	32	12	381	0	23	126	57
1019.8	10	20	14	387	0	23	143	62
1030.0	7	18	12	370	0	22	133	59
1040.2	7	22	11	354	0	25	142	61
1050.2	9	30	11	298	0	24	137	64
1060.3	11	36	12	284	0	28	167	65
1068.9	12	52	11	233	0	52	165	77
1082.2	10	45	8	221	0	43	168	68
1086.7	12	52	11	233	0	52	165	77
1089.8	11	51	11	245	0	48	153	71
1091.0	12	51	11	211	0	41	183	74
1091.6	13	69	9	70	0	78	140	84
1092.8	13	57	12	201	0	53	183	79
1096.3	12	61	10	179	0	64	169	85
1100.8	13	71	12	156	0	91	172	91
1103.7	13	100	13	200	0	71	292	84
1104.9	13	99	12	194	0	71	205	86
1112.0	15	130	16	142	0	110	264	98
1113.5	14	115	13	152	0	14	201	103
1114.7	11	20	19	479	0	14	115	68
1128.7	11	24	16	370	0	19	144	64
1139.1	9	33	13	333	0	15	102	63
1151.3	10	43	15	303	0	18	137	67
1160.0	9	0	18	551	0	12	80	48
1161.5	9	7	18	534	0	12	95	56
1178.2	10	54	12	295	0	10	112	58
1189.8	9	45	11	169	0	11	102	67
1199.0	10	37	12	239	0	14	111	63
1211.0	10	21	16	351	0	25	116	59
1219.1	10	26	14	371	0	25	114	55
1231.2	10	21	13	332	0	26	131	60
1241.5	8	39	12	362	0	20	111	51
1256.3	10	31	13	377	0	18	123	56
1260.8	9	24	12	296	0	17	92	50
1270.4	8	15	13	332	0	20	94	52
1280.5	9	21	12	345	0	17	111	53
1289.7	10	21	14	366	0	22	118	51
1302.8	9	27	12	347	0	23	115	55
1308.6	9	24	12	338	0	25	114	57
1320.8	11	36	13	281	0	26	150	63
1329.2	8	30	9	295	0	22	120	52
1340.1	10	31	12	344	0	28	131	62
1350.6	10	24	13	329	0	31	127	59
1364.0	9	38	11	266	0	36	128	62
1371.9	10	37	11	294	0	36	130	61
1379.1	6	30	4	251	0	33	138	48
1385.0	11	45	10	209	0	45	186	72
1396.0	11	32	12	274	0	40	163	69
1410.2	11	46	11	231	0	45	171	77
1421.1	11	53	11	205	0	40	172	71
1424.3	9	45	9	204	0	40	152	65
1427.4	7	48	3	175	0	51	158	60
1430.3	7	53	3	148	0	46	176	61
1433.3	10	68	9	145	0	57	164	75
1439.1	10	68	8	167	0	41	174	69
1447.3	10	78	8	132	0	12	180	77
1450.1	13	98	9	81	0	12	232	97

Sample	Nb	Ni	Rb	Sr	V	Y	Zn	Zr
1452.8	12	109	8	92	0	9	223	94
1453.3	13	131	9	82	0	12	232	101
1454.4	13	138	7	47	0	11	248	104
1459.6	12	141	8	37	0	10	269	108
1462.7	13	143	8	39	0	10	244	107
1476.2	9	62	15	445	179	9	101	60
1485.9	8	233	3	39	749	5	176	91
1491.0	9	54	12	335	4	10	116	54
1494.0	10	220	5		0	9	198	102
1496.1	9	90	9	151	0	10	128	66
1498.9	9	19	13	344	0	14	103	58
1508.2	7	1	12	477	0	6	79	46
1520.4	10	14	17	488	0	10	94	59
1538.1	5	7	6	369	0	2	78	45
1548.4	9	35	10	225	0	18	110	59
1573.1	9	28	11	266	0	11	135	66
1580.5	10	41	11	266	0	9	144	65
1589.1	10	60	8	180	0	6	169	69
1594.2	9	76	11	241	212	16	134	63
1606.2	9	75	11	250	297	12	195	60
1612.9	9	86	14	373	774	8	128	54
1620.4	8	19	12	395	507	9	79	56
1627.5	9	27	13	398	354	8	126	54
1633.7	9	49	11	327	207	7	118	51
1642.5	9	15	13	428	567	8	79	52
1649.8	9	59	12	259	597	11	112	66

Appendix 10

Eastern Bushveld sample list

Samples selected from the Von Gruenewaldt (1971) investigation, Roossenekal district, eastern Bushveld Complex. The first column lists the names used in this text and the second those used in the Von Gruenewaldt (1971) text for corresponding samples.

Name	Von Gruenewaldt (1971)	Whole Rock	Apatite	Biotite
EB-1D	200	Sample	Sample	No sample
EB-2d	215	Sample	Sample	No sample
EB-3d	216	Sample	Sample	No sample
EB-4d	208	No sample	Sample	No sample
EB-5d	285	Sample	No sample	Sample
EB-6d	368	No sample	Sample	Sample
EB-7d	253	No sample	Sample	No sample
EB-8d	252	Sample	No sample	No sample
EB-9d	257	Sample	Sample	No sample
EB-10d	633	Sample	No sample	No sample
EB-11d	271	Sample	Sample	No sample
EB-12c	642	Sample	Sample	No sample
EB-13c	625	Sample	No sample	No sample
EB-14c	310	Sample	No sample	Sample
EB-15c	621	Sample	No sample	Sample
EB-16c	620	Sample	No sample	Sample
EB-17c	617	Sample	No sample	Sample
EB-18b	350	Sample	No sample	No sample
EB-19b	568	Sample	No sample	Sample
EB-20b	510	Sample	No sample	Sample
EB-21b	400	Sample	No sample	Sample
EB-22a	611	Sample	No sample	No sample

See Von Gruenewaldt (1971) for relative stratigraphic positions.

Appendix 11
Analysis of the Geo-standards

	Abbey NIM-L	Jackson	Current	Abbey SY-3	Current	Evensen Chondrite
La	240	158	169	1350	676	0.2446
Ce	230	201	164	2200	917	0.6379
Pr	15		13	120	105	0.0963
Nd	45	45	29	800	331	0.4738
Sm	6	4.6	1.7	100	49	0.154
Eu	1	1.0	0.5	14	7	0.0580
Gd		1.8	1.2	55	42	0.2043
Dy	3	1.9	1.1	80	50	0.2541
Ho		0.42	0.2	20	10	0.0567
Er		1.2	0.6	50	29	0.166
Tm		0.23				0.0256
Yb	3.5	2.2	0.3	65	50	0.1651
Lu		0.27				0.0253

References

Abbey - Abbey (1983)
Jackon - Jackson and Strelow (1975)
Current - Refers to the values established with the technique employed in this investigation.
Evensen - Evensen et al., (1983)